Investigation of Novel Modular Stator Permanent Magnet Machines

Bo REN

A thesis submitted for the degree of Doctor of Philosophy

Department of Electronic and Electrical Engineering

The University of Sheffield

UK

June 2018

Abstract

This thesis is focused on the novel modular permanent magnet (PM) machines having flux gaps (FGs) in alternate stator teeth. Three research topics are included: 1) the design of multi-phase modular PM machines, 2) cogging torque and torque ripple reduction methods for modular PM machines, 3) the manufacturing tolerance of modular PM machines.

First of all, the influence of FGs on the multi-phase modular PM machines are summarized and some general rules are established which can be used as the design guidelines for the multi-phase modular PM machines. It is worth noting that the 4- and 5-phase modular stator PM machines are only studied through the simulation. Secondly, two cogging torque and torque ripple reduction methods by the slot-opening shift and also the employment of the C-core stator segments are introduced. The proposed methods can effectively reduce the resultant cogging torque and torque ripple of the modular PM machines. Thirdly, the manufacturing tolerances of modular PM machines are also studied in this thesis and it provides an insight into the influence of manufacturing tolerance on the modular PM machines performance. Three possible manufacturing tolerance scenarios, e.g. stator segment radial or circumferential displacement and the PM defects, are investigated. The assessment of the manufacturing tolerance withstand capability of modular PM machines has also been carried out in this thesis.

The prototype machines have been built and the numerical results calculated by both 2D and 3D finite element (FE) have been validated. It is worth mentioning that although the research carried out in this thesis based on the small size modular PM machines (for experimental validation purpose), the conclusions obtained in this thesis may be extended to other large modular PM machines.

Acknowledgements

This thesis completion is attributed to many peoples support and encouragement.

First and foremost, I would like to show my greatest and deepest gratitude to my first supervisor Dr. Guang-Jin LI, for his kind guidance, continuous support and valuable suggestions to me during my PhD research and the writing of this thesis. I am indeed a fortunate man to have Dr. Guang-Jin LI as my supervisor who opened the door of the academic world for me and inspired me both in the research and life. His enthusiastic and rigorous academic attitude set a good example for me. Also, I want to express my sincere gratitude to my second supervisor Prof. Zi-Qiang ZHU, for his instructive advice and insightful advice to this thesis.

I want to thank my dear parents, for their endless support, encouragement and love on me. Without you, the completion of my PhD study and this thesis would not have been possible.

My thanks would also like to go to my colleagues of the EMD group of the University of Sheffield. Thank you, Dr. Yan-Xin LI, Dr. Wen-Qiang CHU, Dr. Jun-Tao SHI, Dr. Xiao. Ge and Dr. Di WU, for their precious advice and valuable technical discussions, which give me deeper sights of my research and lead me to the achievements. I appreciate their kind help and effort.

Last, but not the least, my special and deep gratitude goes to my girl-friend, Dr. Xi-Yun MA for her love and support. The comfort you give me is my most precious gift.

Bo REN

The University of Sheffield

UK

Jun. 2018

List of Abbreviations

Back-EMF	Back electromotive force
EV	Electrical vehicle
FE	Finite element
FG	Flux gap
FP	Frozen permeability
FSPM	Flux-switching permanent magnet
GCD	Greatest common divisor
IPM	Interior permanent magnet
LCM	Least common multiple
MMF	Magneto motive force
PM	Permanent magnet
RMS	Root-mean square
SPM	Surface-mounted permanent magnet
UMF	Unbalanced magnetic force

Nomenclatures

h_{sy}	Stator yoke thickness	mm
E_A, E_B, E_C	Magnitudes of the fundamental phase back-EMFs	V
E_{An}, E_{Bn}, E_{Cn}	Magnitudes of the n^{th} harmonic of phase back-EMFs	V
F_x, F_y	UMF of x-axis or y-axis	N
I_A, I_B, I_C,	Magnitudes of the phase supply currents	A
I_{RMS}	RMS current	A
K_d	Distribution factor	
K_p	Pitch factor	
K_w	Winding factor	
N_{FG}	Number of FGs	
N_c	LCM between N_s and $2p$	
N_{cm}	LCM between N_{FG} and $2p$	
N_s	Slot number	
R_i	Stator inner radius	mm
T_{cogg}	Cogging torque of non-modular PM machine	Nm
$T_{cogg-modualr}$	Cogging torque of modular PM machine	Nm
T_j	The magnitude of the j^{th} cogging torque harmonic	Nm
q_{ph}	Number of slot vectors of one phase	
w_{tb}	Tooth body width	mm

β_{FG}	FG width	mm
λ_s	Split ratio	
σ_{ph}	Angle between two adjacent back-EMF vectors	Elec. Deg.
τ_p	Pole pitch	Mech. Deg.
τ_s	Slot pitch	Mech. Deg.
$\varphi_{An}, \varphi_{Bn}, \varphi_{Cn}$	Phase angles of the n^{th} harmonic of phase back-EMFs	Elec. Deg.
ω_m	Rotation speed	Rad/s
t	Time	s
I	Peak current	A
m	Phase number	
p	Rotor pole pair number	
q	Number of coil per phase	
α	Rotor position	Elec. Deg.
β	Desired shift angle	Elec. Deg.
γ	Desired shift angle	Mech. Deg.
δ	Phase angle of supply current	Elec. Deg.
θ	Angular position	Mech. Deg.
σ	Phase angle between adjacent EMF vectors of one phase	Elec. Deg.
φ	Phase angle of cogging toque harmonic	Elec. Deg.
ω	Electrical speed	Rad/s

Publications

During the PhD study, 5 papers have been published including 4 journal papers and 1 conference papers. Moreover, another 1 conference paper is ready to be submitted.

Papers Directly from Thesis

1. G. J. Li, **B. Ren**, Z. Q. Zhu, Y. X. Li, and J. Ma, "Cogging torque mitigation of modular permanent magnet machines," *IEEE Trans. Magn*., vol. 52, no. 1, Jan. 2016.
2. G. J. Li, **B. Ren**, and Z. Q. Zhu, "Design guidelines for fractional slot multi-phase modular permanent magnet machines," *IET Electr. Power. Appl*., vol. 11, no. 6, pp. 1023-1031, Jul. 2017.
3. G. J. Li, **B. Ren** and Z. Q. Zhu, "Cogging torque and torque ripple mitigation of modular permanent magnet machines," in *IEEE Int. Conf. Electr. Mach. (ICEM)*, Lausanne, Switzerland, Sept. 4-7, 2016, pp. 193-199.

Other Papers

1. **B. Ren**, G. J. Li, Z. Q. Zhu, M. Foster and D. Stone, "Performance comparison between consequent-pole and inset modular permanent magnet machines," *IET journal of engineering*.
2. G. J. Li, **B. Ren**, Z. Q. Zhu, M. Foster and D. Stone, "Demagnetization withstand capability enhancement of surface mounted PM machines using stator modularity," *IEEE Trans. Ind. Appl*., vol. 54, no. 2, pp. 1302-1311, Mar.-Apr. 2018.

CONTENTS

Abstract ..... **I**

Acknowledgements ..... **II**

List of Abbreviations ..... **III**

Nomenclatures ..... **IV**

Chapter 1 Introduction **1**

1.1 Background 2
1.2 Existing Modular Machine Topologies 4
1.2.1 Machines with Modular Stators 5
1.2.2 Machines with Modular Rotors 20
1.3 Summary of the Modular PM Machines 23
1.4 Research Scope and Contributions 25
1.4.1 Research Scope 25
1.4.2 Research Contribution 26

Chapter 2 Design Guidelines for the Fractional-Slot Multi-Phase Modular PM Machines **27**

2.1 Introduction 28
2.2 Winding Arrangement of the Multi-Phase Modular PM Machines 31
2.2.1 Winding Factors of Non-Modular PM Machines 31
2.2.2 Winding Factors of Modular PM Machines 34
2.3 Design of Modular PM Machines 36
2.4 Electromagnetic Performance of Modular PM Machines 38
2.4.1 Air-Gap Flux Density Due to the Armature 38
2.4.2 Air-Gap Flux Density Due to the PMs 45
2.4.3 Phase Back-EMF 50
2.4.4 Cogging Torque 55
2.4.5 On-load Torque and Torque Ripple 56
2.5 Experimental Validation 59
2.5.1 Phase Back-EMF 59
2.5.2 Static Torque 60
2.6 Conclusion 62

Chapter 3 Cogging Torque and Torque Ripple Reduction of Modular PM Machines by Slot-Opening Shift 63

3.1 Introduction 64
3.2 Cogging Torque Prediction of Modular PM Machines 67
3.2.1 Effects of FGs on Cogging Torque 67
3.2.2 Synthesis of Cogging Torque for Modular PM Machines 68
3.3 Cogging Torque Mitigation 72
3.3.1 Theoretical Analysis by FE 72
3.3.2 Calculation of the Desired Shifting Angle 77
3.4 Case Study 80
3.4.1 12-Slot/10-Pole Modular PM Machines 80
3.4.2 12-Slot/14-Pole Modular PM Machines 93
3.4.3 Cogging Torque Mitigation Accounting for Magnetic Saturation 102
3.5 Experimental Validation 106
3.5.1 Prototypes of Modular PM Machines 106
3.5.2 Cogging Torque 107
3.5.3 Phase Back-EMF 107
3.6 Conclusion 109

Chapter 4 Cogging Torque and Torque Ripple Reduction of Modular PM Machines by C-Core Modular Stator 110

4.1 Introduction 111
4.2 Topology of the Investigated PM Machines 114
4.3 Electromagnetic Performance 115
4.3.1 Open-Circuit Flux Linkage 115
4.3.2 Phase Back-EMF 121
4.3.3 Cogging Torque 123
4.3.4 On-Load Torque 125
4.3.5 Torque Ripple Analysis by Using the Frozen Permeability Method 126
4.3.6 Cogging Torque and Torque Ripple of Modular PM Machines Having Dummy Slots 128
4.4 Prototype Machines 132
4.5 Conclusion 133

Chapter 5 Influence of Manufacturing Tolerance on the Performance of Modular PM Machines 134

5.1 Introduction 135
5.2 Modular PM Machines with Radial Stator Segment Displacement 138
5.2.1 Influence of Radial Stator Segment Displacement on Phase Back-EMF 138
5.2.2 Influence of Radial Stator Segment Displacement on On-Load Torque 140
5.2.3 Influence of FG Widths and Slot/Pole Number Combinations on Modular PM Machines with Radial Stator Segment Displacement 143
5.3 Modular PM Machines with Circumferential Stator Segment Displacement 157
5.3.1 Influence of Circumferential Stator Segment Displacement on Phase Back-EMF 158
5.3.2 Influence of Circumferential Stator Segment Displacement on On-Load Torque 161
5.3.3 Influence of Slot/Pole Number Combinations on Modular PM Machines with Circumferential Stator Segment Displacement 164
5.4 Modular PM Machines with PM Defect 174
5.4.1 Influence of PM Defect on Open-Circuit Air-Gap Flux Density and Phase Back-EMFs 175
5.4.2 Influence of FG Widths and Slot/Pole Number Combinations of Modular PM Machines With PM Defect 178
5.4.3 Experimental Validation 192
5.5 Conclusion 198

Chapter 6 Conclusions and Future Works 200

6.1 Conclusions 201
6.2 Future Works 202

References 204

Chapter 1 INTRODUCTION

In this chapter, a general introduction on the modular PM machines is given. The modular stator and rotor topologies have been reviewed in the first place and then the advantages and disadvantages of employing modular machines topologies have been detailed. The machine cooling by taking advantages of modular structure has also been demonstrated. Last but not the least, the research scope and contributions of this thesis has been stated at the end of this chapter.

1.1 BACKGROUND

PM machines, due to their inherently exhibited advantages compared with the electrically excited machines and also induction machines, have attracted increasing interests from both academia and also industry in recent decades. The advantages of PM machines include but not limited to [1]-[2]:

1. Simple structure especially when the brushless topologies are adopted. Therefore, compared to the traditional wound field synchronous machines with mechanical commutators, the PM machines can have higher reliability.
2. Generally high efficiency due to the fact that no extra excitation field is needed, resulting in the elimination of the copper losses in the rotor during the excitation.
3. High torque/power density benefiting from the employment of PMs that have high magnetic energy density.
4. High power factor, etc.

Benefiting from the advantages above, the PM machines can be applied to many applications, such as aerospace, domestic appliances, electric and hybrid electric vehicles (EVs and HEVs), etc. [3]-[5]. In addition, due to high torque and power density as well as high efficiency, the renewable energy such as (onshore and offshore) wind power is another important market sector for PM machines [6]. Two main PM machine topologies are often selected for the wind turbines which are the surface-mounted PM (SPM) generator and the interior PM (IPM) generators although the former is more preferable particularly for offshore wind power applications [7]. By employing the SPM generator, the lower torque ripple can be more easily achieved while when the V-shaped IPM generator is employed, the thinner PMs are allowed due to the flux concentration effect in the rotor [8]. In [7], the performance of two 5MW PM wind power generators having either SPM or IPM rotors are compared. It has concluded that at the average wind speed of 7m/s, the IPM generator has slightly higher efficiency due to its better power factor, which is not common and leaving a surprise.

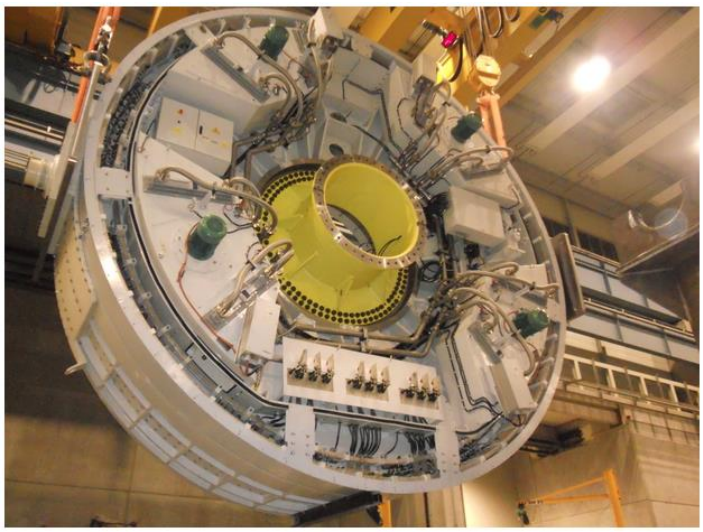

Fig. 1.1 The picture of wind power generator [9].

However, the size of such wind power generators could be very large, as shown in Fig. 1.1. By way of example, the outer diameter can be as large as 8.6 meter for a 5MW wind power generator [10]. Therefore, the manufacturing, transportation, lifting and assembling works on site will be big challenges.

The introduction of modular topology can help to significantly ease the aforementioned difficulties of such large wind power generators and also other large-scaled machines [28]. By employing the modular topology, the manufacturing efficiency in terms of the material consumption, production capability, etc. can be improved as well. Therefore, in this chapter, the modular PM machines having different modular stators or rotors with their characteristics, as well as the advantages and disadvantages of employing the modular topologies are reviewed, providing a powerful insight into the potential of such machines for wind power applications.

1.2 EXISTING MODULAR MACHINE TOPOLOGIES

The modular PM machines, due to advantages such as simple stator construction and winding fabrication as well as good fault-tolerant capability, etc. are attracting growing interest from both industry and academia. Various modular topologies have been proposed in recent years, although some modular rotor structures have been proposed, most of the modular machines employ the modular stator structures in different ways. In the following sections, different modular topologies will be reviewed. A summary of the modular PM machine topologies is given in Fig. 1.2.

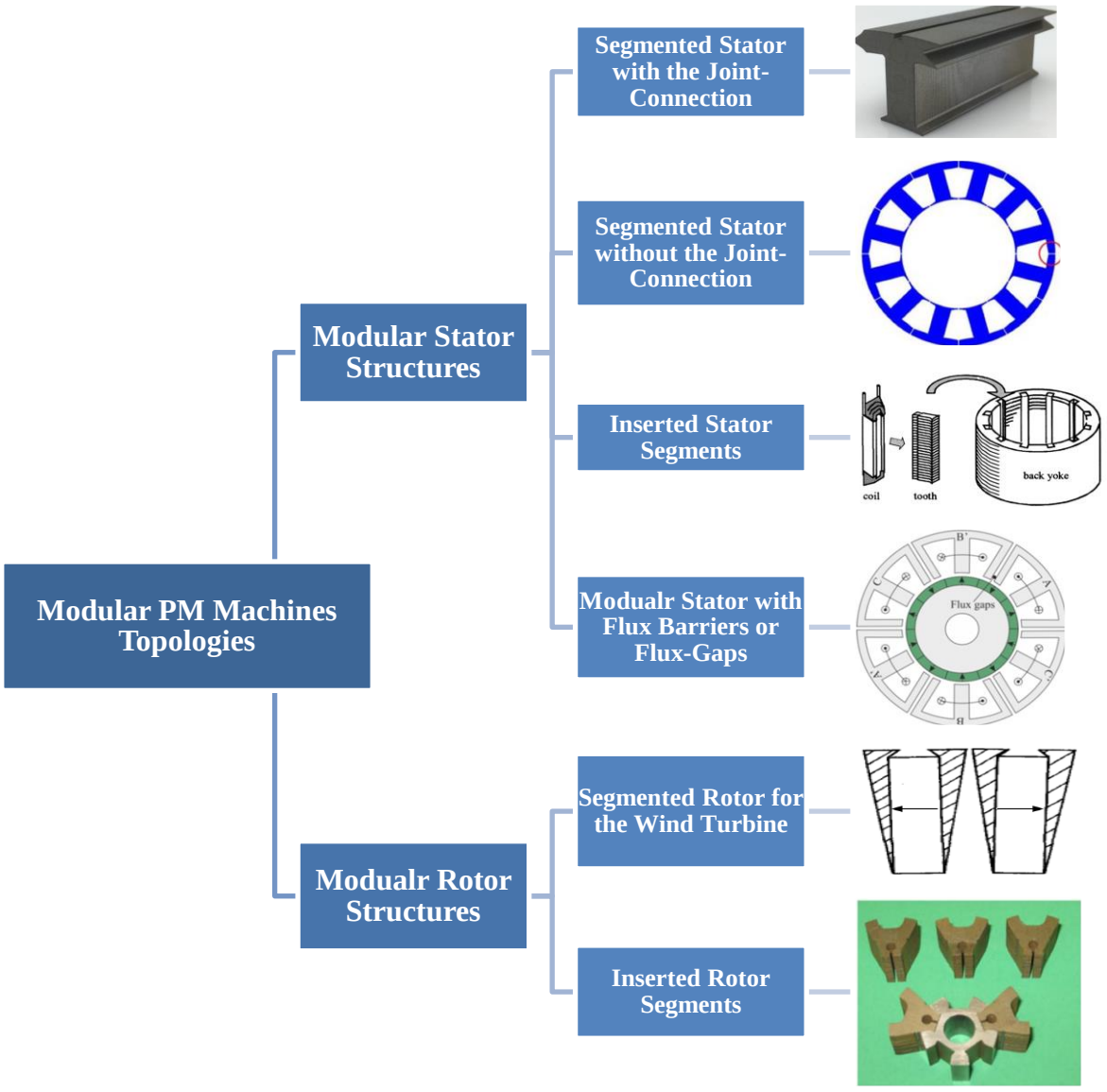

Fig. 1.2 Modular PM machines topologies existed in the literature.

1.2.1 MACHINES WITH MODULAR STATORS

1.2.1.1 SEGMENTED STATOR WITH JOINT-CONNECTION IN STATOR YOKE

H. Akita, *et.al*. have proposed a new stator core structure which can be made into the model of a joint-lapped core [11] and by employing some cylindrical convex or concave joints, the segments are connected together. By doing so, the rotation of the segments are allowed so to obtain a cylindrical stator core, as shown in Fig. 1.3. Additionally, if a non-overlapping winding is employed, the copper wire can be wound around the teeth of such stator core easily and automatically by the winding nozzle, as illustrated in Fig. 1.4. This can largely save the winding time and potentially help to increase the slot fill factor. It is found that the efficiency of the machine with the joint-lapped core can be improved slightly from 93.7% to 95.3% compared with the machine with the conventional core due to the reduction in both copper and iron losses [11]. However, this method requires special tools [12] and extra time to assemble the large number of stator segments, which could increase the manufacturing difficulty and reduce the production efficiency.

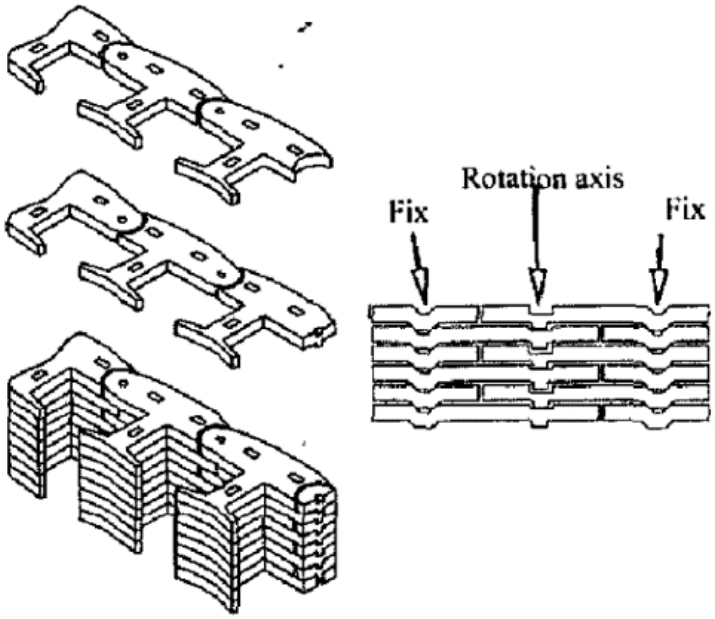

Fig. 1.3 Model of a joint-lapped core [11].

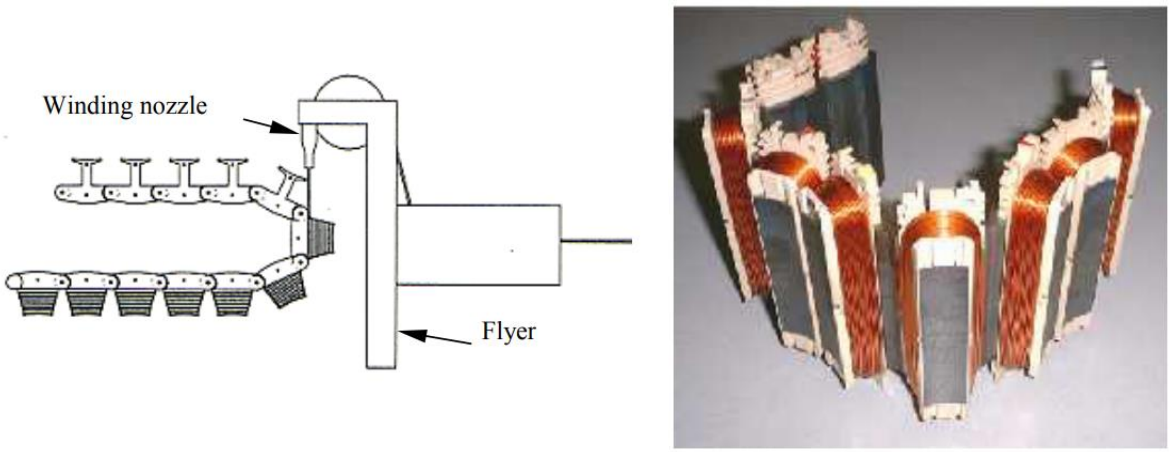

(a) (b)

Fig. 1.4 (a) The flyer winding in the joint-lapped core. (b) Joint-lapped core after winding process [11].

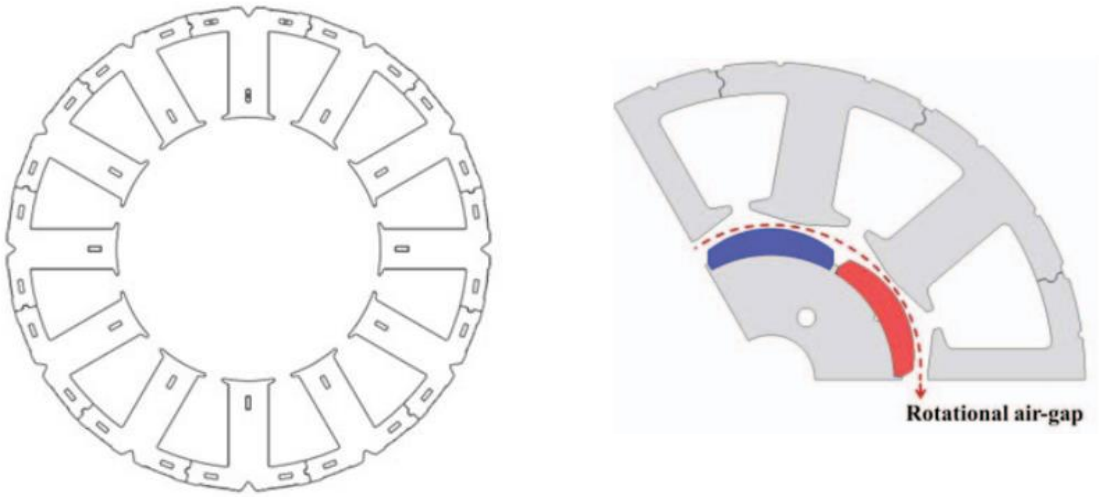

(a) (b)

Fig. 1.5 Modular stators. (a) Modular stator proposed in [13]-[14] . (b) Modular stator proposed in [15].

Similar to the modular topology presented in [11], other modular stator core structures with the joint-connections are shown in [13]-[15], as shown in Fig. 1.5. It can be found that the joint-connection structures and the shape of the stator segments are simpler compared to the structures shown in Fig. 1.3. By doing so, the manufacturing efficiency can be significantly

improved and the stator core material consumption can be greatly saved. The manufacturing method such as preforming winding by winding machine for each stator segment is still feasible for this type of modular structure. It is worth noting that some commercial products have already been launched by companies such as SWD AG [16], Yuma Precision Stamping Co., Ltd [17], as shown in Fig. 1.6.

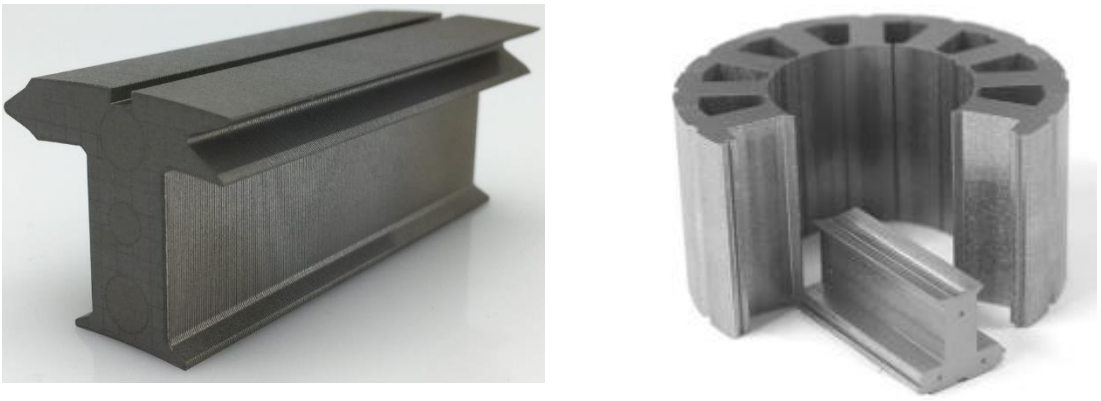

(a) (b)

Fig. 1.6 The pictures of the stator segments. (a) Stator segment produced by [16]. (b) Stator segment produced by [17].

In [18], several other shapes of stator joint-connections are presented, as depicted in Fig. 1.7. However, compared to the stator segments shown in Fig. 1.6, the shape of the stator segments shown in Fig. 1.7 are more complicated. Such complicated joint-connections can help to strengthen the interconnection between the stator segments. However, the precise manufacturing is necessary which need very accurate stamping tool. This will lead to increase in the production cost. On the contrary, due to the relatively simpler joint-connection shape, the stator segments proposed in [13]-[17] can be manufactured and assembled relatively easier and quicker while the strength of the connection will not necessarily be compromised. Therefore, such kind of stator segment shape is more suitable in practice.

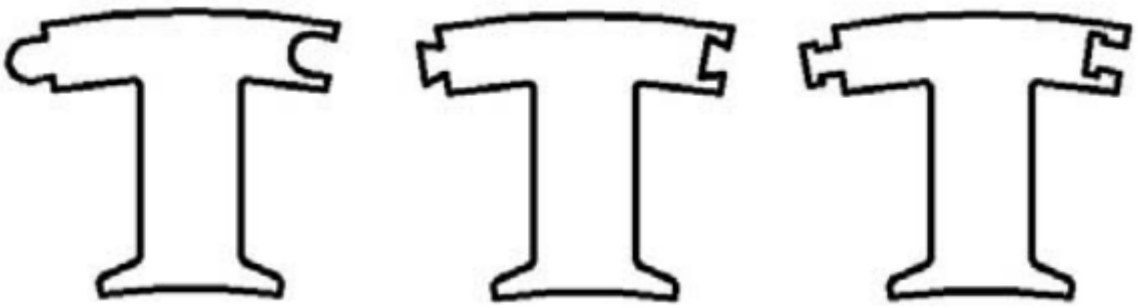

(a) (b) (c)

Fig. 1.7 Stator segments with different joint-connections. (a) Ω shape. (b) Trapezoid shape. (c) T shape [18].

Besides the models proposed above, other modular models with flux-barriers inserting in the stator yoke have been proposed in [19]-[21], as shown in Fig. 1.8. The flux-barriers are made of nonmagnetic material so to reduce the effective stator yoke thickness (rather cutting off the stator yoke partially) and at the same time to maintain a complete stator core. By uniformly displacing the flux-barriers in the stator yoke, the sub-harmonics in the air-gap flux density as well as the iron losses in the machine can be reduced and hence the machine performance can be improved [19].

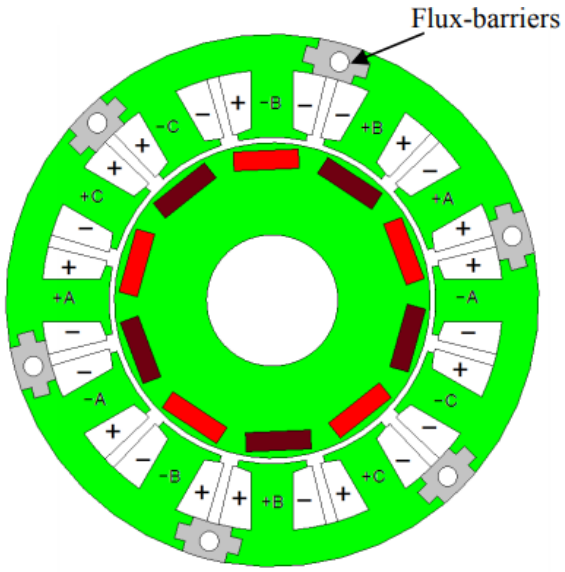

Fig. 1.8 Modular PM machine with flux barrier in the stator yoke [19]-[21].

Nevertheless, the modular structures shown in Fig. 1.5 and Fig. 1.6 still require accurate manufacturing and assembly to build the complete stator core. However, in practice, the 100% accurate manufacturing during the mass production is impossible, and thus, the manufacturing tolerance will always exist, as shown in Fig. 1.9. In [13]-[14], the influence from the manufacturing tolerance of the tooth-bulge on cogging torque has been investigated, as shown in Fig. 1.9 (a). It has found that the tooth-bulge problem leads to extra cogging torque harmonic contents and based on such additional cogging torque harmonics, a quick and easy method for identifying the most sensitive cases of the tooth-bulge problem is introduced.

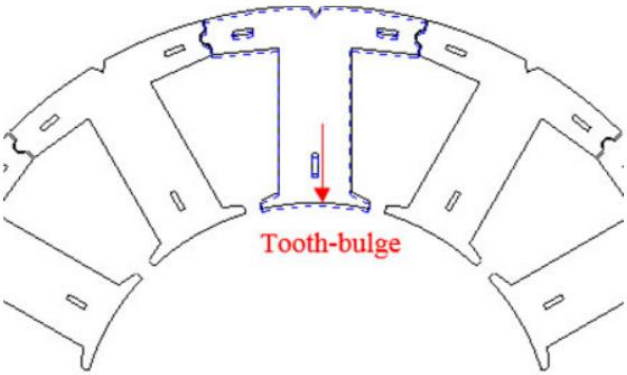

(a)

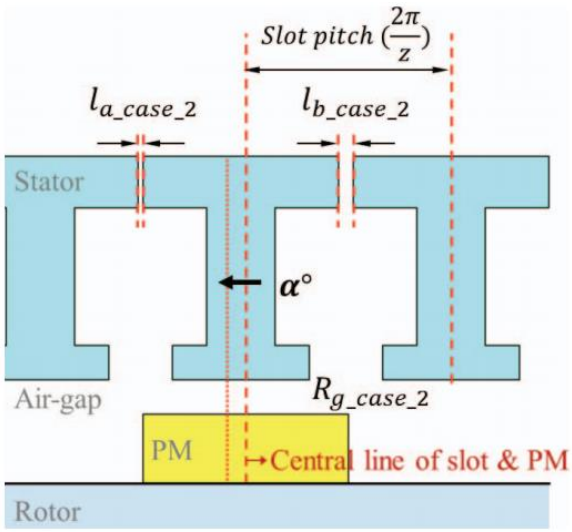

(b)

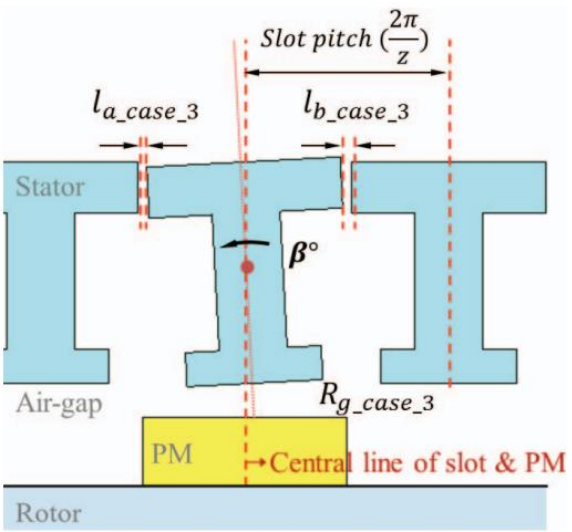

(c)

Fig. 1.9 Modular stator core with the manufacturing tolerance. (a) Tooth-bulge [13]-[14]. (b) Stator segment misaligned [15].

In [15], other two manufacturing tolerance scenarios of the stator core segment misaligned are studied, as shown in Fig. 1.9 (b) and (c). It has found that the inevitable additional air-gaps during the assembly process resulted in the decrease in output power compared with the motor with conventional stator core. This is mainly due to the increase in the effective air-gap reluctance resulted from such additional air-gaps. In addition, it is found that the stator segment misalignment problem increases the peak cogging torque and the periodicity of the cogging torque will be changed at the same time.

1.2.1.2 SEGMENTED STATOR WITHOUT JOINT-CONNECTION IN STATOR YOKE

In 2004, B. C. Mecrow, *et.al.* have proposed a new modular stator core structure, from which the stator core is split into three segments, as shown in Fig. 1.10 [22]. By employing such stator structure, the pre-formed coil can ultimately placed around the teeth easily after passing along the core back. As a result, the high slot fill factor can be achieved [22]. Nevertheless, the proposed manufacturing method still has some drawbacks. Firstly, the working hours for making and assembling the stator segments will increase if the machines have large slot number and pole number such as wind turbine generators. Secondly, when welding the stator segments together, the manufacturing tolerance is more likely to be introduced and possibly result in the non-circular stator core. Thirdly, the soldering spot in the stator yoke will potentially increase the iron losses, so the efficiency of the proposed machines might be reduced.

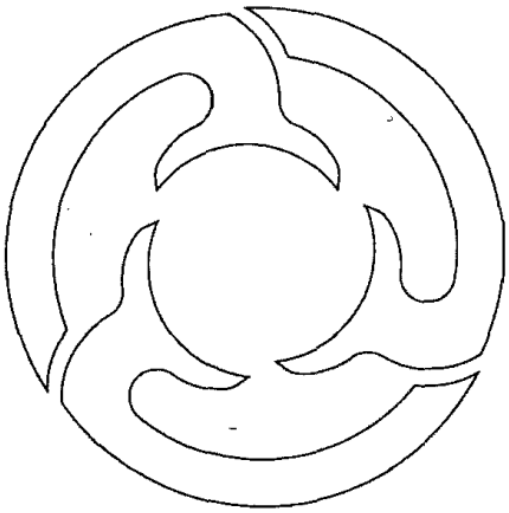

Fig. 1.10 Stator core with three laminated stator segments [22].

F. Libert *et. al*. have compared different modular core shapes together with a summary of their assembling methods in [12]. From Fig. 1.11, the stator iron is split into several segments (or modules). Consequently, such manufacturing method can help to reduce the wasted iron laminations from 80%-90% (by manufacturing in conventional way) to 50%-60% (by manufacturing in modular way) of the total iron material. Since the assembling of stator is achieved via welding the stator segments together, the increase in production time and other materials consumption are still unavoidable. Although the material waste is reduced by applying such production method, as a matter of fact, the waste is still considerable. On the other hand, because the segments are welded together, the local magnetic characteristics are damaged, which leads to an unexpected increase in iron losses [12].

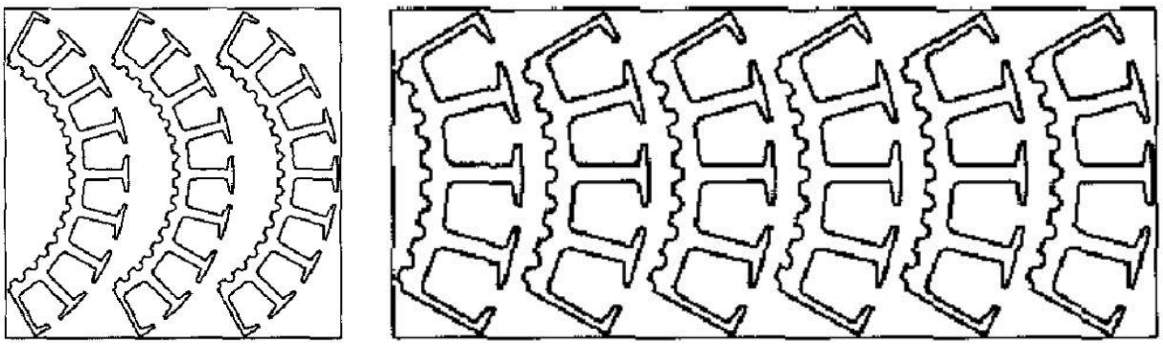

(a) (b)

Fig. 1.11 Stator laminations. (a) 120° segments. (b) 60° segments [12].

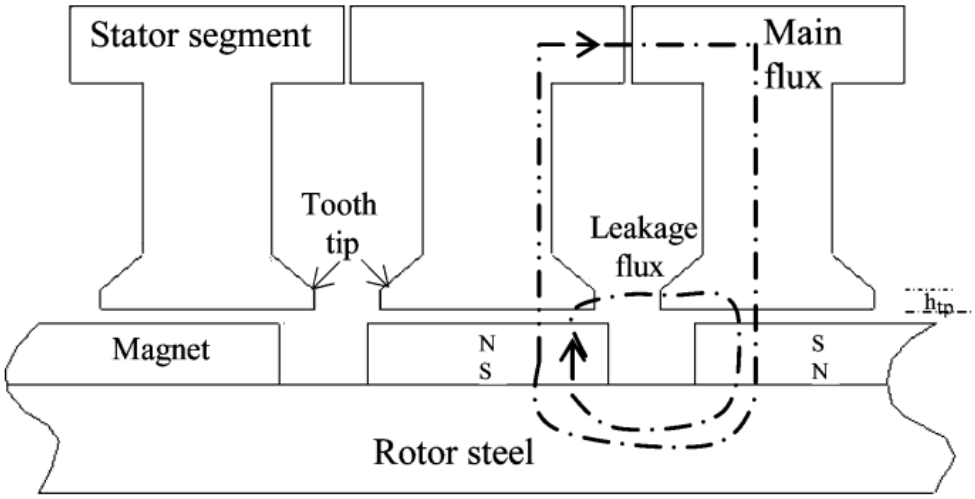

Fig. 1.12 Motor topology with segmented stator core [23].

In [23], the authors have presented a brushless PM motor with a segment stator core and investigated the influence of design parameters on the leakage flux through the tooth tips, as shown in Fig. 1.12. It can be concluded that, compared with the motor with non-segmented stator laminations, the back electromotive force (back-EMF) and the tooth flux density of the motor with the segmented stator laminations are smaller. This is mainly due to higher slot flux leakage and also the increased effective air-gap length [23].

Another similar modular structure is presented in [24], from which the stator core is segmented in the stator yoke, which introduces additional air-gaps due to the manufacturing tolerance, as shown in Fig. 1.13. Moreover, due to manufacturing defects, the additional air-gaps are very likely to be non-uniform, which may lead to a dramatic increase in both resultant cogging torque amplitude and periodicity but they have little impact on the performance of back-EMF waveform [24]. Moreover, such additional air-gaps in the stator yoke may also increase the total reluctance of the PM machine which may result in the degraded performance.

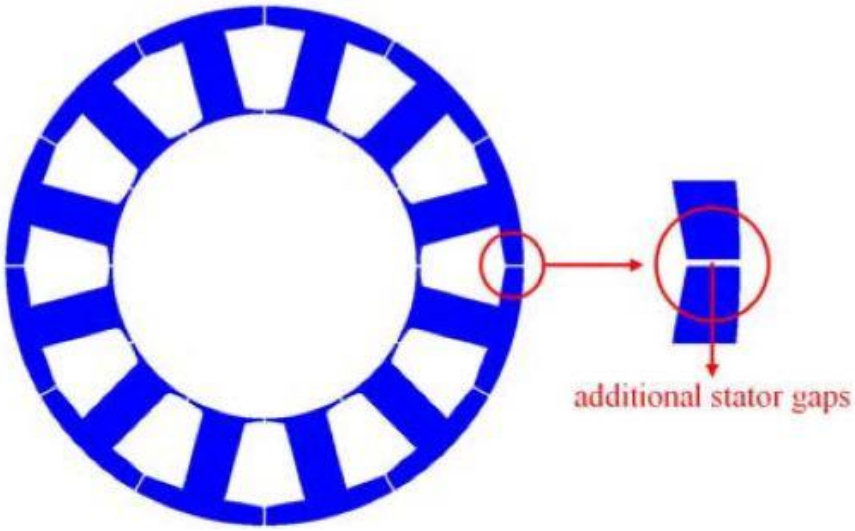

Fig. 1.13 Modular stator structure with individual stator tooth and back-iron [24].

1.2.1.3 INSERTED STATOR SEGMENTS

M. Kitamura *et. al.* [25] investigated the cogging torque due to roundness error of brushless PM machines with segmented stator in 2003, as shown in Fig. 1.14. It can be seen that the stator consists of 12 teeth and a ring-shaped stator yoke. Each tooth is wound by a concentrated coil and by inserting them into the grooves of the stator yoke. Then, a complete stator can be achieved. However, by doing so, the mechanical strength could be compromised and the magnetic field inside the stator will be impacted due to the change of effective air-gap length.

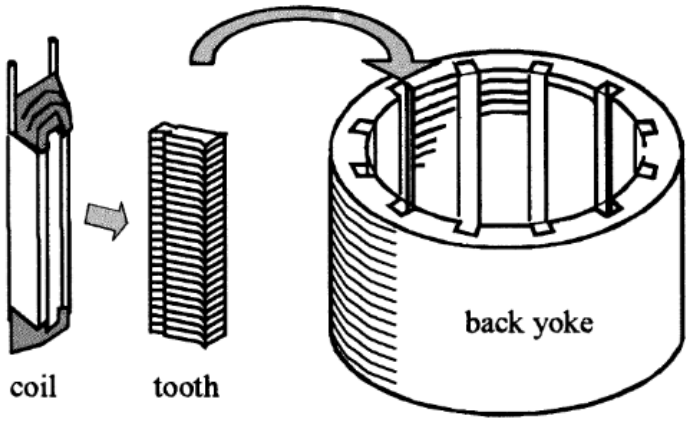

Fig. 1.14 Inserted segmented stator [25].

Several other similar modular structures have been reported in [26]. The segmented stator teeth with the pre-formed coils are inserted into the slots in the solid back iron by the solid joint to make the stator core, as shown in Fig. 1.15. The modular structure shown in Fig. 1.15 (a)-(b) was first proposed by the authors, but it has been found that the iron losses of these two models are very high. In order to solve such problem, the authors have proposed an alternative, in which two arms are added to each side of the teeth, as depicted in Fig. 1.15 (c). Therefore, the equivalent stator yoke can be formed which is the main flux path. As a result, the iron losses of the model shown in Fig. 1.15 (c) can be significantly reduced. It is worth noting that the shape of the solid joint can be different, such as the round shape, as shown in Fig. 1.15 (d) [26]. Both the rectangular and round joint shapes can be made by the existing manufacturing tools easily.

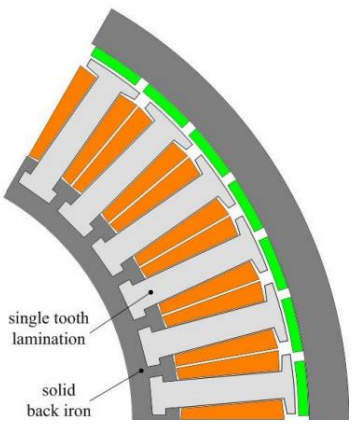

(a)

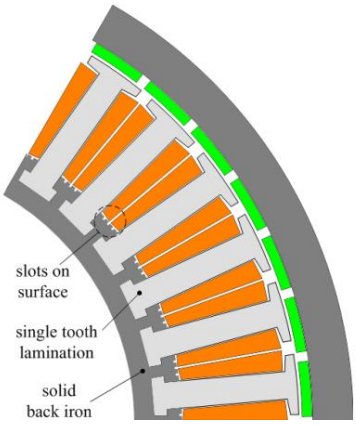

(b)

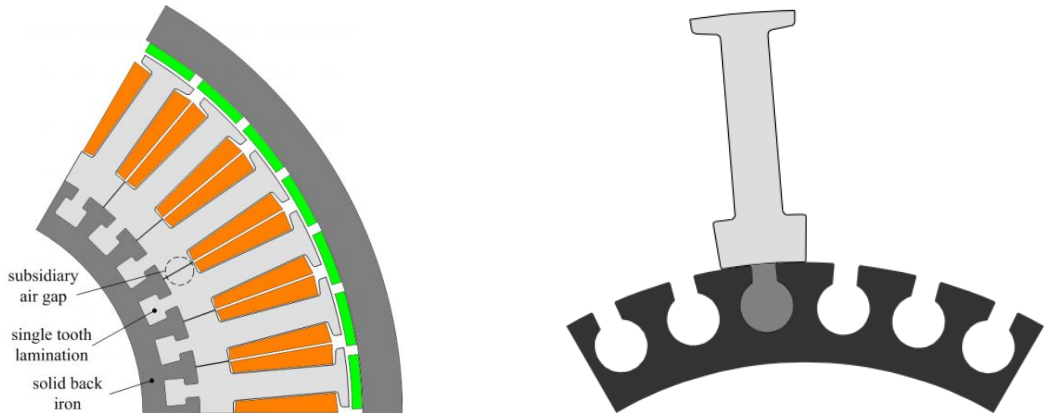

(c) (d)

Fig. 1.15 Modular stator structures with solid joint [26].

However, the drawbacks of the proposed modular structure are still obvious. The stator teeth with the solid joint as well as the solid back iron require very accurate manufacturing. When assembling the stator segmented teeth to the solid back iron via the solid joint, it is difficult to guarantee those components are perfectly fitted into each other during mass production. As a result, non-uniform subsidiary air-gap can occur, which might lead to increased iron losses and also cogging torque.

1.2.1.4 MODULAR STATOR WITH FLUX BARRIERS OR FGS

E. Spooner, *et. al.* have proposed some modular PM wind power generators since 1995 [27]-[32], as shown in Fig. 1.16. The stator core of the introduced modular PM generator is segmented circumferentially, as a result, a large amount of individual E-cores are produced. Each E-core stator segment could carry preformed armature coil and be assembled with other stator segments to form a modular stator [28].

It is found that the proposed modular structure exerts several notable advantages such as: a) reduced active machine mass and slightly increased efficiency compared to the non-modular counterparts [30], b) simple structure and laminations [28], c) ease of assembly [28], d) ease of repair due to the fact that the faulty segments can be removed and replaced rather than removing the entire generator [28]-[29], e) ease of cooling [28]-[29].

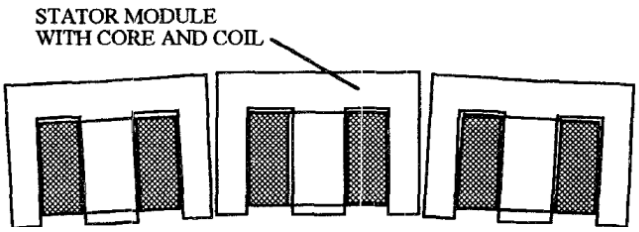

(a)

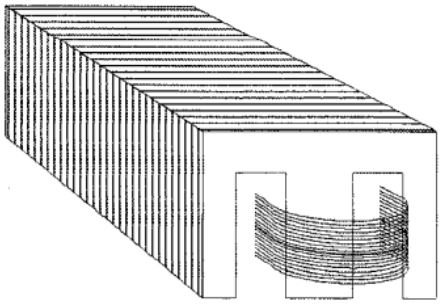

(b)

Fig. 1.16 (a) The Modular stator structure [27]-[32]. (b) The stator segment with coil [29].

Nevertheless, since the modular topology is proposed for wind turbines applications, such electrical machines normally have relatively large slot and pole numbers, which means that more number of mechanical support accessories for the stator segments are required. This will make such modular wind turbines complicated and potentially increase the cost of production although the material can be saved to a certain extent. Because of this, further optimization on this modular topology is necessary.

D. Gerling *et. al.* [33]-[35] have proposed various similar modular structures based on IPM machines. A simple but effective method to achieve modular structures is proposed by placing flux barriers into the alternate stator teeth, as shown in Fig. 1.17. Through inserting flux barriers in specific stator teeth, the drawbacks such as rich content of harmonics in the air-gap magneto motive force (MMF) of the conventional concentrated windings can be overcome. Furthermore, the new modular structure can increase the working harmonic and hence the torque/power density [33]. Different modular topologies have been proposed, e.g. the model (a) employs ‘E’ core structure with single layer winding and model (b) employs ‘C’ core structure.

A 12-slot/14-pole IPM machine with the new modular technology has been investigated. It concluded that the machine's performance has been improved such as a 16% increase in output torque and more than 50% decrease in rotor losses are achieved. Moreover, the new stator topology can reduce up to 20% in material costs [33].

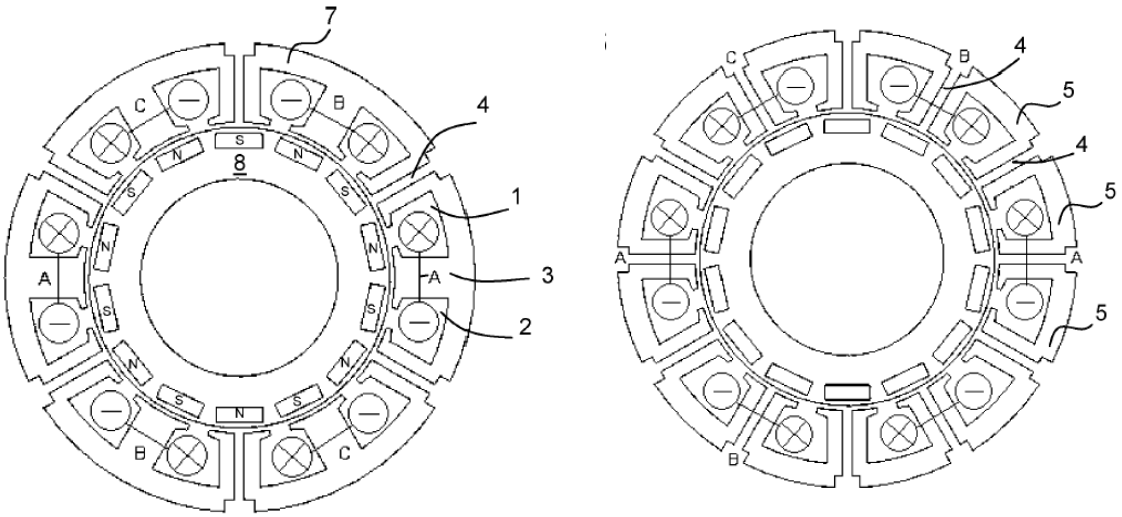

(a) (b)

Fig. 1.17 Various modular configurations [34]. (a) Flux barriers in alternate teeth, (b) Flux barriers in all teeth.

Li *et. al.* [36]-[38] have proposed some novel modular SPM machines, in which, the FGs are inserted into the alternate stator teeth and the single layer winding are wound on the stator teeth without FGs. The structures of conventional and modular SPM machines are described in Fig. 1.18. It is worth noting that the total active tooth body widths in both modular and non-modular machines are kept the same in order to avoid heavy local saturation in stator tooth body.

The electromagnetic performance such as air-gap flux density, phase back-EMF, cogging torque, on-load torque, copper and iron losses, etc. of the novel modular SPM machines influenced by the FGs have been comprehensively investigated and some general rules for modular machines with different slot/pole number combinations have been proposed. Briefly speaking, the FGs between the stator segments have negative effects on the electromagnetic performance for modular PM machines with slot number (N_s) higher than pole number ($2p$), e.g. the average torque is reduced while the torque ripple can be increased. In contrast, if the slot number is lower than the pole number, the electromagnetic performance can be improved

by picking the appropriate FG width. To be specific, the average torque can be increased, but the cogging torque, torque ripple and machines iron losses can be reduced [36].

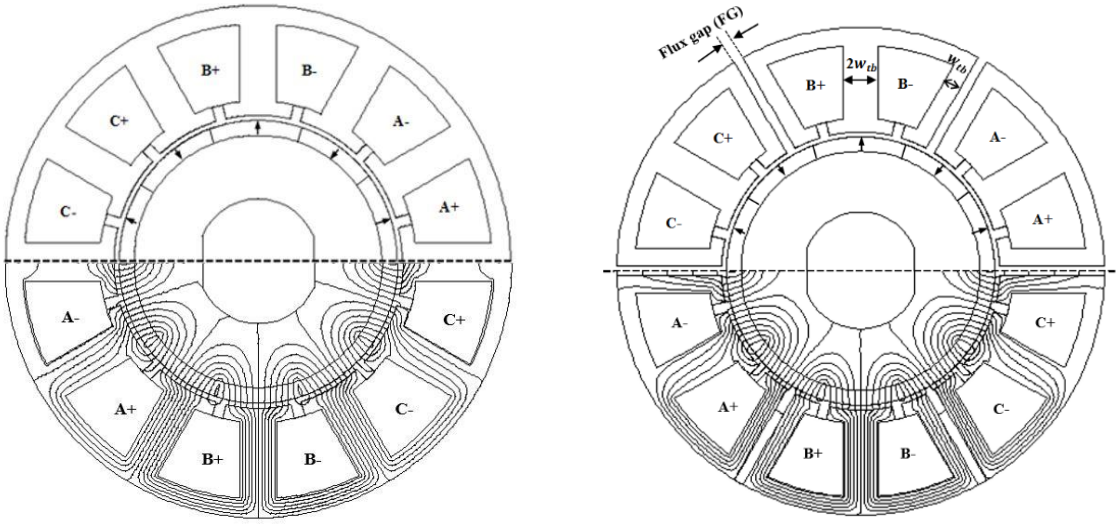

(a) (b)

Fig. 1.18 Cross-sections of the 12-slot/10-pole PM machines [36]. (a) With conventional non-modular stator. (b) With modular stator.

The similar modular PM machine structure but with or without tooth tips are introduced in [37], as shown in Fig. 1.19. The key dimensions of the investigated modular machines are the same as the model proposed in [36]. The influence of FGs and unequal tooth (UNET) width on the performance of modular PM machine are studied.

It is found that for the UNET machines without tooth tips, the winding factors, open-circuit air-gap flux density and the average torque are affected by the UNET widths. While for the UNET machines with tooth tips, the changing of UNET width has limited impacts on the performance. However, for the modular PM machines without tooth tips, when N_s>$2p$, their winding factor and average torque decrease for both modular models. Furthermore, the FGs have flux defocusing effects. On the contrary, when N_s<$2p$, the winding factor and average torque are increased and the FGs have flux focusing effect [37].

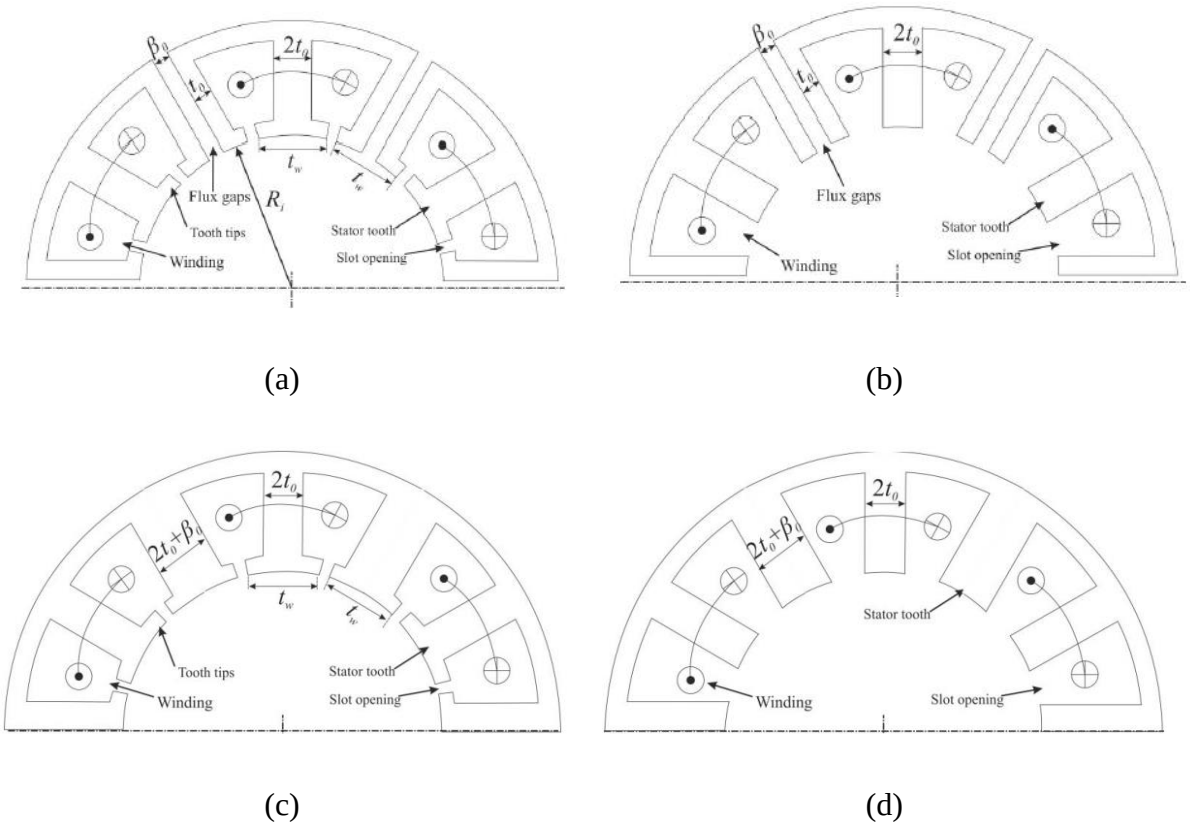

Fig. 1.19 Modular and UNET topologies with or without tooth tip [37]. (a)-(b) Modualr. (c)-(d) UNET.

The modular PM machines with alternate stator teeth having tooth tips are introduced in [38], as shown in Fig. 1.20. Some general conclusions are obtained that for the machines with $N_s > 2p$, the reduced winding factor due to FGs can be compensated by employing tooth tips on the wound teeth. Therefore, the average torque will not be compromised or even improved compared to the non-modular counterparts. However, as mentioned previously, the winding factor increases due to the FGs for the machines with $N_s < 2p$, by applying tooth tips on the unwound teeth, the winding factor can be further improved, so does the average torque. In addition, the torque ripple can be reduced by altering the tooth tip and FG widths [38].

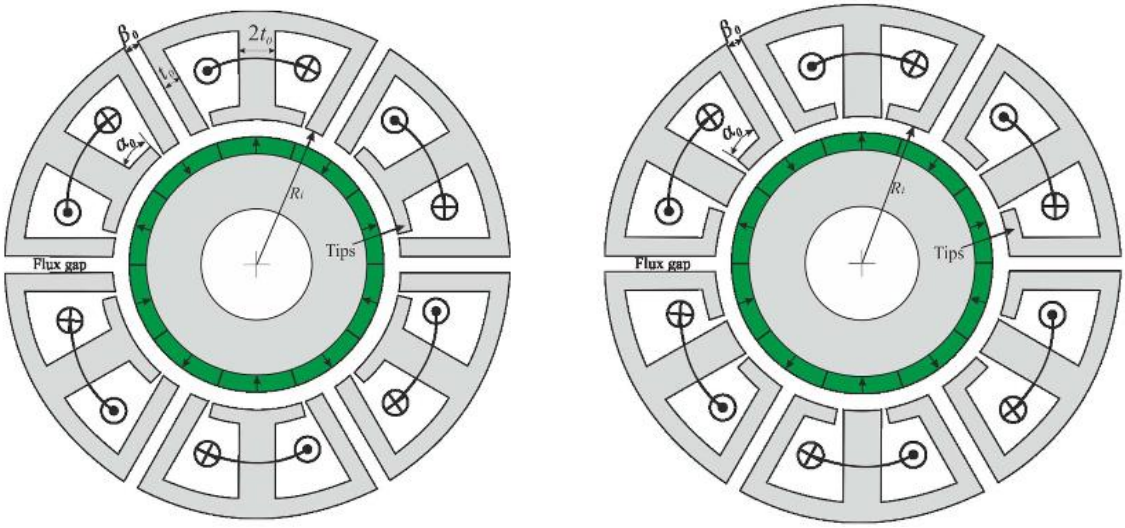

(a) (b)

Fig. 1.20 Modular machines with alternate teeth having tooth tips. (a) Wound teeth having tooth tips. (b) Unwound teeth having tooth tips[38].

1.2.1.5 OTHER PM MACHINES HAVING MODULAR STATOR

In [39], a new linear modular flux-switching permanent magnet (FSPM) machine is introduced by removing the PMs from alternate stator teeth of the conventional linear FSPM machines, as shown in Fig. 1.21. The teeth with flux barriers are unwound and hence, the magnetic coupling between phases can be reduced significantly. Due to the advanced modular configuration, the windings are physically, magnetically and thermally separated, leading to higher fault tolerant capability. It is worth noting that the usage of magnets is more efficient, which leads to nearly 74% more output power under the same PM material volume. Moreover, as for other modular topologies, such modular structure can also make the mass production more cost effective, as studied in [12].

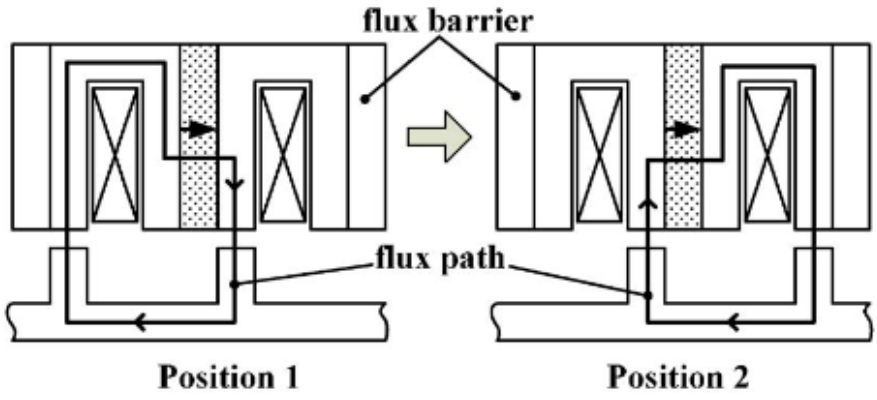

Fig. 1.21 Modular linear SFPM machine structure [39].

1.2.2 MACHINES WITH MODULAR ROTORS

In previous sections, the PM machines with modular stators have been reviewed. However, it is worth noting that although it has not been widely investigated in literature, the rotor core can also be made segmented to achieve modular machines. In this section, some existing examples of PM machines with modular rotors will be given.

1.2.2.1 SEGMENTED ROTOR FOR WIND POWER APPLICATIONS

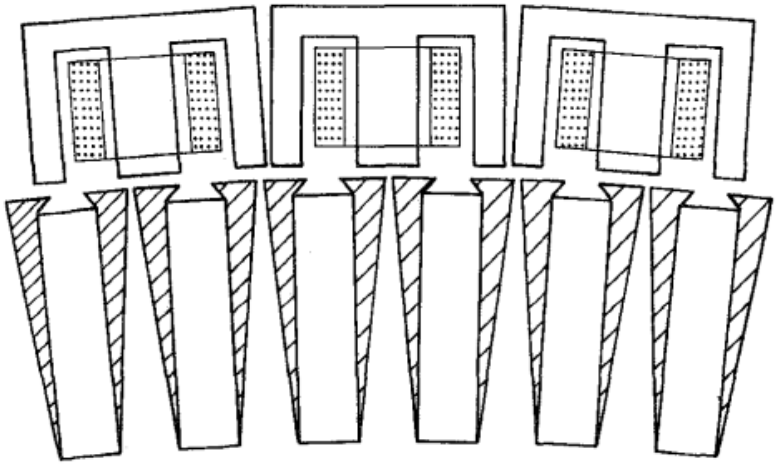

Fig. 1.22 Machines with modular rotor structure [31].

The modular wind power generators proposed by E. Spooner. *et. al*. not only have modular stator but also modular rotor [27]-[32], as illustrated in Fig. 1.22. By doing so, the flux leakage can be lower, leading to optimal utilization of PMs. However, again very high manufacturing and assembling accuracy for the PMs and the pole pieces is required in order to avoid undesirable manufacturing tolerance from the rotor side [29].

1.2.2.2 INSERTED ROTOR SEGMENTS

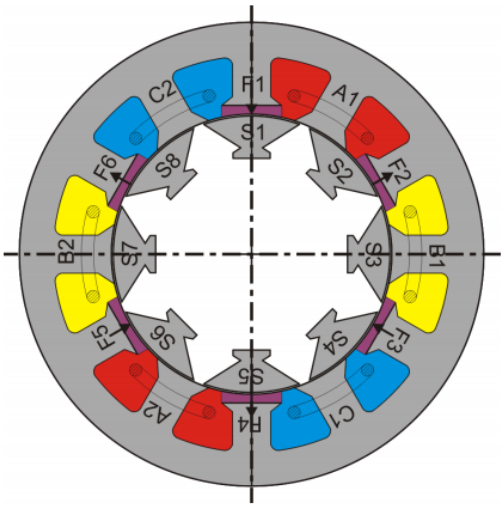

Fig. 1.23 12-slot/8-pole FSPM machines with segmented rotor [40].

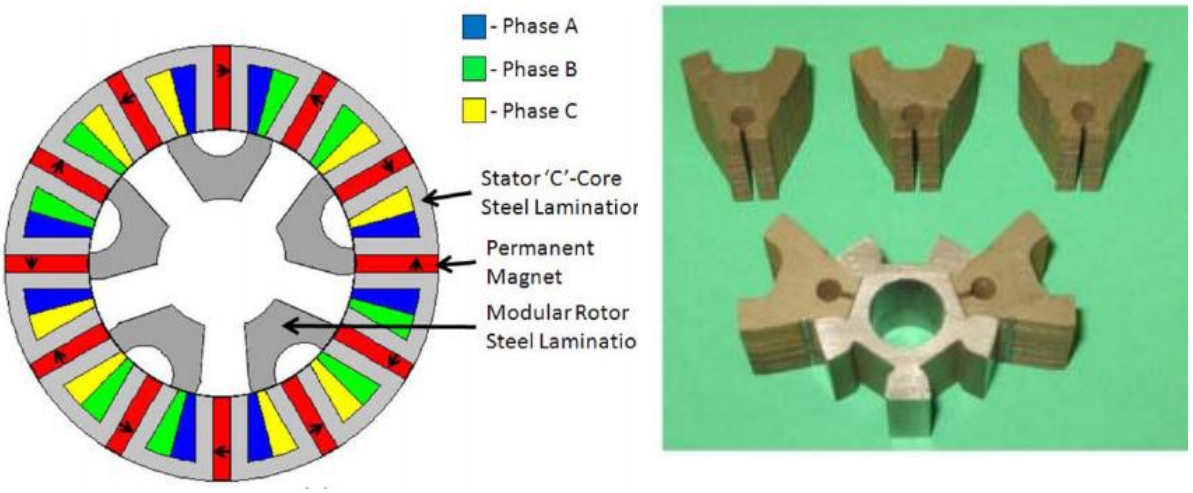

(a) (b)

Fig. 1.24 12-slot/10-pole FSPM machines. (a) Cross-sections. (b) Rotor prototypes [41].

In [40], a FSPM machine with segmented rotor is introduced, as shown in Fig. 1.23 and another similar modular FSPM machine is proposed in [41], as shown in Fig. 1.24. For this modular structure, the rotor segments are manufactured in the first place and then inserted into the rotor back iron to form the complete rotor. By doing so, it is found that the rotor mass can be reduced by 11% compared with the conventional SFPM machines. Furthermore, regarding

the electromagnetic performance, the total losses contributed by the copper losses, iron losses and PM eddy current losses can be reduced by 13% [41].

1.3 SUMMARY OF THE MODULAR PM MACHINES

After introducing the different modular topologies, in this section, the advantages and disadvantages of modular PM machines will be summarized. They are generally advantageous over their conventional non-modular counterparts. By employing the modular structure, several inherent advantages can be obtained [36]-[38]:

1. The manufacturing process as well as winding process can be greatly simplified. Each segment can be manufactured separately and hence, the consumption of materials and the production period can be reduced. As a result, the production efficiency can be improved. Furthermore, it is well known that the transportation for large machines is always a difficult issue, especially for large offshore wind generators or large hydroelectric generators. However, by employing modular structure, each module of the large machines can be transported individually and then be assembled on-site afterwards, and hence significantly ease the transportation process.
2. Better fault-tolerant capability can be achieved by modular structures. Since the stator segments are physically and magnetically separated, the faults cannot propagated from one stator segment to others. In addition, due to the fact that single layer concentrated winding is often employed in modular machines, a high ratio of self/mutual inductance can be achieved [42]-[43]. As a result, the short-circuit current can be reduced which weakens the fault interaction between phases Therefore, the modular machines are very suitable candidates for the safety critical applications [44].
3. The modular machines also show the incomparable advantages in maintenance. The faulty segments can be repaired or replaced by the healthy ones, but avoid replacing the entire machine. This can simplify the maintenance process and extend the lifetime of the machines.
4. The electromagnetic performance of the PM machines can also be improved by the modular structure. Properly choosing the FG widths and slot/pole number combination can increase the winding factor and average torque while the cogging torque, torque ripple and iron losses can be mitigated.
5. The improvement of cooling capability is another remarkable advantage of modular structure. The space (FGs or flux barriers) between the machine modules can be used as cooling channels [45]-[46], as shown in Fig. 1.25. By doing so, the heat exchange

area can be improved and the heat dissipation capability can be enhanced so that the electromagnetic performance can be improved due to the reduction in machine temperature.

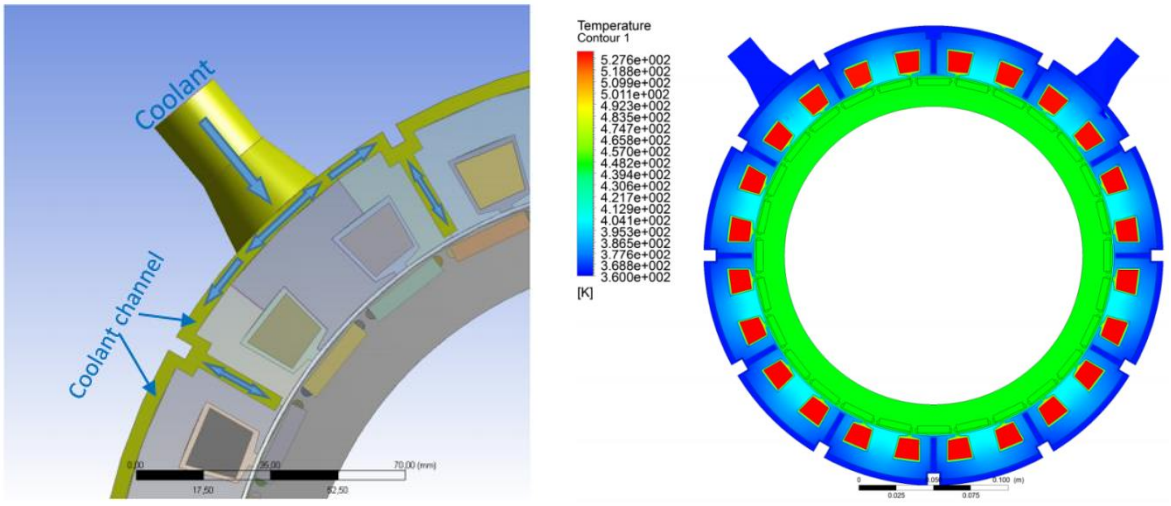

(a) (b)

Fig. 1.25 (a) Radial cooling. (b) Temperature distribution inside the PM machine [45].

However, the disadvantages of modular PM machines compared with the conventional PM machines cannot be overlooked, such as:

1. Due to the novel modular structures, the conventional manufacturing method of PM machines is not applicable. New equipment and new manufacturing methods are required which may increase the cost of the entire PM machines.
2. The manufacturing tolerance is more likely to occur since most of the modular PM machines require relatively more complicated assembly process compared to the conventional non-modular PM machines.
3. The reliability of the modular PM machines may be compromised since the modular PM machines require more mechanical accessories and thus, the structure of the modular PM machines might be more complicated.

1.4 RESEARCH SCOPE AND CONTRIBUTIONS

1.4.1 RESEARCH SCOPE

This thesis is aimed at further investigating the novel modular PM machines shown from Fig. 1.18 to Fig. 1.20. The design of multi-phase modular PM machines, cogging torque and torque ripple reduction methods for modular PM machines and also the studies of the manufacturing tolerance of modular PM machines are covered. The simulation results showed in this thesis are obtained from the commercial FE package of OPERA 2D and 3D. This thesis contains 6 chapters as follows:

- Chapter 1 provides a general introduction about the modular PM machines existing in the literature. The research scope and contributions, publication list are also given in this chapter.
- Chapter 2 investigates the fractional-slot multi-phase modular PM machines. The 3-phase, 4-phase and 5-phase modular PM machines with different slot/pole number combinations are introduced and compared. Several general rules of the multi-phase modular PM machines with the respect to the influence of FG widths on machines performance have been established. The predicted results of the 3-phase modular stator PM machines are validated by experimental tests, while the 4-phase and 5-phase modular PM machines are only studied through the FE simulation.
- Chapter 3 introduces a cogging torque mitigation method by slot-opening shift for the modular PM machines. The analytically predicted desirable shift angle of each group of stator segments for minimizing the resultant cogging torque is derived. The efficiency of the proposed method for mitigating the peak cogging torque for modular PM machines with different slot/pole number combinations is validated by case studies. The experiments based on the existing prototypes are also carried out.
- Chapter 4 proposes the C-core modular PM machines for reducing the cogging torque and torque ripple. The electromagnetic performances of the modular PM machines with the C-core stator segments are investigated.
- Chapter 5 discusses the manufacturing tolerances of the modular PM machines. The manufacturing tolerance scenarios of the modular PM machines studied in this chapter are focused on the radial and circumferential stator segment displacements as well as the PM defect. Through the analyses of the electromagnetic performance,

the manufacturing tolerance withstand capability of the modular PM machines with different slot/pole number combinations are assessed. The prototype with the defective PM has been built and tested for validating the predicted results.

- Chapter 6 gives a general conclusion of this thesis. The future work on the modular PM machines is also proposed in this chapter.

1.4.2 RESEARCH CONTRIBUTION

The main contributions of this thesis are summarized as follows:

- The design guidelines for the multi-phase modular PM machines have been established.
- The cogging torque and torque ripple reduction methods by the slot-opening shift and the employment of the C-core stator segments are proposed. The proposed methods can further improve the performance and enhance the advantages for the modular PM machines.
- The influence of manufacturing tolerances on the electromagnetic performances of the modular PM machines are studied. A method for identifying the most influencing cases of the stator segment displacement is developed and the manufacturing tolerance withstand capability is assessed.

Chapter 2 DESIGN GUIDELINES FOR THE FRACTIONAL-SLOT MULTI-PHASE MODULAR PM MACHINES

This chapter presents the design considerations for fractional slot multi-phase modular PM machines with single-layer concentrated windings. The winding factors for various slot/pole number combinations are calculated to identify the optimal slot/pole number combinations for different phase numbers. In addition, the electromagnetic performance influenced by FGs, such as air-gap flux density (both armature field and also flux density due to PMs), back-EMF, cogging torque, on-load torque and torque ripple, etc., are comprehensively investigated by using a non-linear 2D FE method. Several general rules with respect to the influence of FGs on multi-phase modular PM machines performance are established. The prototypes of modular PM machines are built and the FE results are validated by experiments.

This chapter comes from author's paper [47].

2.1 INTRODUCTION

PM machines have been increasingly applied to various applications such as electric and hybrid vehicles, aerospace actuation and renewable energy, e.g. wind power generators, due to their inherent advantages, including high torque density and efficiency [48]-[49]. However, for some safety-critical applications such as offshore wind power, the PM machines are not only required to have excellent performance (high torque and efficiency) but also good fault-tolerant capability. To achieve such capability, the single-layer concentrated winding layouts [50] are often employed, which can reduce the short-circuit current and limit the fault propagation between phases. In addition, multi-phase (>3) machines can also be employed, which provide extra freedom when dealing with the faults such as armature phase open-circuit or short-circuit [51].

There are many inherent advantages offered by multi-phase machines, e.g. the improvement on reliability, the reduction in the phase current without the increase in phase voltage, and the mitigation of the torque ripple, etc. [51]-[52]. The influence of phase number on the winding factors are comprehensively investigated in [53], which also provides guidelines for selecting the optimal slot/pole number combinations for multi-phase PM machines. Five-phase [54]-[58], six-phase [59]-[61] and dual three-phase [62]-[63] machines (similar to six-phase machines) are the most widely studied multi-phase machines in the existing literature. In [63], a novel dual three-phase, 78-slot/12-pole PM synchronous motor with asymmetric stator winding is proposed (phase shift angle between the phases A1 and B1 is 120.3 Elec. Deg. rather than 120 Elec. Deg. in conventional symmetrical machines) in order to achieve the better performance. It is shown that the proposed dual 3-phase (multi-phase) PM machine offers extremely low cogging torque and torque ripple and also very low back-EMF total harmonic distortion. Furthermore, the torque density can be slightly improved compared with that of the dual 3-phase, 72-slot/12-pole PM machines with symmetrical windings.

Alternatively, the modular topologies with single-layer concentrated windings, such as those shown in Fig. 2.1, can also be employed to improve the fault-tolerant capability. Due to the fact that the segments are separated physically and magnetically in modular machines, the faults would not propagate from one segment to another. This can reduce the short-circuit current and weaken the fault interaction between phases. Hence, the modular machines are excellent options for safety-critical applications.

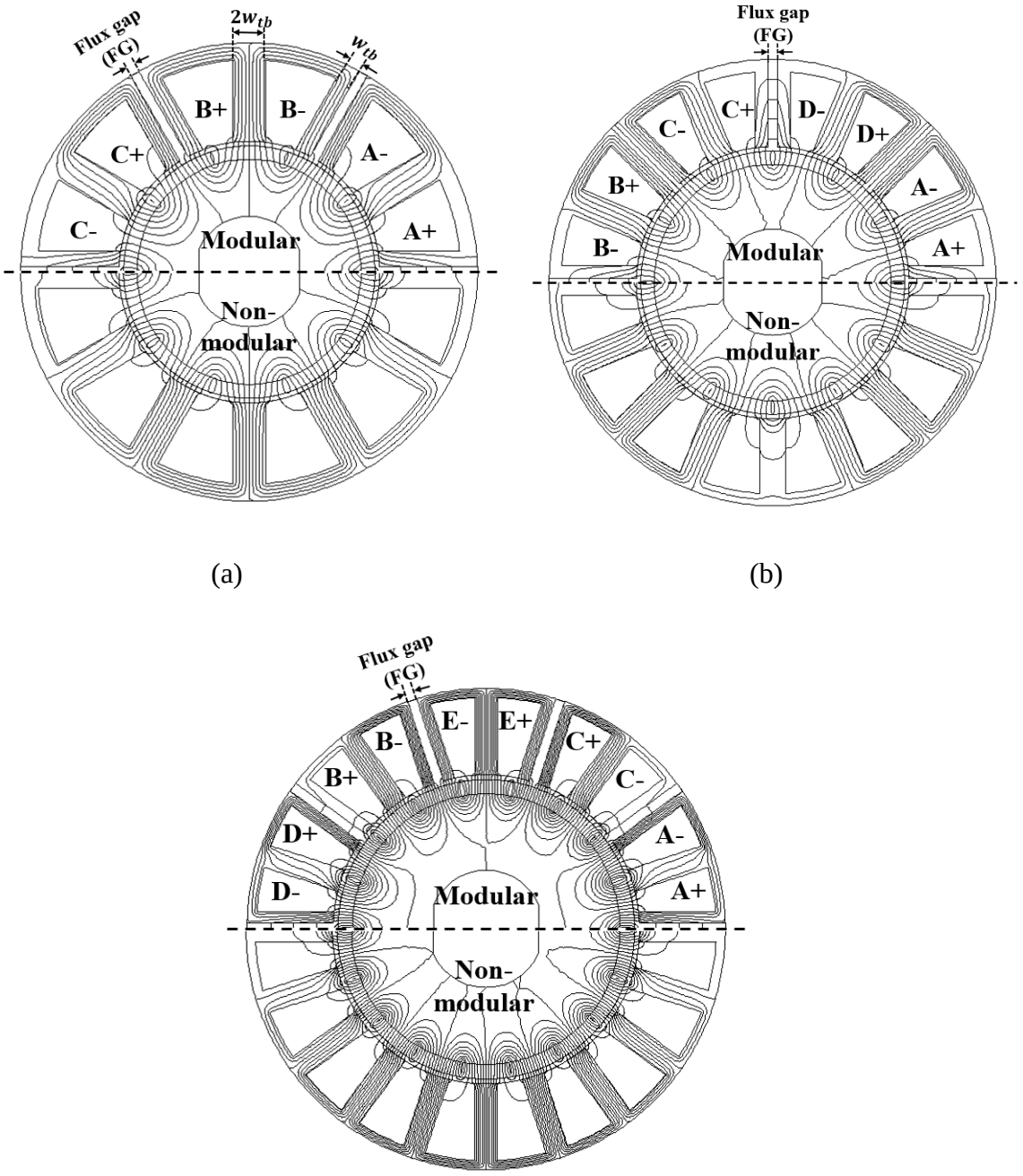

Fig. 2.1 Cross sections of modular and non-modular PM machines with open-circuit flux distributions. (a). 3-phase 12-slot/10-pole [37]. (b) 4-phase 16-slot/12-pole. (c) 5-phase 20-slot/18-pole.

Nevertheless, the existing literature are only focused on 3-phase modular PM machines and very few if not at all studies of the multi-phase modular PM machines have been carried out. Therefore, to fill in this gap, the multi-phase modular PM machines having different slot/pole

number combinations and single-layer concentrated windings will be investigated, with a particular focus on the electromagnetic performance such as air-gap flux density, torque characteristics, etc. Consequently, some general rules which can cover the influence of FGs on the multi-phase modular PM machines will be established and can be used as design guideline for modular machines in practice.

2.2 WINDING ARRANGEMENT OF THE MULTI-PHASE MODULAR PM MACHINES

In this section, the optimal slot/pole number combinations for each modular PM machine with different phase number will be identified first so as to achieve the highest winding factor which is calculated based on its non-modular counterpart. Then, the influence of FGs on the winding factors of multi-phase modular PM machines having different slot/pole number combinations will be investigated.

2.2.1 WINDING FACTORS OF NON-MODULAR PM MACHINES

For classic non-modular and equal tooth width PM machines, without considering the higher order harmonics, the distribution factor (k_d), the pitch factor (k_p), and hence the winding factor (k_w) can be calculated by:

$$k_d = \frac{sin(\frac{q\sigma}{2})}{q\, sin(\frac{\sigma}{2})} \tag{2.1}$$

$$k_p = sin\left(\frac{\tau_s}{\tau_p}\frac{\pi}{2}\right) = sin(\frac{p\pi}{N_s}) \tag{2.2}$$

$$k_w = k_d \times k_p \tag{2.3}$$

where q is the number of coil per phase, σ is the angular phase angle between adjacent EMF vectors of one phase (in Elec. Deg.), $\tau_p = 2\pi/(2p)$ is the pole pitch and the slot pitch is $\tau_s = 2\pi/N_s$. Additionally, N_s is the slot number while p is the rotor pole pair number. As it is well established that k_p depends on the slot/pole number combination rather than on the phase number. Therefore, the calculation of winding factor is focused on the calculations of distribution factors for the fractional slot PM machines with different phase numbers.

Since the multi-phase PM machines studied here have single-layer concentrated windings, the theory developed in [64] for a double-layer concentrated winding structure is no longer applicable, therefore certain modifications have to be taken into account. The improved method is detailed as follows:

- When the phase number is odd (1, 3, 5,…)

$$\begin{cases} k_d = \dfrac{sin\left(\frac{q_{ph}}{2} \times \frac{\sigma_{ph}}{2}\right)}{\left(\frac{q_{ph}}{2}\right) sin\left(\frac{\sigma_{ph}}{2}\right)} & For\ q_{ph}\ is\ even \\ k_d = \dfrac{sin\left(q_{ph} \times \frac{\sigma_{ph}}{4}\right)}{(q_{ph})\, sin\left(\frac{\sigma_{ph}}{4}\right)} & For\ q_{ph}\ is\ odd \end{cases} \tag{2.4}$$

with

$$q_{ph} = \frac{(\frac{N_s}{2})}{m \times t} \tag{2.5}$$

$$\sigma_{ph} = \frac{2\pi}{N_s/(2t)} \tag{2.6}$$

- When the phase number is even (2, 4, 6,…)

$$\begin{cases} k_d = \dfrac{\sin\left(q_{ph} \times \frac{\sigma_{ph}}{2}\right)}{q_{ph} \sin\left(\frac{\sigma_{ph}}{2}\right)} & For\ \sigma_{ph} \neq \dfrac{360}{m} \\ k_d = 1 & For\ \sigma_{ph} = \dfrac{360}{m} \end{cases} \tag{2.7}$$

where m is the phase number, t is the greatest common divisor (GCD) between the slot number divided by 2 (single layer winding) and the pole pair number. This means that the machine is composed by t elementary machines with a slot number of $\frac{N_s}{2t}$ and a pole pair number of $\frac{p}{t}$. q_{ph} is the number of slot vectors which form one phase of the elementary machine while σ_{ph} is the electrical angle between two adjacent back-EMF vectors.

By using the above method, the winding factors for fractional slot single-layer concentrated winding non-modular machines with different phase numbers have been calculated, and hence, the optimal slot/pole number combinations for each phase number can be determined accordingly. The results are shown in Table 2.1, in which only the results for each phase number with its relevant minimum achievable slot number have been given. It is worth noting that the bold figures in Table 2.1 are the optimal winding factors for various slot/pole number combinations and phase numbers.

TABLE 2.1 WINDING FACTORS OF THE SINGLE LAYER CONCENTRATED WINDING N-PHASE MACHINES WITH NON-MODULAR STATORS

	1-phase	2-phase	3-phase	4-phase	5-phase	6-phase
$2p\backslash N_s$	4	8	12	16	20	24
2	0.707	0.271	0.259	0.180	0.156	0.126
4	**1**	**0.707**	0.500	0.383	0.309	0.259
6	0.707	0.653	-	0.513	0.454	-
8	0	-	0.866	-	0.5878	-
10	-0.707	0.653	**0.966**	0.768	-	0.588
12	-1	**0.707**	-	**0.924**	0.809	-
14	-0.707	0.271	**0.966**	0.906	0.891	0.766
16	0	-	0.866	-	0.951	-
18	0.707	-0.271	-	0.906	**0.988**	-
20	**1**	-0.707	0.500	**0.924**	-	**0.966**
22	0.707	-0.653	0.259	0.768	**0.988**	0.958
24	0	-	-	-	0.951	-
26	-0.707	-0.653	-0.259	0.513	0.891	0.958
28	-1	-0.707	-0.500	0.383	0.809	**0.966**

Based on the previous results, it can be concluded that in order to achieve the maximum winding factors for fractional slot modular PM machines with different phase numbers and different slot/pole number combinations, the following rules should be satisfied:

$$N_s = 2p \qquad For\ m = 1 \tag{2.8}$$

$$N_s = 2p \pm 4d \qquad For\ m\ is\ even \tag{2.9}$$

$$N_s = 2p \pm 2d \qquad For\ m\ is\ odd \tag{2.10}$$

where d is an integer and equals to $N_s/(4m)$. By way of example, for 3-phase machines with 12-slot, the pole numbers enabling the machines to have their maximum winding factor are 10-pole and 14-pole; for 4-phase machines with 16-slot, the pole numbers are 12-pole and 20-pole; for 5-phase machines with 20-slot, the pole numbers are 18-pole and 22-pole. Therefore, the slot/pole number combinations mentioned above are chosen for modular PM machines with different phase numbers in order to analyse the influence of FGs on the machines'

electromagnetic performances.

2.2.2 WINDING FACTORS OF MODULAR PM MACHINES

The winding factors for modular machines can be calculated using similar methods as those for classic non-modular machines. However, when the FGs are inserted into the alternate stator teeth, the coil pitch and hence the fundamental k_p need to be modified with the variation of the FG widths (β_{FG}). According to [37], the pitch factor accounting for the influence of FGs can be calculated by:

$$k_p = sin(\frac{(\tau_s - \Delta)}{\tau_p}\frac{\pi}{2}) \tag{2.11}$$

$$\Delta = sin^{-1}(\frac{\beta_{FG}}{2 \times R_i}) \tag{2.12}$$

where R_i is the stator inner radius and again, τ_s and τ_p are the coil pitch and the pole pitch, respectively. The FGs will reduce the coil pitch but they do not influence the pole pitch. Therefore, they will increase the pitch factor for machines with $N_s < 2p$ such as the 12-slot/14-pole 3-phase machine, while reducing it for machines with $N_s > 2p$ such as the 12-slot/10-pole 3-phase machine.

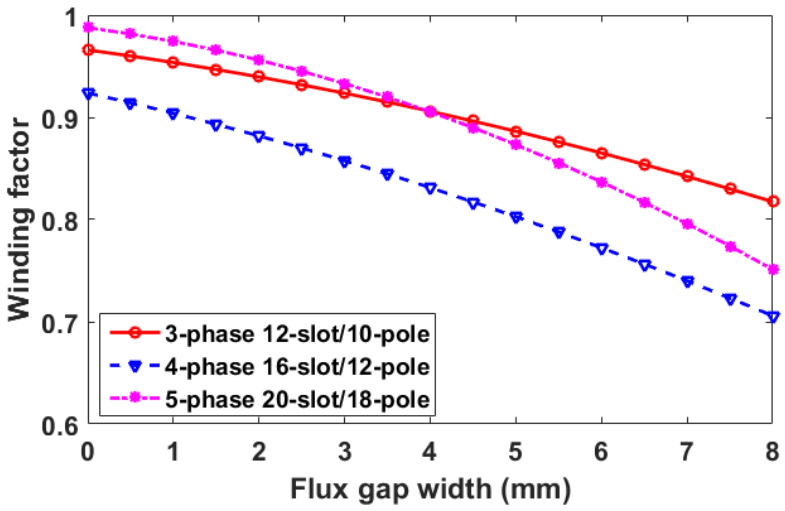

(a)

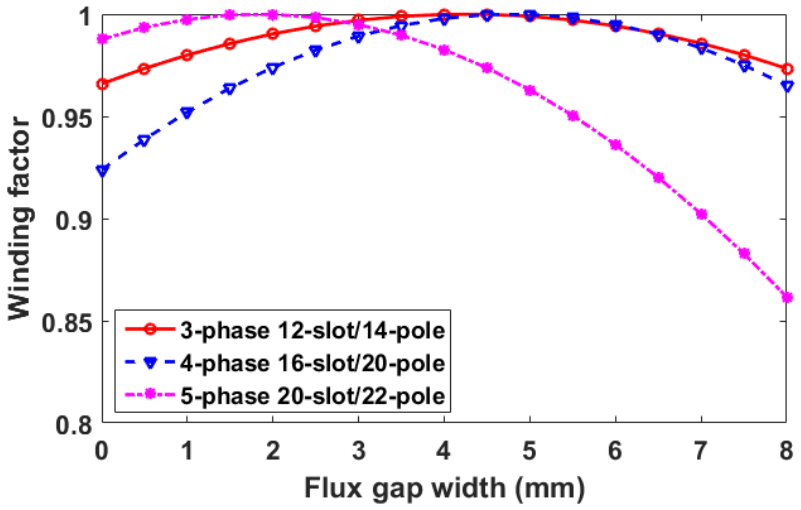

(b)

Fig. 2.2 Winding factors versus FG width of 3-phase, 4-phase and 5-phase modular PM machines with different slot/pole number combinations. (a) $N_s > 2p$. (b) $N_s < 2p$.

Since the distribution factors are unchanged due to the fixed back-EMF and slot vectors distributions for a given slot/pole number combination, the resultant winding factors of modular PM machines with different phase numbers are only affected by the pitch factors, as shown in Fig. 2.2.

It is evident from Fig. 2.2 that for multi-phase modular PM machines having $N_s > 2p$, the winding factors decrease with the increase in FG width. Whereas, when multi-phase modular PM machines having $N_s < 2p$, their winding factors increase with the increasing FG width until they reach the unity and subsequently decrease. The winding factor largely determines the electromagnetic performance. Therefore, the influence of FGs will also be reflected on the machines performances, and will be investigated in the following sections.

2.3 DESIGN OF MODULAR PM MACHINES

The cross sections of modular PM machines with different phase numbers are depicted in Fig. 2.1. The rotors for all machines have surface-mounted, full arc PMs although other rotor topologies can be employed such as interior or inset PMs. Furthermore, it is worth mentioning that the total active tooth body width for the stator teeth with or without FGs is unchanged for different FG widths, as shown in Fig. 2.1. This is to avoid heavy local magnetic saturation occurring in the tooth bodies when large FGs are employed, and hence, the influence of magnetic saturation effect due to FGs will be limited to the minimum. Some of the general design parameters are exactly the same for modular PM machines having different slot/pole number combinations and phase numbers, as shown in Table 2.2.

It is worth noting that the general design parameters showed in Table 2.2 and the 3-phase PM machines design parameters showed in Table 2.3 are contributed by other researchers. While for the other optimized design parameters for the 4-phase and 5-phase PM machines showed in Table 2.3 are contributed by the author of this thesis.

TABLE 2.2 GENERAL DESIGN PARAMETERS OF THE MODULAR PM MACHINES

Phase voltage (V)	36	Stack length (mm)	50
Rated torque (Nm)	5.5	Air-gap length (mm)	1
Rated speed (rpm)	400	Magnet thickness (mm)	3
Stator outer radius (mm)	50	Magnet remanence (T)	1.2
Filling factor k_b	0.37	Number of turns per phase	132
Rated RMS current (A)	7.35	PM material	N35H

TABLE 2.3 OPTIMIZED DESIGN PARAMETERS OF THE MODULAR PM MACHINES

Modular PM machines	λ_s	w_{tb} (mm)	h_{sy} (mm)	I_{RMS} (A)
3-phase	0.57	7.1	3.7	7.35
4-phase	0.61	5.9	2.7	4.83
5-phase	0.64	4.7	1.9	3.41

Some other design parameters are optimized individually in a certain sequence by the assumed constant copper losses, e.g. split-ratio λ_s (ratio of stator inner diameter to stator outer diameter) → tooth body width w_{tb} → stator yoke thickness h_{sy}. In order to determine the

maintained copper losses of 4-phase and 5-phase PM machines as the reference for the optimization, the current density of the designed 3-phase PM machines is calculated in the first place. Then, the initial supply currents, so to the copper losses of the 4-phase and 5-phase PM machines before optimization can be determined by applying the same current density of the 3-phase PM machine. As a result, based on the determined copper losses, the selected design parameters for the 4-phase and 5-phaes PM machines showed in Table 2.3 can be optimized.

It is worth mentioning that the stator outer diameter and active length of the 3, 4 and 5-phase modular PM machines are always the same during the optimization process. Moreover, the 6-phase modular machine is not shown here mainly because its performance is very much similar to that of a 3-phase one.

2.4 ELECTROMAGNETIC PERFORMANCE OF MODULAR PM MACHINES

2.4.1 AIR-GAP FLUX DENSITY DUE TO THE ARMATURE

Although the fractional slot single-layer concentrated winding has advantages as mentioned above, the inherent drawbacks of such a winding layout cannot be overlooked. By way of example, the rich sub-harmonics in the air-gap flux density due to armature windings will result in many undesirable effects on the performance of PM machines, such as increasing PM eddy current loss and core losses, heavy local saturation, acoustic noise and vibrations, etc. Fortunately, the modular structure can help to effectively mitigate those air-gap flux density sub-harmonics as will be demonstrated in this section.

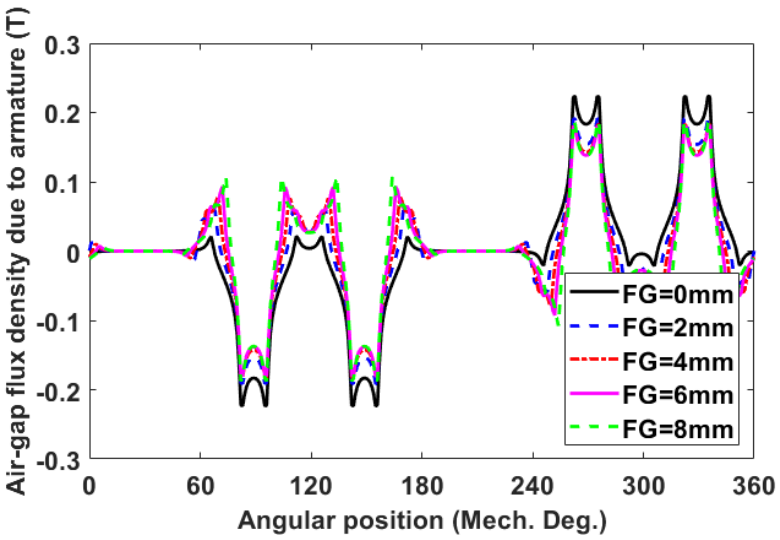

(a)

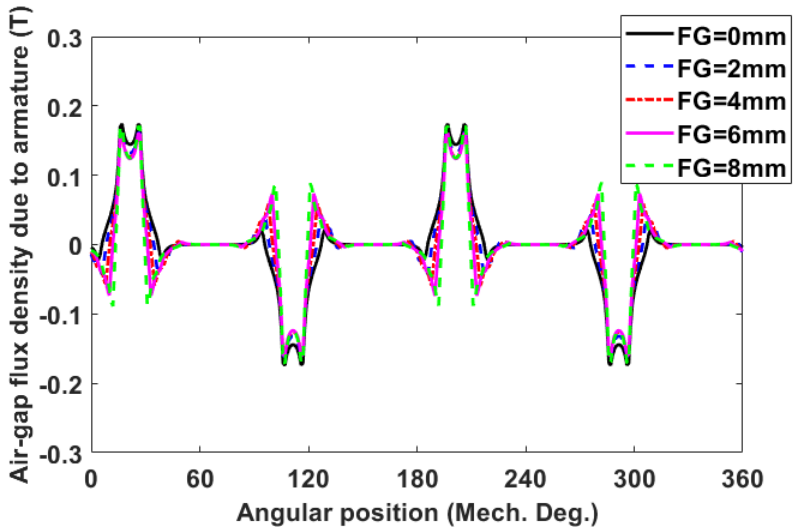

(b)

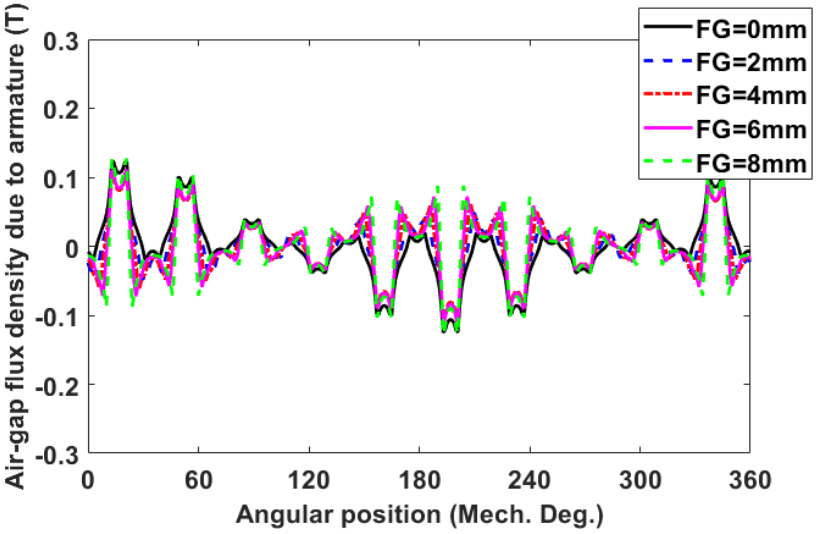

(c)

Fig. 2.3 The waveforms of the air-gap flux dnsity due to the armature windings of the modular SPM machines. (a) 3-phase PM machines. (b) 4-phase PM machines. (c) 5-phase PM machines.

The waveforms and their spectra of the air-gap flux density due to the armature windings for modular PM machines having different slot/pole number combinations and different phase numbers have been calculated by the 2D FE software (Opera 2D). The results of the 3-phase, 4-phase and 5-phase machines are shown in Fig. 2.3 and Fig. 2.4. It has been established that the working (or fundamental) harmonics are 5^{th} or 7^{th} order harmonics depending on the slot/pole number combination for the 3-phase, 6^{th} or 10^{th} for the 4-phase, and 9^{th} or 11^{th} for the

5-phase machines.

The rotating direction of each order harmonic of the air-gap flux density due to armature can be determined by employing the analytical expression. By way of example, for the 3-phase PM machines, the 1st, 7th, 13th, etc. order harmonics rotate in forward direction. While for the 5th, 11th, etc. order harmonics rotate in backward direction. The rotating directions of the harmonics for 4-phase and 5-phase PM machines can be determined by similar method as for the 3-phase PM machines.

As shown in Fig. 2.4, when the FG width changes, the variations of the working harmonics, which produce the electromagnetic torque, are similar to those of the winding factors. This is mainly due to the fact that the working harmonics of the air-gap flux density due to the armature windings are largely determined by the winding factor.

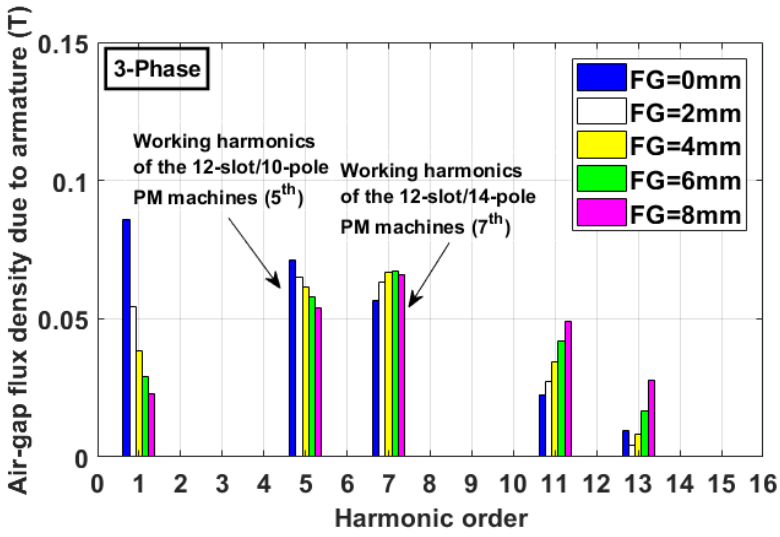

(a)

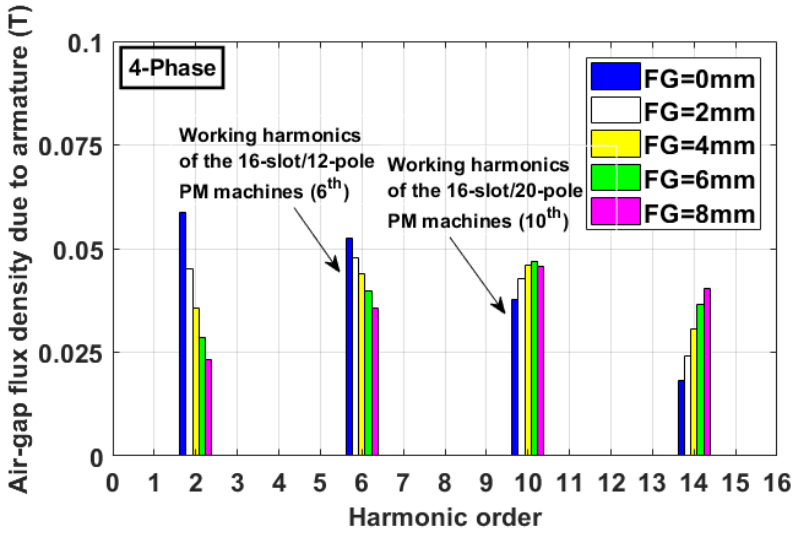

(b)

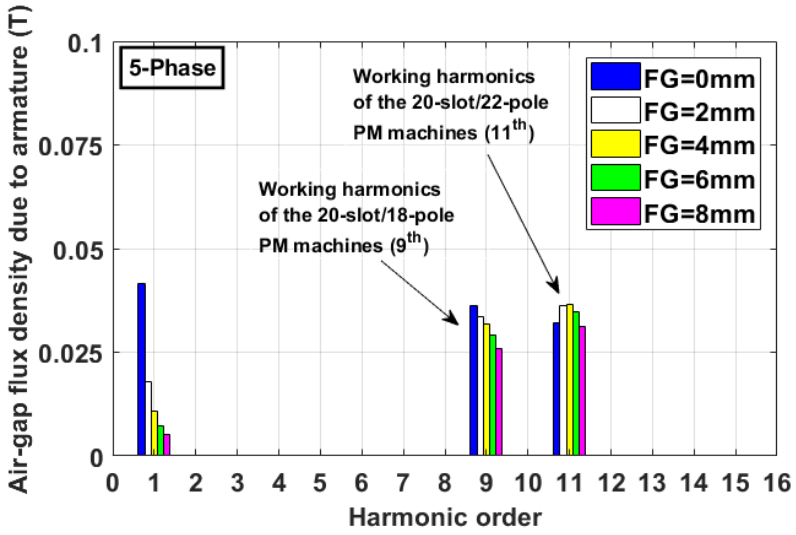

(c)

Fig. 2.4 Spectra of the air-gap flux density due to armature windings of modular SPM machines. (a) 3-phase PM machines. (b) 4-phase PM machines. (c) 5-phase PM machines.

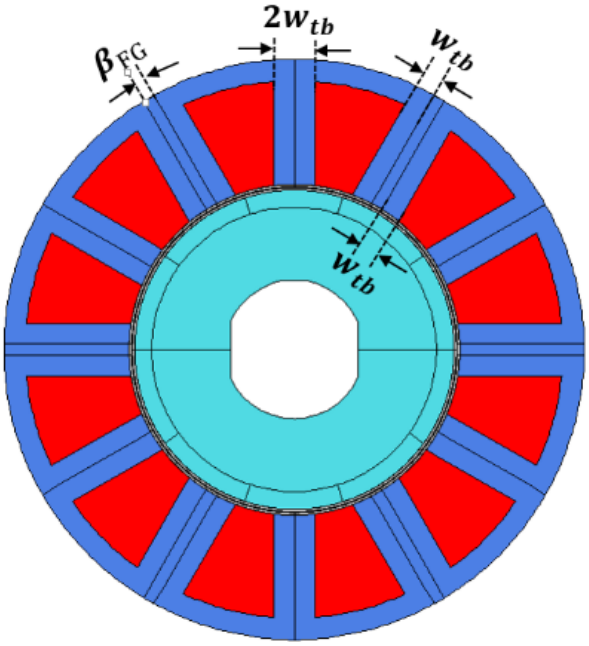

Fig. 2.5 The cross-sections of modular PM machine and non-modular PM machine with UNET.

However, for the 3-phase and 5-phase modular PM machines, the sub-harmonics are mainly contributed by the 1st order harmonic, while for the 4-phase modular PM machines the 2nd order harmonic is the main sub-harmonic. It is evident that for all modular machines, regardless of the slot/pole number combination and phase number, the main sub-harmonics are significantly reduced when the FGs are introduced into the alternate stator teeth. In order to understand the influence of FGs on the air-gap flux density due to the armature windings of modular PM machines, it is necessary to separate the influence of FGs from that of the slot-openings. This is because for modular PM machines, the primary two factors that influence the armature air-gap flux density are the slot-openings and FGs, as can be described by (2.13). Here, the corresponding non-modular PM machines with UNET widths are introduced, as shown in Fig. 2.5, which can be obtained by simply replacing the FGs (air) with the same iron material used for stator and rotor iron cores. This gives an air-gap flux density component due to slot-openings only (B_{UNET}). As a result, the air-gap flux density due to FGs only can be obtained by using the resultant air-gap flux density subtracting the B_{UNET}. This is possible because, to calculate the air-gap flux density due to the armature windings, the PMs are removed and the magnetic saturation can be neglected due to the large effective air-gap length of the SPM machine.

$$B_{modular} = B_{UNET} + B_{Due\ to\ FGs} \tag{2.13}$$

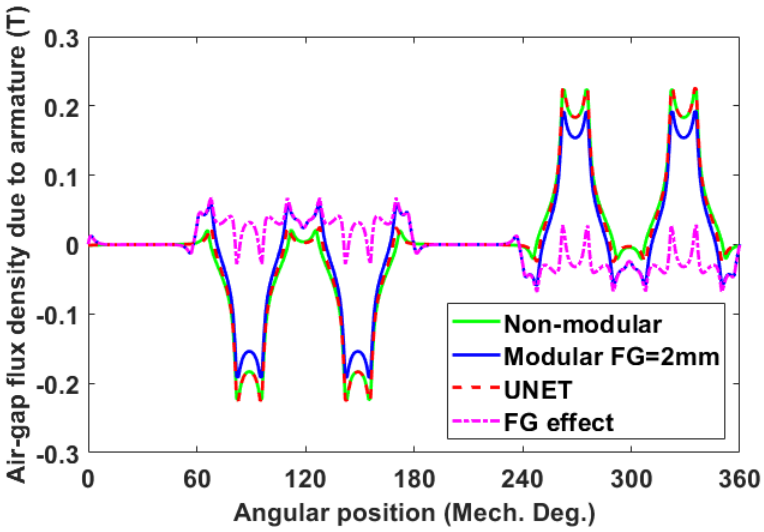

(a)

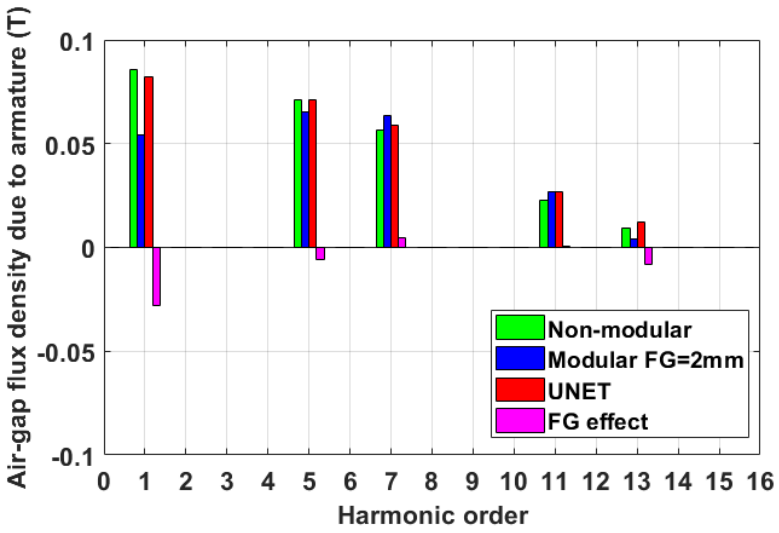

(b)

Fig. 2.6 Influence of FGs on the air-gap flux density due to the armature windings of the 3-phase modular PM machines. (a) Waveforms. (b) Spectra.

Fig. 2.6 depicts the air-gap flux density components (due to slot-openings, FGs) of non-modular and modular PM machines. For the latter, a 3-phase machine with 12-slot/10-pole and FG=2mm is shown as an example. It is evident that the FGs significantly reduce the sub-harmonics while increasing the working harmonics when the slot/pole number combination is properly selected. This is because the sub-harmonic component caused by the FGs is always negative while for certain working harmonics, e.g. the 7^{th} order, the component due to the FGs

can be positive.

In order to further investigate the influence of FGs on the main air-gap flux density sub-harmonics, the flux distribution due to armature currents for the 3-phase, 4-phase and 5-phase non-modular and modular PM machines are shown in Fig. 2.7. It is worth noting that the main sub-harmonic of the air-gap flux density due to the armature windings of the 5-phase machines is similar to that of the 3-phase machines. As expected, the main sub-harmonic of the air-gap flux density due to the armature windings for the 3-phase machine is 2 poles, while for the 4-phase machines it is 4 poles regardless of whether the machines are modular or not. However, when the modular structure is employed as shown in Fig. 2.7 (b) and (d), the FGs in the stator teeth add extra equivalent air-gap length to the flux path of the main armature air-gap flux density sub-harmonic compared to its non-modular counterparts.

Non-modular **Modular**

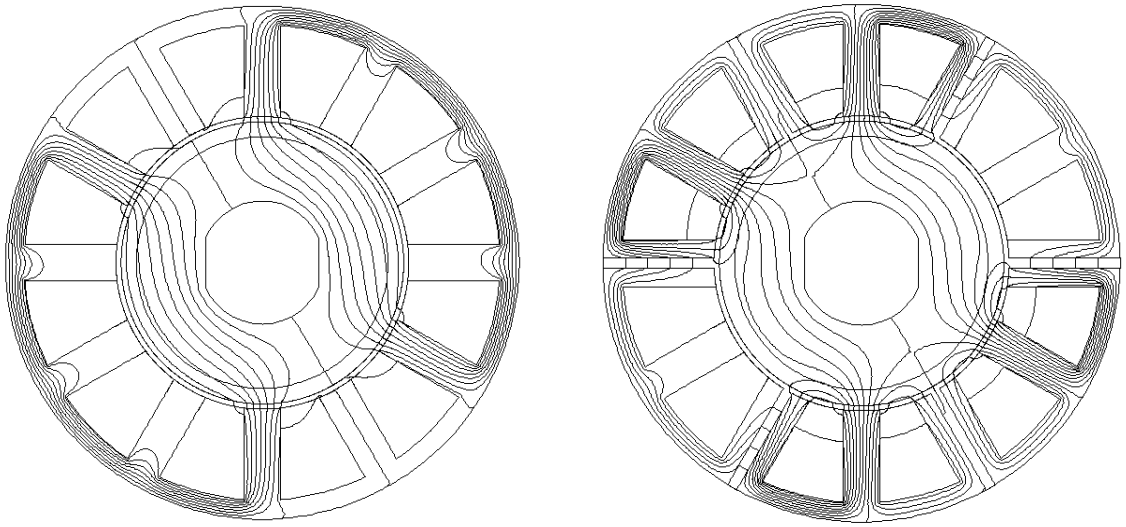

(a) (b)

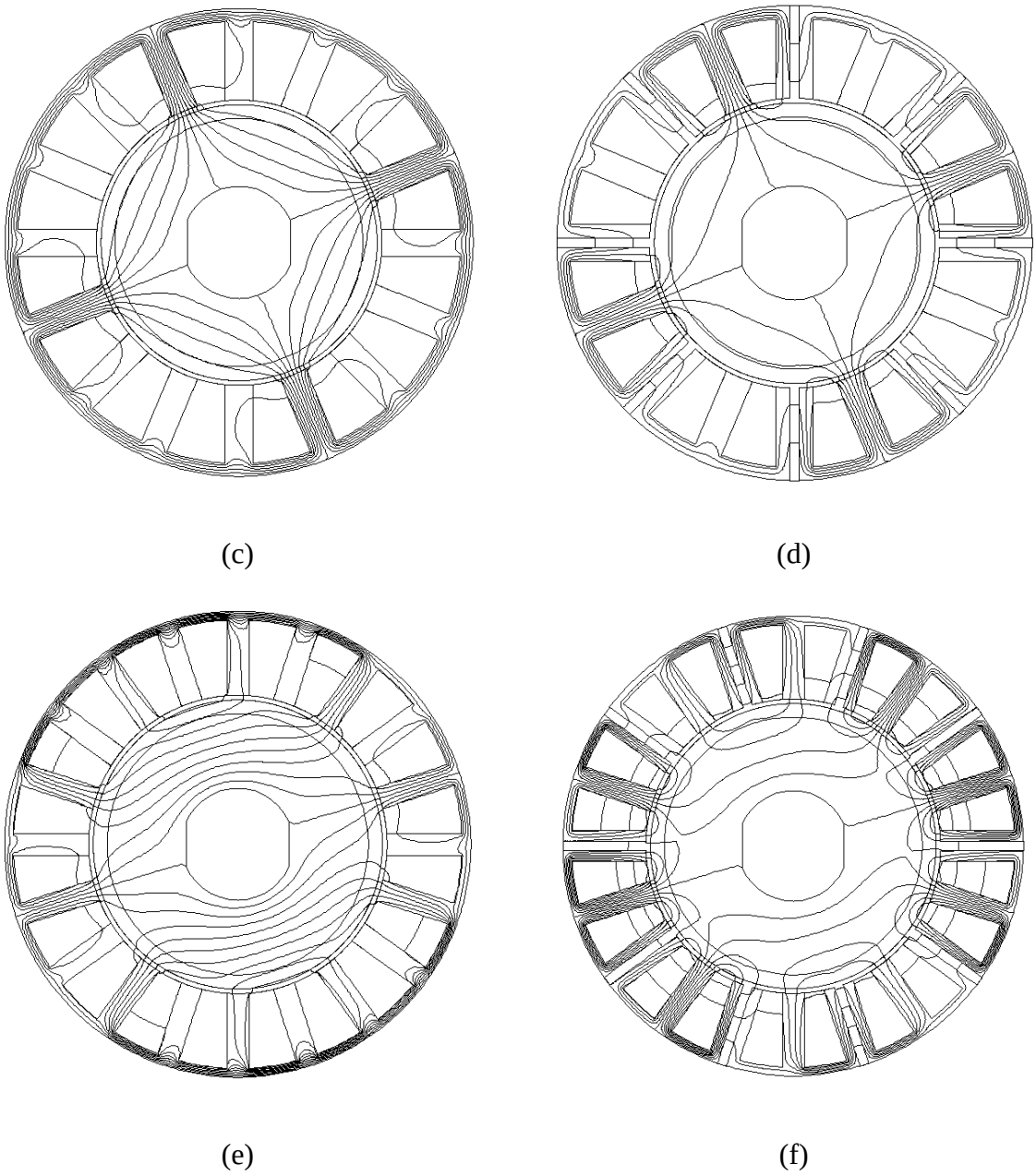

(c) (d)

(e) (f)

Fig. 2.7 Flux distribution due to armature winding only. (a)-(b) 3-phase PM machine. (c)-(d) 4-phase PM machine. (e)-(f) 5-phase PM machine.

2.4.2 AIR-GAP FLUX DENSITY DUE TO THE PMS

In this section, the study on the air-gap flux density due to PMs, which is also known as the open-circuit air-gap flux density will be carried out. From Fig. 2.8 to Fig. 2.10, the waveforms and their spectra of the multi-phase modular PM machines with different FG widths and also different slot/pole number combinations are depicted. It is found that the working harmonics for all the 3-phase, 4-phase, and 5-phase modular PM machines increase in the first place and

then decrease with the increase in the FG widths. This is mainly due to the change of the slot-opening widths interacting with the air-gap flux density due to the PMs and also the iron parts that face the air-gap are constant [37].

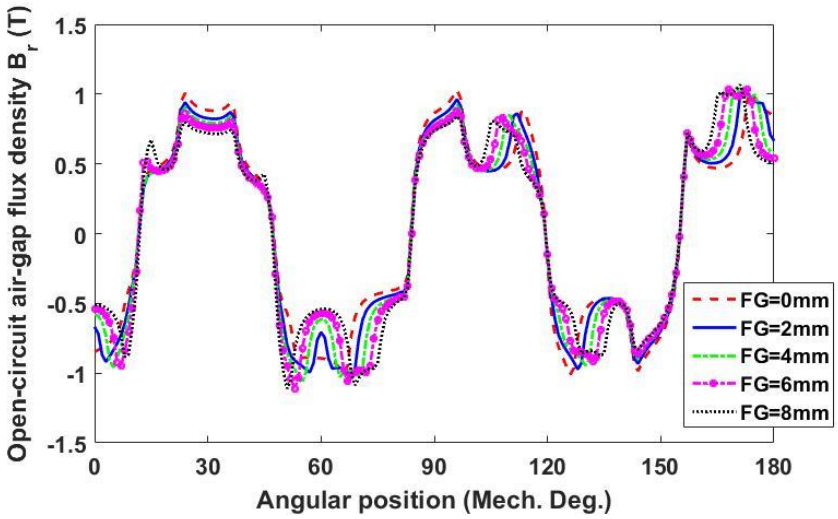

(a)

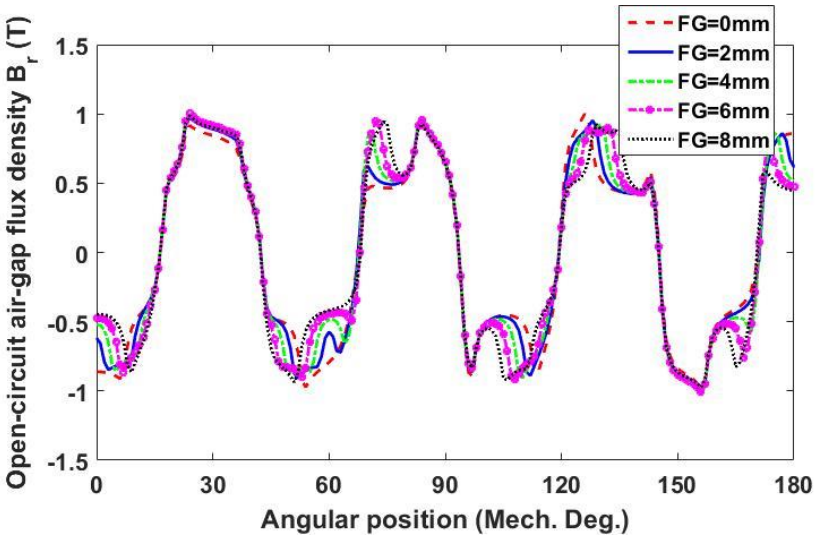

(b)

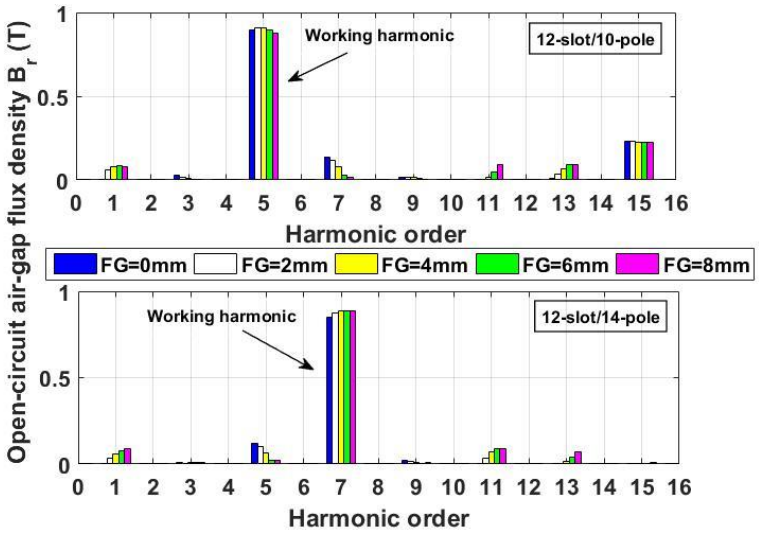

(c)

Fig. 2.8 Waveforms and spectra of the open-circuit air-gap flux density of the 3-phase modular PM machines. (a) Waveforms of the 12-slot/10-pole modular PM machines. (b) Waveforms of the 12-slot/14-pole modular PM machines. (c) Spectra.

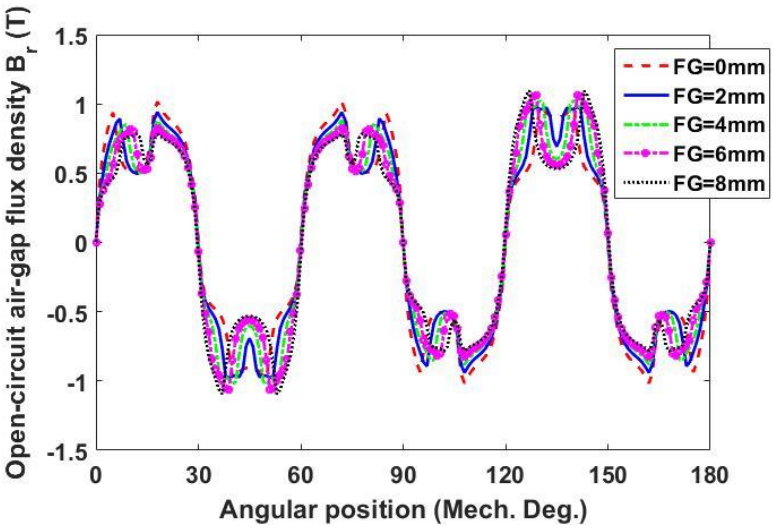

(a)

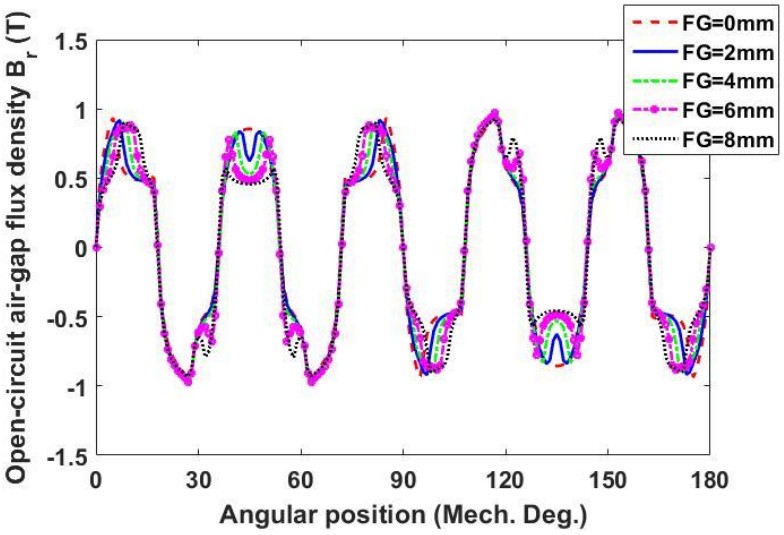

(b)

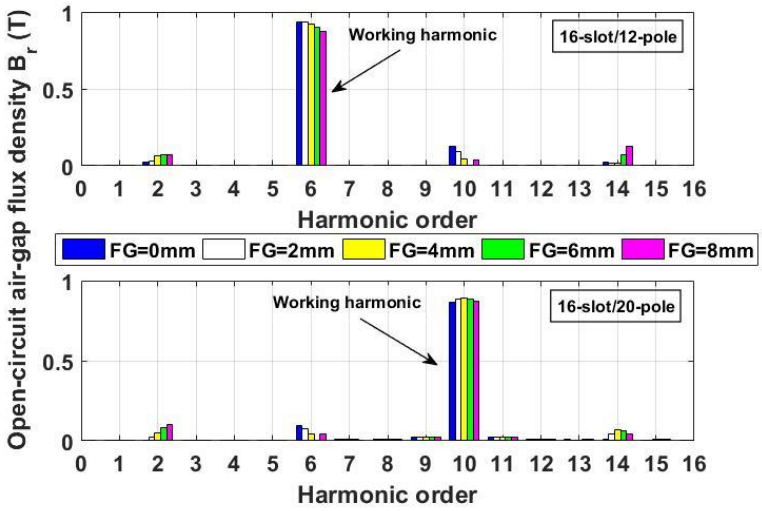

(c)

Fig. 2.9 Waveforms and spectra of the open-circuit air-gap flux density of the 4-phase modualr PM machines. (a) Waveforms the 16-slot/12-pole modular PM machines. (b) Waveforms the 16-slot/20-pole modular PM machines. (c) Spectra.

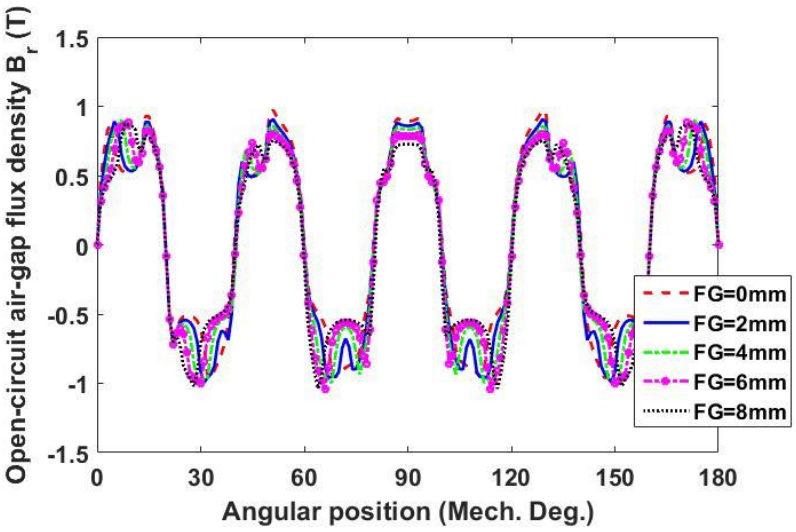
Open-circuit air-gap flux density B_r (T)
1.5
1
0.5
0
-0.5
-1
-1.5
0
30
60
90
120
150
180
Angular position (Mech. Deg.)
FG=0mm
FG=2mm
FG=4mm
FG=6mm
FG=8mm

(a)

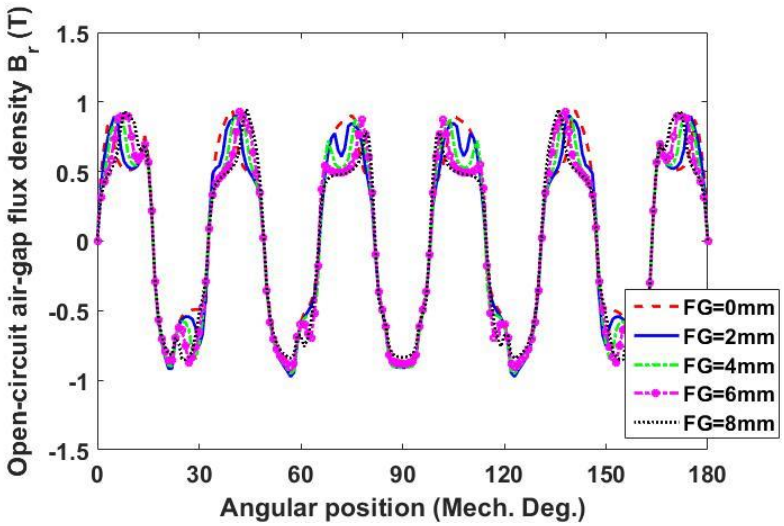
Open-circuit air-gap flux density B_r (T)
1.5
1
0.5
0
-0.5
-1
-1.5
0
30
60
90
120
150
180
Angular position (Mech. Deg.)
FG=0mm
FG=2mm
FG=4mm
FG=6mm
FG=8mm

(b)

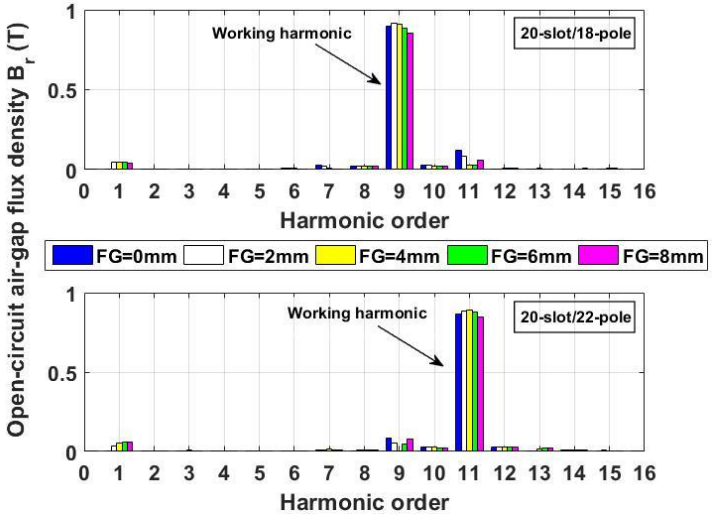

(c)

Fig. 2.10 Waveforms and spectra of the open-circuit air-gap flux density of the 5-phase modualr PM machines. (a) Waveforms the 20-slot/18-pole modular PM machines. (b) Waveforms the 20-slot/22-pole modular PM machines. (c) Spectra.

2.4.3 PHASE BACK-EMF

The phase back-EMF waveforms and their spectra for modular PM machines with different phase numbers and FG widths are shown in Fig. 2.11. Only the results of the phase A are presented. It is found that for multi-phase modular PM machines having $N_s > 2p$, the fundamental phase back-EMFs always decrease with the increase in FG width. When $N_s < 2p$, the fundamental phase back-EMFs can be improved by appropriately selecting the FG widths. Such features are similar to the performance of the air-gap flux density due to the armature windings, as discussed in section 2.4.1, and are mainly due to the influence of FGs on winding factors.

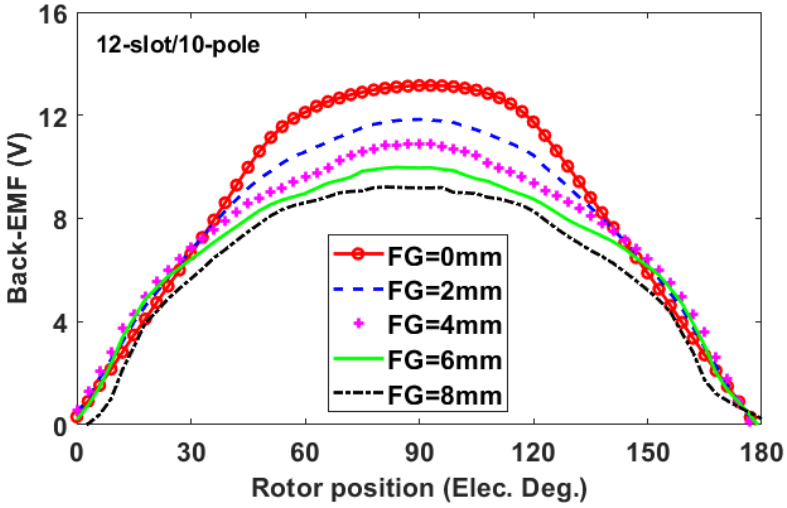
12-slot/10-pole
Back-EMF (V)
Rotor position (Elec. Deg.)
FG=0mm
FG=2mm
FG=4mm
FG=6mm
FG=8mm
0
4
8
12
16
0
30
60
90
120
150
180

(a)

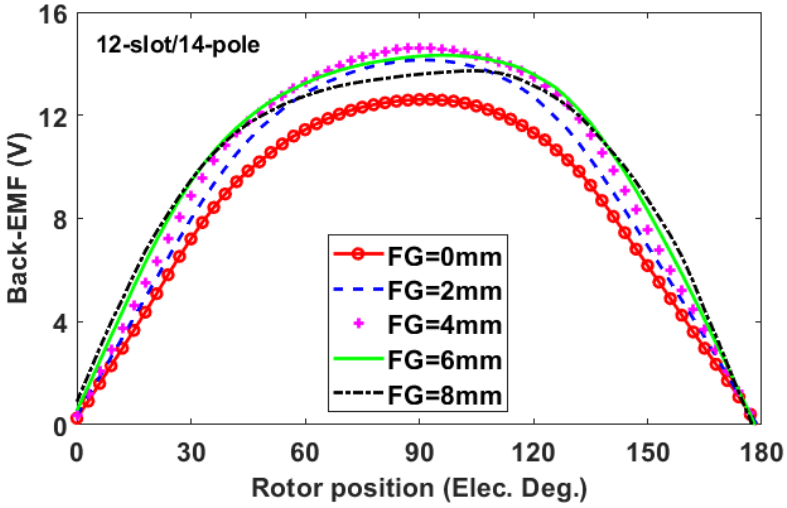
12-slot/14-pole
Back-EMF (V)
Rotor position (Elec. Deg.)
FG=0mm
FG=2mm
FG=4mm
FG=6mm
FG=8mm
0
4
8
12
16
0
30
60
90
120
150
180

(b)

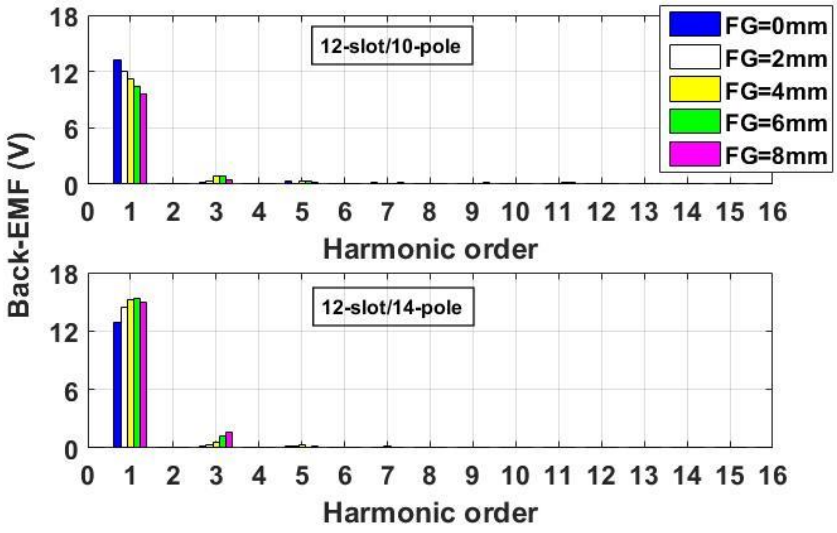
12-slot/10-pole
FG=0mm
FG=2mm
FG=4mm
FG=6mm
FG=8mm
Back-EMF (V)
Harmonic order
12-slot/14-pole
Harmonic order

(c)

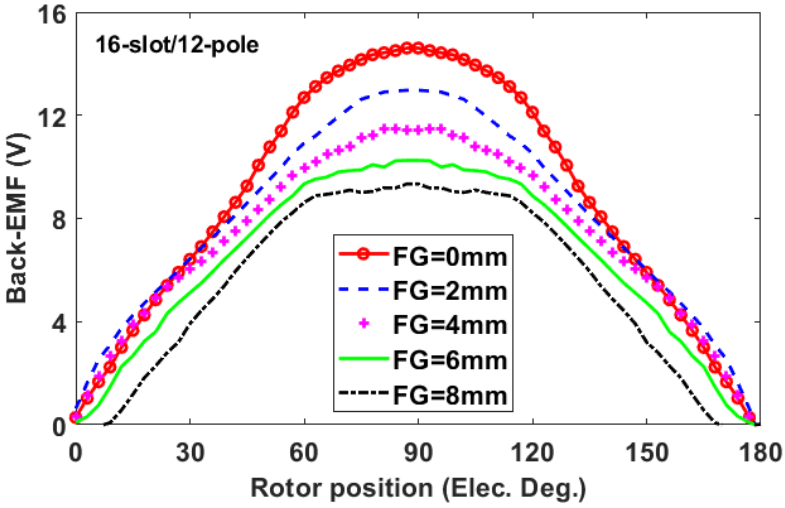
16-slot/12-pole
FG=0mm
FG=2mm
FG=4mm
FG=6mm
FG=8mm
Back-EMF (V)
Rotor position (Elec. Deg.)

(d)

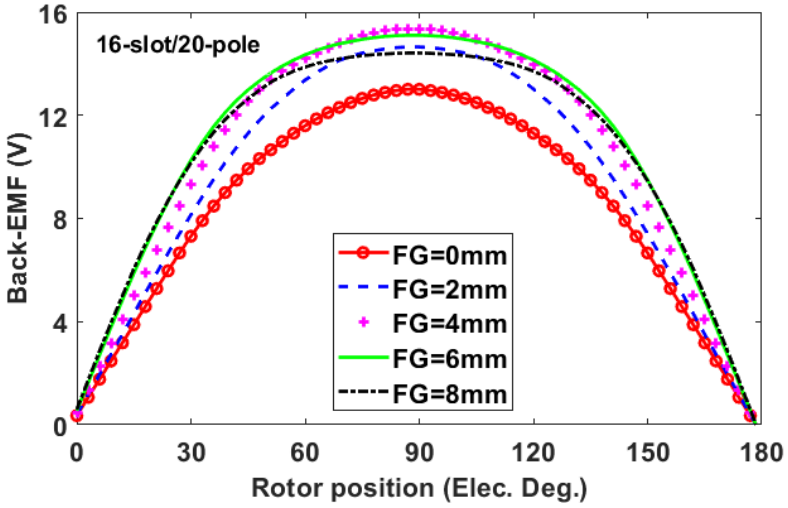
16-slot/20-pole
Back-EMF (V)
Rotor position (Elec. Deg.)
FG=0mm
FG=2mm
FG=4mm
FG=6mm
FG=8mm

(e)

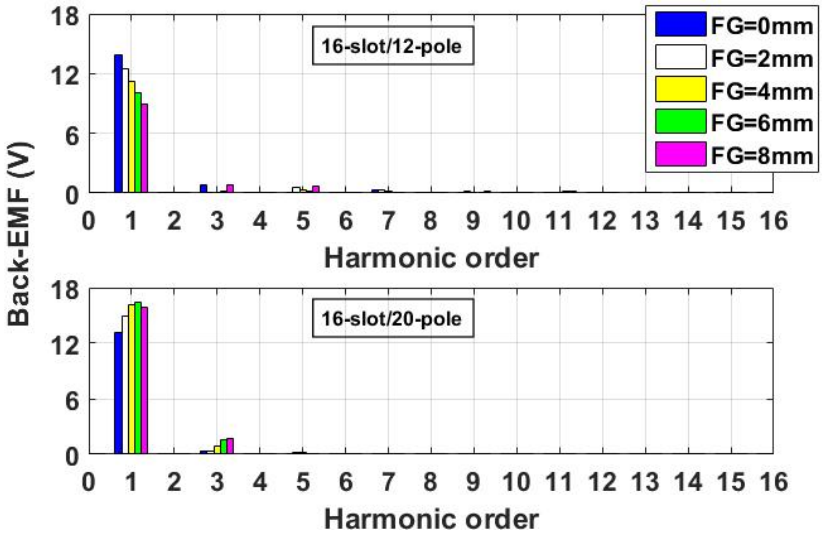
16-slot/12-pole
16-slot/20-pole
Back-EMF (V)
Harmonic order
FG=0mm
FG=2mm
FG=4mm
FG=6mm
FG=8mm

(f)

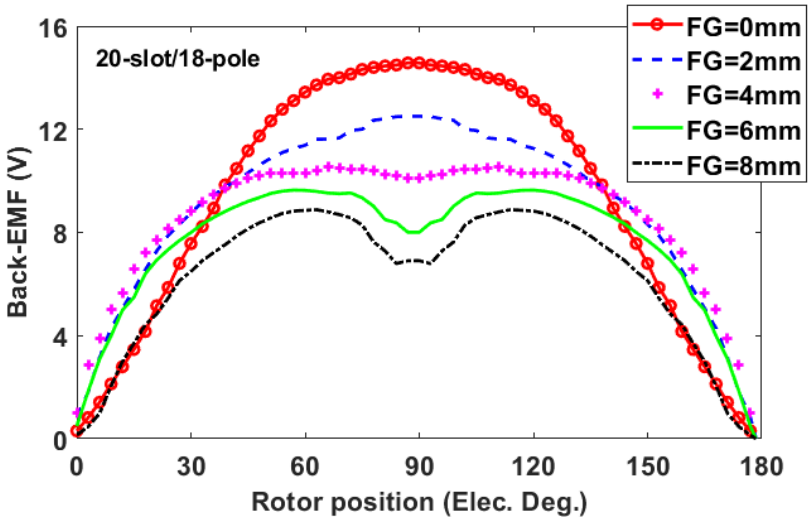
20-slot/18-pole
FG=0mm
FG=2mm
FG=4mm
FG=6mm
FG=8mm
Back-EMF (V)
Rotor position (Elec. Deg.)
0
4
8
12
16
0
30
60
90
120
150
180

(g)

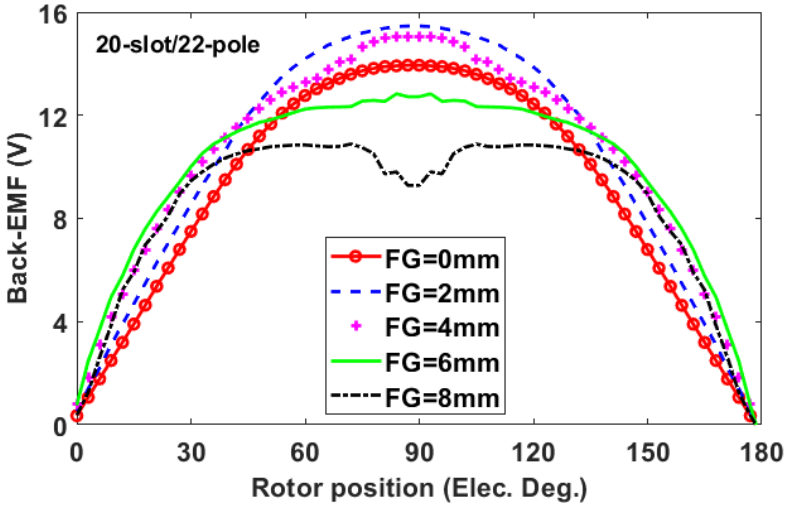
20-slot/22-pole
FG=0mm
FG=2mm
FG=4mm
FG=6mm
FG=8mm
Back-EMF (V)
Rotor position (Elec. Deg.)
0
4
8
12
16
0
30
60
90
120
150
180

(h)

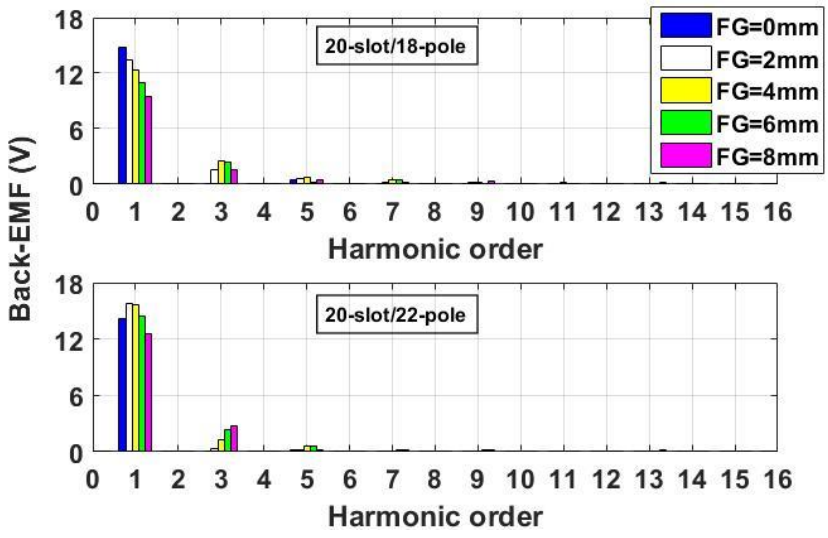

(i)

Fig. 2.11 Back-EMF waveforms and spectra. (a)-(c) 3-phase PM machines. (d)-(f) 4-phase PM machines. (g)-(i) 5-phase PM machines.

2.4.4 COGGING TORQUE

It has been established in [65] that, the periodicity and the amplitude of cogging torque for non-modular PM machines mainly depend on the value of N_c, which is the least common multiple (LCM) between the N_s and the $2p$. The higher the N_c is, the lower the cogging torque will be. However, when the modular structure is employed, the value of N_c becomes N_{cm} due to the change in stator core symmetry. N_{cm} can be obtained by calculating the LCM between $2p$ and the number of FGs [66]. This will be investigated in more detail in the Chapter.

By way of example, the optimal slot/pole number combinations to achieve the highest winding factor for the 4-phase modular PM machines are 16-slot/12-pole and 16-slot/20-pole and the number of FGs is 8. Hence, the values of N_{cm} are 48 and 40, respectively. However, for the 5-phase modular PM machines, the optimal slot/pole number combinations are 20-slot/18-pole and 20-slot/22-pole and the FG number is 10, leading to N_{cm} of 90 and 110, respectively. As a result, the peak-to-peak cogging torques of the 4-phase modular PM machines are always higher than those of the 5-phase modular PM machines, as shown in Fig. 2.12. Moreover, for different multi-phase machines, if the slot/pole number combination and FG width are properly selected, the peak-to-peak cogging torque can be significantly reduced. This will have a profound impact on the torque ripple as studied in the following section.

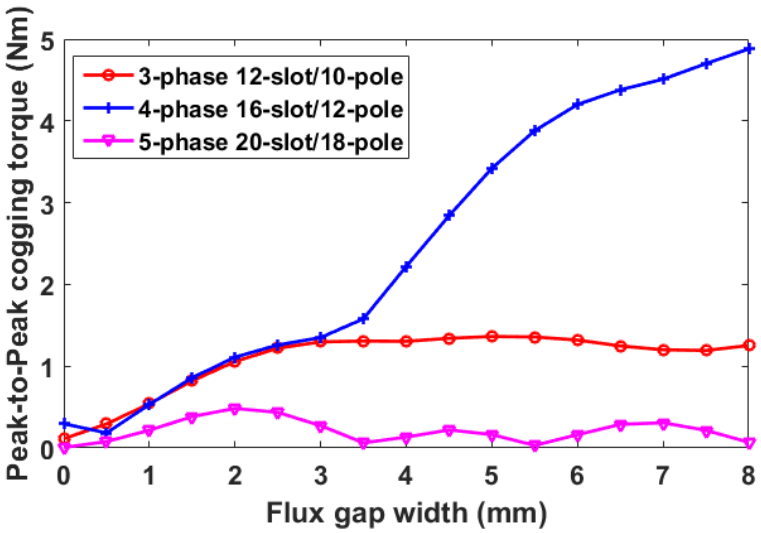

(a)

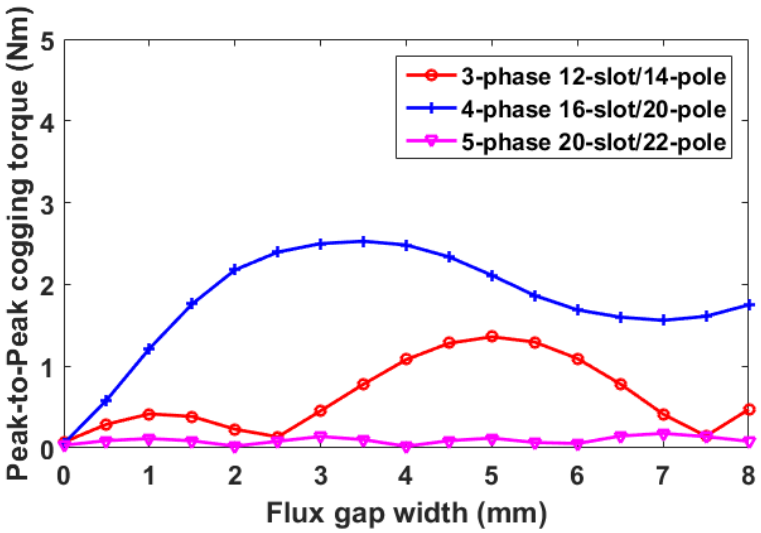

(b)

Fig. 2.12 Peak-to-peak cogging torque of modular PM machines with different phase numbers. (a) $N_s > 2p$. (b) $N_s < 2p$.

2.4.5 ON-LOAD TORQUE AND TORQUE RIPPLE

The results of average torque and torque ripple of modular PM machines with different phase numbers and supplied with sinewave currents (the phase RMS currents are given in Table 2.3) are shown in Fig. 2.13. It can be found that the average torques of the modular PM machines having $N_s > 2p$, decrease with the increasing FG width regardless of the phase

number. However, for the modular PM machines having $N_s < 2p$, the average torques can be maximized by selecting appropriate FG widths. This is mainly due to the impacts of FGs on the working harmonics of the air-gap flux density due to the armature windings and the fundamental phase back-EMFs, as detailed previously.

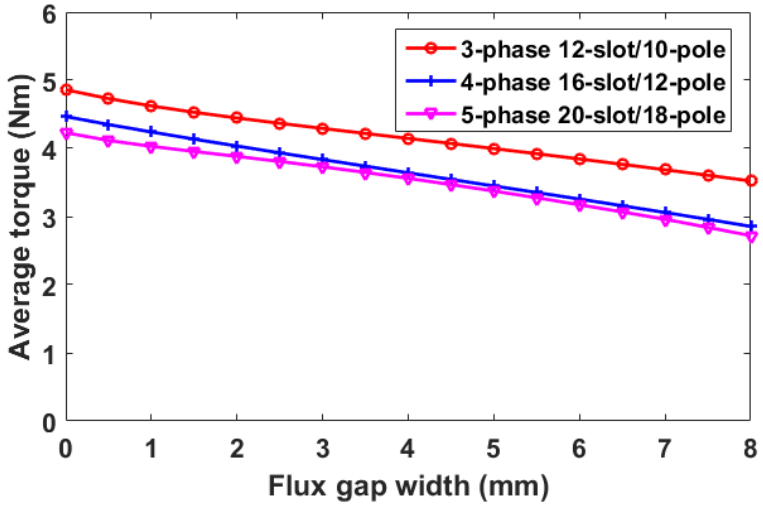

(a)

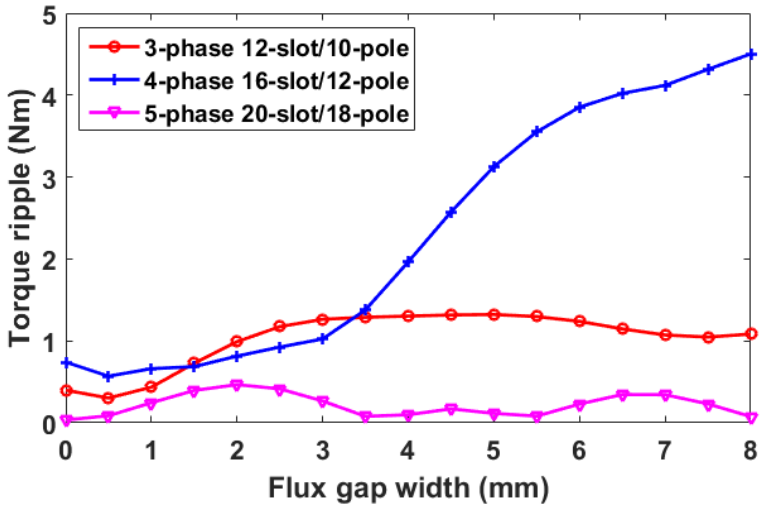

(b)

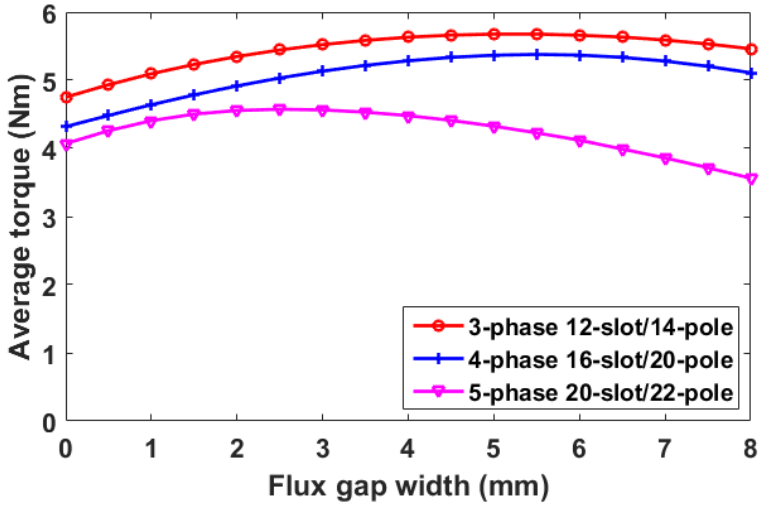

(c)

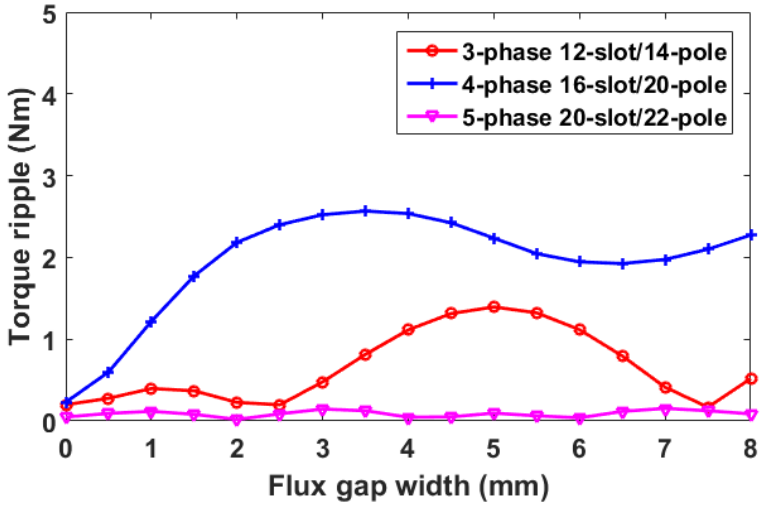

(d)

Fig. 2.13 Average torque and torque ripple versus FG width of modular PM machines with different phase numbers. (a)-(b) $N_s > 2p$. (c)-(d) $N_s < 2p$.

The torque ripples (peak-to-peak torques) follow a similar trend as the peak-to-peak cogging torque. This is mainly due to the fact that higher order harmonics, particularly the 5^{th} and 7^{th}, are quite low in the phase back-EMFs of the modular machines and hence the torque ripples due to the EMF harmonics are much less dominant than those due to the cogging torques.

2.5 EXPERIMENTAL VALIDATION

In order to validate the predictions carried out previously, the existing 3-phase 12-slot/10-pole and 12-slot/14-pole prototype modular PM machines without tooth tips have been employed, as investigated in [37]. The design parameters are given in Table 2.2 and Table 2.3.

2.5.1 PHASE BACK-EMF

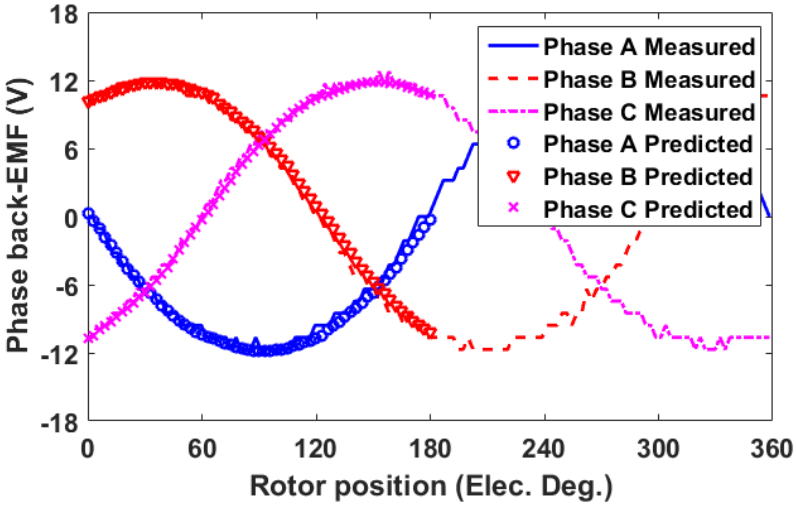

(a)

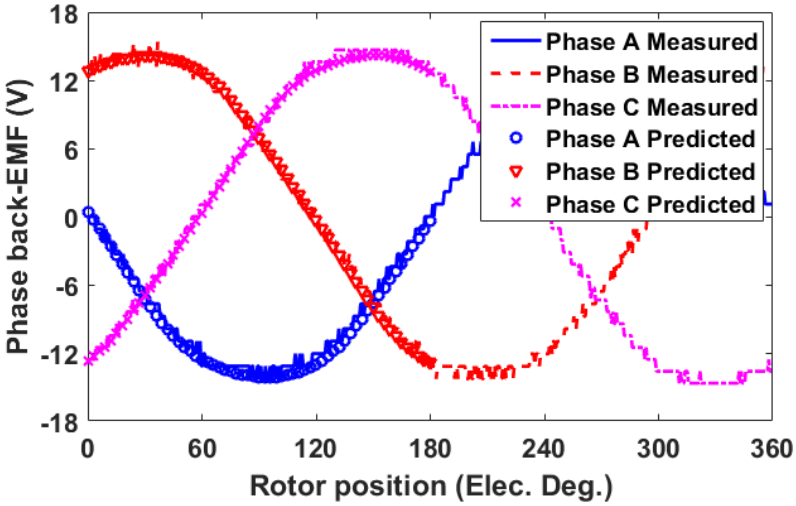

(b)

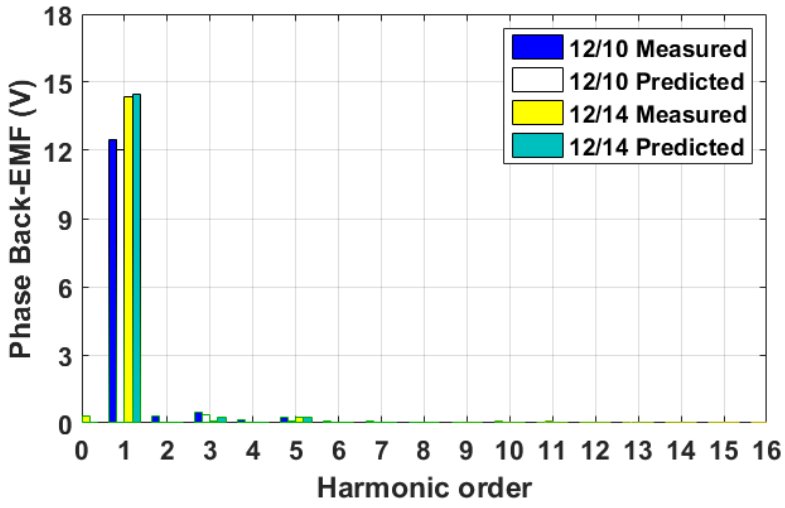

(c)

Fig. 2.14 Predicted and measured phase A back-EMFs. (a) 12-slot/10-pole. (b) 12-slot/14-pole. (c) Spectra of the phase A back-EMFs .

The phase back-EMFs of the prototypes are measured and compared with the corresponding predicted results, as shown in Fig. 2.14. A good match can be obtained between the predicted and measured results.

2.5.2 STATIC TORQUE

The static torque against the rotor position can be measured by employing the method presented in [67] and the test rig is shown in Fig. 2.15 (a). The supply currents to phases A (I_A), B (I_B) and C (I_C) are set as $I_A = -2 \times I_B = -2 \times I_C = I$, where I is a DC and can be changed to represent different load conditions. It is evident from Fig. 2.15 (b) that the predicted and measured results are in good agreement for all prototype machines.

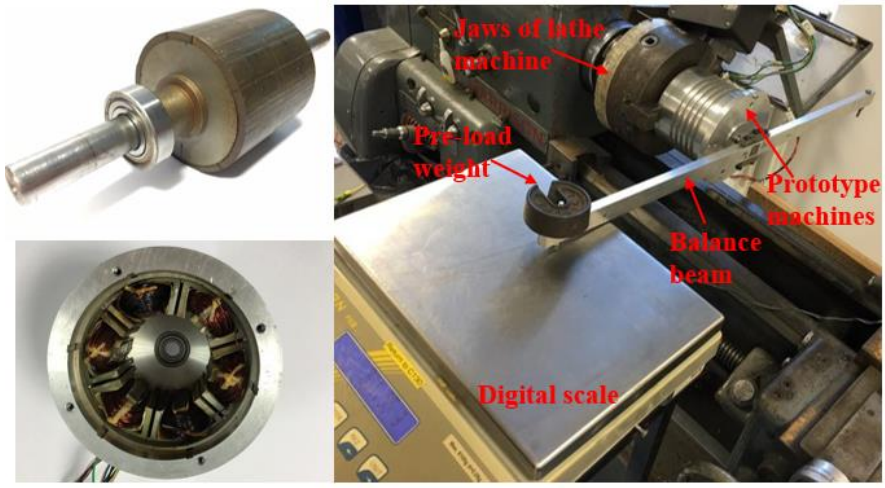

(a)

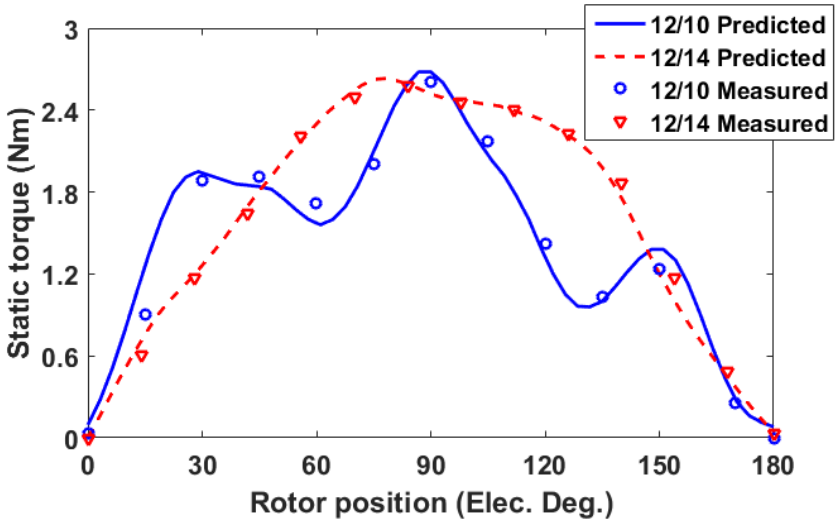

(b)

Fig. 2.15 Static torque measurement (I=5A). (a) The prototype machines and the test rig. (b) Static torque versus rotor position.

2.6 CONCLUSION

The multi-phase modular PM machines with single-layer concentrated windings were investigated in this chapter. The optimal slot/pole number combinations for modular PM machines with different phase numbers were identified. The electromagnetic performance such as winding factors, air-gap flux density due to armature windings or PMs, back-EMF, cogging torque, average torque and torque ripple have been investigated, it demonstrated that:

- The main sub-harmonics of air-gap flux density due to the armature are significantly reduced by employing the modular topologies for multi-phase PM machines. This can largely mitigate the negative effects on the electromagnetic performance due to such sub-harmonics.
- For multi-phase modular PM machines having $N_s > 2p$, the FGs have negative effects on the electromagnetic performance such as decreasing the winding factors, the working harmonics of the air-gap flux density and also the average torques, etc.
- For the multi-phase modular PM machines having $N_s < 2p$, if the FG width is properly selected, the FGs can improve the electromagnetic performance, such as increasing average torques and reducing the torque ripples.

The predictions obtained by 2D FE have been validated by the experiments. The general rules established in this chapter summarize the influence of FGs on the electromagnetic performance of multi-phase modular PM machines. Although only 3, 4 and 5-phase cases are discussed, the conclusions achieved in this chapter can be extended to modular PM machines with all other phase numbers and can be used as design guidelines for multi-phase modular PM machines in practical applications. Furthermore, although only small size machines have been investigated for the experimental validation purpose, the established general rules can also be extended to the design and analysis of large PM machines, e.g. offshore wind generators.

In the following chapter, a cogging torque mitigation method by the slot-opening shift for modular PM machines will be proposed and detailed.

Chapter 3 COGGING TORQUE AND TORQUE RIPPLE REDUCTION OF MODULAR PM MACHINES BY SLOT-OPENING SHIFT

This chapter proposes a novel cogging torque mitigation method for modular PM machines with FGs in alternate stator teeth. The slot-openings of the modular PM machines are divided into two groups in a special way. By shifting the slot-openings of those two groups in opposite directions with the same angle, the cogging torque can be significantly reduced. Analytical formula of the desired shift angle is derived, and can be applicable to other modular machines with different slot/pole number combinations. Meanwhile, the influence of the proposed method on the phase back-EMF and on-load torque are investigated. It is found that the three phase back-EMF waveforms remain balanced for all slot/pole number combinations after slot-opening shifting. Experiments based on existing prototypes are carried out to validate the FE modelling.

This chapter comes from author's paper [66].

3.1 INTRODUCTION

Cogging torque is the consequence of interaction between the PM MMF harmonics and the air-gap permeance harmonics resulted from slot-openings [68]-[69]. Due to the fact that the cogging torque causes torque ripple and hence vibrations and acoustic noise[69], the reduction of cogging torque is of significant importance for designing PM machines. Various methods to reduce the cogging torque have been proposed in recent years. For instance, employing the auxiliary slots [68], [70], [71]-[76], shaping the rotor magnets or stator teeth [77]-[80]. Another effective method for reducing cogging torque is skewing [68], [70], [81]-[83]. Moreover, by appropriately selecting slot/pole number combination [68], [84] or the optimized ratio of pole arc to pole-pitch [70], [85], the cogging torque can be effectively mitigated as well. In addition, the distribution of PMs on the rotor [76] of the PM machines can also affect the cogging torque significantly.

However, the existing methods of mitigating cogging torque still have some drawbacks. Taking the method of skewing as an example, skewing the magnets helps to reduce the cogging torque, along with the reduction in the fundamental of phase back-EMF and hence average torque. Furthermore, it is more difficult to wind the machines after skewing the stator since the effective slot-opening width is decreased slightly [65]. In terms of manufacturing, skewed stator or rotor will be more complex to build, which also increases the cost of production.

Another effective method of minimizing cogging torque such as shifting slot-openings or PMs is proposed for classic SPM machines [70], [86]-[88]. The slot-openings are divided into several groups and each group is shifted by a proper angle so the cogging torque produced by different slot-openings can cancel each other. As a result, the resultant cogging torque can be mitigated. The most significant advantage of using this method is that the symmetry of the three-phase back-EMF remains the same and no extra harmonics are introduced to the back-EMF.

However, the available methods are for conventional machines, so far no cogging torque mitigation method has been proposed for the modular PM machines. Due to the additional air-gaps introduced by modular topologies, the cogging torque could be significantly increased. In [24], the influence of additional air-gaps between the stator teeth and stator back iron on cogging torque has been analysed. When the additional stator air-gaps are uniform, only the magnitude of cogging torque is increased but the non-uniform additional stator air-gaps sharply increase both the amplitude and the periodicity of cogging torque. However, although the

modular stator affects the performance of the PM machines, the superiorities of using modular topologies cannot be neglected, i.e. using modular stator can significantly ease the manufacture process, especially the stator winding, particularly for large machines such as wind power generators, for which the modular/segmented stators are necessary.

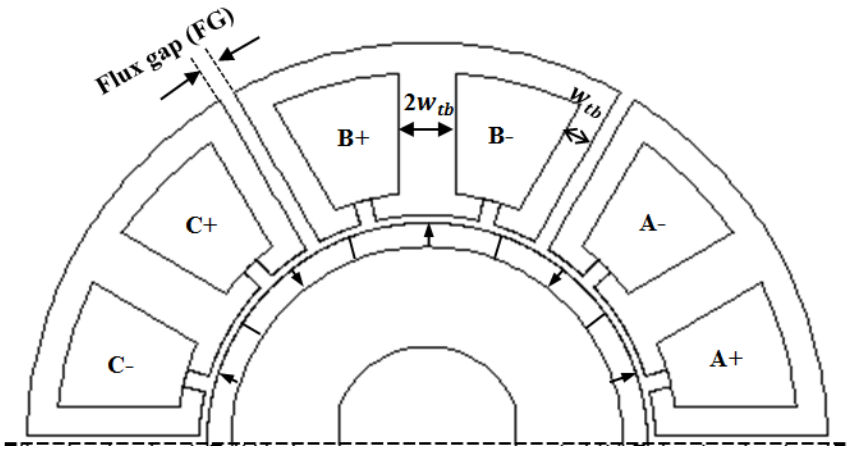

Fig. 3.1 The cross-section of 12-slot/10-pole modular PM machines [33]-[38].

TABLE 3.1 MAIN PARAMETERS OF THE MODULAR PM MACHINES

Phase voltage (V)	36	Tooth body width (mm)	7.1
Rated torque (Nm)	5.5	Slot-opening (mm)	2
Rated current (A_{RMS})	7.35	Stack length (mm)	50
Rated speed (rpm)	400	Air-gap length (mm)	1
Slot number	12	Rotor outer radius (mm)	27.5
Pole number	10/14	Magnet thickness (mm)	3
Stator outer radius (mm)	50	Magnet remanence (T)	1.2
Stator inner radius (mm)	28.5	Number of turns per phase	132
Stator yoke height (mm)	3.7	Filling factor k_b	0.37

Nevertheless, the previous works were focused on studying the influence of various modular topologies on the electromagnetic performances such as cogging torque, phase back-EMF, on-load torque, iron losses, etc., no method of reducing the cogging torque has been proposed. As discussed above, cogging torque is a main design parameter which cannot be overlooked and it is also true for modular PM machines. Therefore, to fill this gap and to further improve the performance of modular PM machine, a novel method of mitigating the cogging torque is proposed in this chapter. It is worth mentioning that different from other mitigation methods, the proposed method uses the cogging torque produced by slot-openings to compensate that

produced by FGs so to reduce the resultant cogging torque.

3.2 COGGING TORQUE PREDICTION OF MODULAR PM MACHINES

3.2.1 EFFECTS OF FGS ON COGGING TORQUE

The previous cogging torque mitigation methods are feasible because of the assumption that resultant cogging torque can be synthesized from the cogging torque produced by each individual slot-opening [65]. So by shifting slots in specific ways, the cogging torque produced by different slot-openings can be cancelled out. According to [68], without accounting for magnetic saturations, the cogging torque for classic non-modular PM machines can be expressed by (3.1), which is the sum of the cogging torques produced by all slot-openings.

$$T_{cogg} = \sum_{n=1,2,3\cdots}^{\infty} T_{N_c n} sin(N_c n\theta) \tag{3.1}$$

where N_c is the least common multiple (LCM) of $2p$ and N_s, and equals to the number of periods of cogging torque over one mechanical revolution. $T_{N_c n}$ is the amplitude of its $N_c n^{th}$ harmonic. θ is the mechanical angle between the stator and rotor.

However, with regard to the modular PM machines, the stator symmetry has been changed since the stator is segmented into several identical sections by the FGs. Taking 12-slot/10-pole PM machine as an example, without stator segmentation, the stator periodicity repeats 12 times over the entire circumference (360 Mech. Deg.). Whereas using stator segmentation, the stator is divided into 6 identical segments (see Fig. 3.1), hence, the stator periodicity repeats 6 times instead of 12 times. Therefore, the value of N_c becomes 30 instead of 60. For this reason, the cogging torque equation of modular PM machine needs to be rewritten by:

$$T_{cogg-modular} = \sum_{n=1,2,3\cdots}^{\infty} T_{N_{cm} n} sin(N_{cm} n\theta) \tag{3.2}$$

where N_{cm} is the LCM of the FG number (N_{FG}) and $2p$. Similar to non-modular PM machine, the frequency of cogging torque depends on the value of N_{cm}. However, the amplitude is determined by the widths of both the slot-openings and FGs and also their interactions. According to [68], the larger the N_{cm}, the higher the frequency of cogging torque and the lower the amplitudes of resultant cogging torque. Therefore, the method of choosing an appropriate

combination of pole and FG numbers is still applicable to mitigate the resultant cogging torque for modular PM machines regardless of the FG width. By way of example, for the 18-slot/16-pole modular PM machine, it has 9 FGs, and the value of N_{cm} is 144. As a result, its peak resultant cogging torque is nearly zero, so this kind of modular machines will not be investigated further in this chapter.

3.2.2 SYNTHESIS OF COGGING TORQUE FOR MODULAR PM MACHINES

For modular PM machines, since the FGs almost eliminate the circumferential flux path (main and leakage fluxes) in the stator iron core, the entire flux distribution inside the stator has been modified, as shown in Fig. 3.2 and Fig. 3.3. This means that, due to FGs, the cogging torque produced by one single slot-opening will be influenced by the presence of adjacent slot-openings and FGs.

Therefore, different from classic non-modular SPM machines, the resultant cogging torque of modular machine cannot be simply written as a sum of cogging torques due to slot-openings and FGs. It should be the resultant cogging torque generated by slot-openings (C_{SO}), FGs (C_{FG}) and the cogging torque due to slot-openings accounting for the FGs influence (C_e), as shown in (3.3).

$$C_{SO} + C_{FG} + C_e = C_{total} \tag{3.3}$$

This chapter introduces a special way to synthesis the resultant cogging torque waveform of modular PM machines from the cogging torque waveforms generated by both slot-openings and FGs. To do so, the stator core has been split into two sub-structures, as shown in Fig. 3.4. Each sub-structure has 6 slot-openings and 6 FGs (the 6 FGs are the same in both sub-structures).

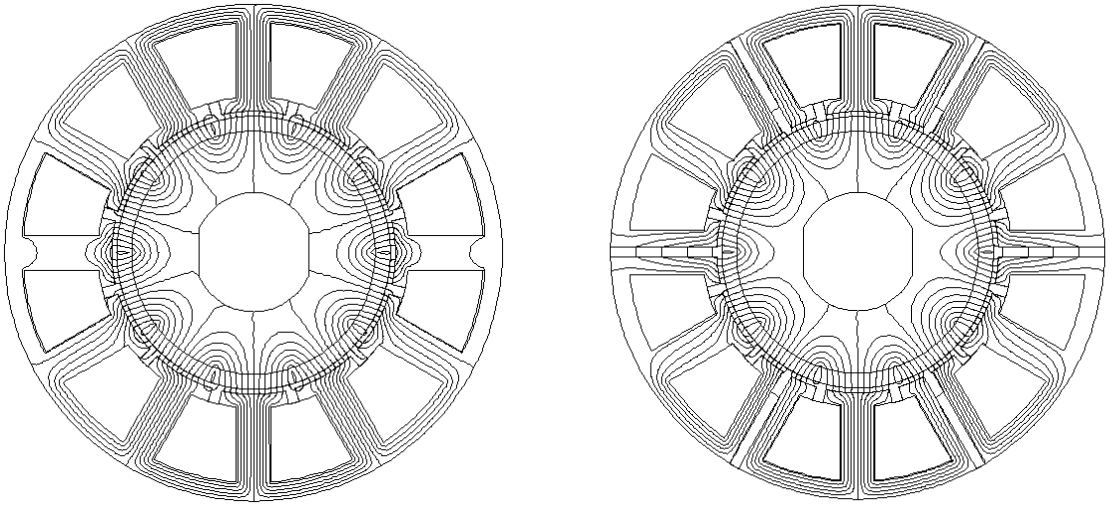

(a) (b)

Fig. 3.2 The flux lines distribution under the open-circuit condition of the 12-slot/10-pole conventional and modualr PM machines. (a) Conventional. (b) Modular (FG=2mm).

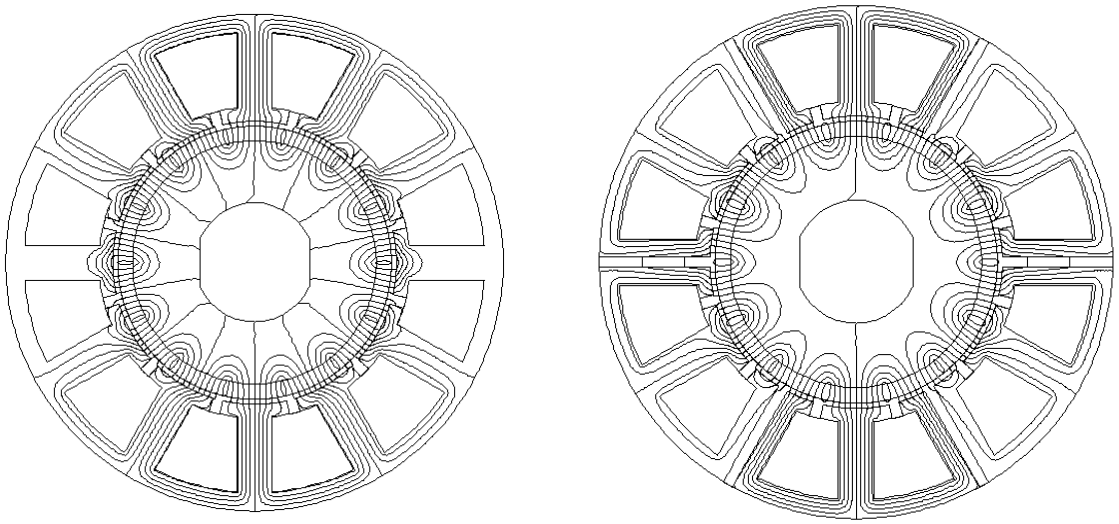

(a) (b)

Fig. 3.3 The flux lines distribution under the open-circuit codition of the 12-slot/14-pole conventional and modular PM machines. (a) Conventional. (b) Modular (FG=2mm).

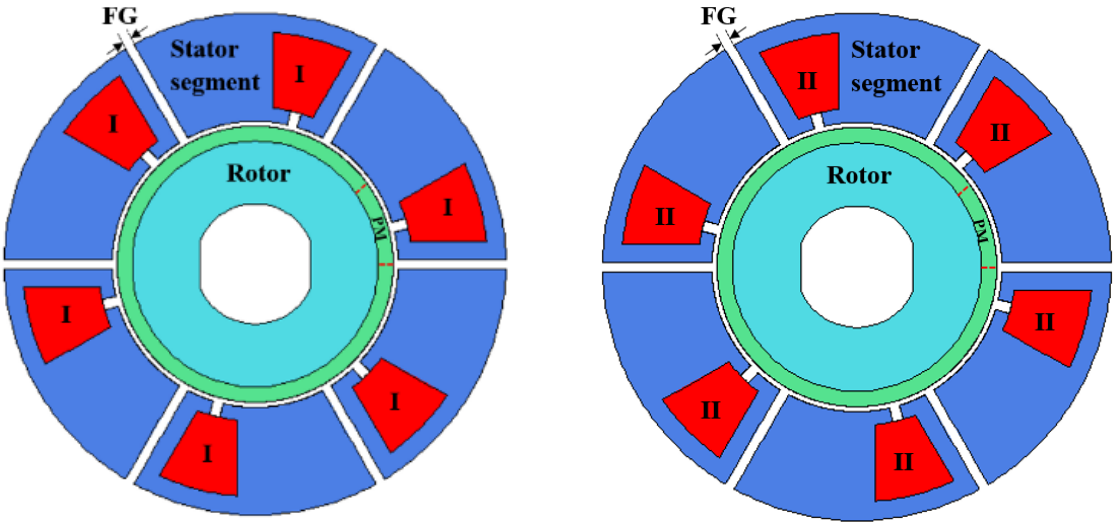

(a) (b)

Fig. 3.4 The two-substructures of stator core for cogging torque synthesis. The rotor is exactly the same for 2 groups. (a) Group I. (b) Group II.

To reassemble groups I and II into one entire stator core so that the resultant cogging torque can be calculated, the equation (3.3) should be rewritten by:

$$\left(C_{groupI} - C_{FG}\right) + \left(C_{groupII} - C_{FG}\right) + C_{FG} = C_{total} \tag{3.4}$$

where $C_{groupI} - C_{FG}$ represents the cogging torque of slot-openings under the influence of FGs in group I, and is named as $C_{groupI}{}'$ for simplicity. Similarly, for group II, $C_{groupII} - C_{FG} = C_{groupII}{}'$. Therefore, (3.4) can be rewritten by:

$$C_{groupI}{}' + C_{groupII}{}' + C_{FG} = C_{total} \tag{3.5}$$

Fig. 3.5 proves the feasibility and accuracy of using (3.4) to predict the resultant cogging torque waveform of modular PM machines. It is worth noting that the cogging torque waveforms of C_{groupI}, $C_{groupII}$, and C_{FG} in (3.4) are obtained from the FE simulation. The waveform named "Synthesized" in the Fig. 3.5 is synthesized by using (3.4), while the waveform named "2D-FEA" is the resultant cogging torque waveform directly from the entire modular PM machines model in the FE.

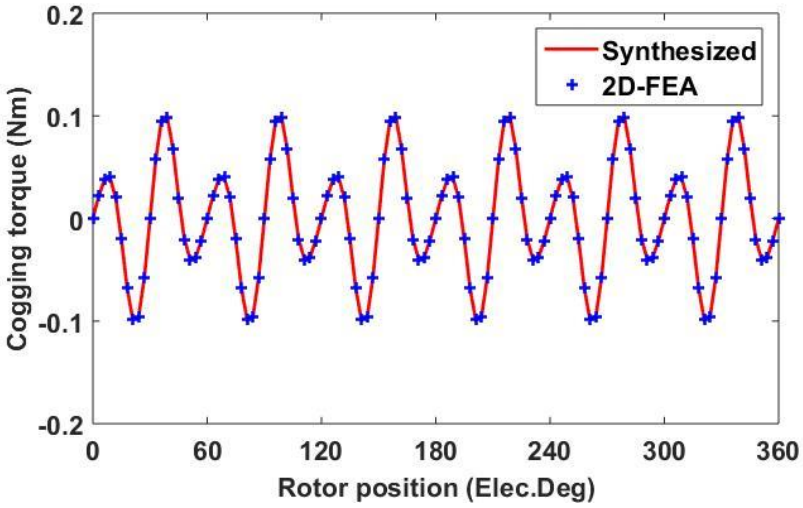

(a)

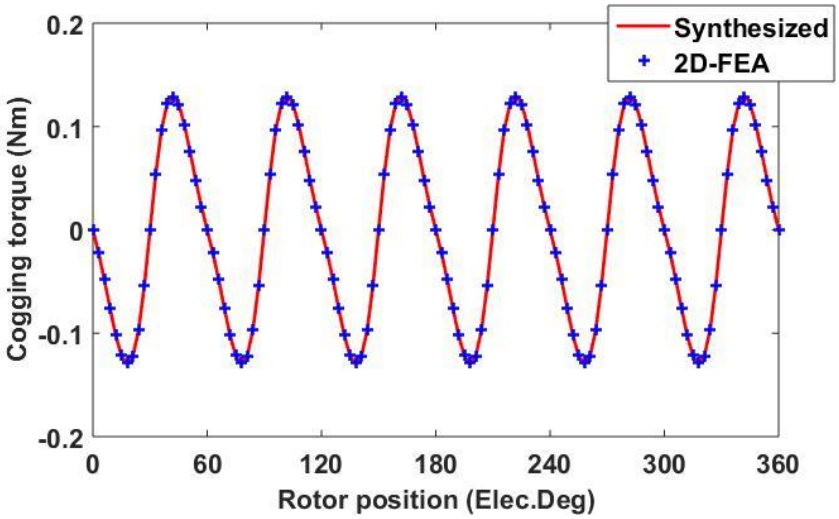

(b)

Fig. 3.5 Comparison of synthesized and direct FE calculated cogging torque waveforms. The FG width is 2 mm for both machines. (a) 12-slot/10-pole. (b) 12-slot/14-pole.

There is no doubt that the quantification of the influence of the FGs on cogging torque using exact analytical expression is very difficult. However, applying (3.4) to predict the resultant cogging torque of modular PM machine can take into account the effect of C_e without the need to calculate its exact expression. This arrangement makes the proposed cogging torque mitigation method possible, as will be detailed later in this chapter.

3.3 COGGING TORQUE MITIGATION

As mentioned previously, the cogging torque of modular machines is produced by both the slot-openings and the FGs. Therefore, only compensating the cogging torque due to the slot-openings will not be sufficient to mitigate the resultant cogging torque. The cogging torque due to FGs is often more dominant and needs to be mitigated. To do so, the slot-openings of the Group I and Group II are shifted in opposite directions with the same shift angle (γ). Whereas, the positions of the FGs are fixed so to maintain the two tooth body widths on two sides of FGs unchanged, as shown in Fig. 3.6. It is worth mentioning that during the shifting process, the slot-opening widths are unchanged. By employing this compensation strategy, effective mitigation of the resultant cogging torque can be achieved if an appropriate shift angle is chosen.

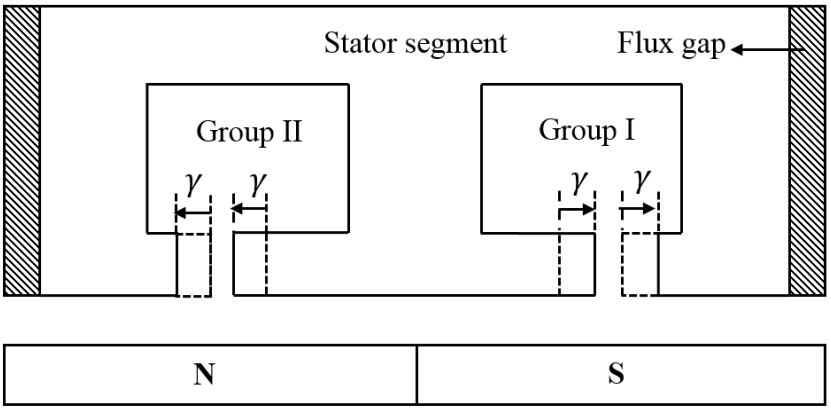

Fig. 3.6 Stator core with slot-openings shifted. Slot-opening of Group II shifted left by γ Mech. Deg., while slot-opening of Group I shifted right by γ Mech. Deg.

Other slot-opening shift methods (e.g. all the slot-openings are shifted in the same direction, and with the same angle, etc.) have also been studied. It is found that these methods cannot help to reduce the cogging torque, some might even increase it and hence, the calculation results will not be shown in this chapter.

3.3.1 THEORETICAL ANALYSIS BY FE

For conventional PM machines, when shifting the slot-openings, the cogging torque components can be shifted in phase accordingly without changing the amplitude. This is still applicable for modular PM machines although the FGs have influence on cogging torque produced by the slot-openings, as shown in Fig. 3.7.

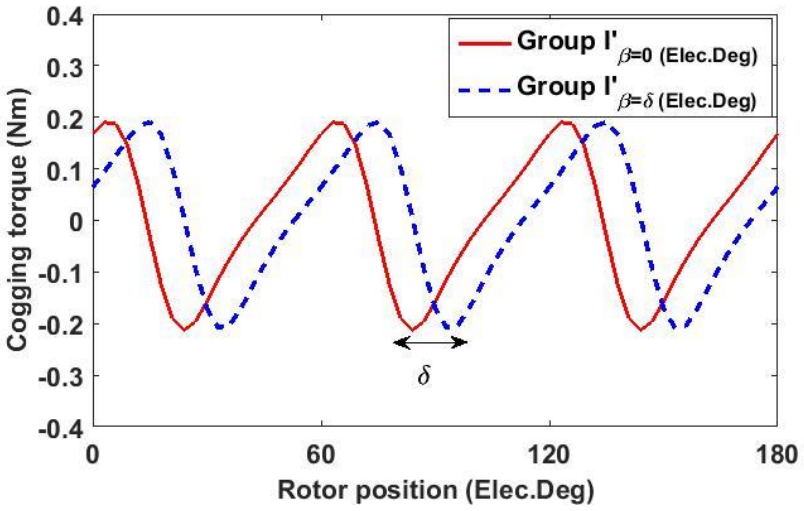

Fig. 3.7 Relevant cogging torque waveforms before and after shifting slot-openings of Group I. β is slot-opening shift angle in Elec. Deg. and δ is an electrical shift angle which can be any value.

Based on (3.1), the cogging torque expressions of ${C_{groupI}}'$ and ${C_{groupII}}'$ are given as:

$$ {C_{groupI}}' = \sum_{n=1,2,3\cdots}^{\infty} T^{I}_{\frac{N_{cm}n}{p}} \sin\left(\frac{N_{cm}n}{p}\alpha + \varphi_{I\frac{N_{cm}n}{p}}\right) \tag{3.6} $$

and

$$ {C_{groupII}}' = \sum_{n=1,2,3\cdots}^{\infty} T^{II}_{\frac{N_{cm}n}{p}} \sin\left(\frac{N_{cm}n}{p}\alpha + \varphi_{II\frac{N_{cm}n}{p}}\right) \tag{3.7} $$

where $T^{I}_{\frac{N_{cm}n}{p}}$ and $T^{II}_{\frac{N_{cm}n}{p}}$ are the respective magnitudes of the $\frac{N_{cm}n^{th}}{p}$ order harmonics of ${C_{groupI}}'$ and ${C_{groupII}}'$ before the slot-opening shift. Through applying the cogging torque data computed by FE to the Fourier analysis program, the values of $T^{I}_{\frac{N_{cm}n}{p}}$ and $T^{II}_{\frac{N_{cm}n}{p}}$ can be obtained. α is the electrical angle between the stator and rotor. $\varphi_{I\frac{N_{cm}n}{p}}$ and $\varphi_{II\frac{N_{cm}n}{p}}$ are the electrical phase angles of ${C_{groupI}}'$ and ${C_{groupII}}'$, respectively and can be acquired by Fourier analysis as well.

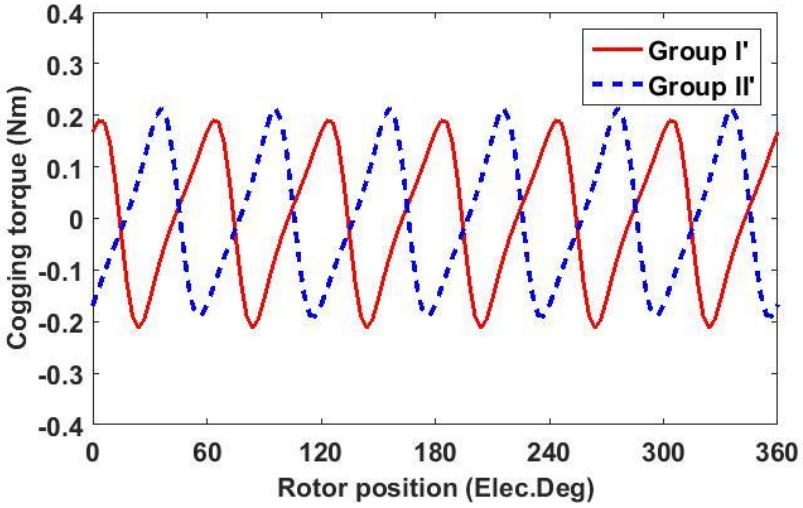

(a)

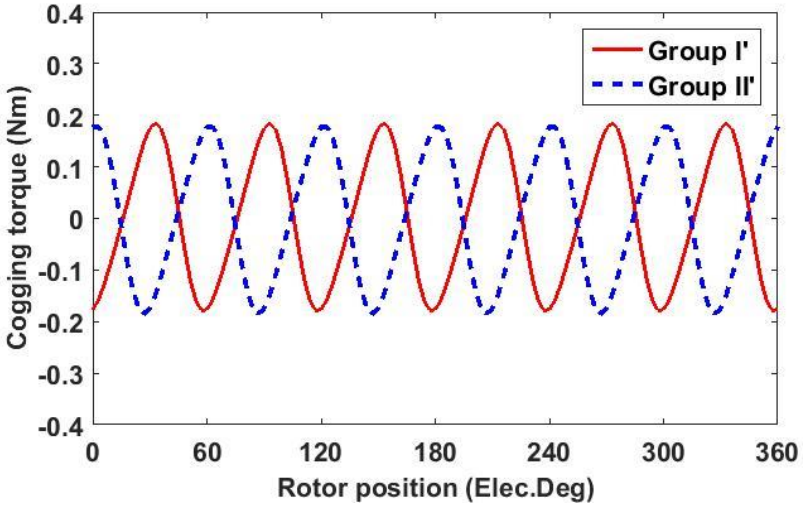

(b)

Fig. 3.8 Cogging torque waveforms of GroupI′ and GroupII′. The FG width is FG = 2 mm for both machines. (a) 12-slot/10-pole. (b) 12-slot/14-pole.

It is worth mentioning that the slot-openings of the two groups have the same dimension. Moreover, the effect of FGs on cogging torque produced by the slot-openings in each group is nearly the same as well due to the symmetrical distribution of FGs in the stator. As a result, the values of $T^{I}_{\frac{N_{cm}n}{p}}$ and $T^{II}_{\frac{N_{cm}n}{p}}$ can be regarded as identical. Hence, (3.7) can be rewritten by:

$$C_{groupII}{}' = \sum_{n=1,2,3\cdots}^{\infty} T^{I}_{\frac{N_{cm}n}{p}} \sin\left(\frac{N_{cm}n}{p}\alpha + \varphi_{II\frac{N_{cm}n}{p}}\right) \tag{3.8}$$

Fig. 3.8 depicts the cogging torque waveforms of $C_{groupI}{}'$ and $C_{groupII}{}'$ before shifting slot-openings for both the 12-slot/10-pole and 12-slot/14-pole modular PM machines. It can be observed that $C_{groupI}{}'$ and $C_{groupII}{}'$ has the following relationship:

$$C_{groupI}{}'\big|_{\alpha=\alpha_1} = -C_{groupII}{}'\big|_{\alpha=\frac{2\pi}{\frac{Ncm}{p}}-\alpha_1} \tag{3.9}$$

where α_1 is an electrical angle which can be any value depending on the relative position between the stator and rotor of Group I'.

Therefore, based on (3.9), the relation between $C_{groupI}{}'$ and $C_{groupII}{}'$ can be described by (3.10)

$$\begin{aligned}\sum_{n=1,2,3\cdots}^{\infty} T^{I}_{\frac{N_{cm}n}{p}} \sin\left(\frac{N_{cm}n}{p}\alpha_1 + \varphi_{I\frac{N_{cm}n}{p}}\right) \\ = -\sum_{n=1,2,3\cdots}^{\infty} T^{I}_{\frac{N_{cm}n}{p}} \sin\left(\frac{N_{cm}n}{p}\left(\frac{2\pi}{\frac{N_{cm}}{p}} - \alpha_1\right) + \varphi_{II\frac{N_{cm}n}{p}}\right)\end{aligned} \tag{3.10}$$

Equation (3.10) can be derived as:

$$\begin{aligned}\sum_{n=1,2,3\cdots}^{\infty} T^{I}_{\frac{N_{cm}n}{p}} \sin\left(\frac{N_{cm}n}{p}\alpha_1 + \varphi_{I\frac{N_{cm}n}{p}}\right) \\ = -\sum_{n=1,2,3\cdots}^{\infty}\left(T^{I}_{\frac{N_{cm}n}{p}} \sin\left(\frac{N_{cm}n}{p}\times\frac{2\pi}{\frac{N_{cm}}{p}}\right)\cos\left(\varphi_{II\frac{N_{cm}n}{p}}\right.\right. \\ \left.\left. - \frac{N_{cm}n}{p}\alpha_1\right) + \cos\left(\frac{N_{cm}n}{p}\times\frac{2\pi}{\frac{N_{cm}}{p}}\right)\sin\left(\varphi_{II\frac{N_{cm}n}{p}} - \frac{N_{cm}n}{p}\alpha_1\right)\right)\end{aligned} \tag{3.11}$$

Equation (3.11) can be simplified to:

$$\sum_{n=1,2,3\cdots}^{\infty} T^{I}_{\frac{N_{cm}n}{p}} \sin\left(\frac{N_{cm}n}{p}\alpha_1 + \varphi_{I\frac{N_{cm}n}{p}}\right)$$
$$= \sum_{n=1,2,3\cdots}^{\infty} \left(T^{I}_{\frac{N_{cm}n}{p}} \cos\left(\frac{N_{cm}n}{p} \times \frac{2\pi}{\frac{N_{cm}}{p}}\right) \sin\left(\frac{N_{cm}n}{p}\alpha_1 - \varphi_{II\frac{N_{cm}n}{p}}\right)\right) \tag{3.12}$$

(3.12) can be further developed, and hence (3.13) is obtained, as shown in section 3.3.

$$\sum_{n=1,2,3\cdots}^{\infty} T^{I}_{\frac{N_{cm}n}{p}} \sin\left(\frac{N_{cm}n}{p}\alpha_1 + \varphi_{I\frac{N_{cm}n}{p}}\right) = \sum_{n=1,2,3\cdots}^{\infty} T^{I}_{\frac{N_{cm}n}{p}} \sin\left(\frac{N_{cm}n}{p}\alpha_1 - \varphi_{II\frac{N_{cm}n}{p}}\right) \tag{3.13}$$

Then, from (3.13), the relationship between the phases angles of $C_{groupI}{}'$ and $C_{groupII}{}'$ ($\varphi_{I\frac{N_{cm}n}{p}}$ and $\varphi_{II\frac{N_{cm}n}{p}}$) can be obtained:

$$\varphi_{I\frac{N_{cm}n}{p}} = -\varphi_{II\frac{N_{cm}n}{p}} + 2k\pi, k \in Z \tag{3.14}$$

as will be verified in the following sections.

Since the focus of this chapter is not on analytically predicting the cogging torque of modular PM machine but on minimizing the resultant cogging torque, the values of $\varphi_{I\frac{N_{cm}n}{p}}$ and $\varphi_{II\frac{N_{cm}n}{p}}$ have been calculated by FE directly without giving their exact analytical formula. Then, they will be used for the following analysis related to the cogging torque mitigation.

By replacing $\varphi_{II\frac{N_{cm}n}{p}}$ using $\varphi_{I\frac{N_{cm}n}{p}}$ such as described by (3.14), (3.8) becomes:

$$C_{groupII}{}' = \sum_{n=1,2,3\cdots}^{\infty} T^{I}_{\frac{N_{cm}n}{p}} \sin\left(\frac{N_{cm}n}{p}\alpha - \varphi_{I\frac{N_{cm}n}{p}}\right) \tag{3.15}$$

By employing similar expression as for $C_{groupI}{}'$ and $C_{groupII}{}'$, the cogging torque due to

FGs can be written as:

$$C_{FG} = \sum_{n=1,2,3\cdots}^{\infty} T^{III}_{\frac{N_{cm}n}{p}} \times sin(\frac{N_{cm}n}{p}\alpha + \varphi_{III\frac{N_{cm}n}{p}}) \tag{3.16}$$

where $T^{III}_{\frac{N_{cm}n}{p}}$ is the amplitude of the $\frac{N_{cm}n^{th}}{p}$ order harmonic, $\varphi_{III\frac{N_{cm}n}{p}}$ is the electrical phase angle of C_{FG} which can be acquired by Fourier analysis as well. However, by defining the position of one single FG as the reference position, the value of $\varphi_{III\frac{N_{cm}n}{p}}$ can only be equal to 0° or 180° Elec. Deg., and hence the analysis can be simplified.

3.3.2 CALCULATION OF THE DESIRED SHIFTING ANGLE

When the desired shift angle is defined as $\beta_{\frac{N_{cm}n}{p}}$ Elec. Deg., (3.6) and (3.15) are modified as:

$$C_{groupI}{}' = \sum_{n=1,2,3\cdots}^{\infty} T^{I}_{\frac{N_{cm}n}{p}} sin\left(\frac{N_{cm}n}{p}\alpha + \varphi_{I\frac{N_{cm}n}{p}} + \frac{N_{cm}n}{p}\beta_{\frac{N_{cm}n}{p}}\right) \tag{3.17}$$

and

$$C_{groupII}{}' = \sum_{n=1,2,3\cdots}^{\infty} T^{I}_{\frac{N_{cm}n}{p}} sin\left(\frac{N_{cm}n}{p}\alpha - \varphi_{I\frac{N_{cm}n}{p}} - \frac{N_{cm}n}{p}\beta_{\frac{N_{cm}n}{p}}\right) \tag{3.18}$$

By replacing $C_{groupI}{}'$, $C_{groupII}{}'$ and C_{FG} in (3.5) using (3.16)-(3.18) respectively, the resultant cogging torque expression of the modular PM machine can be obtained as:

$$\begin{aligned} C_{total=} & \sum_{n=1,2,3\cdots}^{\infty} T^{I}_{\frac{N_{cm}n}{p}} sin\left(\frac{N_{cm}n}{p}\alpha + \varphi_{I\frac{N_{cm}n}{p}} + \frac{N_{cm}n}{p}\beta_{\frac{N_{cm}n}{p}}\right) \\ & + \sum_{n=1,2,3\cdots}^{\infty} T^{I}_{\frac{N_{cm}n}{p}} sin\left(\frac{N_{cm}n}{p}\alpha - \varphi_{I\frac{N_{cm}n}{p}} - \frac{N_{cm}n}{p}\beta_{\frac{N_{cm}n}{p}}\right) \\ & + \sum_{n=1,2,3\cdots}^{\infty} T^{III}_{\frac{N_{cm}n}{p}} \times sin\left(\frac{N_{cm}n}{p}\alpha + \varphi_{III\frac{N_{cm}n}{p}}\right) \end{aligned} \tag{3.19}$$

Equation (3.19) can be derived further as:

$$C_{total=}\sum_{n=1,2,3\cdots}^{\infty} T^{I}_{\frac{N_{cm}n}{p}}\, 2\,sin\left(\frac{N_{cm}n}{p}\alpha\right) cos\left(\varphi_{I\frac{N_{cm}n}{p}}+\frac{N_{cm}n}{p}\beta_{\frac{N_{cm}n}{p}}\right) + \sum_{n=1,2,3\cdots}^{\infty} T^{III}_{\frac{N_{cm}n}{p}}\times sin\left(\frac{N_{cm}n}{p}\alpha+\varphi_{III\frac{N_{cm}n}{p}}\right) \tag{3.20}$$

After simplifying (3.20), (3.21) is obtained.

$$C_{total}\ =\sum_{n=1,2,3\cdots}^{\infty} sin(\frac{N_{cm}n}{p}\alpha)\left(2T^{I}_{\frac{N_{cm}n}{p}}cos(\varphi_{I\frac{N_{cm}n}{p}}+\frac{N_{cm}n}{p}\beta_{\frac{N_{cm}n}{p}})\pm T^{III}_{\frac{N_{cm}n}{p}}\right) \tag{3.21}$$

When $\varphi_{III\frac{N_{cm}n}{p}}$ equals to 0° Elec. Deg., the value of $T^{III}_{\frac{N_{cm}n}{p}}$ is positive. However, when the value of $\varphi_{III\frac{N_{cm}n}{p}}$ is 180° Elec. Deg., $T^{III}_{\frac{N_{cm}n}{p}}$ will be negative.

Let

$$2T^{I}_{\frac{N_{cm}n}{p}}cos(\varphi_{I\frac{N_{cm}n}{p}}+\frac{N_{cm}n}{p}\beta_{\frac{N_{cm}n}{p}})\pm T^{III}_{\frac{N_{cm}n}{p}}=0, n=1,2,3,\cdots \tag{3.22}$$

the resultant cogging torque can then be mitigated.

As a result, the desired slot-opening shift angle (Elec. Deg.) can be calculated by:

$$\beta_{\frac{N_{cm}n}{p}}=\frac{cos^{-1}\left(\frac{\mp T^{III}_{\frac{N_{cm}n}{p}}}{2T^{I}_{\frac{N_{cm}n}{p}}}\right)-\varphi_{I\frac{N_{cm}n}{p}}}{\frac{N_{cm}n}{p}}=p\times\gamma_{\frac{N_{cm}n}{p}}.n=1,2,3,\cdots \tag{3.23}$$

where $\frac{\mp T^{III}_{\frac{N_{cm}n}{p}}}{2T^{I}_{\frac{N_{cm}n}{p}}}$ can be replaced by μ to simplify the analysis.

It has been found out that in some special cases, the value of μ could exceed the range of arccosine function [-1, 1]. In these cases, the maximum or minimum value of the cosine function, i.e. 1 or -1, will be employed to calculate the desired shift angle. It is found when applying the desired shift angle calculated based on μ=1 or -1, the method can still be efficient to mitigate the resultant cogging torque but the mitigation effect could be unsatisfactory. Another similar phenomenon may appear during the application of this method. For some

cases, the value of desired shift angle is beyond the maximum available shift range of slot-openings. In such cases, the solution will be similar, i.e. the boundary value (maximum achievable slot shift angle) will be applied. It is found that the targeted harmonic of cogging torque can also be reduced.

3.4 CASE STUDY

To validate the proposed method, two typical modular PM machines with different slot/pole number combinations as well as different FG widths, i.e. 12-slot/10-pole and 12-slot/14-pole modular PM machines with 2mm or 4mm FG width, have been adopted as examples. The main parameters of the modular PM machines are listed in Table 3.1.

3.4.1 12-SLOT/10-POLE MODULAR PM MACHINES

3.4.1.1 WITH 2MM FG

a. The First Slot-Opening Shift

With regard to the 12-slot/10-pole modular PM machine, the LCM of $2p$ and N_{FG} is 30. The main coefficients for calculating the desired shift angle are shown in Table 3.2. Two slot shift angles are also given to remove the relevant harmonics in the resultant cogging torque.

TABLE 3.2 DESIRED SHIFT ANGLE AND MAIN COEFFICIENTS (12-SLOT/10-POLE AND FG=2MM)

	n=1	n=2
$T^{I}_{\frac{N_{cm}n}{p}}$ (Nm)	0.17	0.06
$T^{III}_{\frac{N_{cm}n}{p}}$ (Nm)	0.02	0.04
$\varphi_{I\frac{N_{cm}n}{p}}$ (Elec.Deg)	98.29	5.35
$\varphi_{II\frac{N_{cm}n}{p}}$ (Elec.Deg)	-98.30	-5.27
$\varphi_{III\frac{N_{cm}n}{p}}$ (Elec.Deg)	0	180
Desired shift angle (Mech. Deg.)	-0.17	1.03
Original peak cogging torque (Nm)	0.1	0.1
Peak cogging torque with shifting (Nm)	0.08(-20%)	0.22(120%)

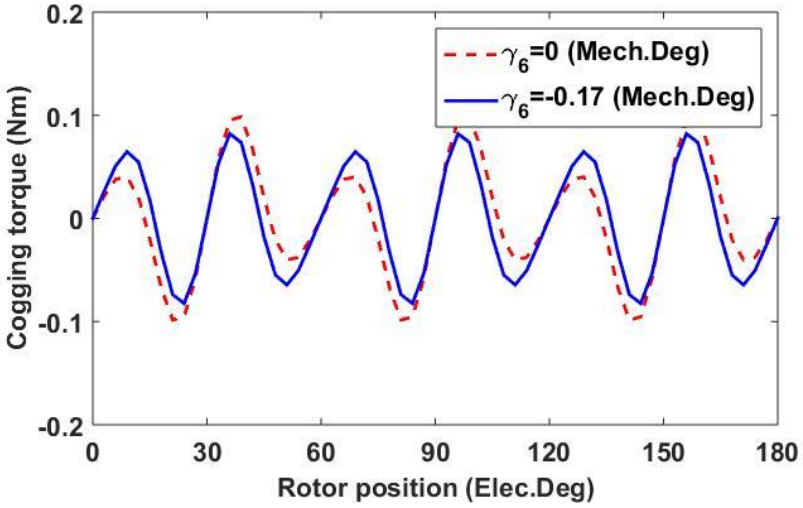

(a)

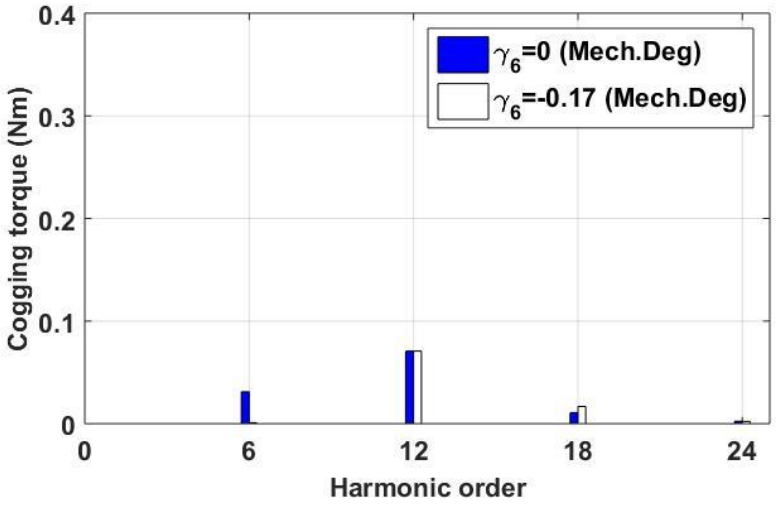

(b)

Fig. 3.9 The reduction of $\frac{N_{cm}}{p}^{th}$ (6^{th}) order harmonic of the resultant cogging torque. (a) Comparison of cogging torque waveforms with or without slot shifting. (b) Spectra. (The machine has 12-slot/10-pole & FG = 2mm.)

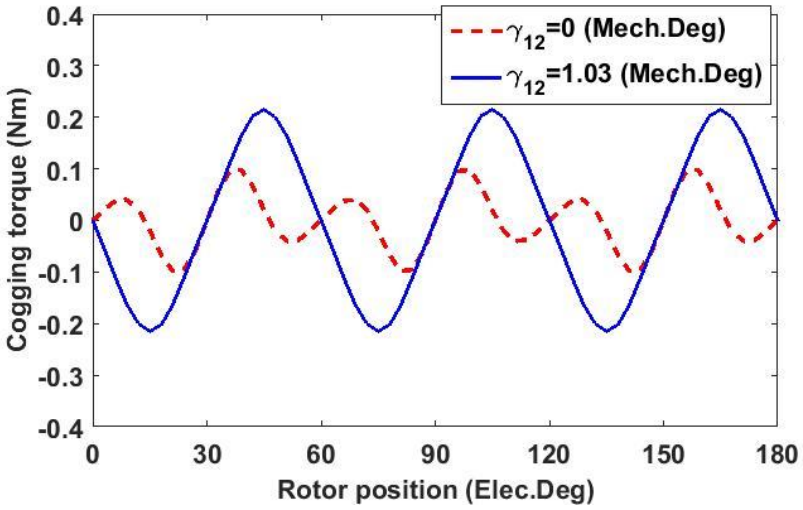

(a)

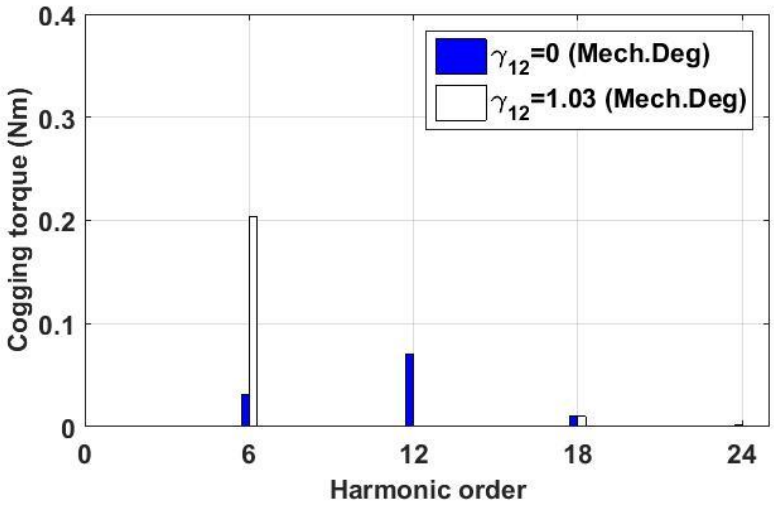

(b)

Fig. 3.10 Reduction of $\frac{N_{cm}\times 2}{p}^{th}$ (12th) order harmonic of the resultant cogging torque. (a) Comparison of cogging torque waveforms with or without slot shifting. (b) Spectra. (The machine has 12-slot/10-pole & FG = 2mm.)

When applying the desired shift angle (-0.17 Mech. Deg.), the targeted $\frac{N_{cm}}{p}^{th}$ (6th) order harmonic is almost eliminated, as shown in Fig. 3.9 (b). This can prove the efficiency of the proposed method for eliminating specific harmonics in cogging torque. However, since the $\frac{N_{cm}\times 2}{p}^{th}$ (12th) order harmonic is dominant in the resultant cogging torque, the mitigation of

resultant cogging torque by only removing the $\frac{N_{cm}}{p}^{th}$ (6^{th}) harmonic is not satisfactory, as shown in Fig. 3.9 (a). Where γ_6 is the desired mechanical shift angle for reducing the 6^{th} order harmonic cogging torque.

Therefore, the question here is why not directly applying the desired shift angle to eliminate the $\frac{N_{cm}\times 2}{p}^{th}$ (12^{th}) order harmonic? This is mainly due to the fact that when focusing on the elimination of the dominant harmonic, the magnitudes of other harmonics are largely out of control due to the interaction between the slot-openings and the FGs. Thus, it is difficult to predict the variation trend of other harmonics after the first slot shifting even if the $\frac{N_{cm}\times 2}{p}^{th}$ (12^{th}) order harmonic can be completely removed. By way of example, if the desired shift angle of 1.03 Mech. Deg. has been chosen, the $\frac{N_{cm}\times 2}{p}^{th}$ (12^{th}) order harmonic is completely eliminated, as shown in Fig. 3.10 (b). Where γ_{12} is the shift angle for reducing 12^{th} order harmonic. However, the amplitude of the $\frac{N_{cm}}{p}^{th}$ (6^{th}) order harmonic is increased dramatically. As a result, the peak cogging torque after shifting the slot-openings becomes even bigger than that of before shifting. In conclusion, the slot-opening shifting method cannot be directly applied to eliminate the $\frac{N_{cm}\times 2}{p}^{th}$ (12^{th}) order harmonic without eliminating the $\frac{N_{cm}}{p}^{th}$ (6^{th}) order harmonic first.

b. The Second Slot-Opening Shift

In order to reduce the dominant order harmonic (12^{th}), the second shift of slot-openings based on the first shift is necessary. However, after the first shift, the symmetry of the modular PM machines has been changed. This means that for the second shift of slot-openings, the groups need to be re-arranged, as shown in Fig. 3.11. The 6 FGs are numbered from FG1 to FG6. Similar grouping method has been proposed in [87]. The re-arranged 2 groups have the same shift angle but shift in the opposite directions as well. Similar to the first shift, the following equation can be derived.

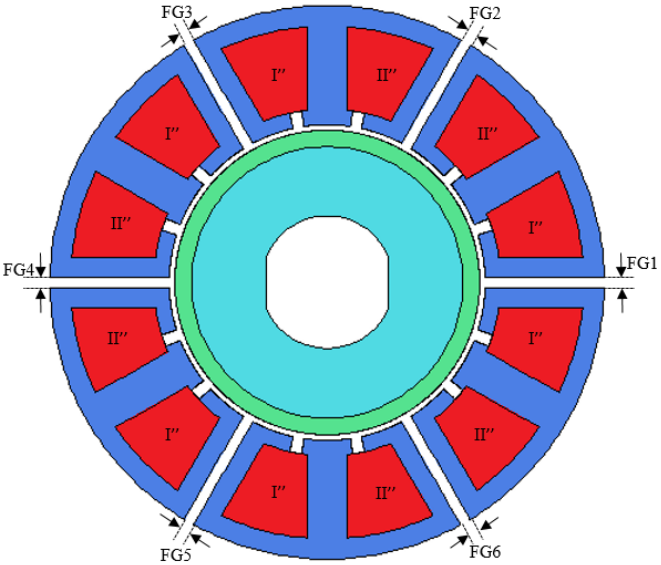

Fig. 3.11 Machine cross section after the first shift to eliminate the $\frac{N_{cm}}{p}^{th}$ (6^{th}) order harmonic in cogging torque.

$$\left(C''_{groupI} - C_{FG135}\right) + \left(C''_{groupII} - C_{FG246}\right) + C_{FG123456} = C''_{total} \tag{3.24}$$

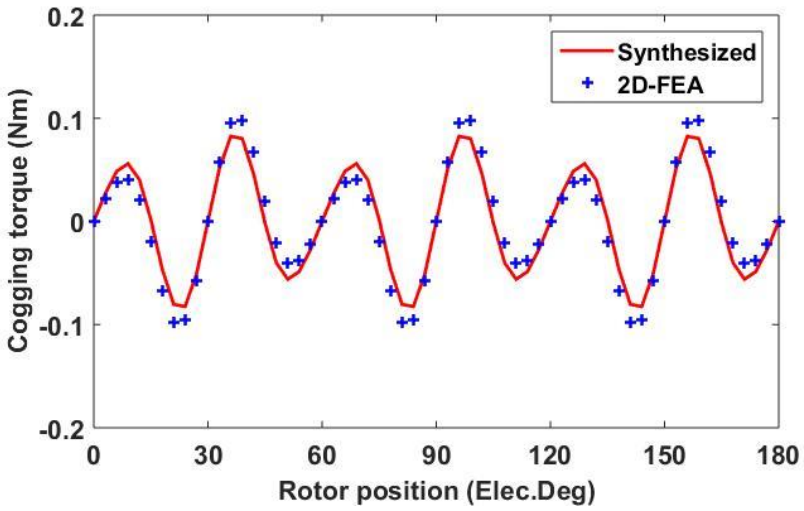

Fig. 3.12 Comparison of synthesized and direct FE calculated cogging torque waveforms before second shift based on (3.24). (12-slot/10-pole & FG=2mm).

The waveforms of the cogging torque obtained by direct FE and by the synthesis method based on (3.24) are compared in Fig. 3.12. An acceptable agreement can be observed with minor discrepancy between the amplitudes (the phases of two cogging torques are exactly the same), which will not compromise the mitigation effectiveness.

The second shift angle is calculated by (3.23) as well. After shifting the slot-openings of two groups in opposite directions with the calculated shift angle (1.03 Mech. Deg.), the synthesized cogging torque waveform of slot-openings is almost the mirror image of the cogging torque waveform due to the FGs, as shown in Fig. 3.13 (a), where γ_6 and γ_{12} represent the shift angles for reducing the first two harmonics by employing the second shift based on the first shift.

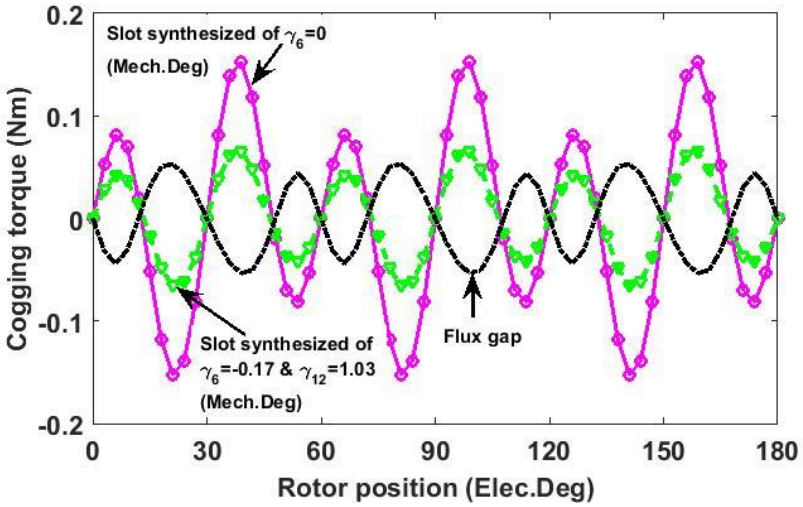

(a)

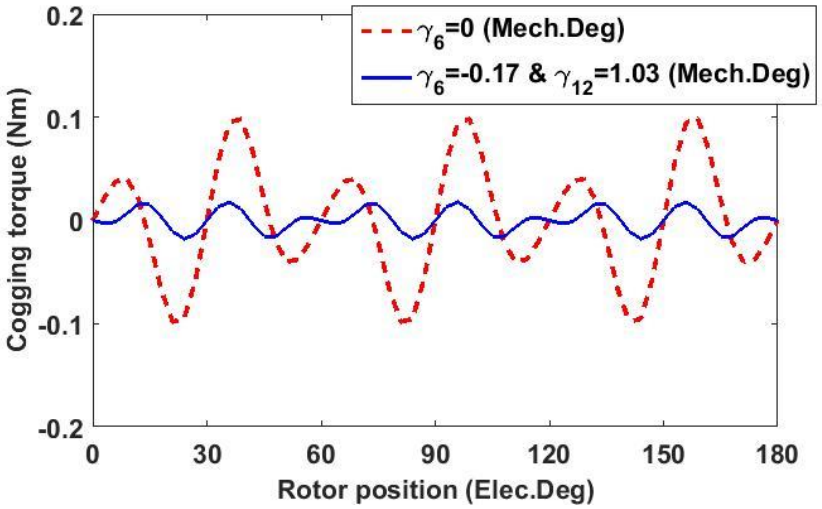

(b)

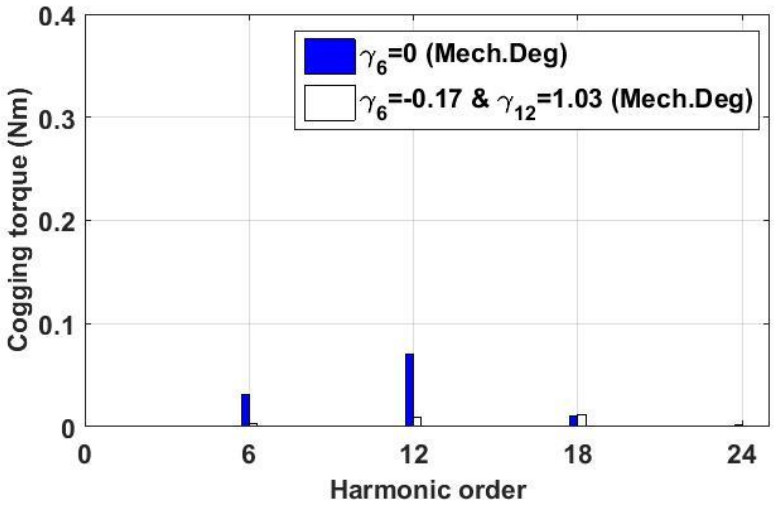

(c)

Fig. 3.13 Reduction of the first two order harmonics of the resultant cogging torque. (a) Cogging torque waveforms of FGs and slot-openings before and after the slot-opening shift. (b) Comparison of resultant cogging torque waveforms. (b) Spectra. (12-slot/10-pole & FG=2mm).

As a result, the resultant peak-to-peak cogging torque is reduced by ~82% after the second shift of slot-openings. However, it is worth mentioning that unless the higher order harmonics are dominant, the second shift is not necessary due to its complexity, such as the case for 12-slot/14-pole in the following section.

c. Back-EMF and On-Load Toque

The back-EMF waveforms of modular PM machines with 2mm FG before and after shift are shown in Fig. 3.14. Here, only the results for phase A are given, for phases B and C, the EMFs of which have the same amplitude but with a phase shift angle of 120 Elec. Deg. It is found that the value of the fundamental decreases slightly, so do the other harmonics. However, this influence on phase back-EMF remains largely negligible for this case, which is different from the stator or rotor skewing method. The tiny decrease in phase back-EMF leads to the decrease in average torque slightly from 5.33 Nm to 5.29 Nm, as shown in Fig. 3.15.

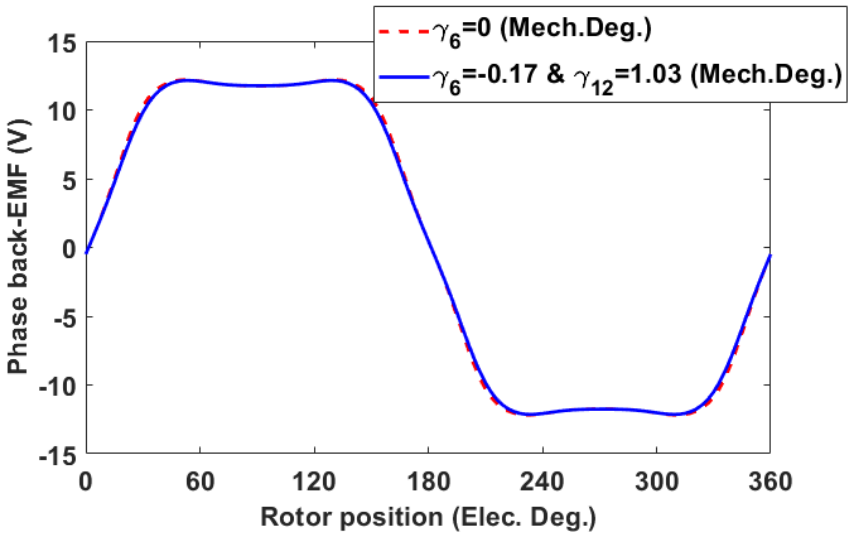

(a)

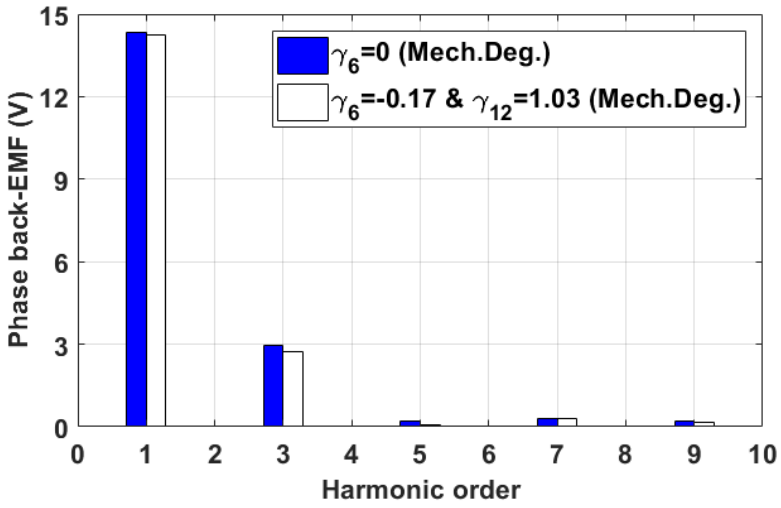

(b)

Fig. 3.14 Phase back-EMFs before and after the slot-opening shift. (a) Waveforms. (b) Spectra (12-slot/10-pole & FG=2mm at 400 rpm).

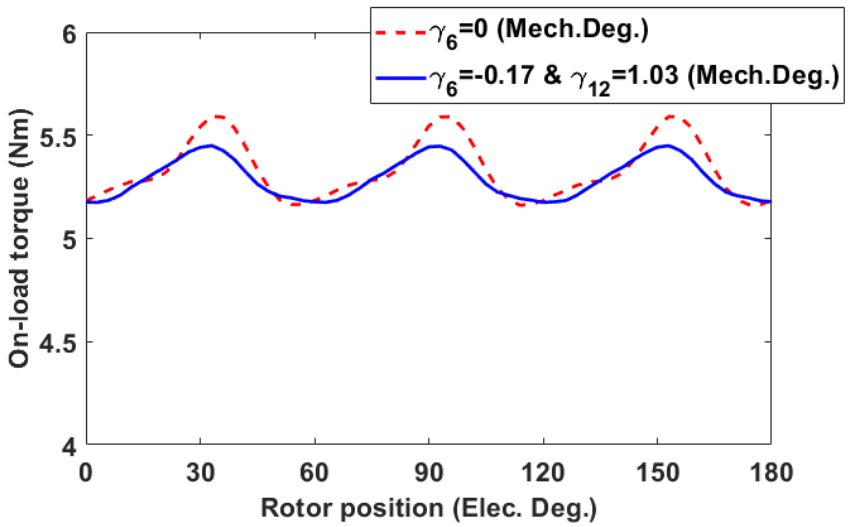

Fig. 3.15 The on-load torque waveforms of the modular PM machine before and after the slot-opening shift (12-slot/10-pole & FG=2mm).

3.4.1.2 WITH 4MM FG

a. The First Slot-Opening Shift

TABLE 3.3 DESIRED SHIFT ANGLE AND MAIN COEFFICIENTS (12-SLOT/10-POLE AND FG=4MM)

	n=1	n=2
$T^{I}_{\frac{N_{cm}n}{p}}$ (Nm)	0.18	0.06
$T^{III}_{\frac{N_{cm}n}{p}}$ (Nm)	0.41	0.04
$\varphi_{I\frac{N_{cm}n}{p}}$ (Elec.Deg)	102.24	8.06
$\varphi_{II\frac{N_{cm}n}{p}}$ (Elec.Deg)	-102.3	-8.09
$\varphi_{III\frac{N_{cm}n}{p}}$ (Elec.Deg)	180	180
Desired shift angle (Mech. Deg.)	-3.41	-
Original peak cogging torque (Nm)	1.04	1.04
Peak cogging torque with shifting (Nm)	0.36(-65%)	-

The main coefficients for calculating the desired shift angle of the 12-slot/10-pole modular PM machine with 4mm FG are listed in Table 3.3. For this case, the value of μ exceeds the range of arccosine function [-1, 1], hence, the value of μ is selected as 1. Therefore, the desired shift angle is calculated as -3.41 Mech. Deg.

As can be seen from Fig. 3.16, the target cogging torque harmonic still can be mitigated efficiently and the resultant peak-to-peak cogging torque is reduced by -65% from 1.04 Nm to just 0.36 Nm.

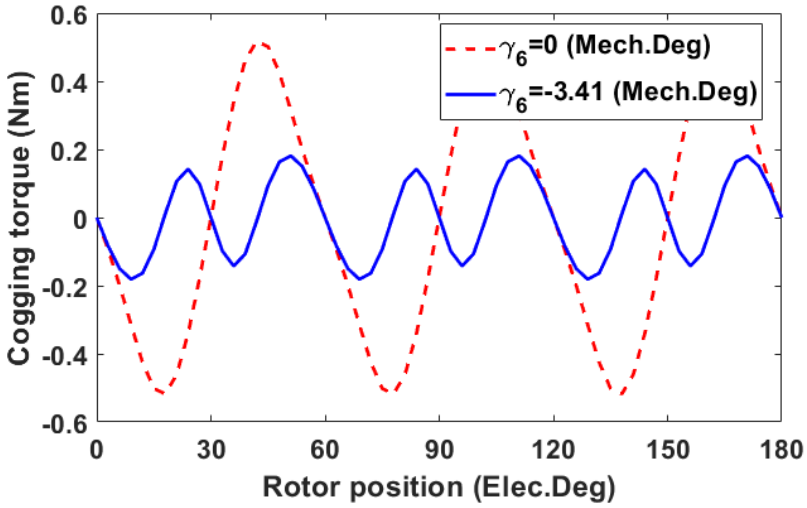

(a)

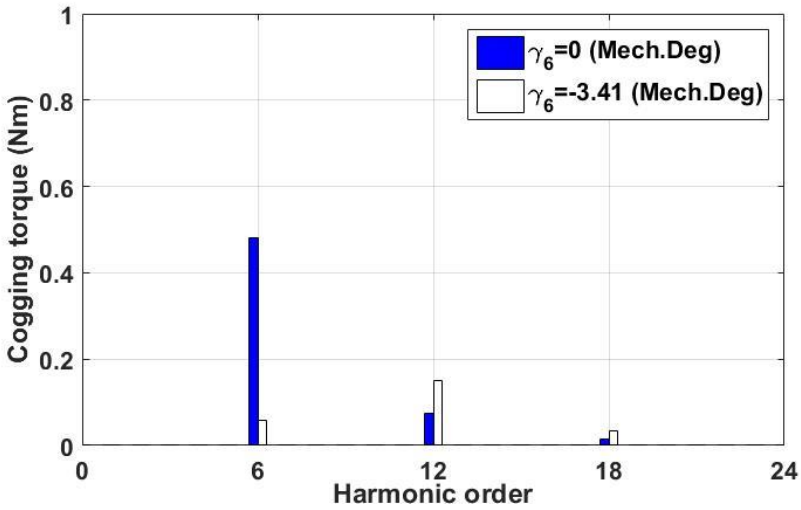

(b)

Fig. 3.16 Reduction of $\frac{N_{cm}}{p}^{th}$ (6^{th}) order harmonic of the resultant cogging torque. (a) Comparison of cogging torque waveforms with or without slot shifting. (b) Spectra. (The machine has 12-slot/10-pole & FG = 4mm.)

b. Back-EMF and On-Load Torque

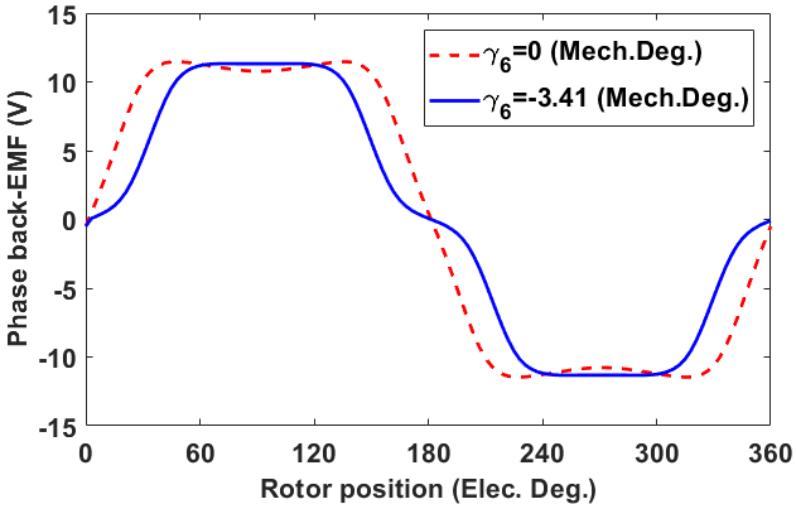

(a)

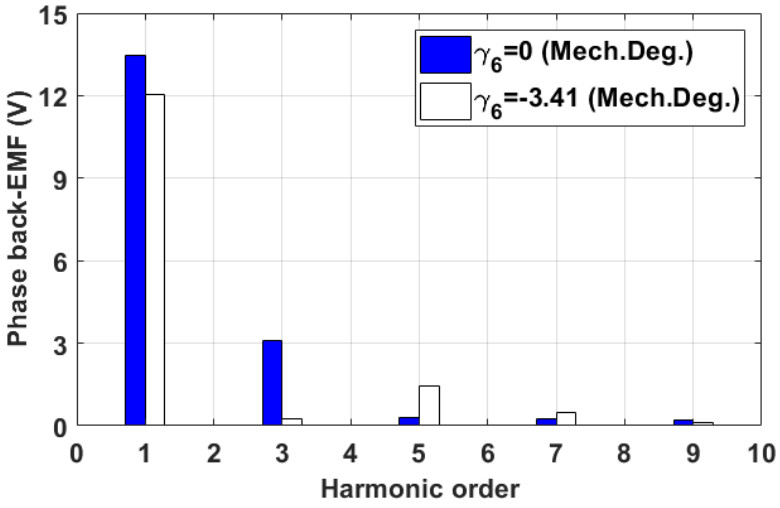

(b)

Fig. 3.17 Phase back-EMFs before and after the slot-opening shift. (a) Waveforms. (b) Spectra (12-slot/10-pole & FG=4mm at 400 rpm).

In Fig. 3.17, the back-EMF waveforms and their spectra of modular PM machines with 4mm FGs before and after slot-opening shift are depicted. Again, only the results for phase A are given. It can be found that the value of the fundamental harmonic of the phase back-EMF decreases from 13.37 V to 12.05 V, which results in the decrease in average torque from 5.01 Nm to 4.48 Nm, as shown in Fig. 3.18. This decrease in phase back-EMF is mainly due to the

relatively bigger reduction in winding factor caused by the slot-opening shift. Thus, in practice, the compromise between reducing the cogging torque and phase back-EMF needs to be considered for this case. Moreover, similar to the previous case studied, there are no extra orders of harmonic introduced and the balance of 3-phase back-EMF waveforms is also maintained.

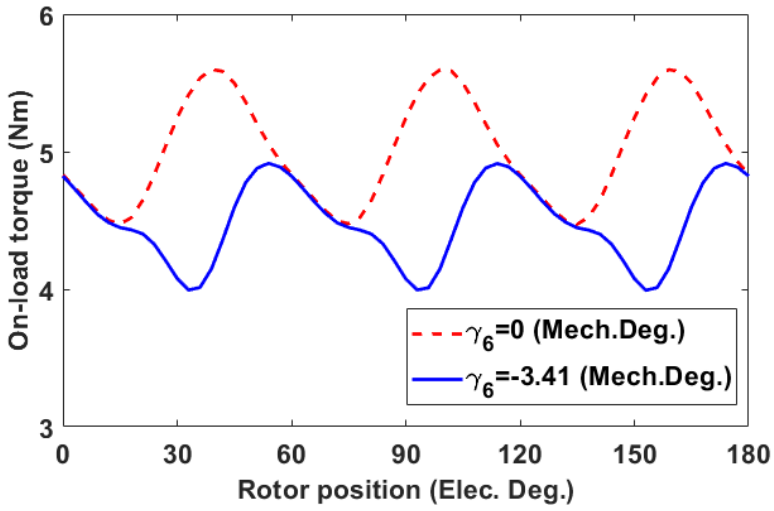

Fig. 3.18 The on-load torque waveforms of the modular PM machine before and after the slot-opening shift (12-slot/10-pole & FG=4mm).

3.4.1.3 WITH DIFFERENT SLOT-OPENING WIDTHS

Fig. 3.19 shows the peak cogging torque versus shift angles and FG widths of the 12-slot/10-pole modular PM machine with various slot-opening widths. It can be found that for different FG and slot-opening widths, although the slot-opening shift angles are different, the proposed method can always be used to reduce the resultant cogging torque effectively. Nevertheless, for the case such as slot-opening=1mm and FG=5mm, the cogging torque reduction is limited. This is mainly due to the fact the resultant cogging torque of the slot-opening is much smaller than that due to the FGs. As a result, they cannot cancel each other.

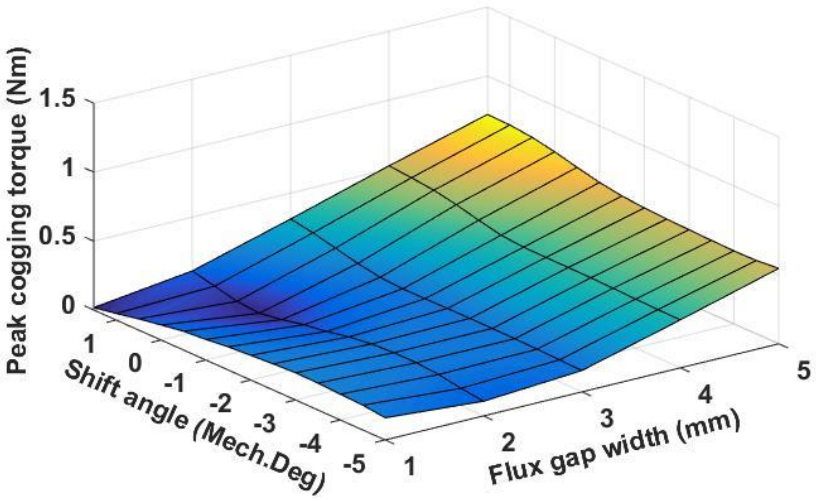
Peak cogging torque (Nm)
1.5
1
0.5
0
1
0
-1
-2
-3
-4
-5
Shift angle (Mech.Deg)
1
2
3
4
5
Flux gap width (mm)

(a)

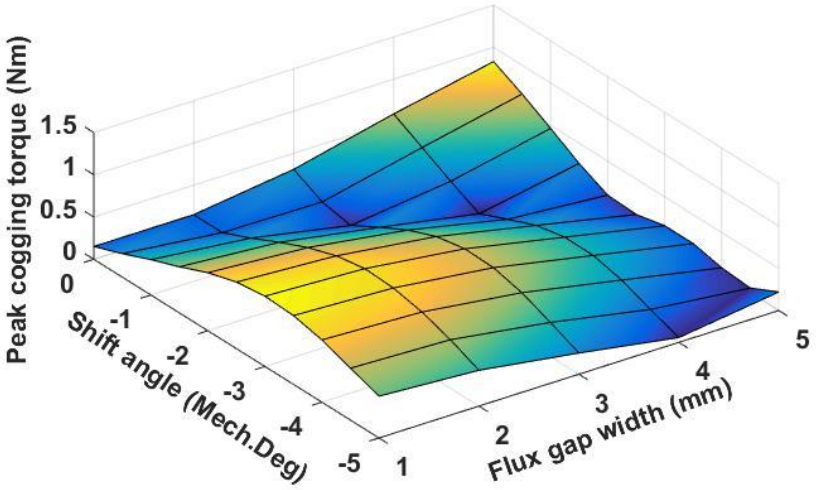
Peak cogging torque (Nm)
1.5
1
0.5
0
0
-1
-2
-3
-4
-5
Shift angle (Mech.Deg)
1
2
3
4
5
Flux gap width (mm)

(b)

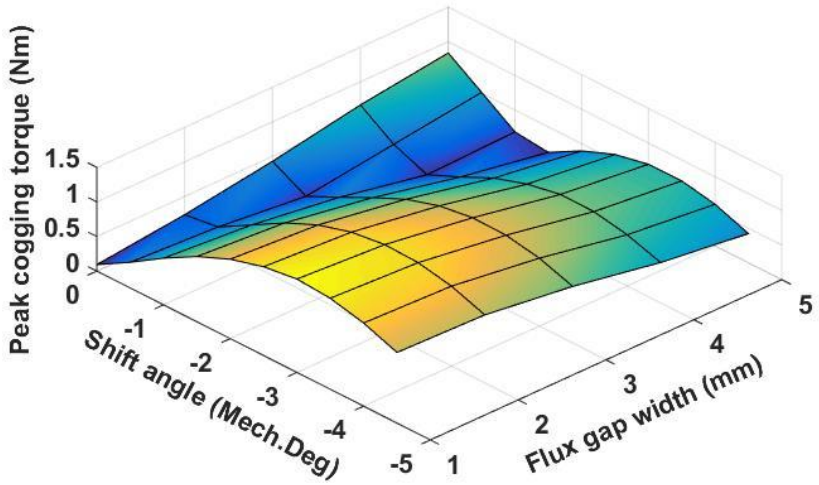

(c)

Fig. 3.19 Peak cogging torque vs FG widths and shift angles of 12-slot/10-pole modular PM machine. (a) Slot-opening=1mm. (b) Slot-opening=3mm. (c) Slot-opening=5mm.

3.4.2 12-SLOT/14-POLE MODULAR PM MACHINES

3.4.2.1 WITH 2MM FG

a. The First Slot-Opening Shift

Another typical slot/pole number combination that has been widely investigated in literature is the 12-slot/14-pole. For this machine, the N_{cm} is 42. Using previously mentioned methods, the main parameters of calculating the desired shift angle have been achieved and listed in Table 3.4.

For the 12-slot/14-pole modular PM machine with 2 mm FGs, the $\frac{N_{cm}}{p}^{th}$ (6^{th}) order harmonic is the most dominant one. Therefore, only the first shift is necessary to mitigate its resultant cogging torque. When the desired shift angle for cancelling the $\frac{N_{cm}}{p}^{th}$ (6^{th}) order harmonic is applied, the cogging torque waveforms synthesized from slot-openings (under the effect of FGs) is almost opposite to that produced by the FGs, as shown in Fig. 3.20 (a). As a result, the amplitude of the $\frac{N_{cm}}{p}^{th}$ (6^{th}) order harmonic can be significantly decreased. Furthermore, the $\frac{N_{cm}\times 2}{p}^{th}$ order harmonic is reduced slightly at the same time. Consequently, a 85% reduction

in the resultant cogging torque has been achieved.

TABLE 3.4 DESIRED SHIFT ANGLE AND MAIN COEFFICIENTS (12-SLOT/14-POLE AND FG=2MM)

	n=1	n=2
$T^{I}_{\frac{N_{cm}n}{p}}$ (Nm)	0.18	0.02
$T^{III}_{\frac{N_{cm}n}{p}}$ (Nm)	0.09	0.02
$\varphi_{I\frac{N_{cm}n}{p}}$ (Elec.Deg)	-94.5	-2.32
$\varphi_{II\frac{N_{cm}n}{p}}$ (Elec.Deg)	94.48	2.41
$\varphi_{III\frac{N_{cm}n}{p}}$ (Elec.Deg)	180	180
Desired shift angle (Mech. Deg.)	-4.55	-
Original peak cogging torque (Nm)	0.13	0.13
Peak cogging torque with shifting (Nm)	0.02(-85%)	-

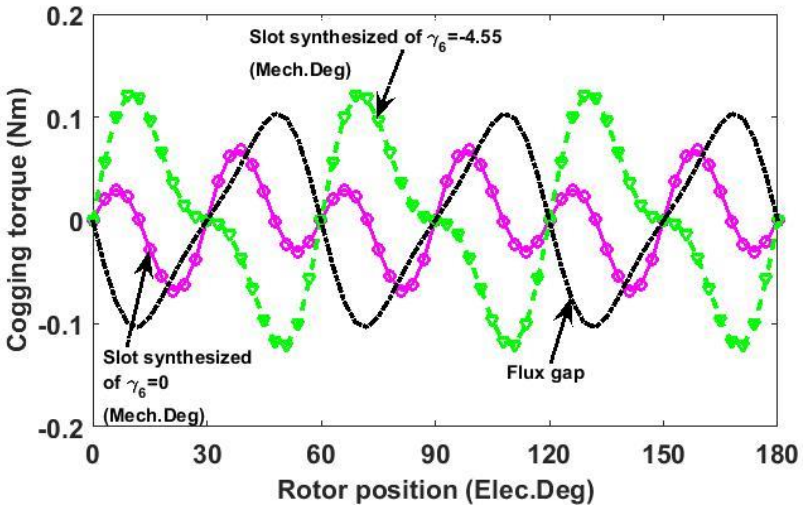

(a)

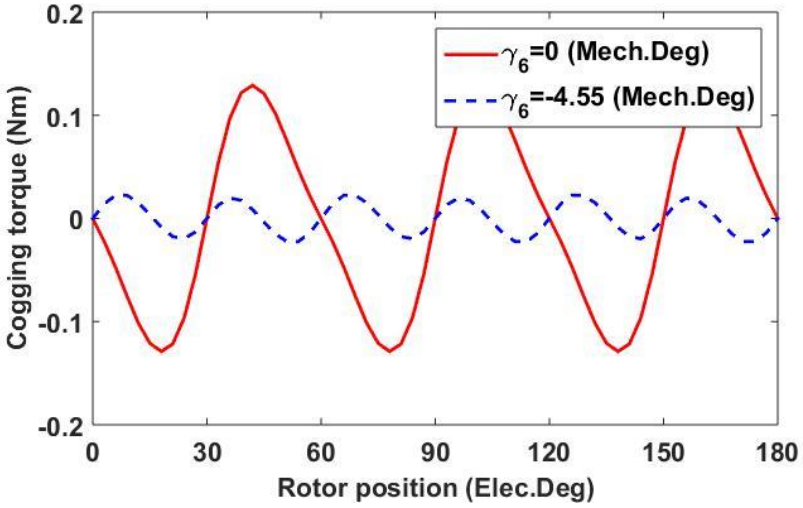

(b)

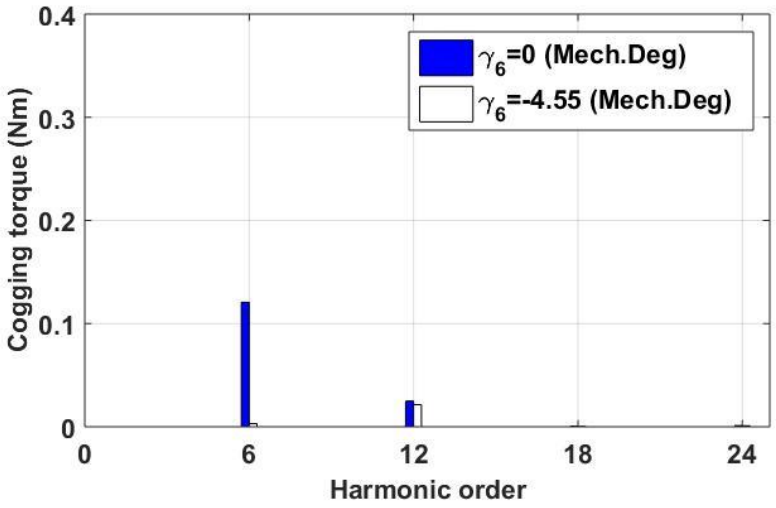

(c)

Fig. 3.20 Reduction of the first two order harmonic of the resultant cogging torque. (a) Cogging torque waveforms of FGs and slot-openings before and after shifting. (b) Comparison of resultant cogging torque waveforms. (b) Spectra. (12-slot/14-pole & FG=2mm).

b. Back-EMF and On-Load Torque

Fig. 3.21 compares the waveforms of back-EMF before and after applying the slot-opening shift. Again, only the results of the phase A are given. The shift of slot-openings weakens the magnitude of the fundamental back-EMF leading to potential decrease in the average torque from 6.33 Nm to 6.06 Nm, as shown in Fig. 3.22. The reason for the decrease in the

fundamental harmonic of the phase back-EMF and also the average torque has been demonstrated in section 3.4.1.2 b. Similarly, there are no extra harmonics introduced into the phase back-EMF after slot-opening shifting and the three-phase back-EMFs still remain balanced.

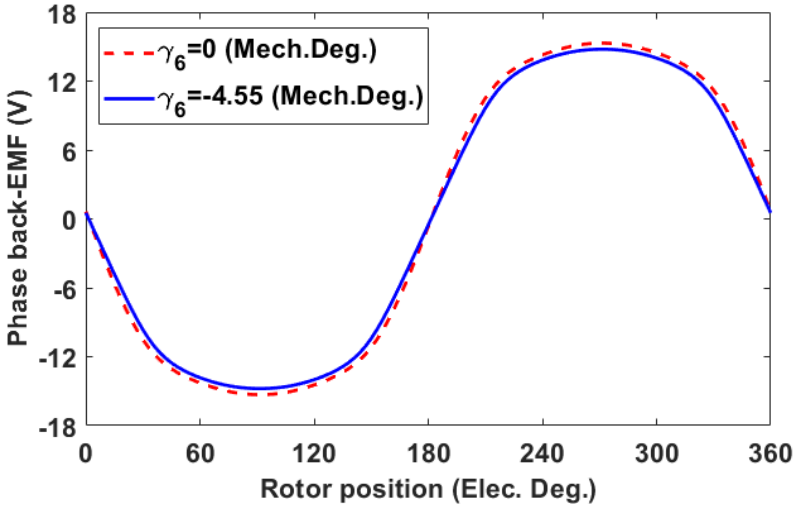

(a)

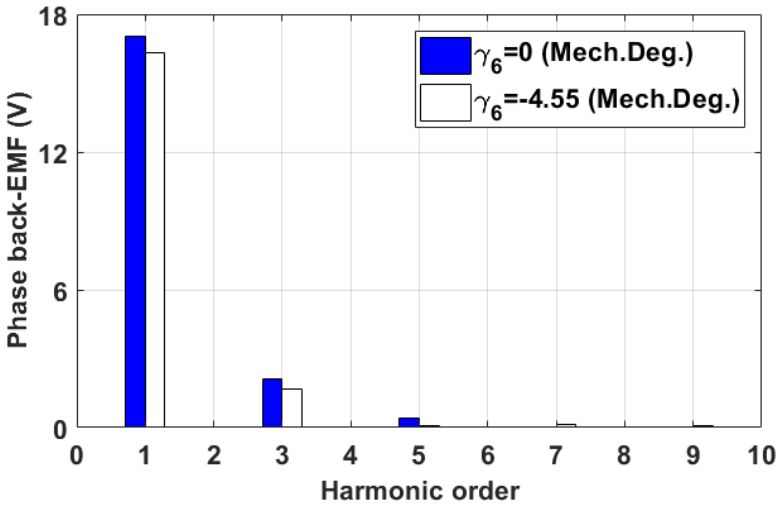

(b)

Fig. 3.21 Phase back-EMFs before and after the slot-opening shift. (a) Waveforms of phase A. (b) Spectra. (12-slot/14-pole & FG=2mm at 400rpm)

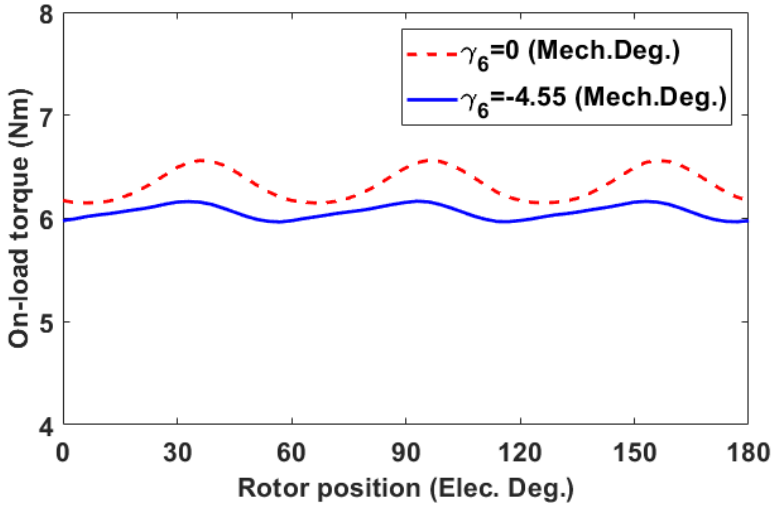

Fig. 3.22 The on-load torque waveforms of the modular PM machine before and after the slot-opening shift (12-slot/14-pole & FG=2mm).

3.4.2.2 WITH 4MM FG

a. The First Slot-Opening Shift

TABLE 3.5 DESIRED SHIFT ANGLE AND MAIN COEFFICIENTS (12-SLOT/14-POLE AND FG=4MM)

	n=1	n=2
$T^{I}_{\frac{N_{cm}n}{p}}$ (Nm)	0.18	0.02
$T^{III}_{\frac{N_{cm}n}{p}}$ (Nm)	0.34	0.02
$\varphi_{I\frac{N_{cm}n}{p}}$ (Elec.Deg)	-95.4	-3.49
$\varphi_{II\frac{N_{cm}n}{p}}$ (Elec.Deg)	95.39	3.48
$\varphi_{III\frac{N_{cm}n}{p}}$ (Elec.Deg)	180	0
Desired shift angle (Mech. Deg.)	-5.99	-
Original peak cogging torque (Nm)	0.74	0.74
Peak cogging torque with shifting (Nm)	0.1(-86%)	-

For the case of the 12-slot/14-pole modular PM machine with 4mm FG, the main coefficients for calculating the desired shift angle are shown in Table 3.5. The desired shift angle is -5.99 Mech. Deg. and the resultant cogging torque waveforms as well as their spectra before and after the slot-opening shift are depicted in Fig. 3.8. As a result, the peak-to-peak

cogging torque can be reduced effectively by 86%.

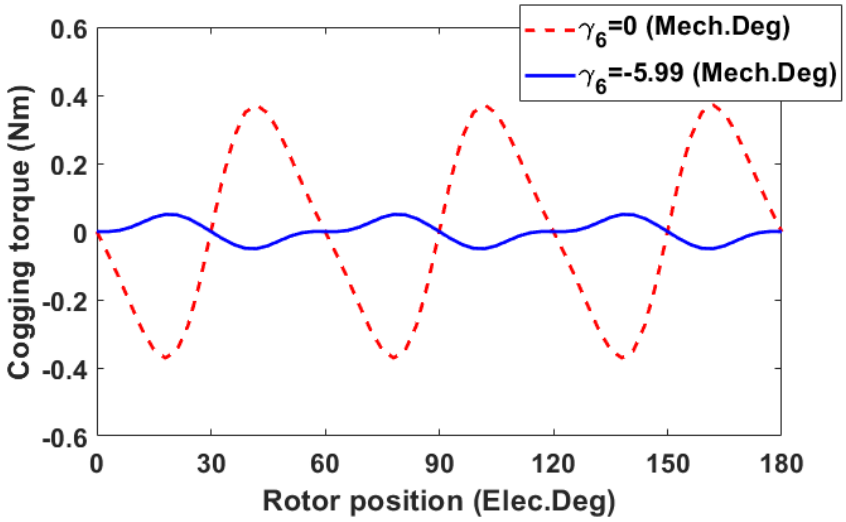

(a)

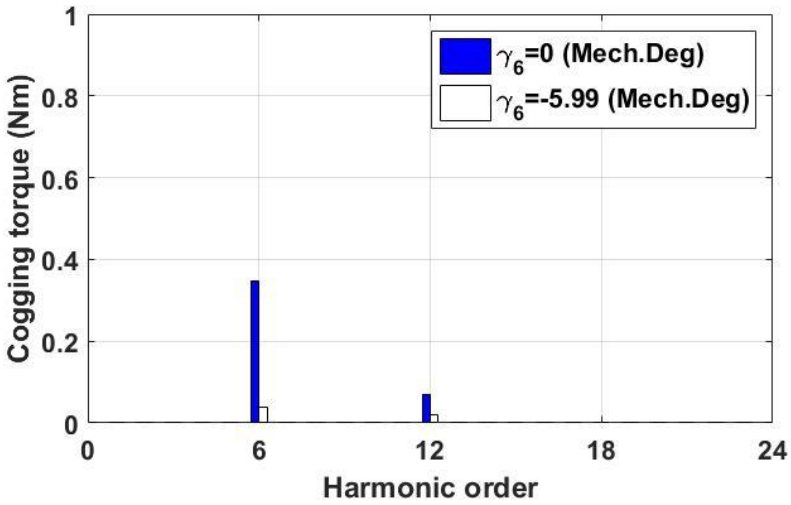

(b)

Fig. 3.23 Reduction of $\frac{N_{cm}\times 1^{st}}{p}$ (6^{th}) order harmonic of the resultant cogging torque. (a) Comparison of cogging torque waveforms with or without slot shifting. (b) Spectra. (The machine has 12-slot/14-pole & FG = 4mm.)

b. Back-EMF and On-Load Torque

The back-EMF waveforms before and after the slot-opening shift are compared in Fig. 3.24. Again, only the results of the phase A are given. The magnitude of the fundamental back-EMF

are weakened due to the slot-opening shift which leading to the reduction in the average torque from 6.47 Nm to 5.7 Nm, as shown in Fig. 3.25.

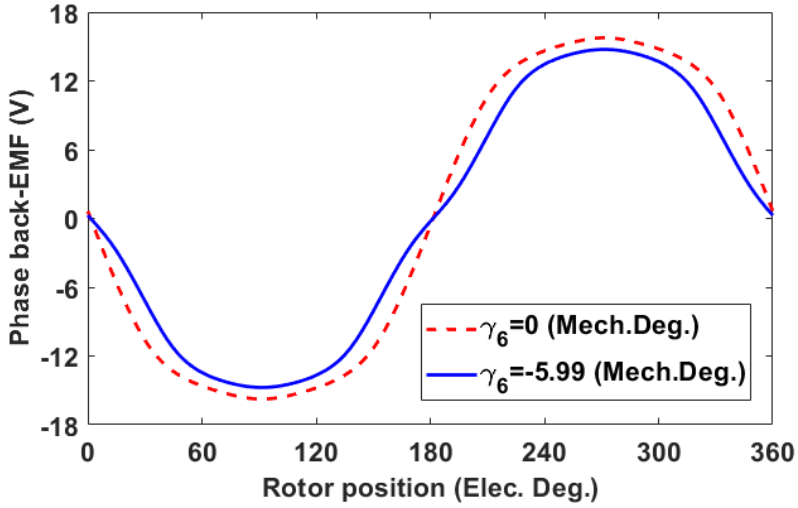

(a)

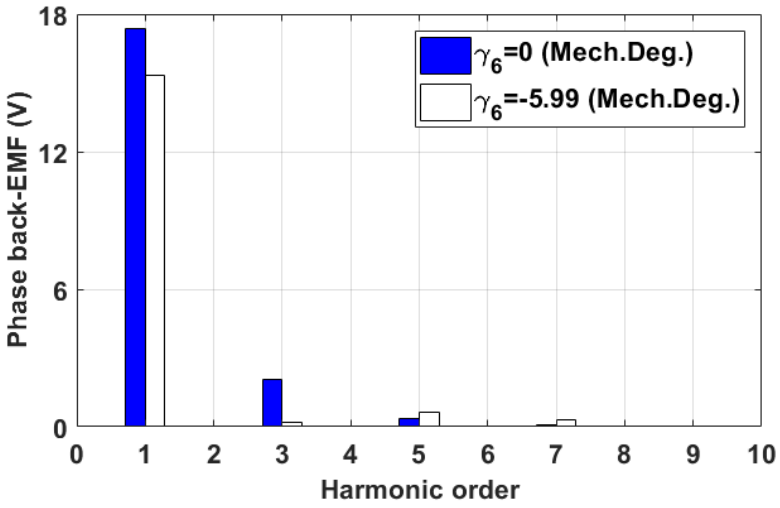

(b)

Fig. 3.24 Phase back-EMFs before and after the slot-opening shift. (a) Waveforms of phase A. (b) Spectra. (12-slot/14-pole & FG=4mm at 400rpm).

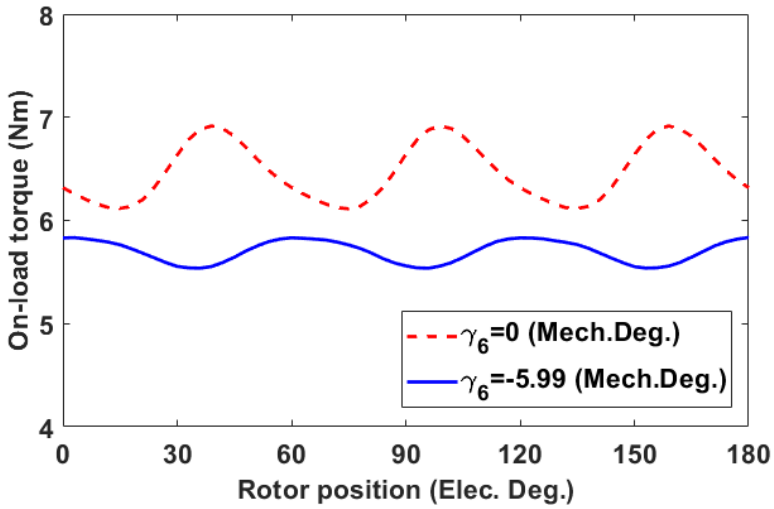

Fig. 3.25 The on-load torque waveforms of the modular PM machine before and after the slot-opening shift (12-slot/14-pole & FG=4mm).

3.4.2.3 WITH DIFFERENT SLOT-OPENING WIDTHS

Peak cogging torque versus shift angles and FG widths of the 12-slot/14-pole modular PM machine with various slot-opening widths are shown in Fig. 3.26. Again, as for the 12-slot/10-pole modular machines, the slot-opening shift method can be applied to effectively reduce the resultant cogging torque. Other slot/pole number combinations have also been investigated. However, they are not presented to avoid repetition. It can be concluded that the proposed method can be applicable for different modular machines with different slot/pole number combinations, FG width, slot-opening widths, etc. Although for some specific topologies, the reduction by employing the proposed method may not be as significant as expected. This is mainly due to the difference between the cogging torque produced by FGs and that could be potentially achieved by synthesising the cogging of individual slot-openings.

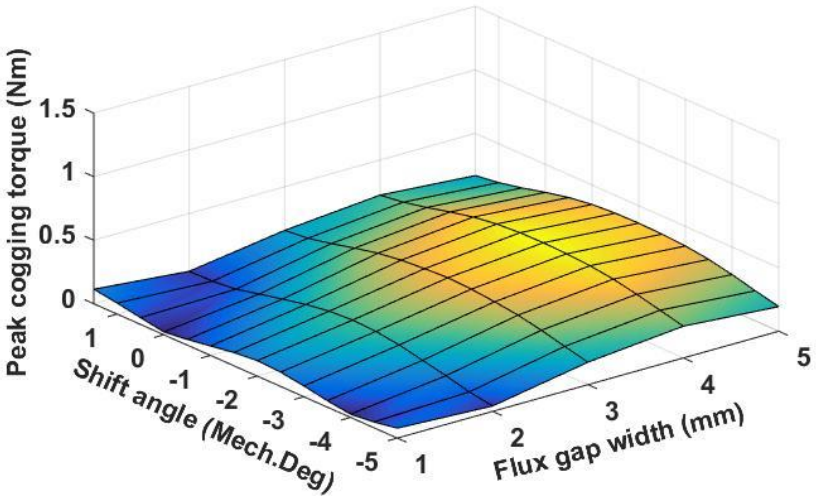
Peak cogging torque (Nm)
1.5
1
0.5
0
1
0
-1
-2
-3
-4
-5
Shift angle (Mech.Deg)
1
2
3
4
5
Flux gap width (mm)

(a)

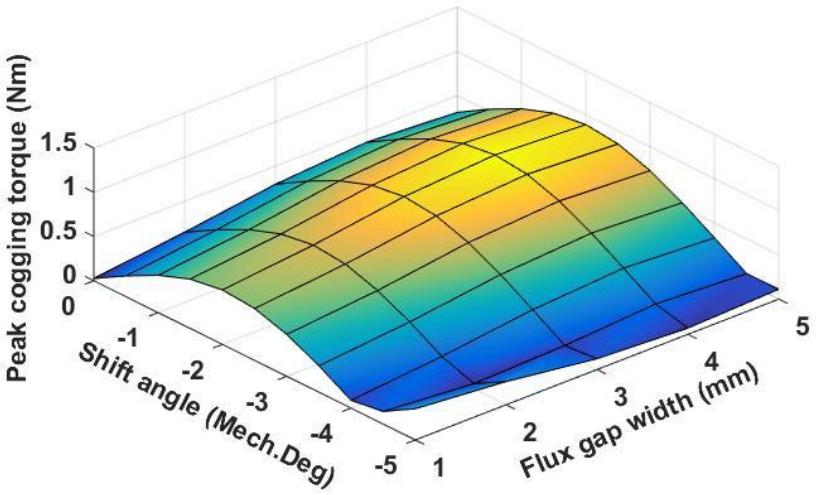
Peak cogging torque (Nm)
1.5
1
0.5
0
0
-1
-2
-3
-4
-5
Shift angle (Mech.Deg)
1
2
3
4
5
Flux gap width (mm)

(b)

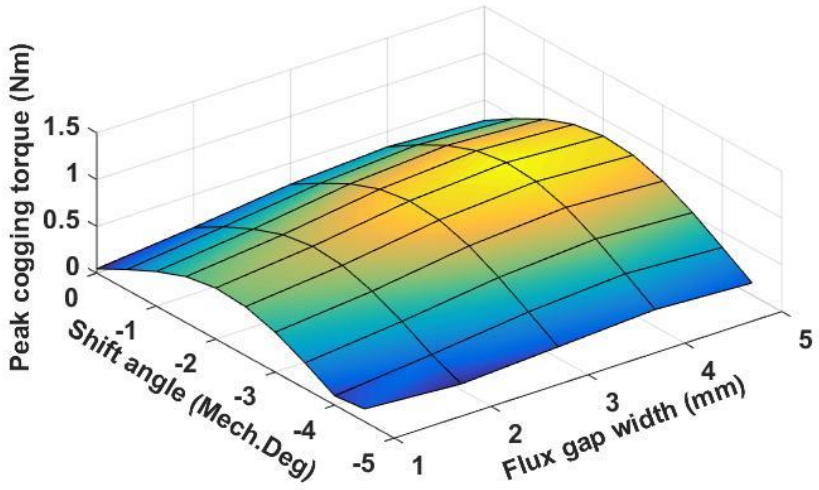

(c)

Fig. 3.26 Peak cogging torque versus FG widths and shift angles of 12-slot/14-pole modular PM machine. (a) Slot-opening=1mm. (b) Slot-opening=3mm. (c) Slot-opening=5mm.

3.4.3 COGGING TORQUE MITIGATION ACCOUNTING FOR MAGNETIC SATURATION

It is well known that the local magnetic saturation has important influence on the cogging torque. Therefore, the following section is dedicated to investigate its influence on the proposed method. By way of example, the 12-slot/10-pole modular PM machine with 2mm FGs has been adopted. The main calculation parameters accounting for magnetic saturation are listed in Table 3.6

The cogging torques before and after the first slot-opening shift have been calculated using non-linear 2D FE, as shown in Fig. 3.27. It can be seen that although the targeted harmonic reduction is not as good as linear case, the resultant cogging torque can be reduced even more due to the influence of saturation (45% for non-linear against 20% for linear). This can show the effectiveness of the proposed cogging torque mitigation method.

The phase back-EMF waveforms and their spectra accounting for the magnetic saturation effect of the modular PM machines before and after the first and second slot-opening shifts are depicted in Fig. 3.27. Similar to the results obtained by the linear 2D FE model, the fundamental phase back-EMF is slightly decreased from 13.61 V to 13.28 V. This will lead to a slight

decrease in the average torque from 4.91 Nm to 4.83 Nm, as shown in Fig. 3.29. Moreover, the torque ripple is decreased from 0.59 Nm to 0.45 Nm, which means that the proposed cogging torque reduction method for the modular PM machines in this chapter could also help to mitigate the torque ripple.

TABLE 3.6 DESIRED SHIFT ANGLE AND MAIN COEFFICIENTS (CLASSIC 12-SLOT/10-POLE MODULAR PM MACHINE AND FG=2MM)

	n=1	n=2
$T^{I}_{\frac{N_{cm}n}{p}}$ (Nm)	0.17	0.05
$T^{III}_{\frac{N_{cm}n}{p}}$ (Nm)	0.02	0.04
$\varphi_{I\frac{N_{cm}n}{p}}$ (Elec.Deg)	120	81.78
$\varphi_{II\frac{N_{cm}n}{p}}$ (Elec.Deg)	-120	-82.2
$\varphi_{III\frac{N_{cm}n}{p}}$ (Elec.Deg)	0	180
Desired shift angle (Mech. Deg.)	-0.91	-0.3
Original peak cogging torque (Nm)	0.2	0.2
Peak cogging torque with shifting (Nm)	0.11(-45%)	-

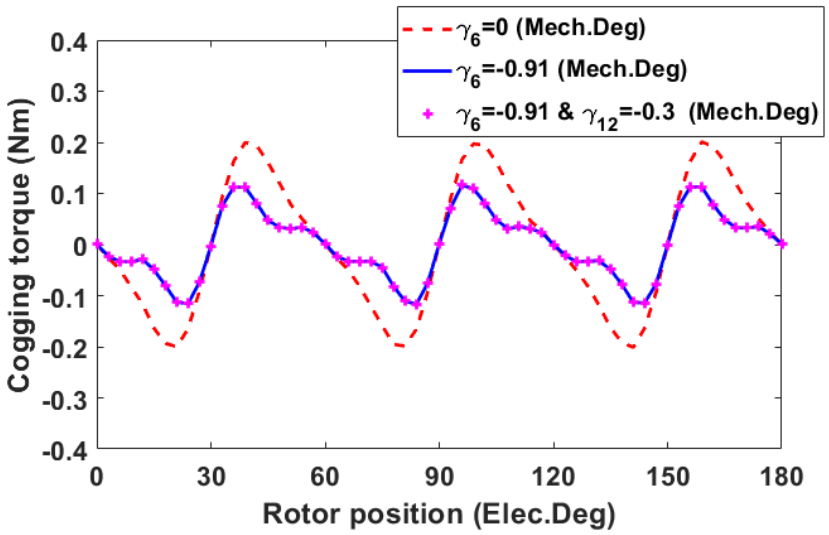

(a)

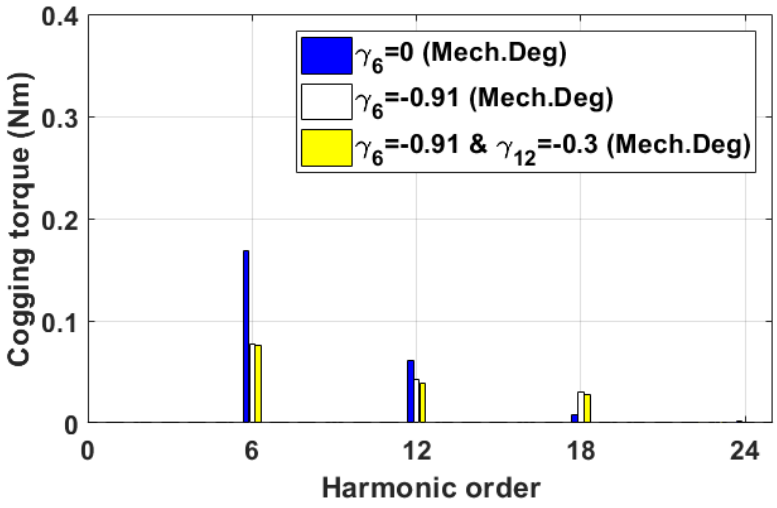

(b)

Fig. 3.27 Reduction of the resultant cogging torque obtained by non-linear 2D FE. (a) Comparison of cogging torque waveforms with or without slot shifting. (b) Spectra (12-slot/10-pole & FG=2mm).

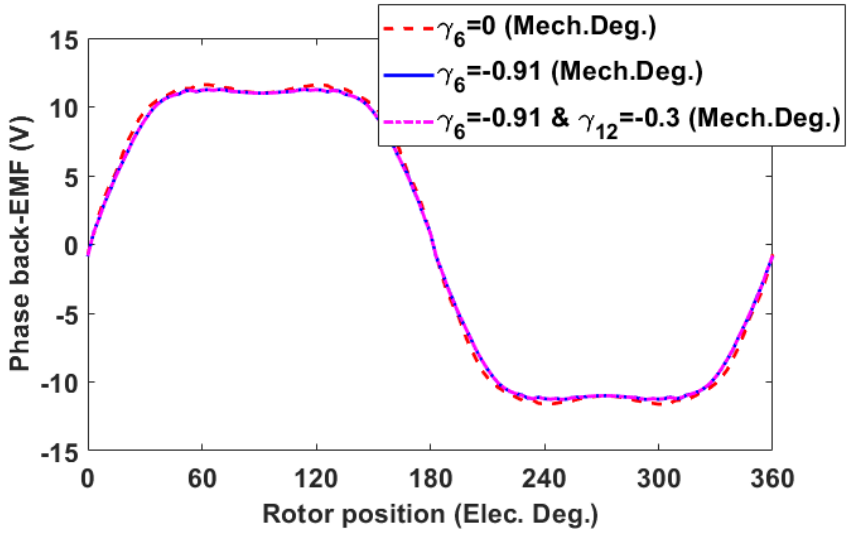

(a)

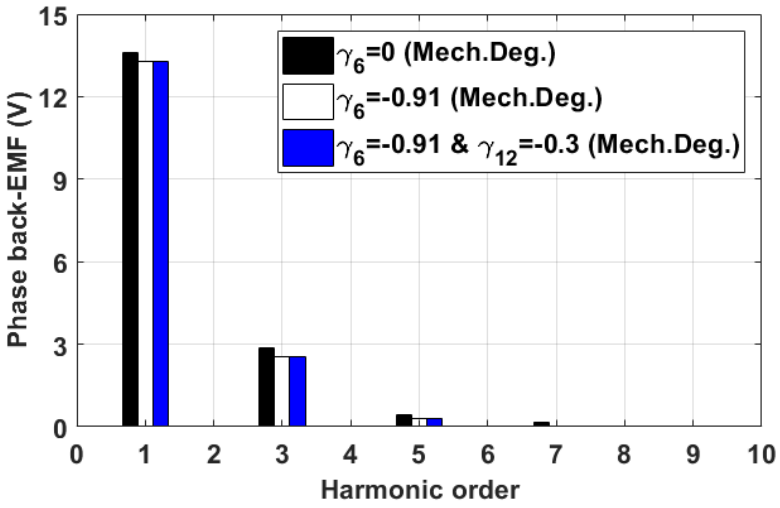

(b)

Fig. 3.28 Phase back-EMFs before and after the slot-opening shift obtained by non-linear 2D FE. (a) Waveforms of phase A. (b) Spectra. (12-slot/10-pole & FG=2mm at 400rpm).

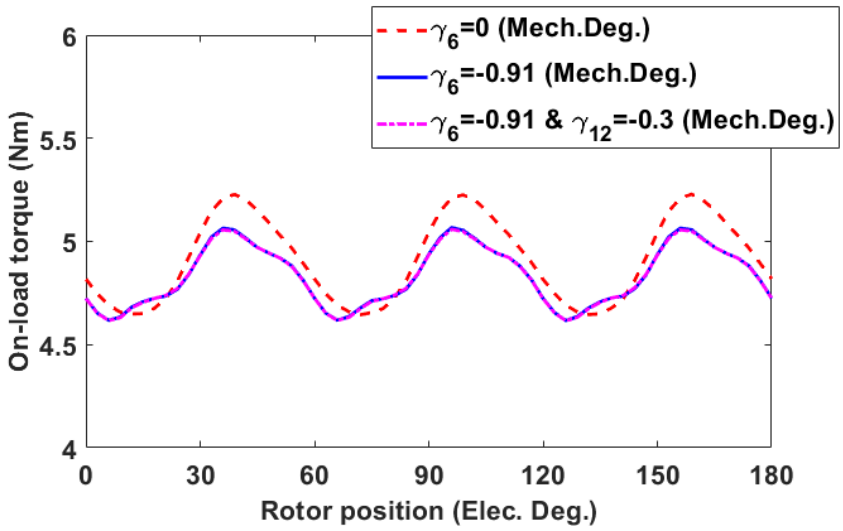

Fig. 3.29 The on-load torque waveforms of the modular PM machine before and after the slot-opening shift obtained by non-linear 2D FE (12-slot/10-pole & FG=2mm).

3.5 EXPERIMENTAL VALIDATION

3.5.1 PROTOTYPES OF MODULAR PM MACHINES

In order to verify the slot-opening shift method discussed in this chapter, the existing 12-slot/10-pole and 12-slot/14-pole modular prototype PM machines with the FGs of 3 mm have been used. The design parameters are shown in Table 3.1.

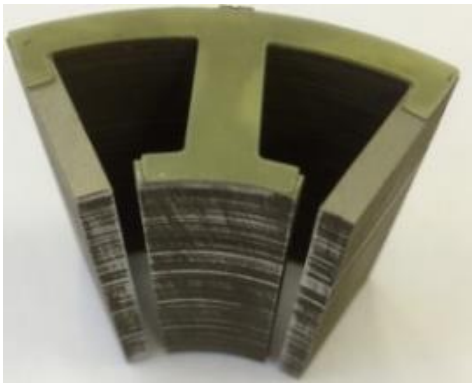

(a)

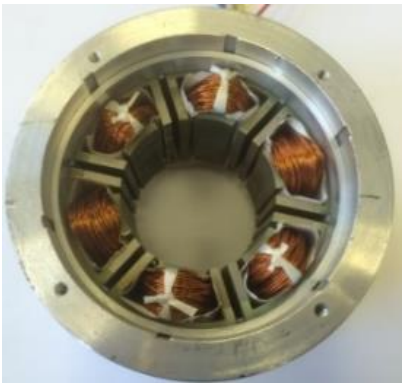

(b)

(c)

Fig. 3.30 Prototype machine. (a) Stator segment. (b) Wounded stator with frame. (c) 10-pole SPM rotor (FG=3 mm, Slot-opening=2.4 mm).

Fig. 3.30 depicts the structures of the stator, the rotor and the stator segment which are built based on the limited cases analysed in this chapter. It is worth mentioning that due to cost issues, the prototype machines with desired slot shift angle have not been built. The used prototype machines were initially built to achieve the highest phase back-EMF by shifting the slot-openings, which is similar to the proposed method of mitigating the cogging torque in this

chapter. Therefore, this shift angle in prototype machines will not be optimal for reducing the resultant cogging torque as will be seen in Fig. 3.31. However, the FE results after shifting slot-opening by a specific angle can still be validated by experiments. This can indirectly prove the effectiveness of the proposed cogging torque mitigation method which has already been validated by the same FE method.

3.5.2 COGGING TORQUE

The cogging torque measured according to the method described in [67] and the test rig shown in Fig. 2.15 (a). The cogging torques of 12-slot/10-pole and 12-slot/14-pole modular PM machines are measured and compared against their predicted counterparts in Fig. 3.31. A good agreement has been observed with only minor discrepancy due to manufacturing tolerance, measuring errors, etc.

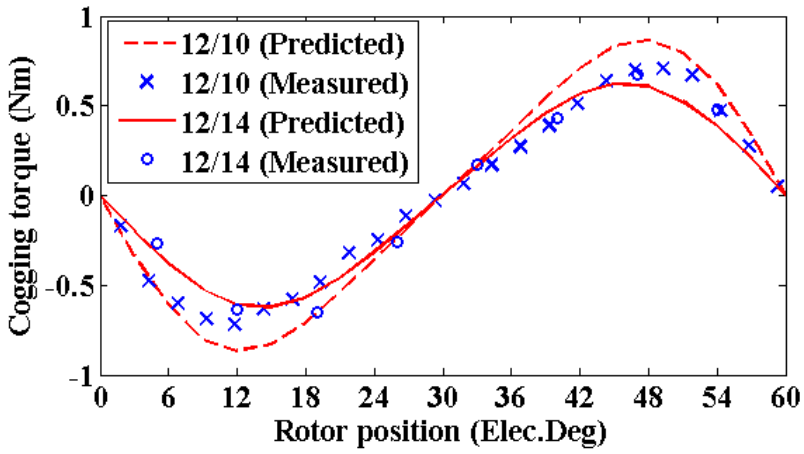

Fig. 3.31 Predicted and measured cogging torques for 12-slot/10-pole and 12-slot/14-pole modular machines.

3.5.3 PHASE BACK-EMF

By way of example, only the predicted and measured phase back-EMFs of the 12-slot/10-pole modular PM machine are shown in Fig. 3.32. It is found that after the slot-opening shift, the balance of 3-phase back-EMFs is maintained, as expected.

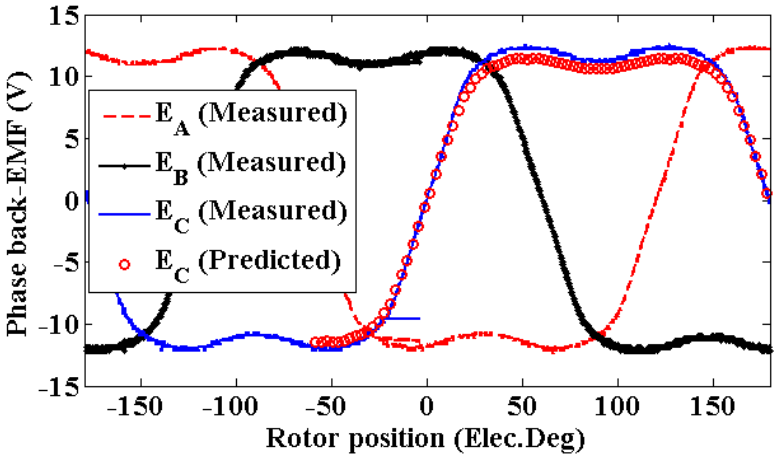

(a)

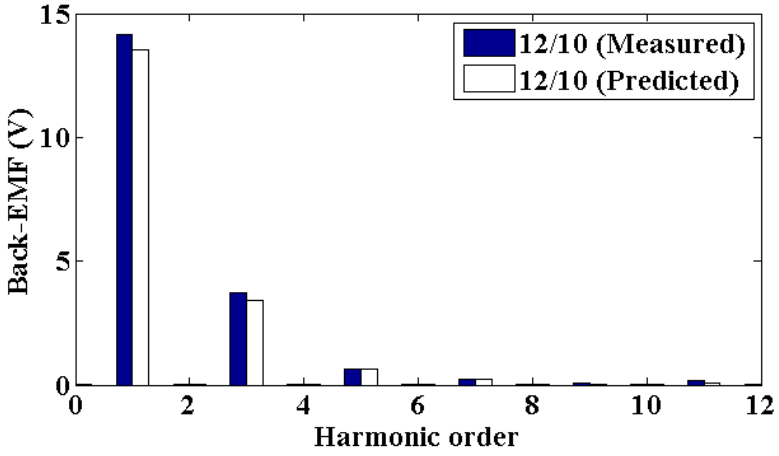

(b)

Fig. 3.32 Predicted and measured phase back-EMF waveforms at 400 rpm. (a) Waveforms (b) Spectra.

3.6 CONCLUSION

In this chapter, an effective method of mitigating cogging torque for modular PM machines is presented. The slot-openings have been divided into two groups. By shifting the two groups in opposite directions with a desired shift angle, the synthesised cogging torque due to the slot-openings could be almost opposite to that produced by the FGs (fixed during slot-opening shift), and hence cancel each other. The general expression of the desired shift angle has also been derived.

Several slot/pole number combinations have been investigated and the 12-slot/10-pole and 12-slot/14-pole with 2mm or 4mm FGs have been presented to validate the proposed method. Although slightly different mitigation approaches are needed for the investigated machines due to different dominant cogging torque harmonics, a reduction by up to 86% in the resultant cogging torque can be achieved. The performances of phase back-EMF and on-load torque are studied as well. After employing slot-opening shift, the balance of three phase back-EMF waveforms is maintained and no extra back-EMF harmonics are introduced. The FE results have been validated by experiments.

In the following chapter, another cogging torque and torque ripple reduction method by employing the C-core stator segments for modular PM machines will be investigated.

Chapter 4 COGGING TORQUE AND TORQUE RIPPLE REDUCTION OF MODULAR PM MACHINES BY C-CORE MODULAR STATOR

In order to minimize the cogging torque and torque ripple for modular SPM machines, this chapter proposes a C-core modular stator which can be obtained by inserting FGs into every stator tooth rather than in the alternate stator teeth (E-core modular machines) as in the previous chapters. The electromagnetic performances of C-core modular PM machines such as open-circuit flux linkage, phase back-EMF, cogging torque and torque ripple, etc. are comprehensively investigated. By employing the C-core modular structure, the resultant cogging torque of modular PM machines can be significantly mitigated, and simultaneously, the torque ripple can be reduced effectively if the FG width is chosen properly. It is found that the resultant cogging torque and torque ripple can be reduced by up to 96.4% and 57.6%, respectively. Especially, when C-core modular stator is employed, the average torque can become bigger than that of the E-core modular PM machines if the slot/pole number combination is properly selected. Furthermore, the cogging torque and torque ripple of modular PM machines having dummy slots are studied as well. It shows that, using dummy slots, the cogging torque and torque ripple of modular PM machines can be further reduced.

This chapter comes from author's chapter [89].

4.1 INTRODUCTION

PM machines have been widely used due to their inherent advantages such as high torque density, high efficiency, etc. [90]. However, for applications which require high performance such as direct-drive wind turbines, servo motors, EVs, etc. the torque ripple needs to be minimized [91]-[92]. Since cogging torque is one of the main sources of torque ripple, the reduction of cogging torque is of great significance for the reduction of torque ripple [68]. However, in some cases, due to the effect of saturation, the on-load cogging torque, which can be obtained by applying the frozen permeability method [91], [93], could contribute more to the torque ripple compared with the open-circuit one.

Various torque ripple reduction methods have been reported in the previous studies. By way of example, shaping the PMs [92] or rotor configurations [94] could reduce the torque ripple effectively. Skewing is another effective method to suppress the torque ripple. However, when the conventional skewing method is applied, although the cogging torque can be eliminated the torque ripple may become even bigger than that without skewing. Therefore, in [95], an improved skewing method for torque ripple reduction by optimizing both the current phase advanced angle and skewing angle has been proposed. Additionally, the symmetry of the machines might also influence the torque ripple and by employing asymmetric rotor pole, the torque ripple can be reduced significantly [96].

However, little work has been done on the torque ripple improvement for modular PM machines with E-core stators as shown in Fig. 4.1 (b). To reduce the cogging torque and torque ripple for modular PM machines, a reduction method has been proposed in [66]. The introduced method divides the slot-openings into two groups, through shifting those two groups of slot-openings in opposite direction by a desired shift angle, the cogging torque due to slot-openings can be compensated with that due to FGs. Consequently, the resultant cogging torque of modular PM machines can be reduced effectively, so does the torque ripple.

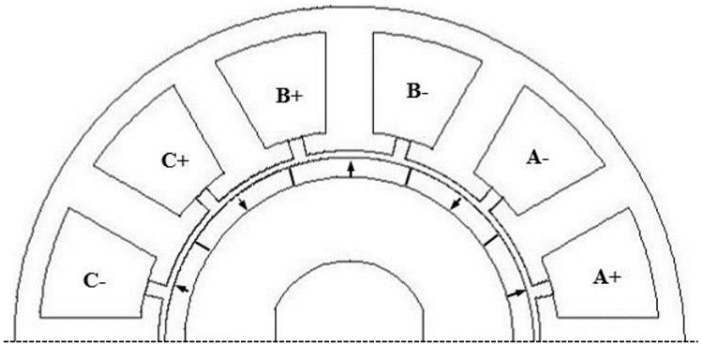

(a)

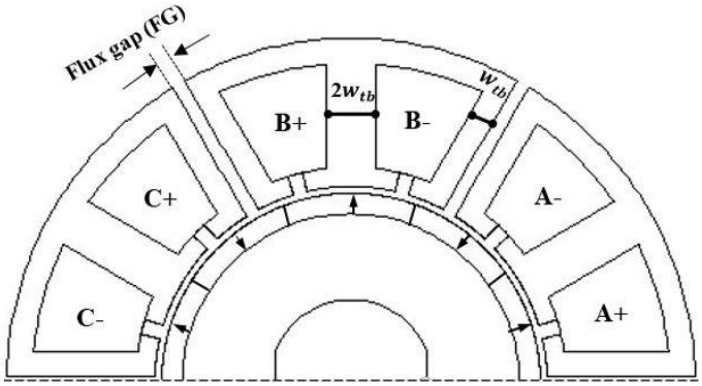

(b)

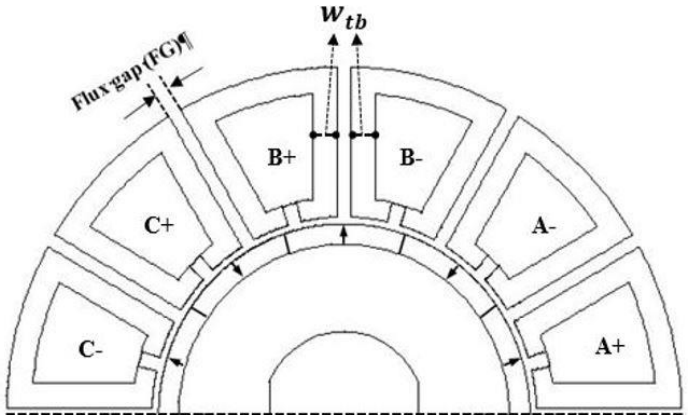

(c)

Fig. 4.1 Cross-sections of the investigated PM machines having 12-slot/10-pole. FG=2mm for modular machines. (a) Conventional non-modular PM machine. (b) E-core machine [28]-[36].(c) C-core machine.

Alternatively, in order to achieve a balance between torque ripple reduction and performance improvement, a modular PM machine with FGs in every stator tooth, leading to C-core stator as shown in Fig. 4.1 (c), is proposed in this chapter. In [33], a similar C-core modular interior PM machine without tooth tips has been proposed but there is no electromagnetic performance investigation on this topology. Therefore, this chapter will further investigate the influence of FGs on electromagnetic performances with a particular focus on cogging torque and torque ripple of C-core modular PM machines with different slot/pole number combinations. Moreover, the influence of employing dummy slots on cogging torque and torque ripple of modular PM machines is also investigated in this chapter.

4.2 TOPOLOGY OF THE INVESTIGATED PM MACHINES

Due to the fact that modular stator segments showed in [36]-[38] have similar shape with the letter ‘E’, hence, they can be named as E-core modular PM machines, as depicted in Fig. 4.1 (b). Different from the E-core modular PM machines, the FGs are inserted into every stator tooth in C-core modular PM machines, as shown in Fig. 4.1 (c). Both modular topologies employ surface mounted full arc PM rotor, and the main design parameters such as the stator and rotor outer radii, air-gap length, slot-opening width, stator yoke height, etc. are identical as detailed in Table 3.1 for simplifying the comparison.

As can be seen from Fig. 4.1 (b), for the E-core machine, in order to avoid the heavy local saturation, the total iron section width of the teeth with FGs is the same as that of teeth without FGs [36]. This is the same for C-core model. Moreover, similar to the E-core modular PM machines, the single layer concentrated winding is also employed for the C-core modular machine. It is worth mentioning that the original slot area will be partially occupied by FGs when modular topologies are employed. Hence, the copper loss will be increased if the packing factor and total number of turns are assumed to be constant since the copper wire diameter has been reduced accordingly. For example, the copper loss of conventional PM machine is 45.4W. While for its E-core and C-core counterparts having FG width of 2mm, the copper losses are 49.2W and 53.6W, respectively.

4.3 ELECTROMAGNETIC PERFORMANCE

The following electromagnetic performance analyses are based on the 12-slot/10-pole and 12-slot/14-pole modular PM machines. This is mainly due to the fact that the non-modular conventional PM machines with those two slot/pole number combinations have the maximum winding factor compared with other 12-slot alternatives. However, it is worth mentioning that the findings in this chapter are applicable to other slot/pole number combinations.

4.3.1 OPEN-CIRCUIT FLUX LINKAGE

The open-circuit flux linkages of the C-core and E-core modular PM machines with various slot/pole number combinations are depicted in Fig. 4.2. It is evident that for machines with C-core stator, the flux reduces with the increase in FG width, regardless of slot/pole number combination. However, as investigated in [36], for E-core modular machines, the FGs increases flux linkage for machines with lower slot number than pole number while reduces it for machines with higher slot number than pole number.

It has found that the FGs have influence on winding factor, flux focusing/defocusing and also the open-circuit air-gap flux density. However, for C-core machines, the effect on winding factor will be cancelled due to FGs in all stator teeth. Therefore, the FGs will only have influence on flux focusing/defocusing and open-circuit flux density. In order to deeply investigate the open-circuit flux linkage of C-core modular PM machines, the studies on the flux focusing or defocusing effect due to FGs and on the open-circuit air-gap flux density have been carried out.

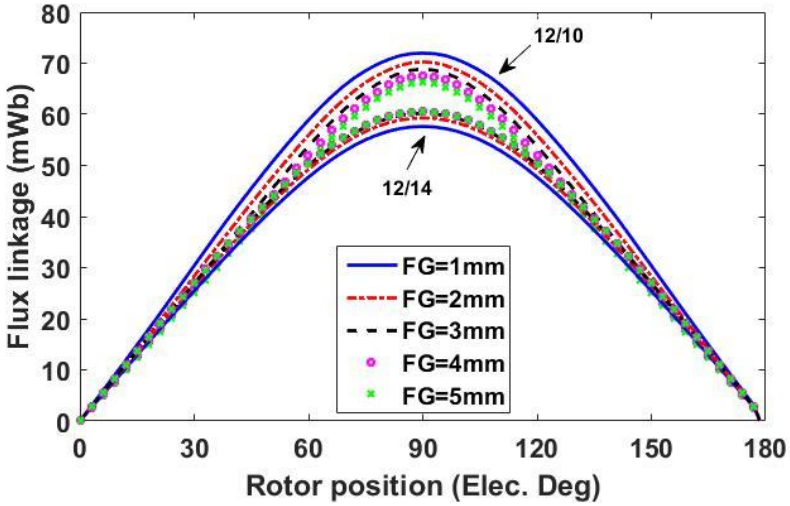
12/10
12/14
FG=1mm
FG=2mm
FG=3mm
FG=4mm
FG=5mm
Flux linkage (mWb)
Rotor position (Elec. Deg)
0
10
20
30
40
50
60
70
80
0
30
60
90
120
150
180

(a)

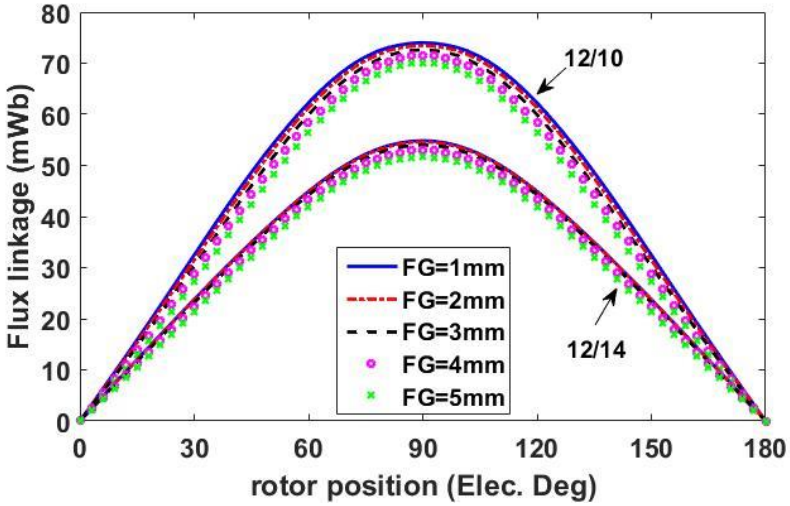
12/10
12/14
FG=1mm
FG=2mm
FG=3mm
FG=4mm
FG=5mm
Flux linkage (mWb)
rotor position (Elec. Deg)
0
10
20
30
40
50
60
70
80
0
30
60
90
120
150
180

(b)

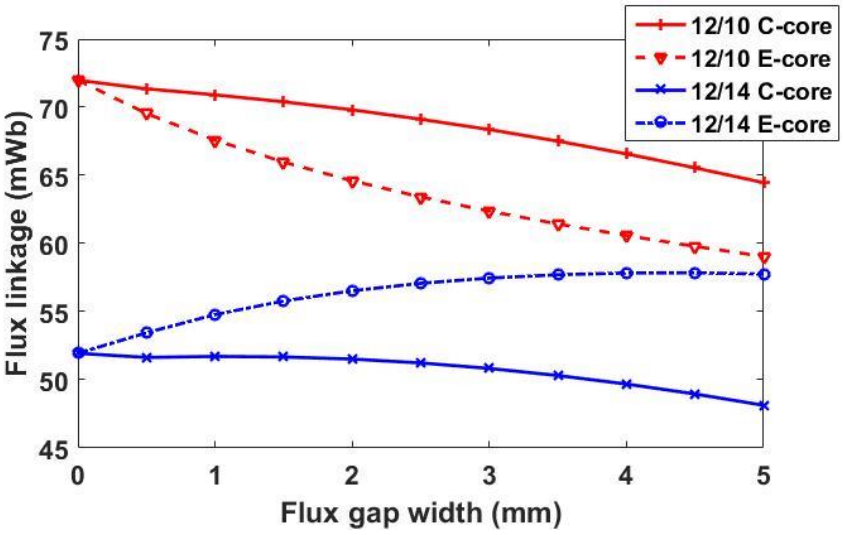

(c)

Fig. 4.2 The open-circuit phase flux linkage versus different FG widths. (a) E-core modular PM machines. (b) C-core modular PM machines. (c) Fundamental flux linkages versus FG width.

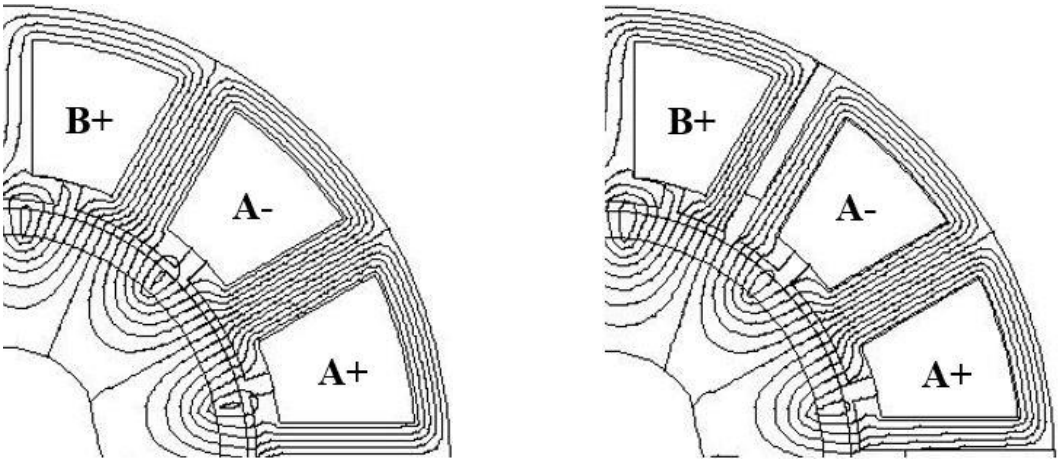

(a) (b)

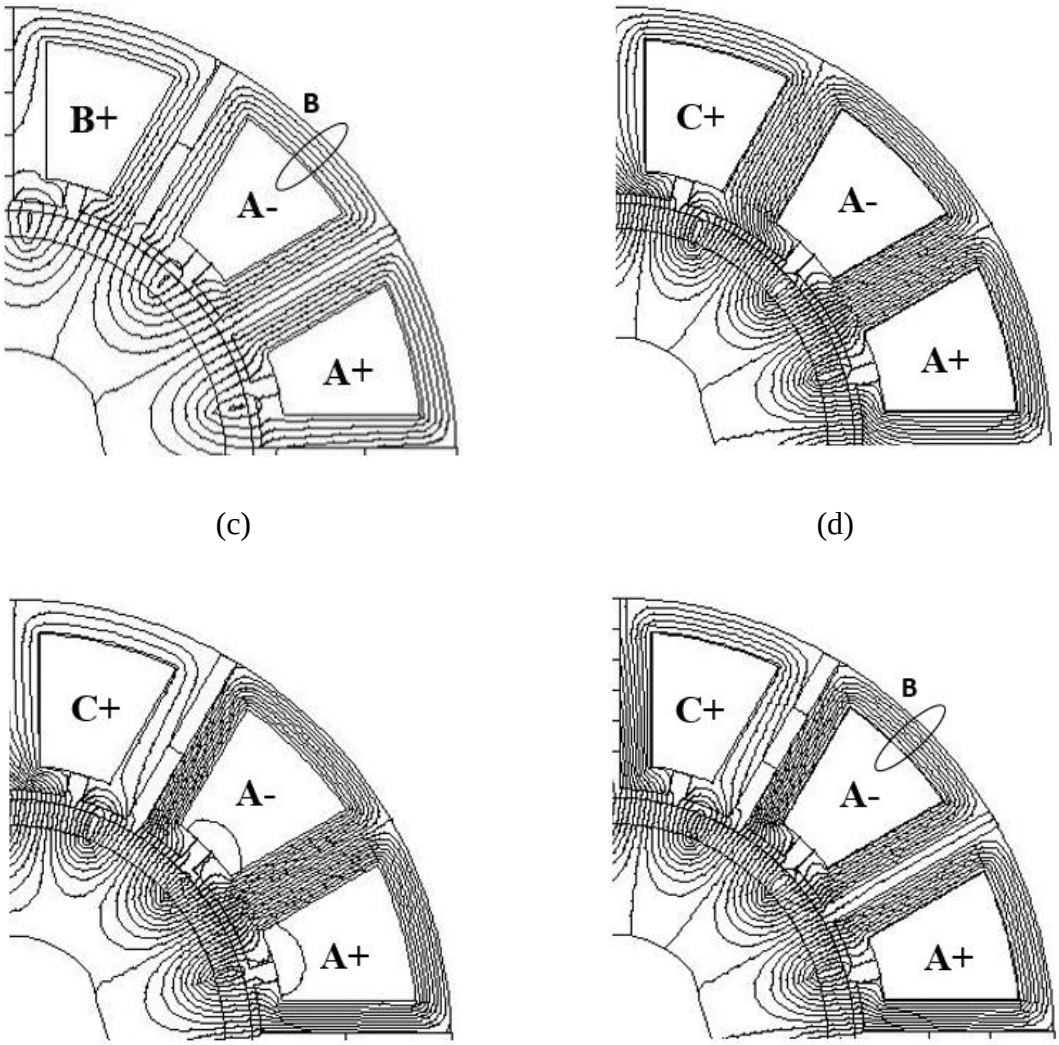

(c) (d)

(e) (f)

Fig. 4.3 The open-circuit flux distributions of convention non-modular, C-core modular and E-core modular PM machines. (a)-(c) 12-slot/10-pole. (d)-(f) 12-slot/14-pole.

The open-circuit flux distributions of the conventional non-modular, C-core and E-Core modular PM machines are shown in Fig. 4.3, in which the rotor is at the position where the phase A has its maximum flux linkage. It is found in [36] that for the PM machines with slot number higher than pole number, as shown in Fig. 4.3 (a) to (b), the FGs exhibit flux defocusing effect. This is because the FGs divert some flux away from the phase A. Contrarily, the FGs in E-core machines with slot number lower than pole number have an influence of flux focusing effect, as shown in Fig. 4.3 (d) and (e). This is because the FGs concentrate some flux, which will enter into phases B and C if no FGs exist, into phase A.

However, it will be difficult to observe the flux focusing/defocusing effect of C-core modular machines only based on flux distribution, as shown in Fig. 4.3 (c) and (f). To do so, the analysis on the average flux density of stator yoke has been carried out, as shown in Fig. 4.4. The test position in stator yoke is highlighted by a small circle. It is evident that the average flux densities in stator yoke decreases with the increase of FG width for C-core modular machines regardless of the slot/pole number combinations. Therefore, the FGs in C-core modular machines exert flux defocusing effect.

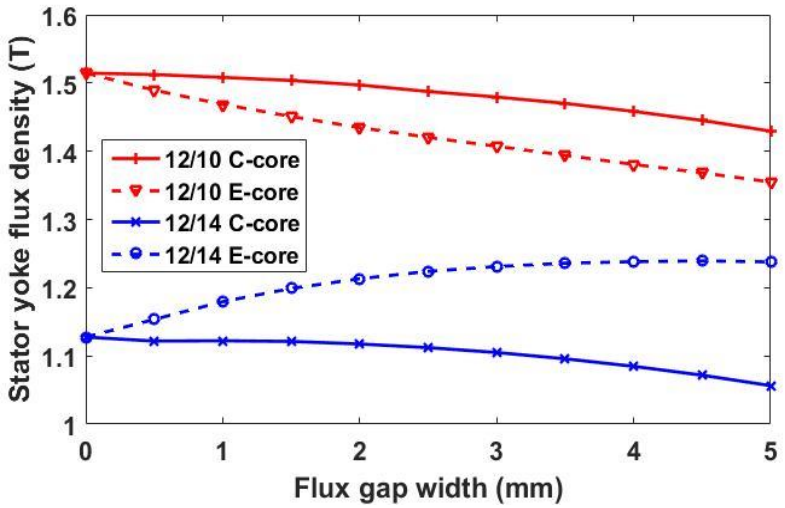

Fig. 4.4 The average flux density of stator yoke for C-core and E-core modular PM machines with various slot/pole number combinations.

As studied previously, for C-core modular machines, the flux linkage is not only influenced by flux focusing/defocusing, but also the open-circuit air-gap flux density. Hence, the working harmonics of open-circuit flux density of C-core modular machines are investigated and shown in Fig. 4.5. It is worth noting that for the 12-slot/10-pole modular PM machines, the 5^{th} order harmonic of the open-circuit air-gap flux density is the working harmonic while for the 12-slot/14-pole modular PM machines, it is the 7^{th} order harmonic. As indicated in Fig. 4.5, for both 12-slot/10-pole and 12-slot/14-pole C-core modular PM machines, the working harmonics decrease with the increase in FG width but for 12-slot/10-pole machine, it decreases faster.

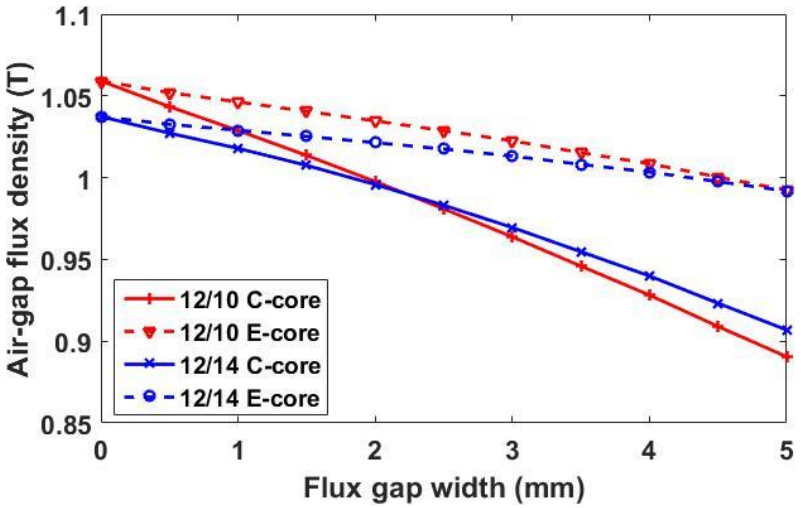

Fig. 4.5 The working harmonic of open-circuit air-gap flux density versus FG widths for 12-slot/10-pole and 12-slot/14-pole modular PM machines with C-core and E-core stator segments.

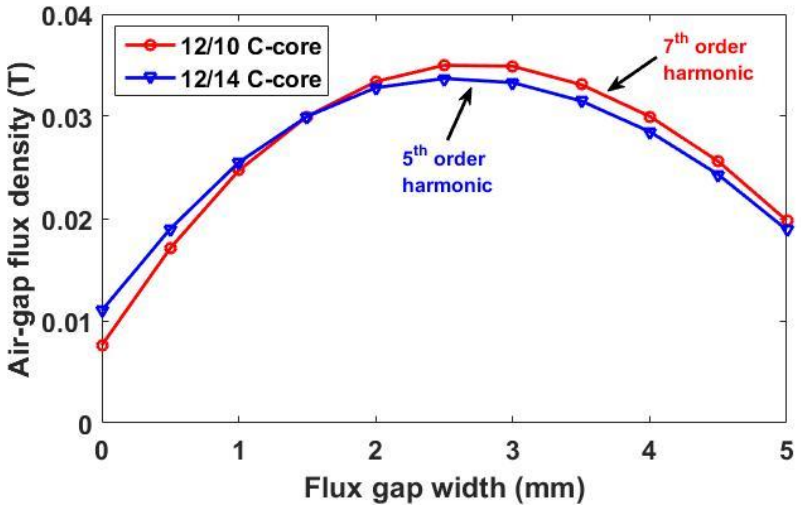

Fig. 4.6 The harmonics of generating PM eddy current losses in open-circuit air-gap flux density versus FG widths for 12-slot/10-pole and 12-slot/14-pole modular PM machines with C-core stator segments.

In conclusion, due to the flux defocusing effect together with the decrease in the open-circuit air-gap flux density, the open-circuit flux linkages decline with the increase of FG width for C-core modular PM machines regardless of the slot/pole number combinations. Moreover, the flux linkage of the 12-slot/10-pole C-core modular machine decreases faster than that of the 12-slot/14-pole one. Additionally, the FGs affect not only the working harmonics in the open-

circuit air-gap flux density, but also other harmonic contents, which mainly contribute to the PM eddy current losses.

By observing the spectra of the open-circuit air-gap flux density, only the 7th order harmonic of the 12-slot/10-pole machine and the 5th order harmonic of the 12-slot/14-pole machine are relatively significant and hence can be treated as the main source of the PM eddy current losses. It can be found that for both the 12-slot/10-pole and 14-pole C-core modular PM machines, their PM eddy current losses would increase with the FG width till 2.5 mm and reduce thereafter, as shown in Fig. 4.6.

4.3.2 PHASE BACK-EMF

The investigation of the phase back-EMFs for both the C-core and E-core modular machines has been carried out at the rated motor speed (400 rpm), as shown in Fig. 4.7 and Fig. 4.8. It is worth noting that when FG=0mm, the machine is a conventional non-modular one. Since the phase back-EMF is proportional to the flux linkage, all influence of FGs on the flux linkage will be introduced into the phase back-EMF.

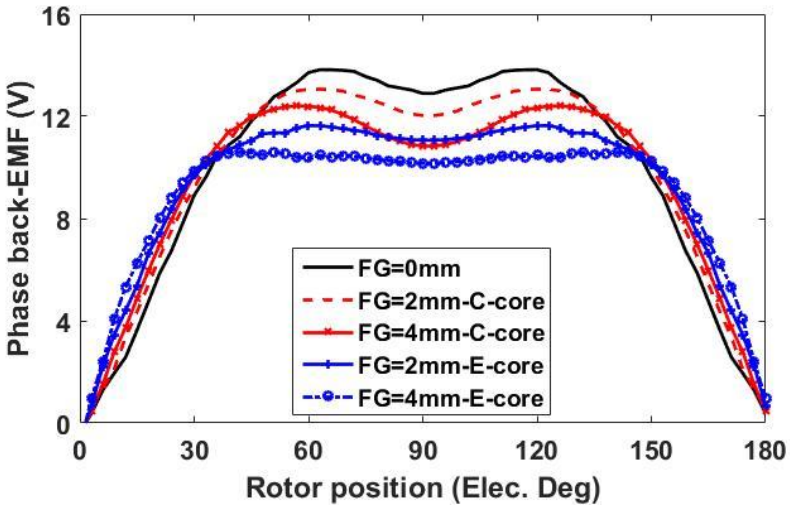

(a)

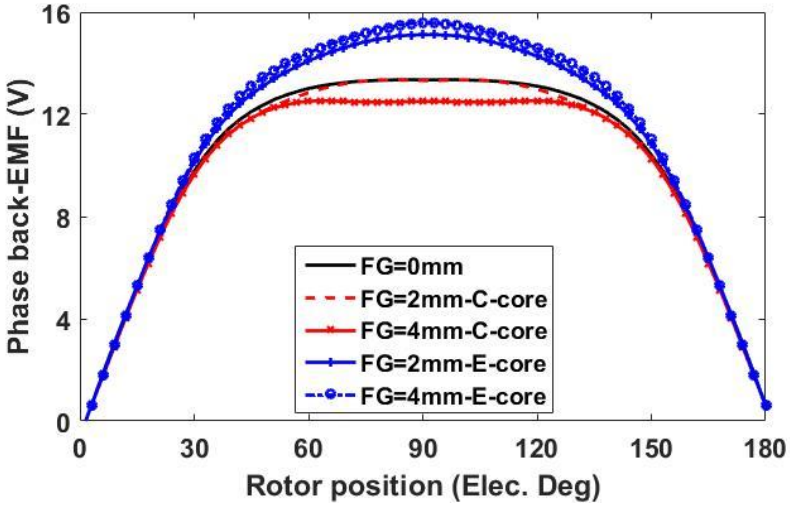

(b)

Fig. 4.7 The phase back-EMF waveforms of C-core and E-core modular PM machines versus FG widths. (a) 12-slot/10-pole. (b) 12-slot/14-pole.

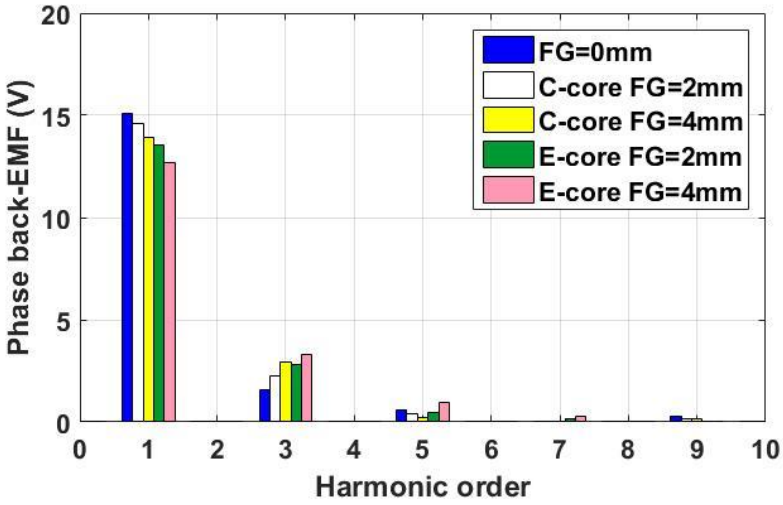

(a)

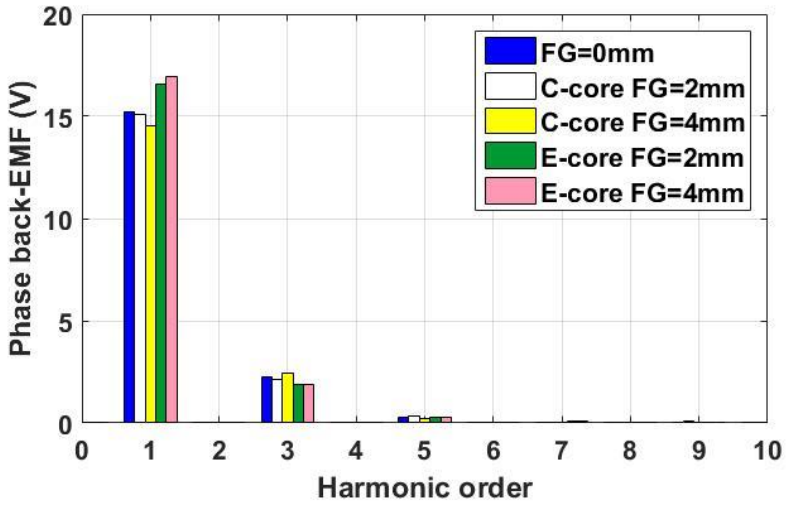

(b)

Fig. 4.8 The spectra of phase back-EMFs of C-core and E-core modular PM machines versus FG widths. (a) 12-slot/10-pole. (b) 12-slot/14-pole.

4.3.3 COGGING TORQUE

It is well established that the cogging torque of PM machines depends on the N_c. For conventional non-modular PM machines, different slot/pole number combinations will result in different N_c. However, when the modular structures are employed, the stator symmetry will be changed since the stator is segmented into several modules. It is worth mentioning that the periodicity is dominated by the number of FGs. By way of example, for the 12-slot/10-pole non-modular PM machines, the stator repeats 12 times over a mechanical period (360°). However, for the E-core modular PM machine, the stator is divided into 6 identical segments while the C-core model has 12 identical segments. Hence, the periodicity of the E-core stator repeats 6 times while the C-core stator repeats 12 times. As a result, for modular PM machines, the constant N_c should be re-written as N_{cm} [66]. This means that for the C-core modular PM machines with 12-slot/10-pole, the value of N_{cm} is 60 while the E-core counterpart has a N_{cm} of 30. In other words, the number of periods of cogging torque for the 12-slot/10-pole C-core modular PM machines is 12 over one electrical period, as shown in Fig. 4.9.

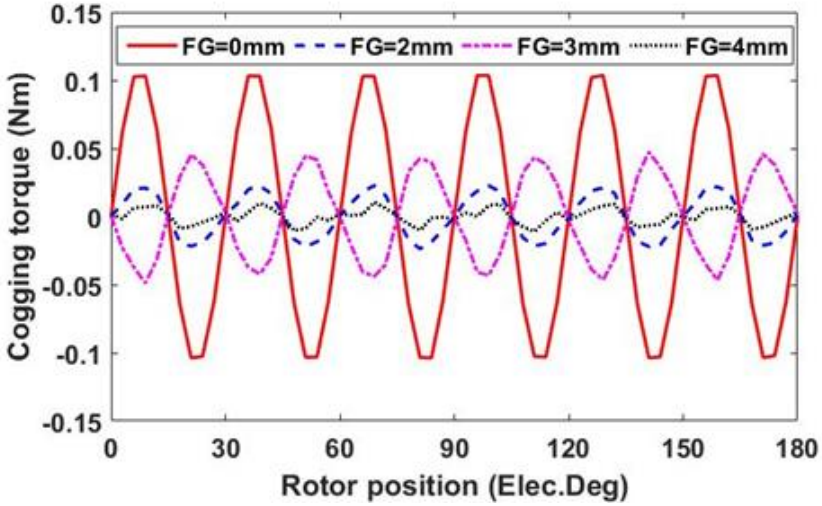

(a)

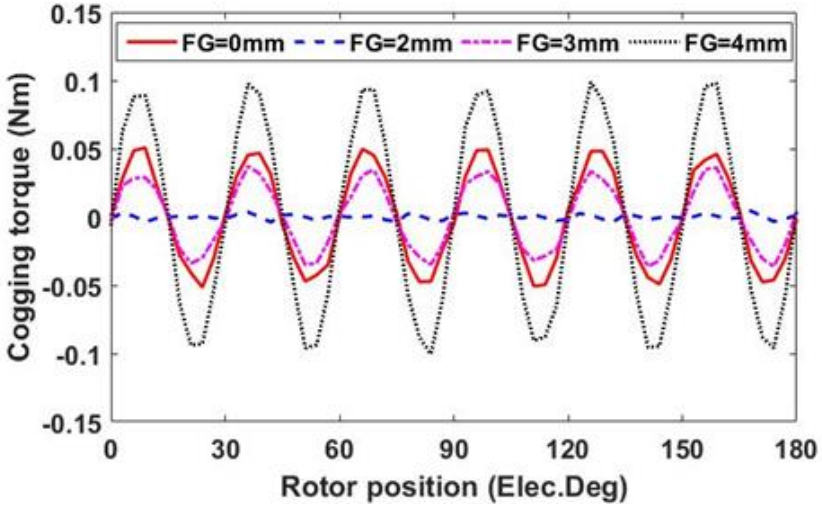

(b)

Fig. 4.9 The cogging torque waveforms of the C-core modular PM machines versus rotor position and various FG widths. (a) 12-slot/10-pole. (b) 12-slot/14-pole.

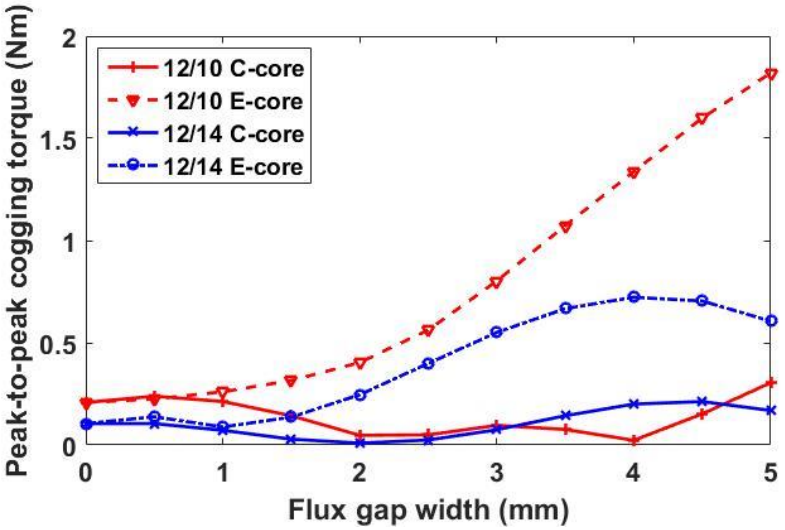

Fig. 4.10 Peak-to-peak cogging torque versus FG width of the C-core and E-core modular PM machines with various slot/pole number combinations.

The peak-to-peak cogging torques versus FG width of the E-core and C-core modular PM machines are shown in Fig. 4.10. It is found that the peak values of resultant cogging torque of the C-core models are smaller than those of the E-core models regardless of the slot/pole number combinations. This is mainly due to the fact that according to [68], the higher the frequency (determined by N_{cm}) of the cogging torque, the smaller the magnitude of the resultant cogging torque.

In summary, when the FG width is 2mm or 4mm, the much smaller resultant cogging torque for the 12-slot/10-pole C-core modular PM machines is achieved. However, for the 12-slot/14-pole C-core modular PM machine, the minimum resultant cogging torque appears when the FG width equals to 2mm.

4.3.4 ON-LOAD TORQUE

By supplying the rated sinewave currents to the investigated PM machines, the on-load torque can be calculated, as shown in Fig. 4.11. It is found that:

1. For the modular PM machines with $N_s > 2p$, i.e., 12-slot/10-pole, the average torque of C-core model is higher than the average torque of the E-core model. The reason of such a phenomenon is mainly due to the significant influence of FGs on the phase flux linkage and the phase back-EMF as described previously. Additionally, similar to the E-core machine, the increasing FG width of the C-core

model reduces the average torque as well.

2. For the modular PM machines with $N_s < 2p$, i.e. 12-slot/14-pole, the E-core model improves the average torque, while the average torque declines slightly with the increasing FG width for the C-core modular structure.

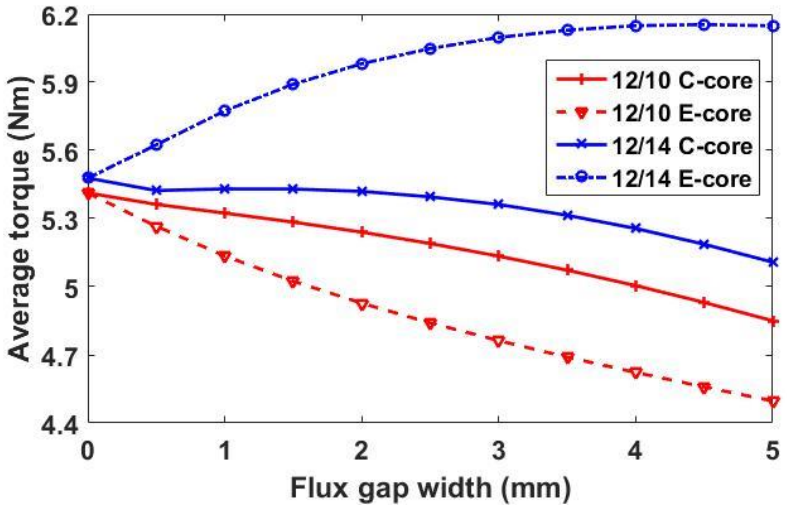

Fig. 4.11 Average torques versus FG width of the C-core and E-core modular PM machines with various slot/pole number combinations.

4.3.5 TORQUE RIPPLE ANALYSIS BY USING THE FROZEN PERMEABILITY METHOD

In this chapter, the torque ripple is defined as the peak-to-peak on-load torque. Benefited from the remarkable reduction of cogging torque when employing the C-core machine, its torque ripple is mitigated significantly as well. However, the reductions in the cogging torque and in the torque ripple are not directly proportional. By way of example, when the FG width is properly selected, the peak-to-peak cogging torque for the 12-slot/10-pole and 12-slot/14-pole C-core modular PM machines can almost be eliminated. Nevertheless, it can be found from Fig. 4.12 that the smaller torque ripples of both 12-slot/10-pole and 12-slot/14-pole machines with the C-core stator and 2mm FG can be achieved which are 0.25 Nm and 0.19 Nm, respectively. This is mainly due to the fact that the torque ripple is not due to the open-circuit cogging torque but mainly due to the on-load cogging torque and the phase back-EMF harmonics.

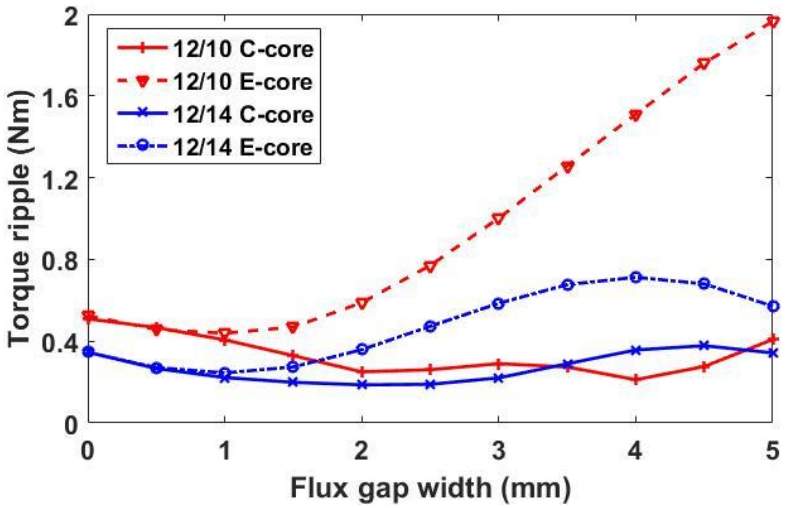

Fig. 4.12 Torque ripples versus FG width of the C-core and E-core modular PM machines with various slot/pole number combinations.

According to [91] the on-load cogging torque can be calculated by employing the frozen permeability (FP) method together with the virtual work principle. The FP method can help to accurately calculate the on-load cogging torque and the on-load phase back-EMF. Therefore, the source of torque ripple can be identified and analysed.

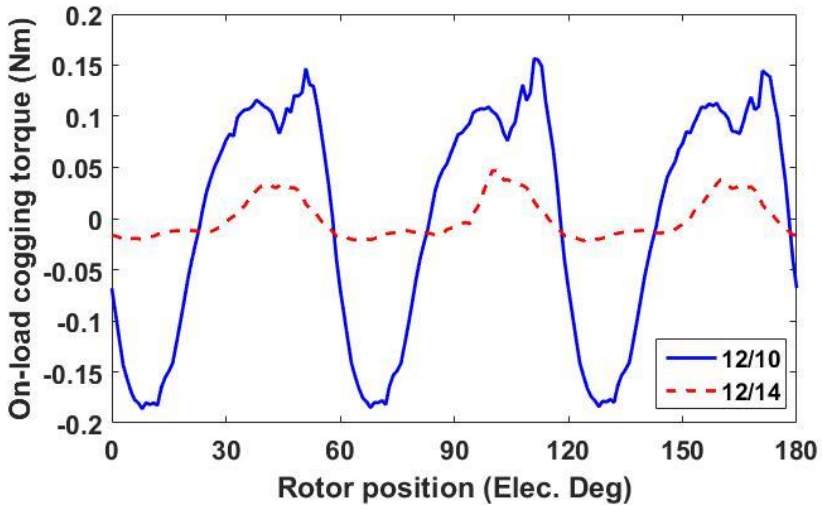

Fig. 4.13 On-load cogging torque waveforms calculated using the FP method for the C-core modular PM machines. (FG=2mm.)

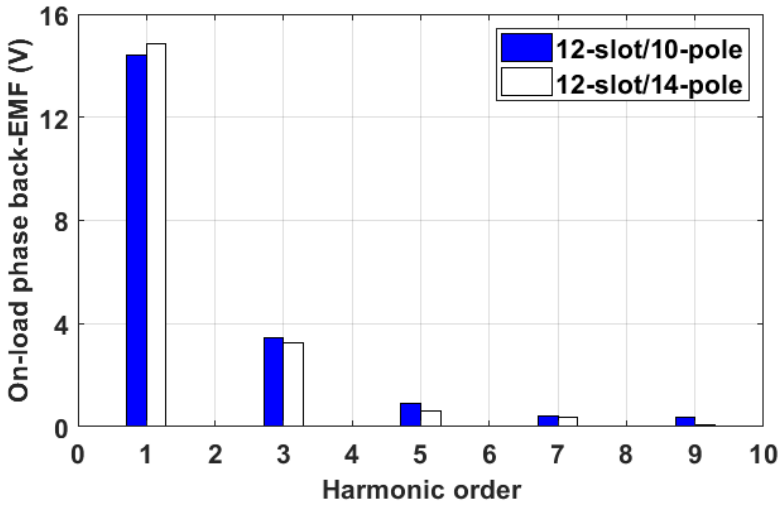

Fig. 4.14 The spectra of the on-load phase EMF calculated using the FP method for the C-core modular PM machines. (FG=2mm.)

The on-load cogging torque waveforms of the 12-slot/10-pole and 12-slot/14-pole modular PM machines with 2mm FG width are depicted in Fig. 4.13. It is shown that the peak on-load cogging torques of the 12-slot/10-pole and 12-slot/14-pole machines are 0.16 Nm and 0.05 Nm, respectively. Together with the torque ripple components generated by the on-load phase back-EMF harmonics (mainly 5^{th} and 7^{th}, as shown in Fig. 4.14), the torque ripple features observed above can be explained.

As a result, when the FG width equals to 2mm, the best torque performance is obtained. For the 12-slot/10-pole C-core modular PM machines, the torque ripple is reduced by 57.6% with a 6.3% increase in average torque compared with the E-core counterparts. However, for the 12-slot/14-pole C-core modular PM machine, the average torque is reduced by 9.4% but the torque ripple is reduced by 47.2% compared with the E-core counterparts.

4.3.6 Cogging Torque and Torque Ripple of Modular PM Machines Having Dummy Slots

Apart from the aforementioned methods, dummy slots can also be employed for cogging torque and torque ripple reduction of the modular PM machines. As shown in Fig. 4.15, this can be achieved by adding dummy slots in stator teeth with coils of the E-core modular PM machines, or by adding iron bridges to stator teeth with coils of the C-core modular PM machines. The optimized dummy slot width is assumed to be equal to the slot-openings (2mm)

to achieve the minimum cogging torque and torque ripples. It is also worth mentioning that the E-core with dummy slots and the C-core with iron bridges have similar effect on cogging torque and torque ripple if saturation effect can be neglected. Therefore, the following section will only focus on the E-core modular machines with dummy slots.

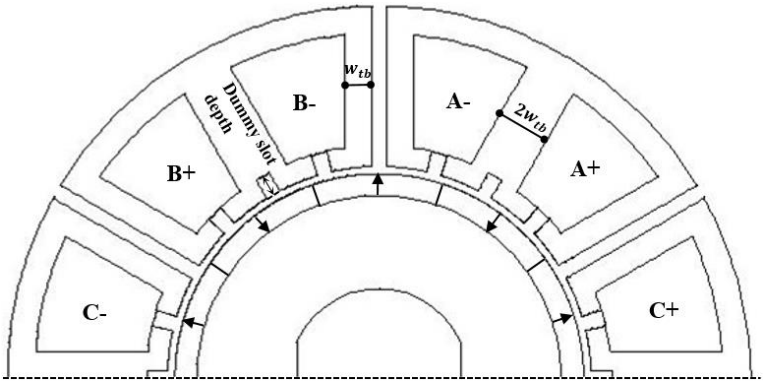

(a)

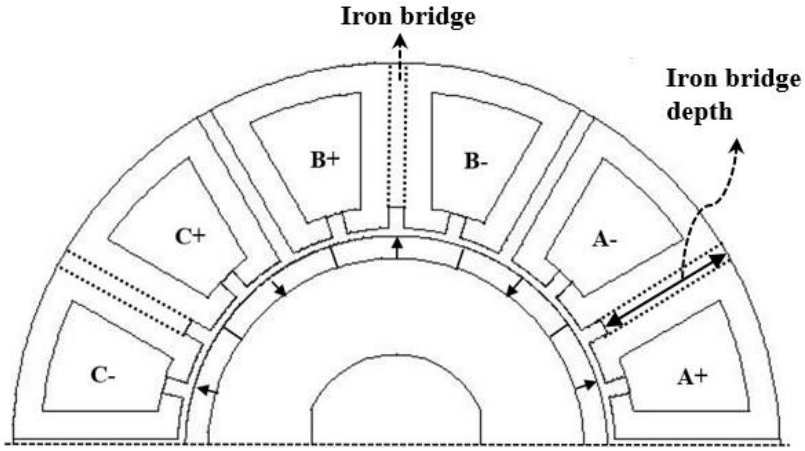

(b)

Fig. 4.15 The cross-sections of modular machines. (a) E-core modular machines with dummy slots, (b) C-core modular machine with iron bridges.

The peak-to-peak cogging torques of the E-core modular PM machines with dummy slots are depicted in Fig. 4.16. It is evident that when the FG widths are bigger than 1mm, the peak-to-peak cogging torque can be reduced effectively by appropriate selection of the dummy slot depth for both the 12-slot/10-pole and 12-slot/14-pole modular machines. However, when the FG width is 1mm, the peak-to-peak cogging torque is increased. This is mainly due to heavy local saturation in the tooth tips.

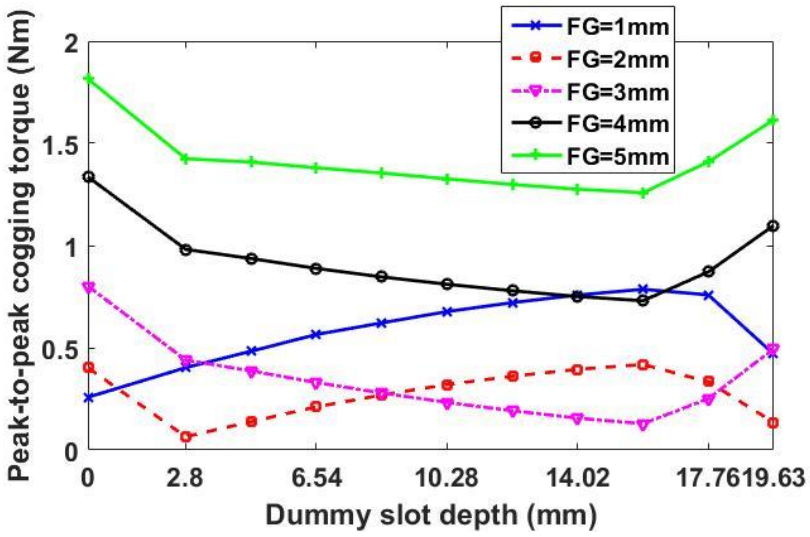

(a)

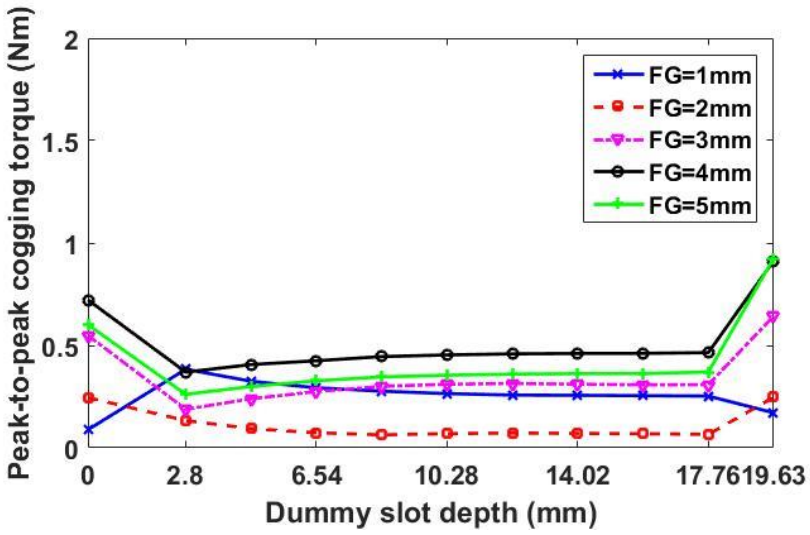

(b)

Fig. 4.16 The peak-to-peak cogging torque versus dummy slot depth of the E-core modular PM machines. (a) 12-slot/10-pole. (b) 12-slot/14-pole.

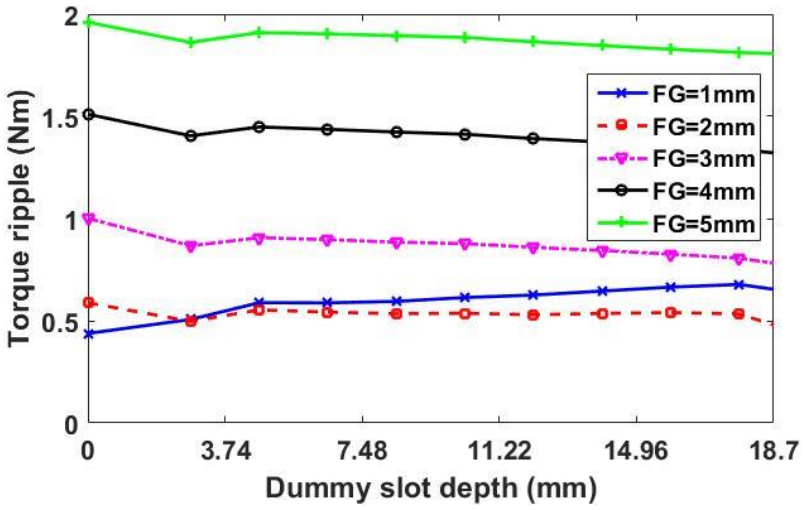

(a)

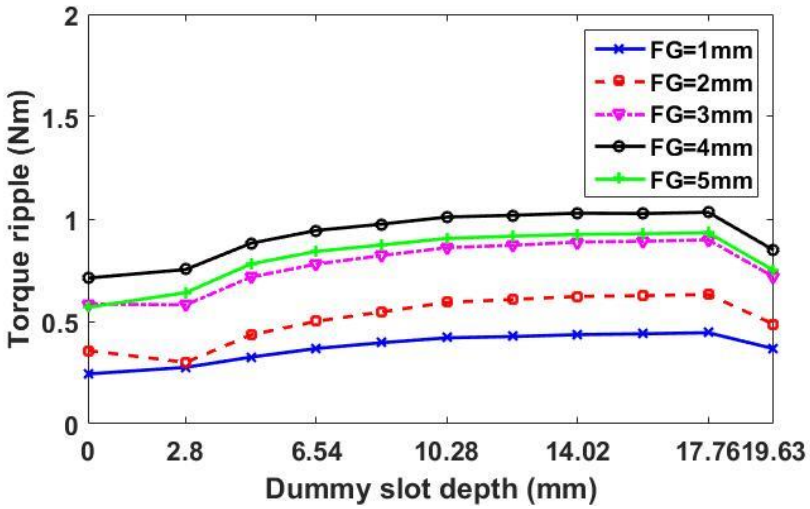

(b)

Fig. 4.17 The torque ripple versus dummy slot depth of the E-core modular PM machines. (a) 12-slot/10-pole. (b) 12-slot/14-pole.

Fig. 4.17 shows the influence of dummy slot depth on the torque ripple. It can be found that when the FG width is bigger than 1mm, a slight reduce in the torque ripple of the 12-slot/10-pole modular PM machines with dummy slots can be achieved. However, for the 12-slot/14-pole machines, the dummy slots have negative effect on the torque ripple. Therefore, it can be concluded that employing dummy slots for the modular PM machines is useful for cogging torque reduction. Nevertheless, this method also has limited effect on torque ripple reduction.

4.4 PROTOTYPE MACHINES

The prototype machine with C-core stator segments has been newly built, as can be seen from the Fig. 4.18. The test results from this machines will be covered in the future related papers.

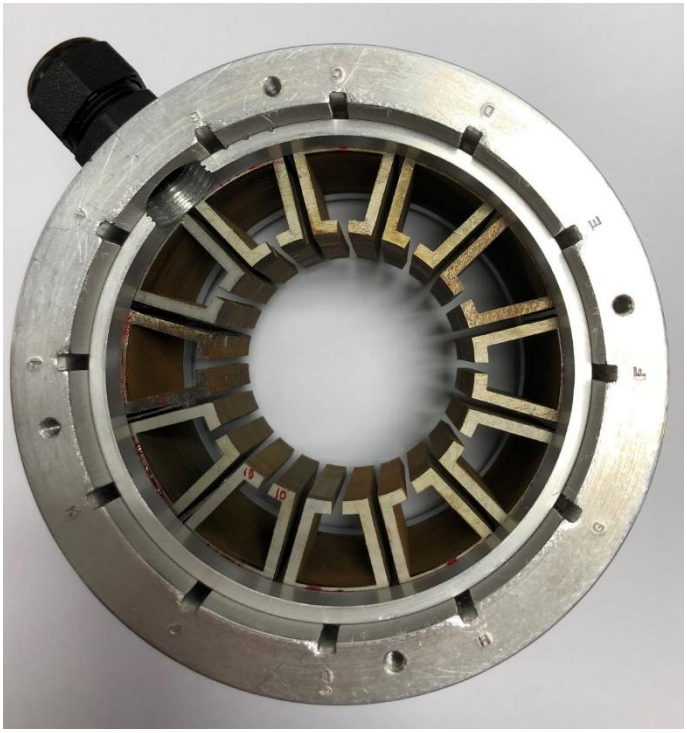

Fig. 4.18 The prototype machines with C-Core stator segments.

4.5 CONCLUSION

In this chapter, for reducing cogging torque and torque ripple, the modular PM machines with C-core stator segments have been proposed. Their electromagnetic performances such as the open-circuit flux linkage, phase back-EMF, open-circuit and on-load cogging torques as well as on-load torque have been investigated. The best torque performances for both the 12-slot/10-pole and 12-slot/14-pole C-core modular PM machines are achieved when the FG width equals to 2mm, as detailed in Table 4.1. It is also found that by employing dummy slots for the E-core modular PM machines or iron bridges for the C-core modular PM machines, the resultant cogging torque can be further reduced by properly choosing the depth of dummy slots and the FG width. However, they have limited effect on the reduction of torque ripple. Moreover, by applying the modular structure, the copper loss are also affected due to the changing slot area and the maintained packing factor. By way of example, the copper loss of conventional non-modular PM machine is 45.4W. However for its E-core and C-core counterparts having FG width of 2mm, the copper losses are 49.2W and 53.6W, respectively.

TABLE 4.1 COGGING TORQUE, TORQUE RIPPLE AND AVERAGE TORQUE OF THE INVESTIGATED PM MACHINES

	Slot/pole	Non-modular	E-core	C-core	
Cogging torque (Nm)	(12/10)	0.1	0.4	0.04	-90%
	(12/14)	0.05	0.25	0.009	-96.4%
Torque ripple (Nm)	(12/10)	0.51	0.59	0.25	-57.6%
	(12/14)	0.35	0.36	0.19	-47.2%
Average torque (Nm)	(12/10)	5.41	4.93	5.24	+6.3%
	(12/14)	5.48	5.98	5.42	-9.4%

- For modular machines, the FG width is 2 mm.
- The percentages of the C-core modular PM machines is based on those values of the E-core modular PM machines.

The manufacturing tolerance and its influence on modular PM machines will be studied in the following chapter.

Chapter 5 INFLUENCE OF MANUFACTURING TOLERANCE ON THE PERFORMANCE OF MODULAR PM MACHINES

In this chapter, the investigation about the influence of manufacturing tolerance on the electromagnetic performance of modular PM machines with segmented stator has been carried out. It is worth noting that the manufacturing tolerance is defined as the variations in dimensions and relative position compared to normal values. Two typical slot/pole number combinations such as 12-slot/10-pole and 12-slot/14-pole have been chosen for case studies. The manufacturing tolerance scenarios are focused on the stator segment displacement (both radial and circumferential) and the PM defect. Firstly, the influence on phase back-EMF as well as on-load torque is investigated. By doing so, the most significant influenced cases of stator segment displacement can be identified. This allows for further studying the influence of FG widths on the performance of modular PM machines. While for the PM defect scenario, two representative cases are selected, e.g. 5% or 10% area of one magnet pole is defected. Through the analyses of the back-EMF, on-load torque and cogging torque, etc., the manufacturing tolerance withstand capability of the 12-slot/10-pole and 12-slot/14-pole modular PM machines can be assessed. It is found that the 12-slot/10-pole modular PM machines have better manufacturing tolerance withstand capability compared with the 12-slot/14-pole modular PM machines.

5.1 INTRODUCTION

PM machines, due to their inherent advantages such as high power/torque density, high efficiency, etc., have become prominent candidate for various industrial applications [97]. However, during the mass production, the manufacturing tolerance is inevitable and many possible scenarios of the manufacturing tolerance can be observed. By way of example, stator and rotor asymmetry [98]-[99], PMs magnetization error [100]-[101], the variation of coil number of turns [102] and rotor eccentricity [103]-[105], etc.

When the manufacturing tolerance occur, the performance of PM machines will be affected, especially cogging torque and torque ripple, which are very sensitive parameters and are prone to the influence of manufacturing tolerance. In [106], the extra introduced cogging torque harmonics of SPM machines due to the assembly tolerance and material imperfection have been investigated. It is found that the additional cogging torque harmonics are heavily influenced by the PMs assembly and the thickness variations while not much influenced by the PM width variations. X. Ge *et. al.* have studied the cogging torque sensitivities under the tooth-bulge and PM diversity of the IPM machines with various slot/pole number combination in [13] and with eccentricity as well as the sinusoidal rotor shape in [14]. The authors have introduced a method of detecting the most sensitive cases amongst numerous possible distributions of tooth-bulge and PM diversity by employing the additional cogging torque vectors diagram.

Given the facts that the manufacturing tolerance will degrade the performance of the PM machines such as increasing cogging torque and torque ripple and reducing average torque, etc., researchers have made great effort to mitigate such negative impact. In [82], the efficiency of the existing cogging torque mitigation methods such as shaping the PMs, skewing, etc., has been evaluated based on the brushless DC PM motors. In [107], it is reported that employing the dummy slots placed partially in axial direction of the stator teeth is an effective method to reduce the cogging torque of SPM machines under the influence of manufacturing tolerance.

As a matter of fact that the rear-earth PMs, for instance, SmCo, NdFeB, etc. are very brittle and quite easily to be fractured [108]. Hence, the PM defect or damaged [109]-[110] during the manufacturing and assembly processes are also a common scenarios of manufacturing tolerance. A general investigation on the PM defect fault of PM synchronous machines has been carried out in [111]. According to the influence of the different defective PMs on the phase back-EMF and current spectra, it is found that the most critical coefficient of the PM defect is the overall defective volume rather than the shape and the direction of the defective

zone in the PMs.

In addition, the tiny fracture on the PMs due to the manufacturing tolerance may result in total damage of the PMs during operation and hence dramatic failure of the PM machines. As a result, the PM defect should be detected in the early stage to avoid such potential hazards. Various indexes have been selected to detect the PM defect in the literatures, such as back-EMF [112], phase current spectrum [113] and leakage flux [114], etc.

However, for modular PM machines, since their stators are segmented, compared to their non-modular counterparts, they could be even more prone to manufacturing tolerance during the assembly process. This needs to be investigated in order to reveal the full potential of modular PM machines. Therefore, in this chapter, the influence of the manufacturing tolerances such as the stator segment radial or circumferential displacement as well as the PM defect of modular PM machines will be comprehensively studied. The most serious cases of stator segment displacements in the respect of average torque can be identified. Two PM defect scenarios are studied in this chapter which are the 5% and 10% area of one magnet pole is defected.

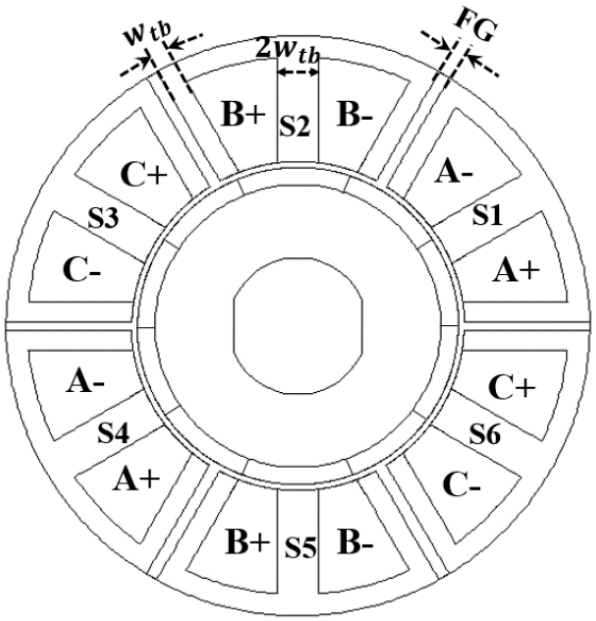

Fig. 5.1 The healthy modular PM machine topology with 12-slot/10-pole [37].

The cross-sections of the modular PM machines investigated in this chapter is depicted in Fig. 5.1 and the general design parameters are listed in Table 2.2. The SPM rotor topology having full pole-arc is employed. The winding type is single-layer concentrated windings. The machine performance without considering the manufacturing tolerance has been fully

investigated in [36]. Again, it is worth noting that to avoid heavy local saturation, the widths of iron section of teeth with or without FGs are kept the same. For simplifying the future analyses, the six stator segments can be numbered from S1 to S6 in anticlockwise direction, as shown in Fig. 5.1.

In practice, the manufacturing process of modular PM machines is different from their conventional non-modular counterparts. The stator segment laminations of modular PM machines are cut and welded first. Benefit from the modular structure, the coils can be wound on the teeth of stator segments outside the machine. This could significantly simplify the winding process and also improve the slot fill factor. After then, the stator segments with coils will be inserted into the notches on the inner surface of the frame, forming a complete stator for modular machines.

However, during the assembly process of these segments, the manufacturing tolerance may occur, resulting in the different inner radii for different segments, etc. Therefore, the manufacturing tolerance such as the stator segment radial or circumferential displacement will be introduced. Moreover, during the rotor manufacturing process, other manufacturing tolerance scenarios may occur, such as the PM defect, which will also be detailed in this chapter.

Two representative modular PM machines having 12-slot/10-pole and 12-slot/14-pole are employed to investigate the influence of the manufacturing tolerance. The calculations of the other cases such as 12-slot/8-pole modular PM machines have also been carried out. It is found that the influence of manufacturing tolerance on the 12-slot/8-pole modular PM machine is similar as that for the 12-slot/10-pole counterparts. Due to the fact that the 12-slot/10-pole and 12-slot/14-pole cases are more typical, in this chapter, the study of the manufacturing tolerance will be mainly based on these two modular PM machines.

5.2 MODULAR PM MACHINES WITH RADIAL STATOR SEGMENT DISPLACEMENT

In reality, the scenarios of the manufacturing tolerance could be random. By way of example, for the radial stator segment displacement, the stator segments can be displaced randomly in different directions and distances. Due to these infinite possible cases of the manufacturing tolerance and for simplifying the studies carried out in this chapter, several assumptions and definitions have to be made. For example, the displacement distance is assumed to be 0.25mm. The stator segments displacing towards the machine centre are named as -Sn. Otherwise, they are named as +Sn.

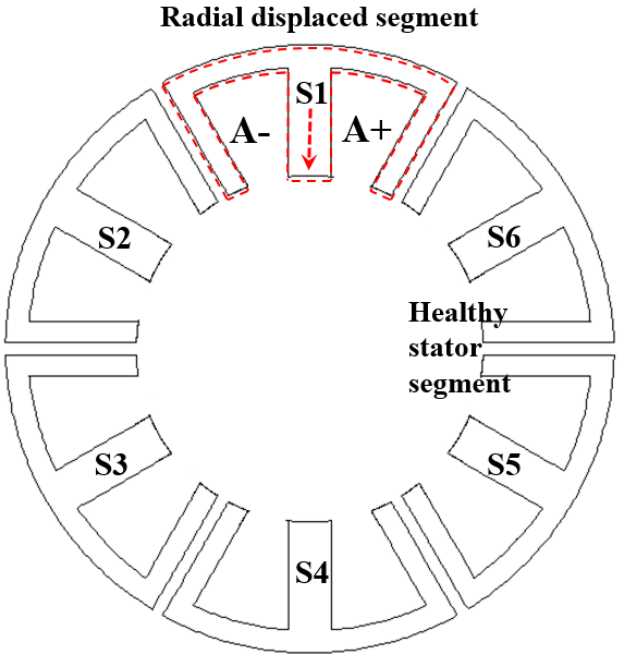

Fig. 5.2 The stator cross section of modular PM machine topology with the radial stator segments displacement (Case –S1).

5.2.1 INFLUENCE OF RADIAL STATOR SEGMENT DISPLACEMENT ON PHASE BACK-EMF

The stator cross-section of modular PM machine with one stator segment radially displaced is depicted in Fig. 5.2. For the radial stator segment displacement, the angles between the adjacent stator segments will not be changed. Hence the angles between the adjacent back-EMF vectors are maintained the same. This can be validated by the results shown in Table 5.1,

in which the phase angles of the phase back-EMFs of the 12-slot/10-pole modular PM machines having 2mm FG width either with or without radial stator segment displacement are calculated by the 2D FE model.

TABLE 5.1 THE PHASE ANGLES OF PHASE BACK-EMFS OF MODULAR PM MACHINES WITH OR WITHOUT RADIAL STATOR SEGMENT DISPLACEMENT

Phase angles (Elec. Deg.)	Phase A	Phase B	Phase C
Healthy	28.5	-91.5	148.5
-S1	28.5	-91.5	148.5
+S1	28.5	-91.5	148.5

However, because the air-gap length changes due to the radial stator segment displacement, the magnitudes of phase back-EMF vectors will be changed accordingly. Again, the 12-slot/10-pole modular PM machine having 2mm FG width with the radial stator segment displacements such as cases -S1 and +S1 are taken as examples. Since the stator segment S1 is displaced, leading to reduced or increased air-gap length for segment S1, the magnitude of E1 is increased or decreased accordingly, so does the resultant phase A back-EMF vector, as shown in Fig. 5.3 (a) and Fig. 5.4 (a). Whereas for the magnitudes of the resultant back-EMF vectors of the phases B and C, the influence from such radial stator segment displacement cases is limited.

To validate such predictions on the magnitudes of phase back-EMFs, the spectra of resultant three phase back-EMFs of cases +S1 and -S1 are calculated and compared in Table 5.2. It can be clearly seen that the magnitude of phase A is changed while the magnitudes of phases B and C remain largely unaffected.

TABLE 5.2 THE PHASE BACK-EMF MAGNITUDES OF MODULAR PM MACHINES WITH OR WITHOUT RADIAL STATOR SEGMENT DISPLACEMENT

Magnitudes (V)	Phase A	Phase B	Phase C
Healthy	12.36	12.36	12.36
-S1	12.74	12.37	12.37
+S1	12	12.36	12.37

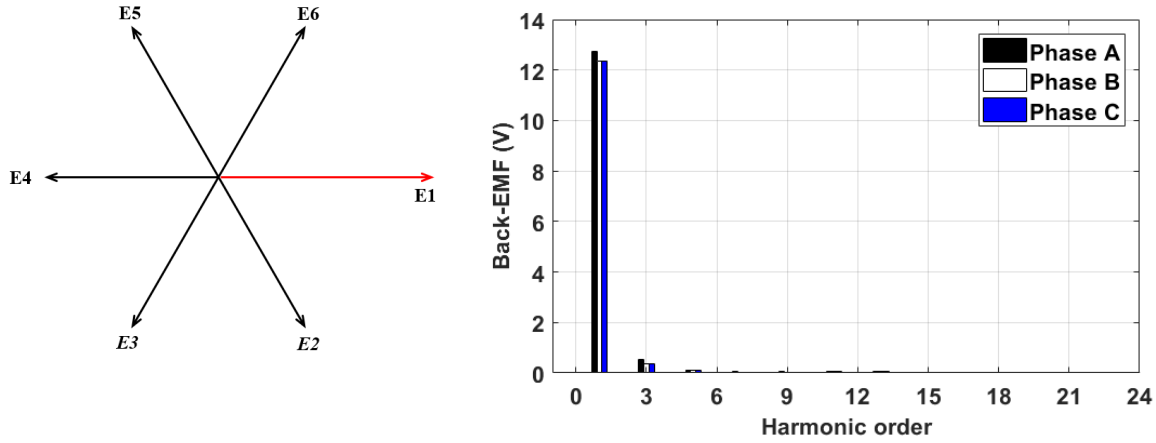

(a) (b)

Fig. 5.3 The Phase back-EMFs of 12-slot/10-pole modular PM machines with the radial stator segment of the case -S1. (a) Vector diagram. (b) Spectra.

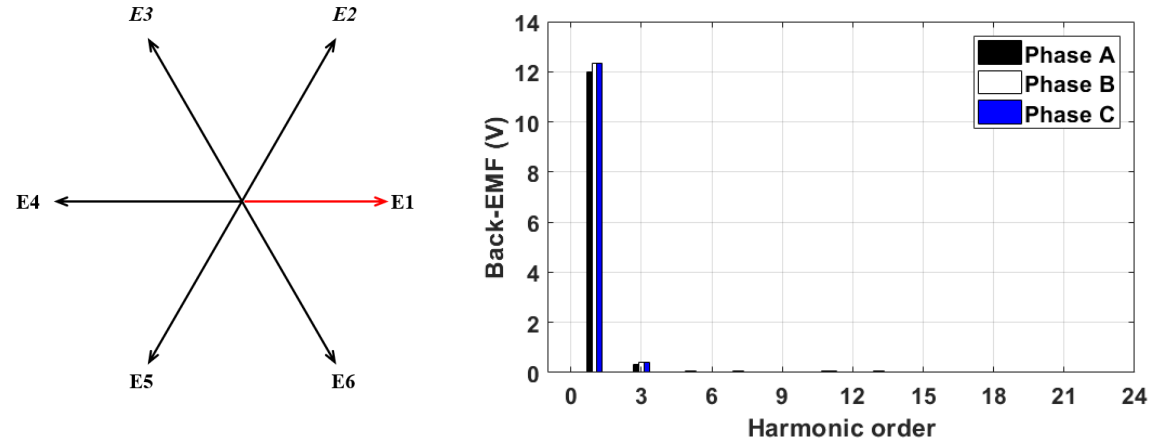

(a) (b)

Fig. 5.4 The Phase back-EMF of the 12-slot/10-pole modular PM machines with the radial stator segment of the case +S1. (a) Vector diagram. (b) Spectra.

5.2.2 Influence of Radial Stator Segment Displacement on On-Load Torque

Without considering the magnetic saturation, the on-load torque of the PM machines will be directly proportional to the phase back-EMFs and the supply phase currents, as detailed in (5.1). Therefore, the influence of the radial stator segment displacement on the phase back-

EMF will be reflected in the on-load torque as well.

$$T = \frac{E_A I_A + E_B I_B + E_C I_C}{\omega_m} \tag{5.1}$$

where E_A, E_B, E_C are the magnitudes of the three-phase back-EMFs. I_A, I_B, I_C are the three-phase supply currents and ω_m is the rotation speed.

The phase back-EMFs can be written as (5.2).

$$\begin{cases} E_A = \sum_{n=1,2,3,\cdots}^{\infty} E_{An}\, cos(n\omega t + \varphi_{An}) \\ E_B = \sum_{n=1,2,3,\cdots}^{\infty} E_{Bn}\, cos\left[(n\omega t - \frac{2n\pi}{3}) + \varphi_{Bn}\right] \\ E_C = \sum_{n=1,2,3,\cdots}^{\infty} E_{Cn}\, cos\left[(n\omega t + \frac{2n\pi}{3}) + \varphi_{Cn}\right] \end{cases} \tag{5.2}$$

where E_{An}, E_{Bn} , E_{Cn}, φ_{An}, φ_{Bn}, and φ_{Cn} are the magnitudes and the phase angles of the n^{th} order harmonics of the three-phase back-EMFs, respectively. ω denotes the electrical rotation speed and t is the time.

Similarly, the ideal three-phase currents can be expressed as (5.3)

$$\begin{cases} I_A = I\, cos(\omega t + \delta) \\ I_B = I\, cos(\omega t - \frac{2\pi}{3} + \delta) \\ I_C = I\, cos(\omega t + \frac{2\pi}{3} + \delta) \end{cases} \tag{5.3}$$

where I is the peak value. δ, denotes the phase angle of the supply currents.

By substituting the variables in (5.1) by (5.2)-(5.3) the equation can be rewritten as (5.4).

$$
\begin{aligned}
T \times \omega_m &= \sum_{n=1,2,3,\cdots}^{\infty} E_{An}I + E_{Bn}I + E_{Cn}I \\
&= \sum_{n=1,2,3,\cdots}^{\infty} E_{An}I \left\{ \frac{cos[(n-1)\omega t + \varphi_{An} - \delta]}{2} \right. \\
&\left. + \frac{cos[(n+1)\omega t + \varphi_{An} + \delta]}{2} \right\} \\
&+ \sum_{n=1,2,3,\cdots}^{\infty} E_{Bn}I \left\{ \frac{cos\left[(n-1)(\omega t - \frac{2\pi}{3}) + \varphi_{Bn} - \delta\right]}{2} \right. \\
&\left. + \frac{cos\left[(n+1)\left(\omega t - \frac{2\pi}{3}\right) + \varphi_{Bn} + \delta\right]}{2} \right\} \\
&+ \sum_{n=1,2,3,\cdots}^{\infty} E_{Cn}I \left\{ \frac{cos\left[(n-1)(\omega t + \frac{2\pi}{3}) + \varphi_{Cn} - \delta\right]}{2} \right. \\
&\left. + \frac{cos\left[(n+1)\left(\omega t + \frac{2\pi}{3}\right) + \varphi_{Cn} + \delta\right]}{2} \right\}
\end{aligned}
\tag{5.4}
$$

Under the healthy condition, when n equals 1, the average torque is given by (5.5). In other words, the fundamental harmonics of the three-phase back-EMFs contribute to the average torque.

$$
\begin{aligned}
T_{Average} \times \omega_m = E_{A1}I \left[\frac{cos(\varphi_{A1} - \delta)}{2}\right] + E_{B1}I \left[\frac{cos(\varphi_{B1} - \delta)}{2}\right] \\
+ E_{C1}I \left[\frac{cos(\varphi_{C1} - \delta)}{2}\right]
\end{aligned}
\tag{5.5}
$$

Therefore, the average torque can be employed as an index to assess the severity of the influence of manufacturing tolerance on the performance of the modular PM machines. In addition, it also can help to identify quickly the most serious cases from various possible radial stator segment displacements without the need for intensive FE simulations.

As have been demonstrated, due to the radial stator segment displacement, the magnitudes of the phase back-EMFs are affected, so does the average torque, as can be seen from (5.5). However, since the accurate analytical prediction on the increase or decrease in the phase back-EMF magnitudes due to the radial stator segment displacement is hardly achievable, in this

chapter, the coefficient τ is introduced to denote the variation of the back-EMF vector due to the radial stator segment displacement for simplicity.

TABLE 5.3 THE PREDICTED INFLUENCE OF THE AVERAGE TORQUE DUE TO THE RADIAL STATOR SEGMENT DISPLACEMENT

Case	Contribution	Case	Contribution
+S1	$-\frac{\tau I}{2\omega_m}$	+S1&+S2&+S4&+S5	$-\frac{2\tau I}{\omega_m}$
-S1&-S4	$\frac{\tau I}{\omega_m}$	+S1&+S2&-S4&-S5	0
+S1&-S4	0	+S1&-S2&+S4&-S5	0
-S1&-S2&-S3	$\frac{3\tau I}{2\omega_m}$	-S1&-S2&-S3&-S4&-S5	$\frac{5\tau I}{2\omega_m}$

In Table 5.3, the predicted influence of the average torque due to the radial stator segment displacement cases are listed. It is found that the cases where the stator segments are displaced in the same direction and the displaced stator segments belong to the same phase have the most severe influence on the average torque, e.g. case -S1&-S4. However, for the cases where the stator segments displaced in different directions, their influence on the on-load torque is limited, e.g. case +S1&-S4.

Moreover, due to the unequal magnitudes of the phase back-EMFs, the vector sum of the 2nd order harmonic is no longer zero. In other words, the radial stator segment displacement will lead to extra 2nd, 4th, 8th, etc. harmonics in the on-load torque, as shown in Fig. 5.9 and Fig. 5.10. This phenomenon can be explained by (5.4).

According to the severity assessment, the cases -S1, -S1&-S4, -S1&-S2&-S4&-S5, which have the most significant influence on machine performance, are selected for further investigating the influence of FG widths on modular PM machines with radial stator segment displacement.

5.2.3 INFLUENCE OF FG WIDTHS AND SLOT/POLE NUMBER COMBINATIONS ON MODULAR PM MACHINES WITH RADIAL STATOR SEGMENT DISPLACEMENT

To simplify the analyses, a changing ratio of the electromagnetic performance between

modular PM machines with or without manufacturing tolerance is introduced, as can be seen from (5.6),

$$Changing\ ratio = \frac{\sigma - \sigma_0}{\sigma_0} \times 100\% \tag{5.6}$$

where σ and σ_0 are the indexes of the electromagnetic performance of modular PM machines with or without manufacturing tolerance respectively.

The smaller the changing ratio is, the better the manufacturing withstand capability will be. However, it is worth noting that the changing ratio will not be employed to analyse the unbalanced magnetic force (UMF) since the initial UMF is zero for the healthy modular PM machines.

5.2.3.1 PHASE BACK-EMF

In this section, the analysis on the influence of FG widths as well as the slot/pole number combinations on fundamental phase back-EMFs of modular PM machines with the radial stator segment displacement is carried out. As an example, only the results for the phase A are shown in Fig. 5.5. It is found that the influence of FG widths on fundamental phase back-EMF of modular PM machines under the radial stator segment displacement is similar to the influence on healthy modular PM machines regardless of the slot/pole number combinations.

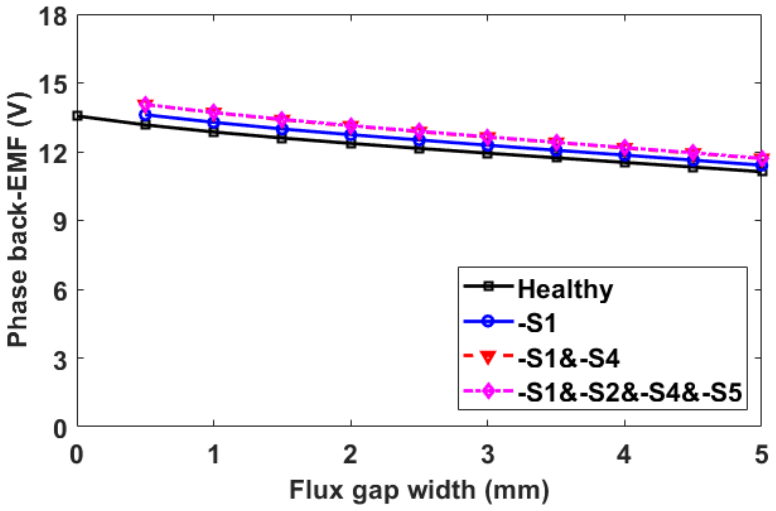

(a)

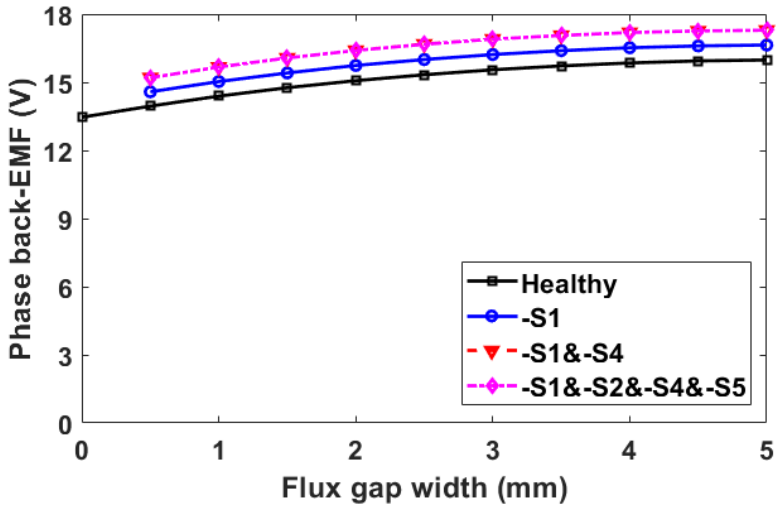

(b)

Fig. 5.5 The fundamental harmonics of phase A back-EMF versus FG width of modular PM machines with various radial stator segment displacements. (a) 12-slot/10-pole. (b) 12-slot/14-pole.

TABLE 5.4 THE CHANGING RATIOS OF THE FUNDAMENTAL HARMONICS OF THE PHASE A BACK-EMF OF MODULAR PM MACHINES WITH RADIAL STATOR SEGMENT DISPLACEMENT

FG widths (mm)	Case:-S1 (12slot-10pole/12slot-14pole)	Case: -S1&-S4 (12slot-10pole/12slot-14pole)	Case: -S1&-S2&-S4&-S5 (12slot-10pole/12slot-14pole)
0.5	3.35% / 4.52%	6.69% / 8.96%	6.77% / 8.96%
1.0	3.29% / 4.45%	6.55% / 8.9%	6.63% / 8.9%
1.5	3.15% / 4.4%	6.32% / 8.88%	6.48% / 8.88%
2.0	3.08% / 4.45%	6.15% / 8.83%	6.31% / 8.83%
2.5	3.03% / 4.37%	5.99% / 8.81%	6.16% / 8.74%
3.0	2.9% / 4.31%	5.83% / 8.68%	6% / 8.68%
3.5	2.8% / 4.26%	5.7% / 8.52%	5.79% / 8.52%
4.0	2.78% / 4.23%	5.47% / 8.45%	5.64% / 8.45%
4.5	2.67% / 4.14%	5.32% / 8.28%	5.49% / 8.28%
5.0	2.57% / 4.13%	5.18% / 8.2%	5.27% / 8.2%

It can be seen that the changing ratio of the fundamental back-EMF is slightly decreased with the increase in FG widths for both 12-slot/10-pole and the 12-slot/14-pole modular PM machines. In other words, the severity of the influence on the fundamental phase back-EMFs from the radial stator segment displacement can be mitigated with the increase in the FG widths, as listed in Table 5.4. Besides, it is worth noting that the changing ratios of the 12-slot/10-pole modular PM machines are generally smaller than those of the 12-slot/14-pole machines. As a result, one can conclude that the 12-slot/10-pole modular PM machines have the better radial stator segment displacement withstand capability in terms of phase back-EMFs.

5.2.3.2 COGGING TORQUE

It has been found that the cogging torque is sensitive to the design parameters of PM machines such as the machine symmetry, slot/pole number combinations, and stator structure, etc. This is also true for their modular counterparts. It is evident that when the manufacturing tolerance occurred, the symmetry of modular PM machines will be changed, and thus, could exert significant impact on the cogging torque characteristics.

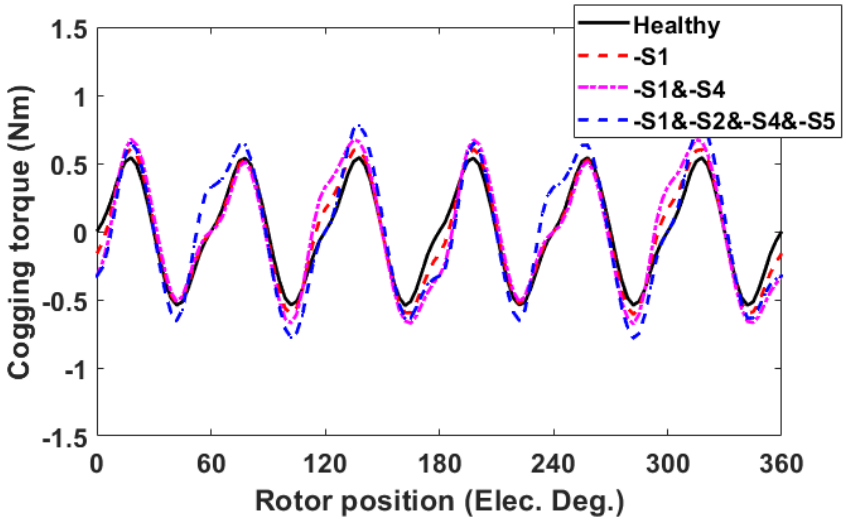

(a)

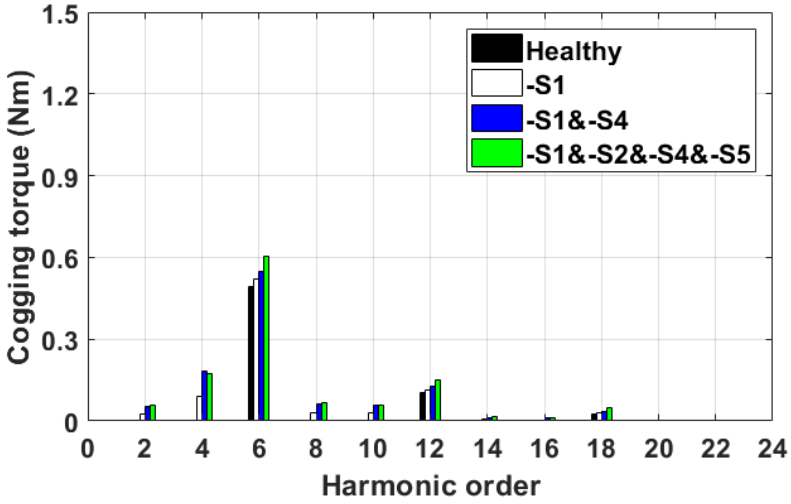

(b)

Fig. 5.6 Cogging torque of the 12-slot/10-pole modular PM machines with the radial stator segment displacement. (a) Waveforms. (b) Spectra. (FG=2mm).

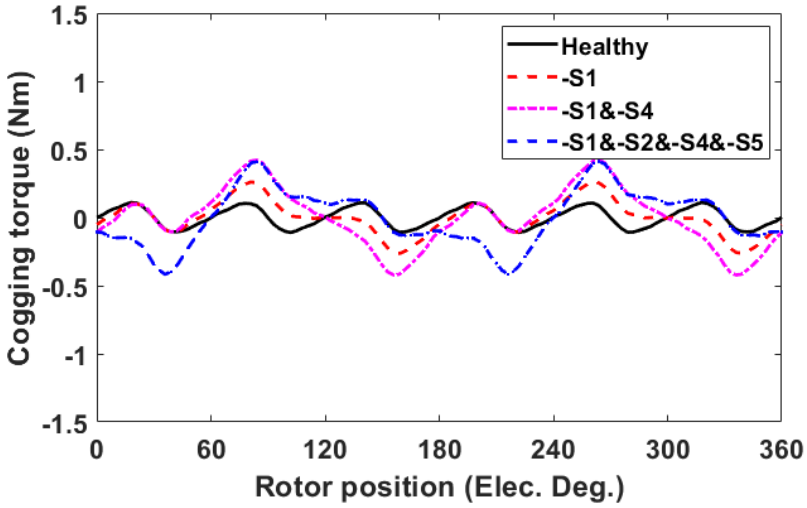

(a)

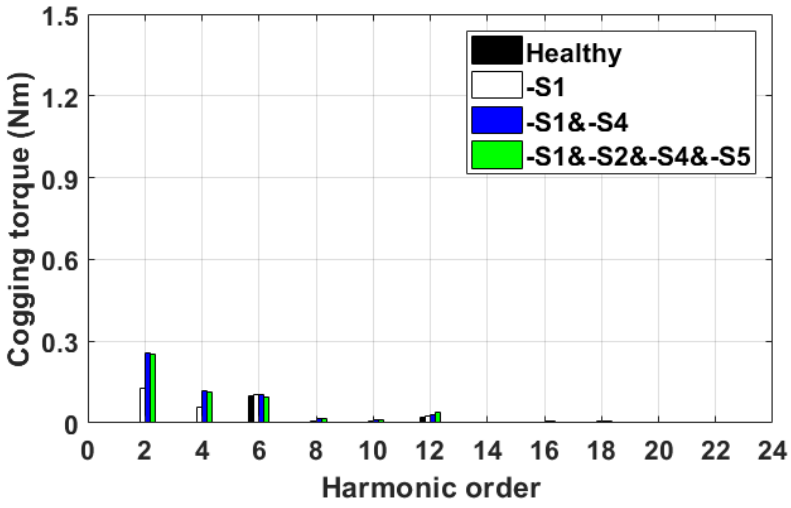

(b)

Fig. 5.7 Cogging torque of the 12-slot/14-pole modular PM machines with the radial stator segment displacement. (a) Waveforms. (b) Spectra. (FG=2mm).

The cogging torque periodicity is mainly determined by the rotor pole number and the stator symmetry. For the healthy modular PM machines, the stator symmetry is determined by the N_{FG} [66]. However, for the modular PM machines with radial stator segment displacement, the stator symmetry is determined by the distribution of the displaced stator segments rather than the N_{FG}. Because of this, the cogging torque periodicity of the modular PM machines with radial stator segment displacement will be changed.

By way of example, for the 12-slot/10-pole modular PM machines under radial stator segment displacement of the case -S1, the stator symmetry is changed from 6 to 1 and hence, the LCM between $2p$ and the stator symmetry is changed to 10. This means that the N_{cm} of such modular PM machines within a mechanical revolution is 10 and 2 within an electrical revolution. This means that the first appeared harmonic of the cogging torque will be the 2nd order harmonic.

For validating this prediction, the cogging torque waveforms and their spectra within one electrical revolution of the 12-slot/10-pole and 12-slot/14-pole modular PM machines are depicted in Fig. 5.6 and Fig. 5.7. It can be clearly seen that the additional 2nd, 4th, and 8th, etc. harmonics are introduced due to the radial stator segment displacement.

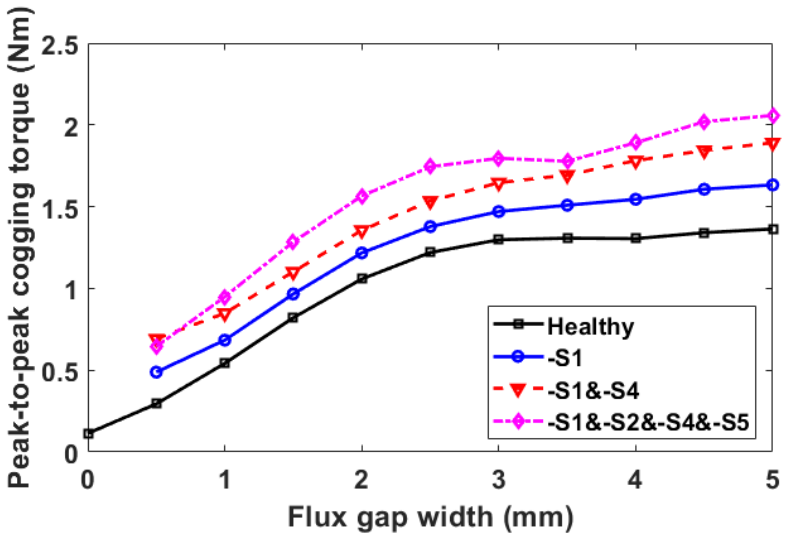

(a)

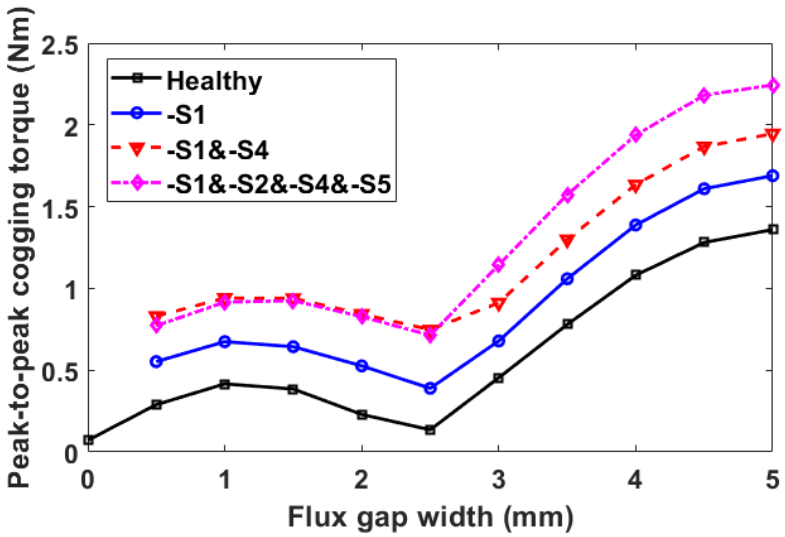

(b)

Fig. 5.8 The peak-to-peak cogging torque versus FG width of modular PM machines with radial stator segment displacement. (a) 12-slot/10-pole. (b) 12-slot/14-pole.

The peak-to-peak cogging torques of modular PM machines under the selected cases are depicted in Fig. 5.8. It is found that the influences of FG widths on the peak-to-peak cogging torque of modular PM machines with or without radial stator segment displacement conditions are similar for all the slot/pole number combinations.

The changing ratio of the peak-to-peak cogging torque of modular PM machines are illustrated in Table 5.5. It is found that for both the 12-slot/10-pole and the 12-slot/14-pole

modular PM machines, the changing ratio can be decreased significantly by selecting the proper FG widths. Additionally, the changing ratios of the peak-to-peak cogging torque of the 12-slot/14-pole modular PM machines are generally bigger than those of the 12-slot/10-pole machines. Therefore, regarding the peak-to-peak cogging torque, the 12-slot/10-pole modular PM machines again have the better radial stator segment displacement withstand capability.

TABLE 5.5 THE CHANGING RATIOS OF THE PEAK-TO-PEAK COGGING TORQUE OF MODULAR PM MACHINES WITH RADIAL STATOR SEGMENT DISPLACEMENT

FG widths (mm)	Case:-S1 (12slot-10pole/12slot-14pole)	Case: -S1&-S4 (12slot-10pole/12slot-14pole)	Case: -S1&-S2&-S4&-S5 (12slot-10pole/12slot-14pole)
0.5	63.93% / 89.89%	132.36%/185.36%	116.36% / 165.36%
1.0	23.78% / 63.57%	53.65% / 128.22%	71.8% / 122.26%
1.5	14.45% / 70.45%	30.51% / 148.7%	52.1% / 145.02%
2.0	12.15% / 139.39%	24.9% / 283.67%	44.21% / 276.22%
2.5	10.63% / 148%	23.2% / 376.1%	40.02% / 354.52%
3.0	11.41% / 38.33%	24.77% / 85.85%	36.08% / 133.11%
3.5	13.05% / 27.78%	26.87% / 56.79%	33.19% / 89.82%
4.0	16.71% / 20.75%	34.58% / 42.24%	42.83% / 68.6%
4.5	17.41% / 18.09%	34.77% / 36.99%	47.6% / 60.06%
5.0	17.33% / 17.38%	35.85% / 35.22%	47.86% / 55.91%

5.2.3.3 ON-LOAD TORQUE

From Fig. 5.9 to Fig. 5.10, the on-load torque waveforms and their spectra of modular PM machines investigated in this section with the radial stator segment displacement are depicted. The reasons of the increased average torque with the increase in the number of radial stator segment displacement in the same direction can be explained by theory detailed in section 5.2.2.

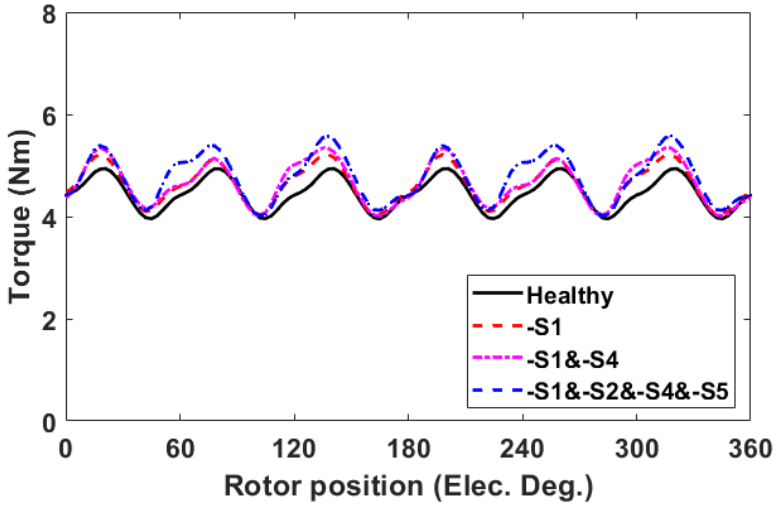

(a)

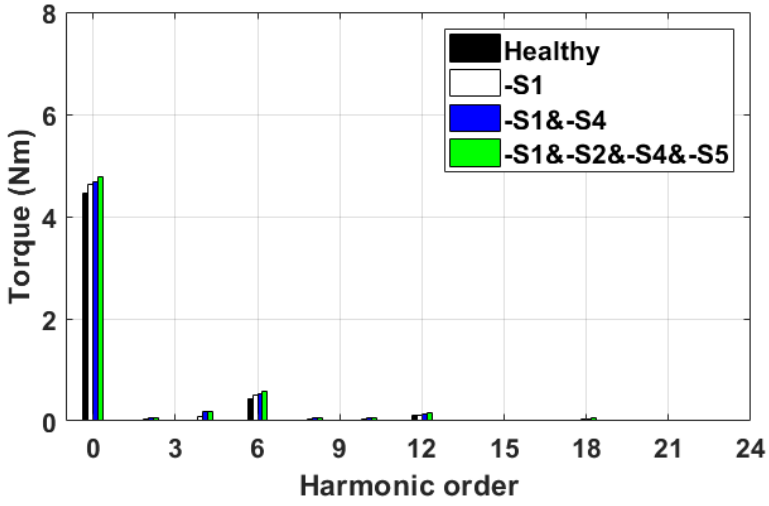

(b)

Fig. 5.9 On-load torque of the 12-slot/10-pole modular PM machines with radial stator segment displacement. (a) Waveforms. (b) Spectra. (FG=2mm).

Clearly, it can be found that the first appeared torque ripple harmonics of the 12-slot/10-pole and 12-slot/14-pole modular PM machines are the 2nd order harmonics rather than the 6th order harmonics of healthy modular PM machines. Such additional 2nd order harmonics come from three sources: 1) the 2nd order harmonic of cogging torque that has been demonstrated previously. 2) the contribution from the unbalanced fundamental three phase back-EMFs. 3) the contribution from the unbalanced 3rd order harmonics of the phase back-EMFs, as detailed

in (5.4). The average toque versus FG widths of modular PM machines with the radial stator segment displacement are shown in Fig. 5.11. It is found that the influences of FG widths on the average torque of modular PM machines either with or without radial stator segment displacement are similar.

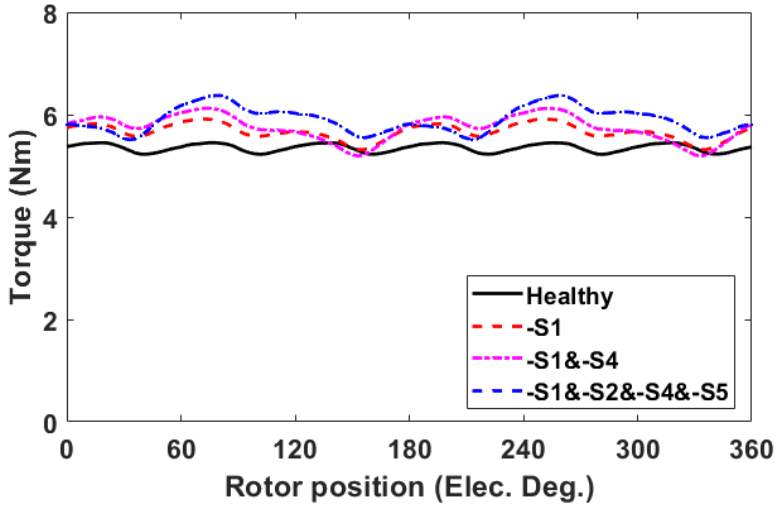

(a)

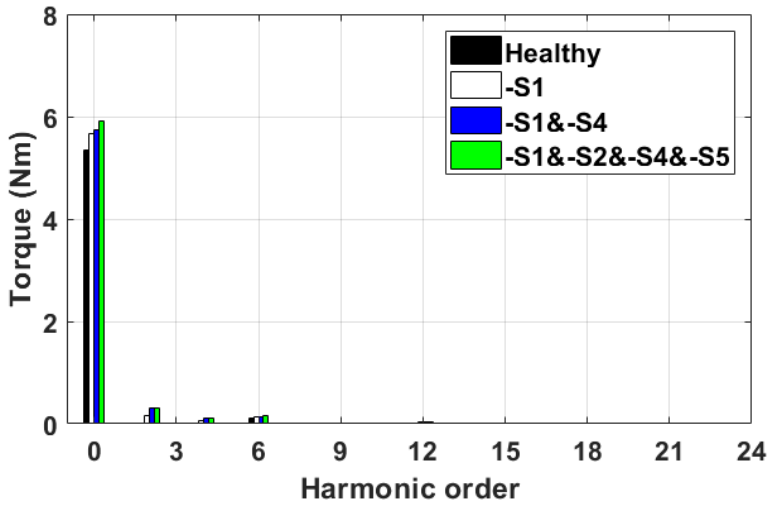

(b)

Fig. 5.10 On-load torque of the 12-slot/14-pole modular PM machines with the radial stator segment displacement. (a) Waveforms. (b) Spectra. (FG=2mm).

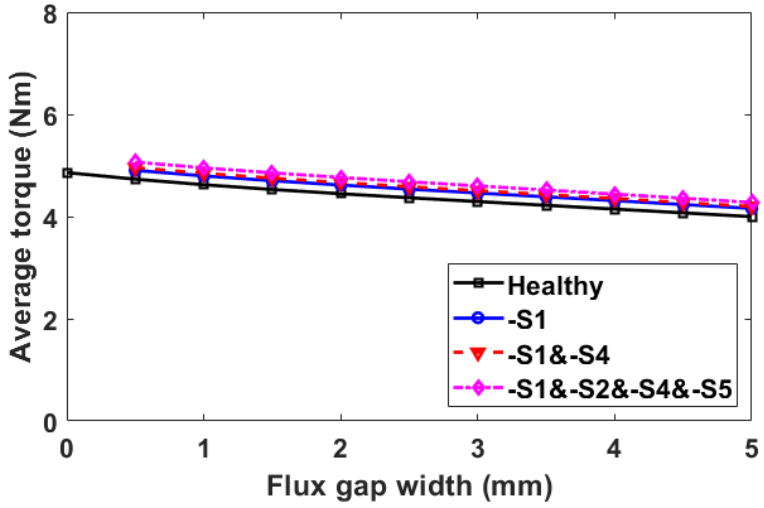

(a)

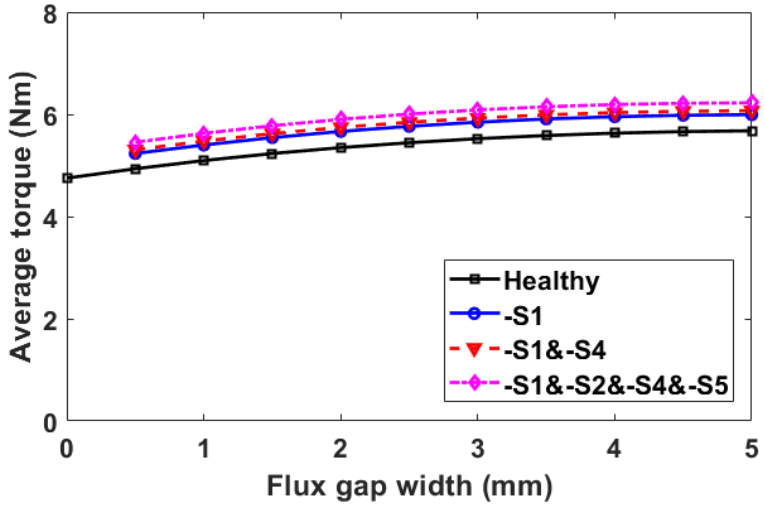

(b)

Fig. 5.11 The average torque versus FG widths of modular PM machines with the radial stator segment displacement. (a) 12-slot/10-pole. (b) 12-slot/14-pole.

The changing ratios of average torque are listed in Table 5.6. Overall, the influence of FG widths on the changing ratio of the average torque is limited for both the 12-slot/10-pole and the 12-slot/14-pole modular PM machines. However, for the 12-slot/14-pole modular PM machines, the changing ratio can be slightly decreased by selecting a proper FG width. Furthermore, the changing ratios of the 12-slot/10-pole modular PM machines are smaller. This means that they also have the better radial stator segment displacement withstand capability in

terms of average torque compared with their 12-slot/14-pole counterparts. Since the cogging torque is dominant in torque ripple contributions, the influence of FGs on the cogging torque will be reflected in the performance of torque ripple. Hence, the same conclusion as for the cogging torque can be drawn for torque ripple as well.

TABLE 5.6 THE CHANGING RATIOS OF THE AVERAGE TORQUE OF MODULAR PM MACHINES WITH RADIAL STATOR SEGMENT DISPLACEMENT

FG widths (mm)	Case:-S1 (12slot-10pole/12slot-14pole)	Case: -S1&-S4 (12slot-10pole/12slot-14pole)	Case: -S1&-S2&-S4&-S5 (12slot-10pole/12slot-14pole)
0.5	3.65% / 6.07%	4.78% / 7.54%	7.07% / 10.51%
1.0	3.72% / 6.01%	4.85% / 7.50%	7.13% / 10.46%
1.5	3.78% / 6.16%	4.89% / 7.64%	7.16% / 10.6%
2.0	3.83% / 5.92%	4.93% / 7.4%	7.18% / 10.33%
2.5	3.87% / 5.88%	4.95% / 7.36%	7.16% / 10.28%
3.0	3.91% / 5.84%	4.97% / 7.3%	7.14% / 10.19%
3.5	3.95% / 5.79%	4.99% / 7.22%	7.11% / 10.07%
4.0	3.98% / 5.72%	4.99% / 7.13%	7.06% / 9.94%
4.5	4.01% / 5.65%	5% / 7.04%	7.02% / 9.79%
5.0	4.05% / 5.76%	5.01% / 7.13%	6.99% / 9.84%

5.2.3.4 UMF

The UMF causes vibrations and acoustic noise and also leads to the undesired negative effect on the shaft and reduces the lifetime of bearings. In this section, the UMF due to the radial stator segment displacement is investigated. As shown in Fig. 5.12, the UMF under on-load condition of 12-slot/10-pole modular PM machines having 2mm FG width with radial stator segment displacement is calculated. For the healthy modular PM machines, due to the symmetrical stator and rotor structures, the UMF should be zero, as proven by the results shown in Fig. 5.12.

However, for the modular PM machines under some of the typical cases of radial stator segment displacement, the stator structures are still remained symmetrical, which results in zero UMF as well. By way of example, for the selected case -S1&-S4 and case -S1&-S2&-

S4&-S5, the UMFs of both x-axis (F_x) and y-axis (F_y) are zero, as proven by the results shown in Fig. 5.12.

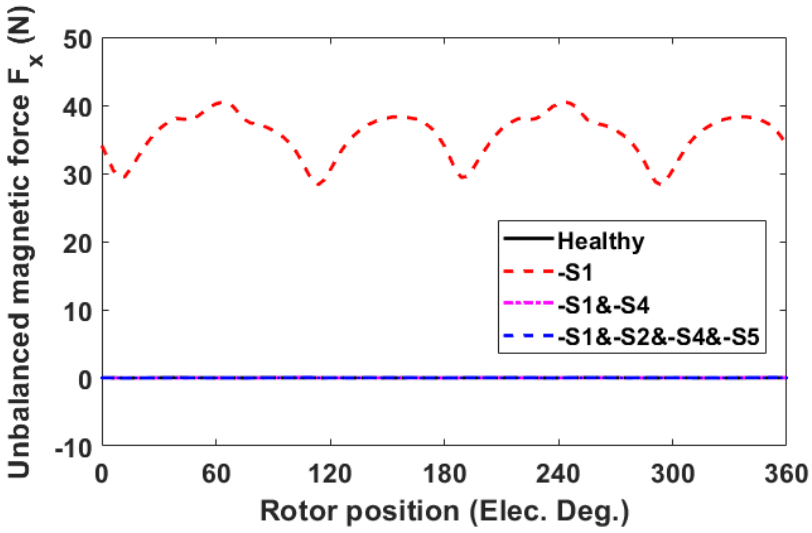

(a)

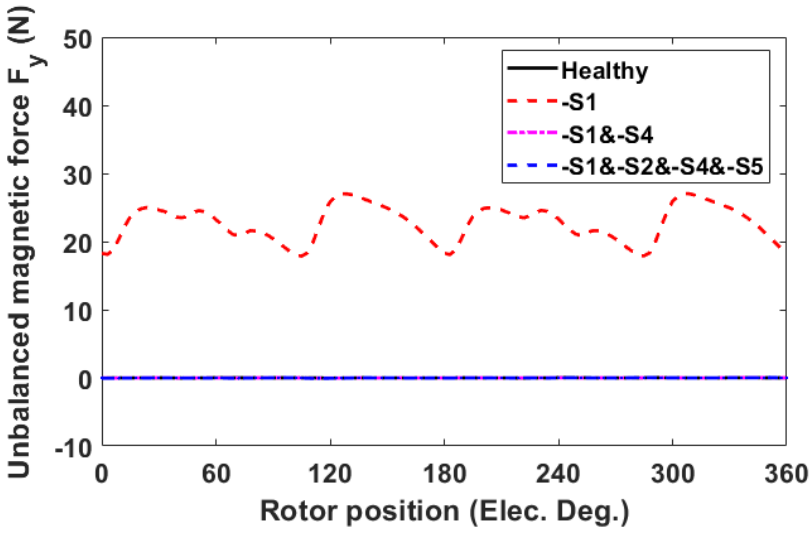

(b)

Fig. 5.12 The UMF waveforms of the 12-slot/10-pole modular PM machines. (a) F_x. (b) F_y.

Nevertheless, for the modular PM machines with radial stator segment of case -S1, the stator structure becomes asymmetric which lead to the non-zero UMF, as shown in Fig. 5.12. It is worth noting that the UMFs of x-axis are bigger than those of y-axis regardless of slot/pole number combinations. This is mainly due to the position of the stator segment S1, which is closer to the x-axis but far from the y-axis.

In Fig. 5.13, the influence of FG widths on the magnitudes of on-load UMFs of modular PM machines under the radial stator segment of case -S1 is depicted. It is found that for the F_x of both 12-slot/10-pole and the 12-slot/14-pole modular PM machines, the magnitudes are increased with the increase in FG widths. However, for the UMF of F_y, the magnitudes are decreased. Furthermore, it can be found from Fig. 5.13 that the UMF magnitudes of the 12-slot/14-pole modular PM machines are generally higher than those of 12-slot/10-pole modular PM machines. This helps further to prove that the 12-slot/10-pole modular PM machines have better radial stator segment displacement withstand capability.

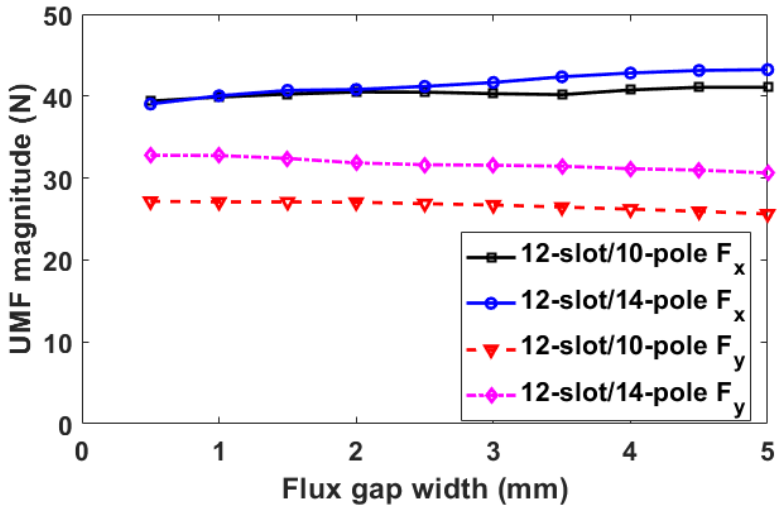

Fig. 5.13 The UMF magnitudes versus FG widths of modular PM machines with radial stator segment displacement of case -S1.

5.3 MODULAR PM MACHINES WITH CIRCUMFERENTIAL STATOR SEGMENT DISPLACEMENT

In the section 5.2, the influence of manufacturing tolerance due to radial stator segment displacement on performance of modular PM machines has been investigated. In this section, another possible manufacturing tolerance scenario such as circumferential stator segment will also be investigated, as shown in Fig. 5.14.

Similarly, the stator segments are numbered from S1 to S6. The stator segment displaced in anti-clockwise is named as S1, S1&S4, etc., while for the stator segments displaced in clockwise they are named as -S1, -S1&-S4, etc. Moreover, for all the cases studied in this section, the circumferentially displaced angles of stator segments are assumed to be 25% of the maximum possible displaced angle, which depends on the FG width. By doing so, the displaced angles of modular PM machines having different FG widths can be different, as can be seen from Table 5.7. It is worth noting that the displaced angles for all the affected stator segments are assumed to be the same.

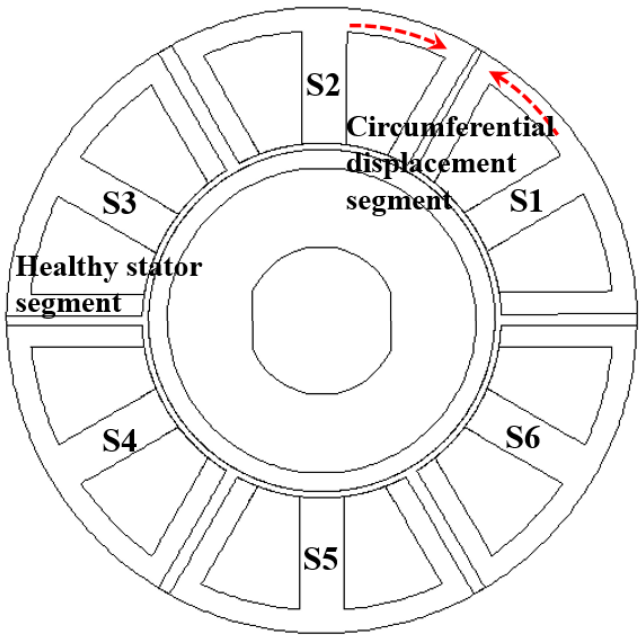

Fig. 5.14 The stator cross section of the modular PM machines topologies with the circumfermtial stator segments displacement (Case S1&-S2).

TABLE 5.7 THE MAXIMUM POSSIBLE DISPLACED ANGLES AND THE ACTUAL DISPLACED ANGLES AGAINST DIFFERENT FG WIDTHS

FG width (mm)	Maximum displaced angle (Mech. Deg.)	Displaced angle (Mech. Deg.)	FG width (mm)	Maximum displaced angle (Mech. Deg.)	Displaced angle (Mech. Deg.)
0.5	0.5	0.125	1.0	1.1	0.275
1.5	1.7	0.425	2.0	2.2	0.55
2.5	2.8	0.7	3.0	3.4	0.85
3.5	4	1.00	4.0	4.5	1.125
4.5	5.1	1.275	5.0	5.7	1.425

5.3.1 INFLUENCE OF CIRCUMFERENTIAL STATOR SEGMENT DISPLACEMENT ON PHASE BACK-EMF

As have been addressed above, the radial stator segment displacement exerts significant influence on the magnitudes of back-EMFs due to the change of air-gap length. However, for the modular PM machines under circumferential stator segment displacement, the phase angles of phase back-EMFs will be influenced more significantly than their magnitudes. This is mainly due to the fact that the angles between two adjacent stator segments, and thus the angles between two adjacent coils, will be changed due to the circumferential stator segment displacement.

By way of example, as can be seen in Fig. 5.15, the back-EMF vector diagram of the 12-slot/10-pole modular PM machines having 2mm FGs with the circumferential stator segment displacement of case S1&S4 are depicted. Under such a circumstance, the displaced angle is 0.55 Mech. Deg. In this case, the phase angle of the phase A back-EMF will be expected to be displaced by 2.75 Elec. Deg. as calculated in (5.7). However, the magnitudes of the resultant three-phase back-EMF vectors would remain the same.

$$0.55\ Mech.Deg. \times 5 = 2.75\ Elec.Deg. \tag{5.7}$$

where 5 is the pole pair number for a 12-slot/10-pole machine.

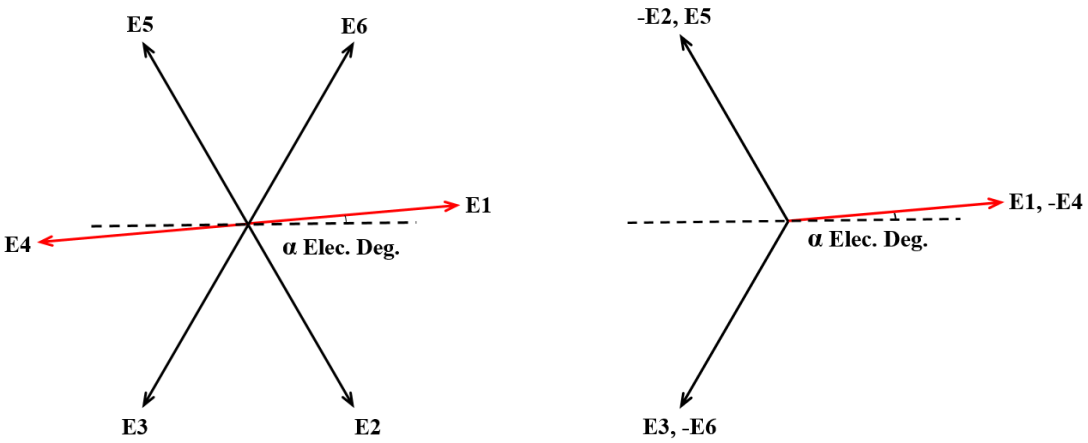

(a) (b)

Fig. 5.15 The fundamental phase back-EMFs of the modular PM machines with circumferential stator segment displacement. (a) Back-EMF vectors of each coil. (b) The resultant three phase back-EMF vectors. (Case S1&S4).

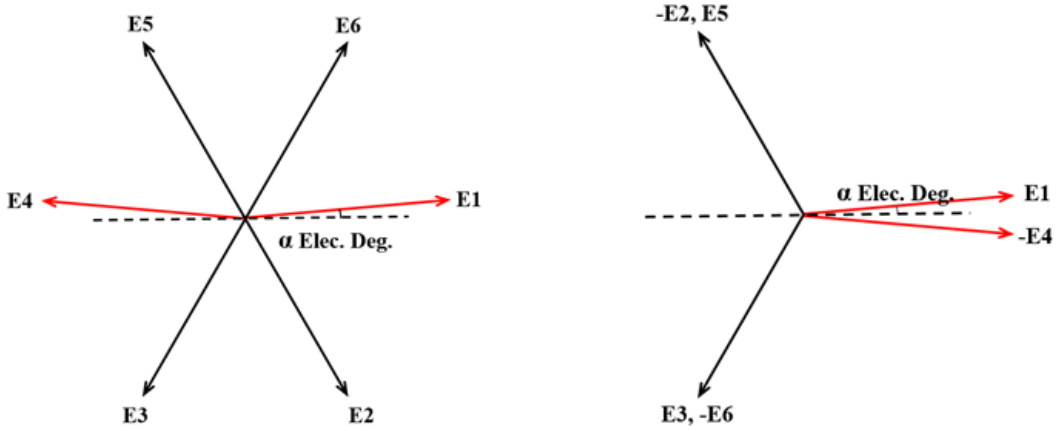

(a) (b)

Fig. 5.16 The fundamental phase back-EMFs of the modular PM machines with circumferential stator segment displacement. (a) Back-EMF vectors dof each coil. (b) The resultant three phase back-EMF vectors. (Case S1&-S4).

Nevertheless, although the magnitudes of the back-EMF vectors due to each coil will be maintained, it is still possible that the resultant phase back-EMFs under the influence of circumferential stator segment displacement will be decreased. By way of example, for the case of S1&-S4, as shown in Fig. 5.16., the back-EMF vector of phase A is decreased. However, it

is worth noting that such decrease in the resultant phase back-EMF vectors is too tiny and can be neglected.

The predicted and calculated magnitudes and phase angles of phase back-EMFs of 12slot/10-pole modular PM machines having 2mm FG with cases S1&S4 or S1&-S4 are listed in Table 5.8. The magnitudes and phase angles of phase back-EMFs of modular PM machines without the circumferential stator segment displacement can be calculated by FE first. As demonstrated above, for the case of S1&S4, the magnitudes of phase back-EMFs are expected to be maintained, but the phase angle of phase A back-EMF is expected to be displaced by 2.75 Elec. Deg. theoretically. Then, the new phase angle of the phase A back-EMF under the influence of the case S1&S4 can be predicted as:

$$28.5\ Elec.Deg. - 2.75\ Elec.Deg. = 25.75\ Elec.Deg. \tag{5.8}$$

TABLE 5.8 THE PREDICTED AND CALCULATED MAGNITUDES AND PHASE ANGLES OF MODULAR PM MACHINES WITH CIRCUMFERENTIAL STATOR SEGMENT

	Case S1&S4			Case S1&-S4		
Fundamental phase Back-EMFs	Phase A	Phase B	Phase C	Phase A	Phase B	Phase C
Magnitude (Predicted)	12.36V	12.36V	12.36V	12.31V	12.36V	12.36V
Magnitude (Calculated)	12.37V	12.35V	12.37V	12.33V	12.37V	12.37V
Phase angle (Predicted)	25.75 Elec. Deg.	-91.5 Elec. Deg.	148.5 Elec. Deg.	28.5 Elec. Deg.	-91.5 Elec. Deg.	148.5 Elec. Deg.
Phase angle (Calculated)	24.98 Elec. Deg.	-91.1 Elec. Deg.	148.9 Elec. Deg.	28.5 Elec. Deg.	-91.43 Elec. Deg.	148.4 Elec. Deg.

From Table 5.8, it can be found that the calculated phase angle using direct FE for case S1&S4 circumferential stator segment displacement is 24.98 Elec. Deg., which is very close to the predicted 25.75 Elec. Deg. While the phase angles and magnitudes of other phase back-EMFs are unchanged, as compared in Table 5.8. Therefore, it can be concluded that the above theoretical predictions made on magnitudes and phase angles of phase back-EMFs under the influence of circumferential stator segment are validated.

5.3.2 INFLUENCE OF CIRCUMFERENTIAL STATOR SEGMENT DISPLACEMENT ON ON-LOAD TORQUE

As aforementioned, the circumferential stator segment displacement impacts the phase angles of phase back-EMFs but has limited influence on their magnitudes. Therefore, in this section, we will only investigate the influence of phase angles of phase back-EMFs on the on-load torque.

As can be seen from (5.5), when the phase angles of fundamental phase back-EMFs are changed, the average torque will be influenced accordingly. However, it is found that such influence is also very minor. By way of example, the 12-slot/10-pole modular PM machines having 5mm FG and two cases such as S1&S4 and S1&S2&S3 are considered, of which the displaced angle is 0.55 Mech. Deg. For the case of S1&S4, the predicted on-load average torque only decreases by 0.26% while for the case of S1&S2&S3, the on-load average torque is decreased by 0.19%. This is mainly due to the fact that the minor change in the phase angles cannot exert dramatic influence on the average torque, as can be proved by (5.5).

Because of the limited influence on average torque from the circumferential stator segment displacement, the average torque cannot be applied as the index to assess the sensitivity of such type of manufacturing tolerance. However, similar to the radial stator segment displacement, the circumferential stator segment displacement also introduces an extra 2nd order harmonic to the on-load torque waveform. Hence, the 2nd order harmonic of on-load torque has been selected for further study in this section.

The 2nd order harmonic of on-load torque contributed by the fundamental phase back-EMFs, i.e. $T_{2ndFunda}$, can be expressed as (5.9). Given the fact that the magnitudes of phase back-EMFs are not significantly affected, $T_{2ndFunda}$ will mainly be generated by the variations of phase angle.

$$
\begin{aligned}
T_{2ndFunda} \times \omega_m \\
&= E_{A1} I \left\{ \frac{cos[2\omega t + \varphi_{A1} + \varphi]}{2} \right\} \\
&+ E_{B1} I \left\{ \frac{cos\left[2\left(\omega t - \frac{2\pi}{3}\right) + \varphi_{B1} + \varphi\right]}{2} \right\} \\
&+ E_{C1} I \left\{ \frac{cos\left[2\left(\omega t + \frac{2\pi}{3}\right) + \varphi_{C1} + \varphi\right]}{2} \right\}
\end{aligned} \tag{5.9}
$$

TABLE 5.9 THE PREDICTED AND CALCULATED $T_{2ndFunda}$ WITH THE RESULTANT CALCULATED 2ND ORDER HARMONIC OF ON-LOAD TORQUE

Case	$T_{2ndFunda}$ (Predicted)	$T_{2ndFunda}$ (Calculated)	T_{2nd} Resultant (Calculated)
S1	0.04	0.05	0.09
-S1	0.04	0.05	0.1
S1&S2	0.04	0.05	0.09
S1-S2	0.06	0.09	0.17
S1&S4	0.07	0.1	0.18
S1-S4	0.002	0.002	0.01
S1&S2&S4&S5	0.07	0.1	0.19
S1&S2&-S4&-S5	0.002	0.003	0
S1&-S2&S4&-S5	0.13	0.18	0.35
S1&-S2&-S4&-S5	0.08	0.08	0.2
S1&S2&S3&S4&S5&S6	0	0.001	0
S1&S2&S3&-S4&-S5&-S6	0	0.003	0.03
S1&-S2&S3&S4&-S5&S6	0.15	0.2	0.39
S1&-S2&-S3&S4&-S5&-S6	0.15	0.2	0.37

It can be predicted from (5.9) that the bigger difference between the phase angles of resultant phase back-EMFs such as ($\varphi_{A1} - \varphi_{B1}$) and the original 120 Elec. Deg., the bigger $T_{2ndFunda}$ will be. By way of example, for the 12-slot/10-pole modular PM machines having 2mm FG width, the phase angle difference of cases S1&S2 and S1&S4 are 1.375 Elec. Deg. and 2.75 Elec. Deg., respectively. This means that the case S1&S4 will have the slightly bigger

$T_{2ndFunda}$ than case S1&S2.

For validating the theoretical predictions of $T_{2ndFunda}$, the predicted and calculated $T_{2ndFunda}$ as well as the calculated resultant 2^{nd} order harmonics of the on-load torque are listed and compared in Table 5.9. The modular PM machines having 12-slot/10-pole and 2mm FGs with various circumferential stator segment displacement cases. It is worth noting that the predicted $T_{2ndFunda}$ is calculated by the theoretically predicted phase angles and magnitudes of phase back-EMFs. But the calculated $T_{2ndFunda}$ is computed using the phase angles and magnitudes of phase back-EMFs obtained from the FE results. The resultant T_{2nd} is calculated using direct FE.

As can be seen from Table 5.9, there are some error between the predicted and calculated $T_{2ndFunda}$. This is because of the inevitable error between the predicted and calculated phase angles and magnitudes of phase back-EMFs. However, it is still true that the smaller the predicted $T_{2ndFunda}$ is, the smaller the calculated $T_{2ndFunda}$ will be, and vice versa.

As has been demonstrated that the T_{2nd} of on-load torque of modular PM machines under the radial stator segment is generated by three sources, as detailed in the section 5.2.3.3. This is also true for the circumferential stator segment scenario. However, due to the much smaller 3rd order harmonics of the phase back-EMFs compared with the fundamental ones, the phase angles and magnitudes cannot be accurately predicted. Similarly, the 2nd order harmonics of the cogging torque due to the circumferential stator segment displacement are also very difficult to predict. Nevertheless, from Table 5.9, it is found that the bigger the predicted $T_{2ndFunda}$ is, the bigger T_{2nd} will be, and vice versa. This means that although T_{2nd} is difficult to predict, the influence from various cases of the circumferential stator segment displacement on $T_{2ndFunda}$ can fully reflect the performance of T_{2nd}.

Based on the analysis carried out above, the severity of the influence from circumferential stator segment displacement in respect to T_{2nd} of the modular PM machines can be assessed. The bigger T_{2nd} is, the more influence it will have on the machine performance. Based on this, the cases of S1&S4, S1&-S2&S4&-S5, and S1&-S2&S3&S4&-S5&S6, which have the relatively bigger T_{2nd} compared with other cases, will be selected for further studying.

5.3.3 INFLUENCE OF SLOT/POLE NUMBER COMBINATIONS ON MODULAR PM MACHINES WITH CIRCUMFERENTIAL STATOR SEGMENT DISPLACEMENT

In this section, the influence of slot/pole number combination of modular PM machines with the selected cases of circumferential stator segment displacement will be studied. It is worth noting that the influence of FG widths on the electromagnetic performance of modular PM machines will not be investigated due to the fact that the displaced angles are different, which depend directly on the FG widths. Moreover, the changing ratio will not be employed neither due to the same reason. In this section, only the research of the influence of the slot/pole number combination on modular PM machines with the circumferential stator segment displacement will be carried out.

5.3.3.1 PHASE BACK-EMF

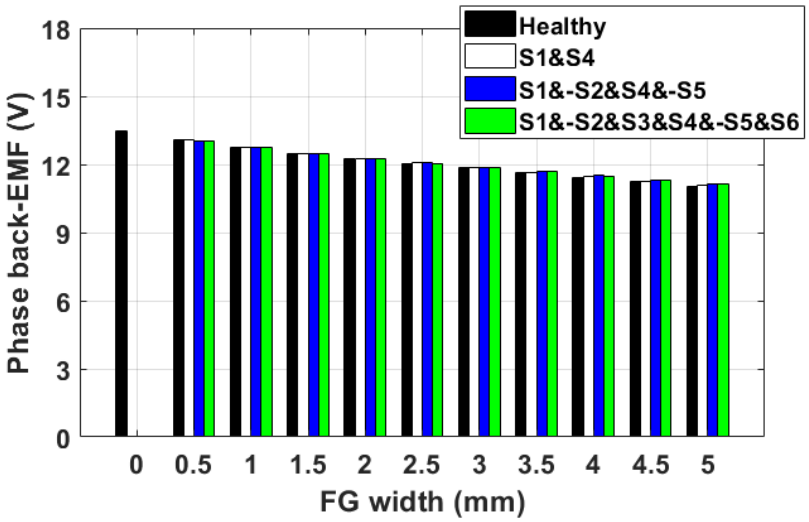

(a)

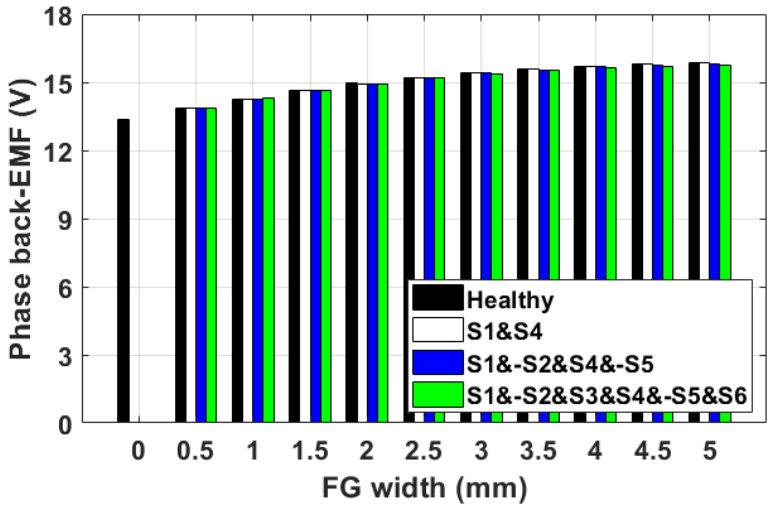

(b)

Fig. 5.17 The fundamental back-EMF of the phase A versus FG width of modular PM machines with various circumferential stator segment displacements. (a) 12-slot/10-pole. (b) 12-slot/14-pole.

In Fig. 5.17, the magnitudes of fundamental phase A back-EMF of modular PM machines with the selected circumferential stator segment displacement cases are depicted. As concluded in the previous sections, the circumferential stator segment displacement mainly affects the phase angles of phase back-EMFs but has limited influence on their magnitudes. From Fig. 5.17, such conclusion can be further validated. It can be found that for the same FG width, the magnitudes of the fundamental phase back-EMFs with different circumferential segment displacement cases are largely unchanged for both 12-slot/10-pole and 12-slot/14-pole modular PM machines.

5.3.3.2 COGGING TORQUE

The cogging torque waveforms and their spectra of modular PM machines with or without the circumferential stator segment displacement are shown in Fig. 5.18 and Fig. 5.19. Similar to the radial stator segment displacement scenario, the extra 2^{nd}, 4^{th}, 8^{th}, etc. order harmonics are introduced due to the change of stator symmetry.

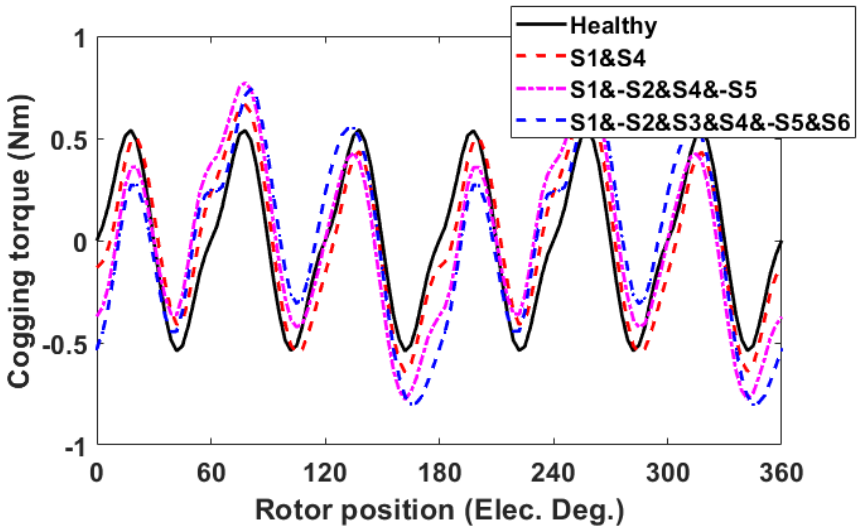

(a)

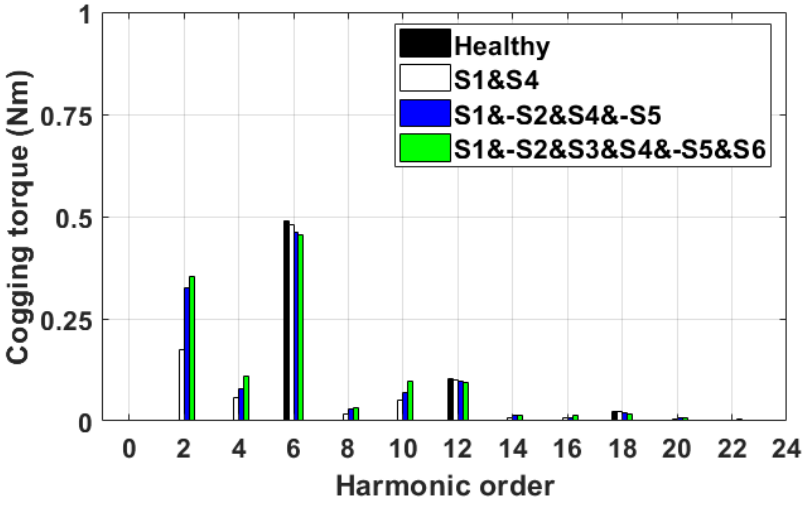

(b)

Fig. 5.18 Cogging torque of the 12-slot/10-pole modular PM machines with circumferential stator segment displacement. (a) Waveforms. (b) Spectra. (FG=2mm)

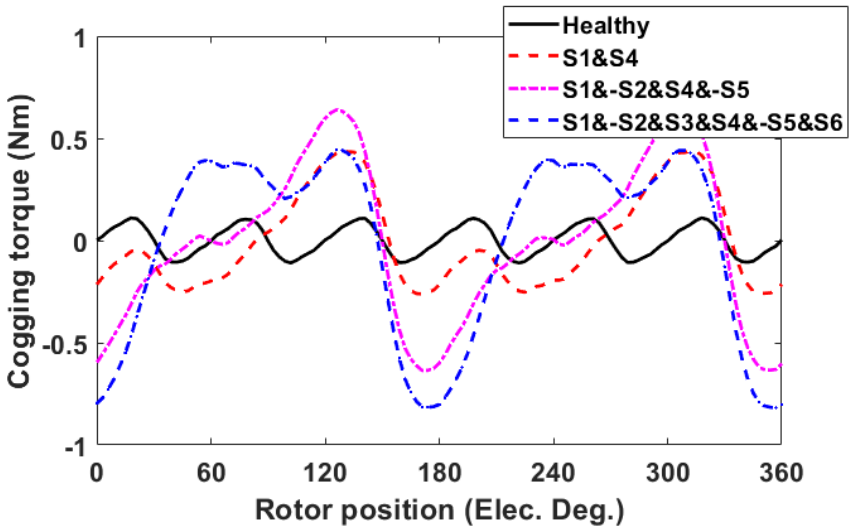

(a)

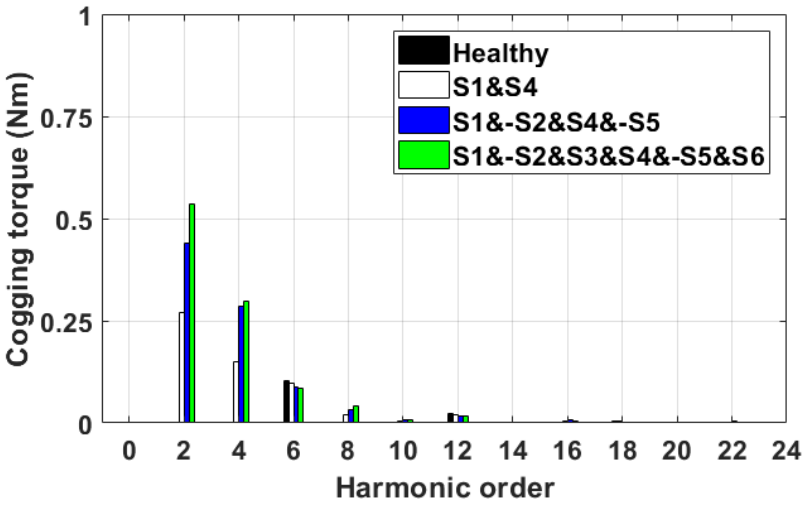

(b)

Fig. 5.19 Cogging torque of the 12-slot/10-pole modular PM machines with circumfernetial stator segment displacement. (a) Waveforms. (b) Spectra. (FG=2mm)

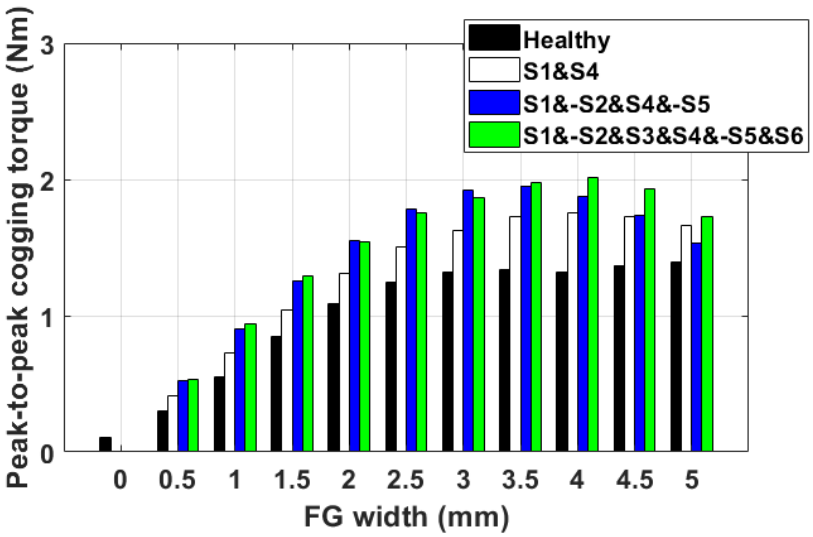

(a)

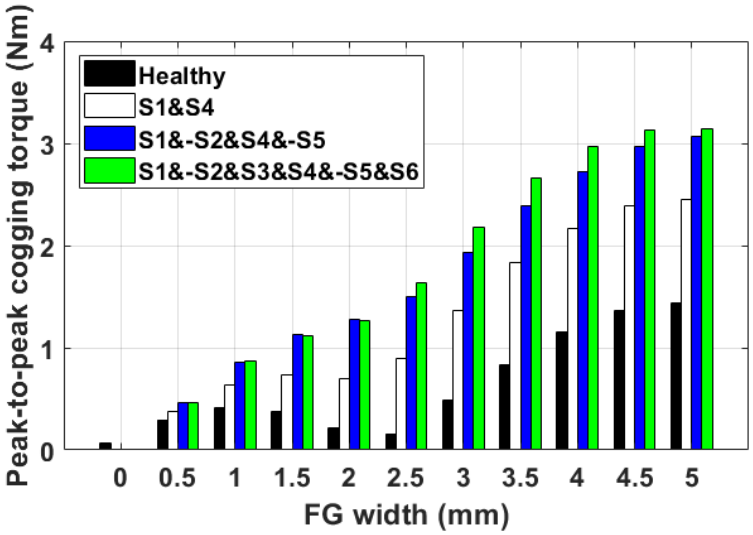

(b)

Fig. 5.20 The peak-to-peak cogging torque versus FG width of modular PM machines with circumferential stator segment displacement. (a) 12-slot/10-pole. (b) 12-slot/14-pole.

The peak-to-peak cogging torque of modular PM machines with the selected cases of circumferential stator segment displacement are compared in Fig. 5.20. It is found that for the case of S1&S4, when the FG width is ≤ 3mm, the peak-to-peak cogging torque of 12-slot/10-pole modular PM machines is bigger compared with that of 12-slot/14-pole modular PM machines. While for the case S1&-S2&S4&-S5 and the case S1&-S2&S3&S4&-S5&S6, when the FG width is bigger than 2.5mm, the peak-to-peak cogging torque of 12-slot/14-pole

modular PM machine becomes bigger than that of 12-slot/10-pole machine. Overall, the peak-to-peak cogging torques are significantly increased due to the circumferential stator segment displacement.

5.3.3.3 ON-LOAD TORQUE

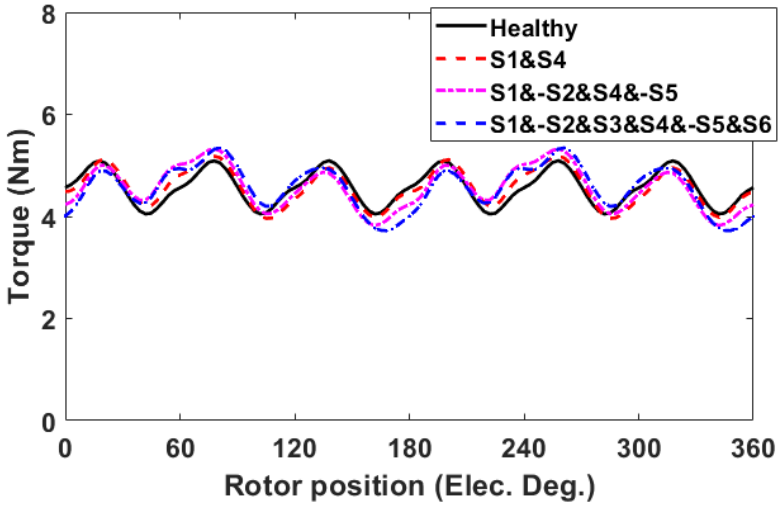

(a)

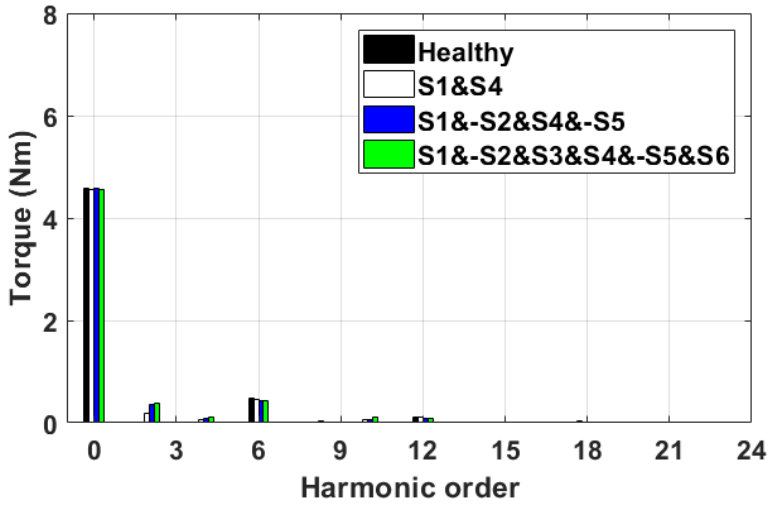

(b)

Fig. 5.21 On-load torque of the 12-slot/10-pole modular PM machines with radial stator segment displacement. (a) Waveforms. (b) Spectra. (FG=2mm)

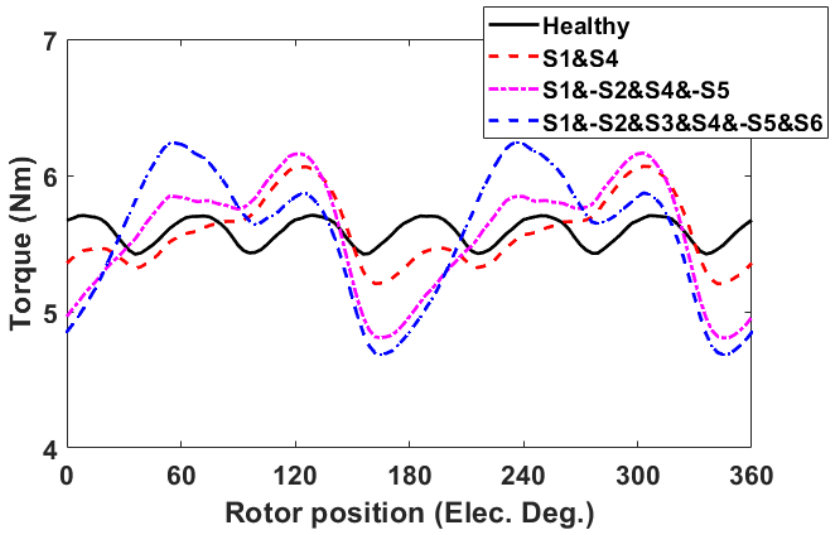

(a)

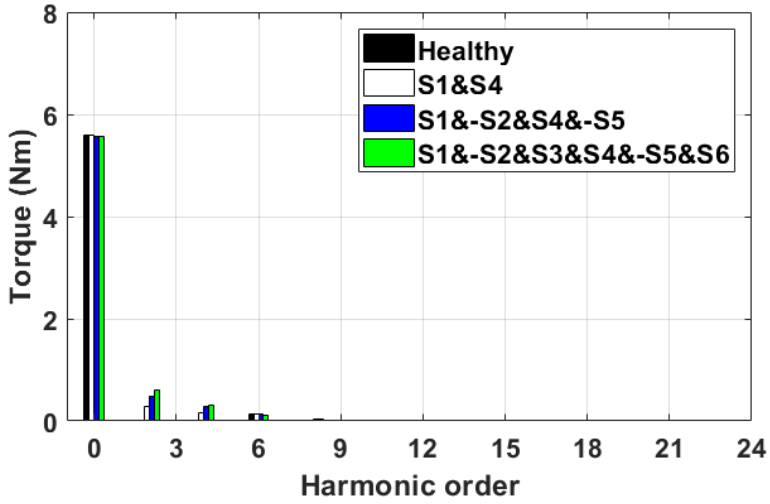

(b)

Fig. 5.22 On-load torque of the 12-slot/14-pole modular PM machines with radial stator segment displacement. (a) Waveforms. (b) Spectra. (FG=2mm)

The on-load waveforms and their spectra of 12-slot/10-pole and 12-slot/14-pole modular PM machines having 2mm FG with circumferential stator segment displacement are shown in Fig. 5.21 and Fig. 5.22. Similarly, the extra 2^{nd}, 4^{th}, 8^{th}, etc. order harmonics are observed. The reasons of such extra order harmonics have already been addressed previously and will not be detailed in this section.

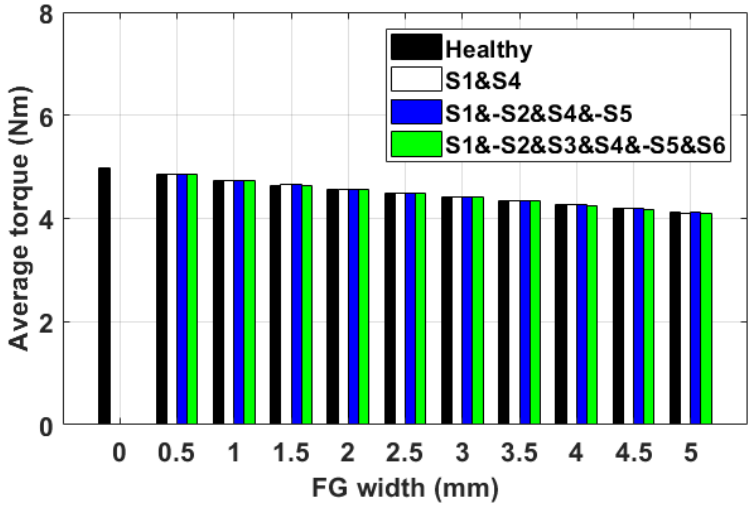

(a)

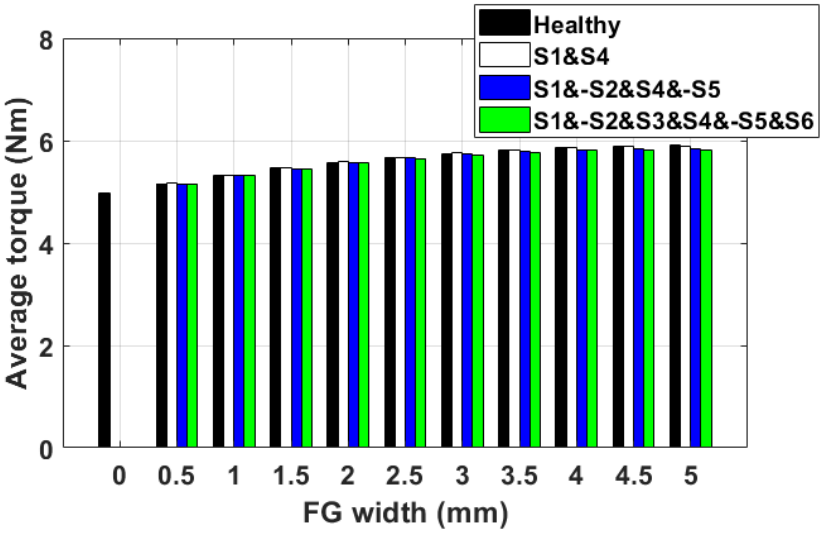

(b)

Fig. 5.23 The average torque versus FG widths of modular PM machines with the circumferential stator segment displacement. (a) 12-slot/10-pole. (b) 12-slot/14-pole.

The average torque of modular PM machines having different slot/pole number combinations with and without the circumferential stator segment displacement are shown in Fig. 5.23. It can be found that the average torques are maintained. This is because of the limited influence of circumferential stator segment displacement on phase back-EMFs. In addition, it also can be found that the average torque of 12-slot/14-pole modular PM machines is always bigger than that of 12-slot/10-pole modular PM machines when they have the same FG width

and the same case of circumferential stator segment displacement.

Similar to the radial stator segment cases, the torque ripple is mainly contributed by the cogging torque. Hence, the influence of FGs on cogging torque will be reflected in the performance of torque ripple as well.

5.3.3.4 UMF

Since the stator of modular PM machines with the selected circumferential stator segment cases (e.g. case S1&S4, case S1&-S2&S4&-S5, and case S1&-S2&S3&S4&-S5&S6) are still symmetry, therefore, the UMFs will be zero. In order to investigate the influence of circumferential stator segment displacement on UMF performance, the alternate case such as S1 is selected and its UMF waveforms are depicted from Fig. 5.24.

In Fig. 5.25, the magnitudes of UMFs of 12-slot/10-pole and 12-slot/14-pole modular PM machines are depicted. Comparing the UMF magnitudes of F_x and F_y of 12-slot/10-pole and 12-slot/14-pole machines, it is found that the magnitudes of F_x are similar. However, the 12-slot/14-pole modular PM machines have generally higher magnitudes of F_y. Overall, in terms of UMF, the 12-slot/10-pole modular PM machines have better circumferential segment displacement withstand capability.

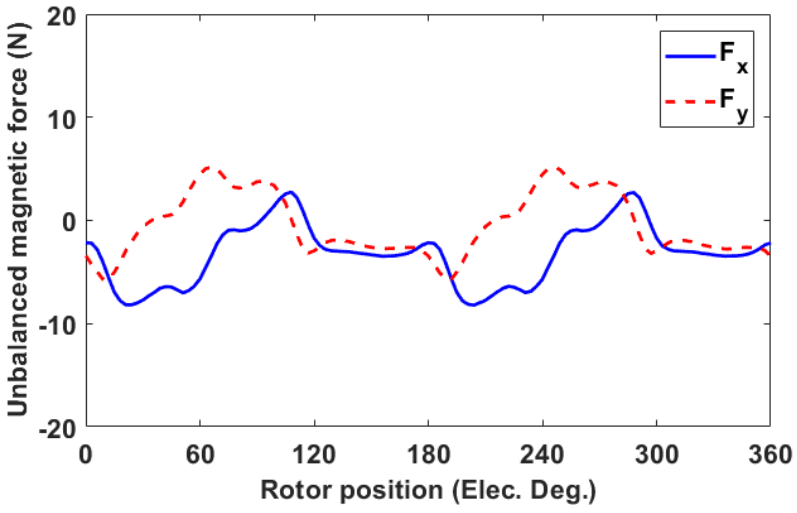

(a)

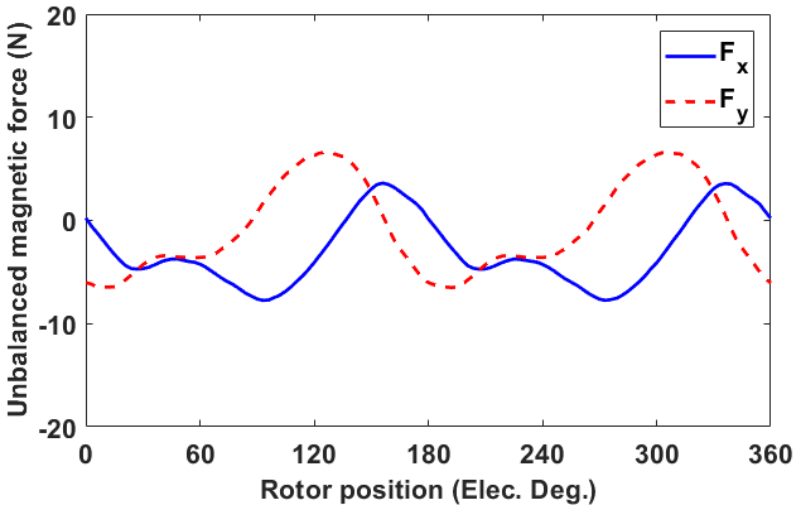

(b)

Fig. 5.24 The UMF waveforms of modualr PM machines with circumferential stator segment displacement. (a) 12-slot/10-pole. (b) 12-slot/14-pole. (FG=2mm)

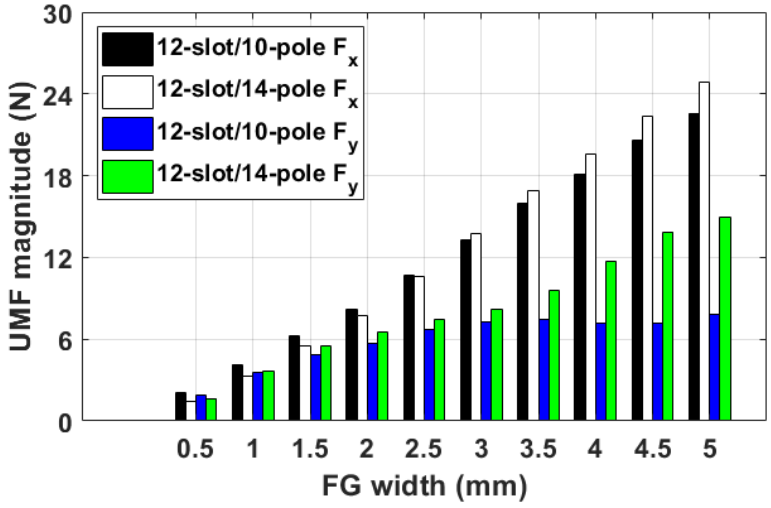

Fig. 5.25 The UMF magnitudes versus FG widths of modular PM machines with circumferential stator segment displacement of case S1.

5.4 MODULAR PM MACHINES WITH PM DEFECT

The manufacturing tolerance occurred during the PM production is another common issue in practice, such as, PM imperfect magnetization, PM demagnetization, broken PMs, etc. Unquestionably, such problems exert significant effect on the performance of PM machines. Therefore, in this section, the influence of PM defect on the electromagnetic performance of modular PM machines will be investigated. In order to simulate the PM defect problem, the 3D FE models with modular stators and defective rotors have been built, as shown from Fig. 5.26 and Fig. 5.27. It is worth noting that the general design parameters of the 3D FE models are exactly the same as the 2D FE models which are listed in Table 2.2.

In this section, two representative PM defect cases are studied which are 5% and 10% defective area of one PM pole, as can be seen from Fig. 5.27. It is worth noting that such defective zone is chosen to be within one piece of a N-pole PM.

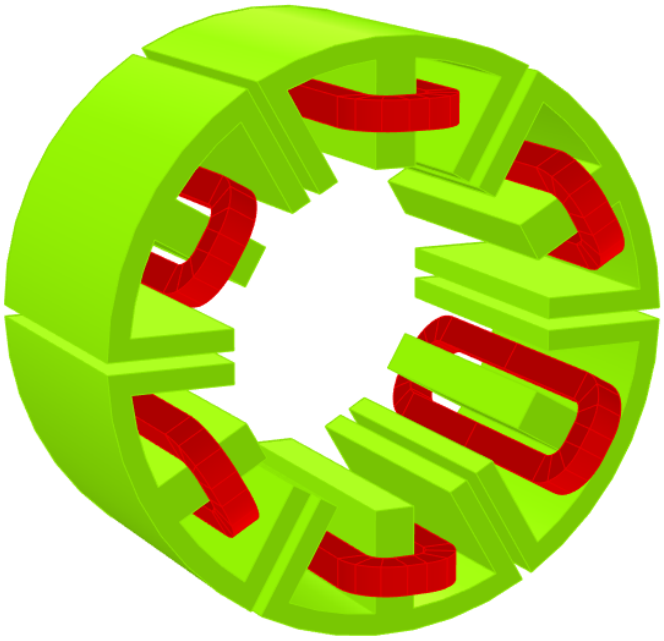

Fig. 5.26 The 3D model of the modualr stator segments with the single layer concentrated windings.

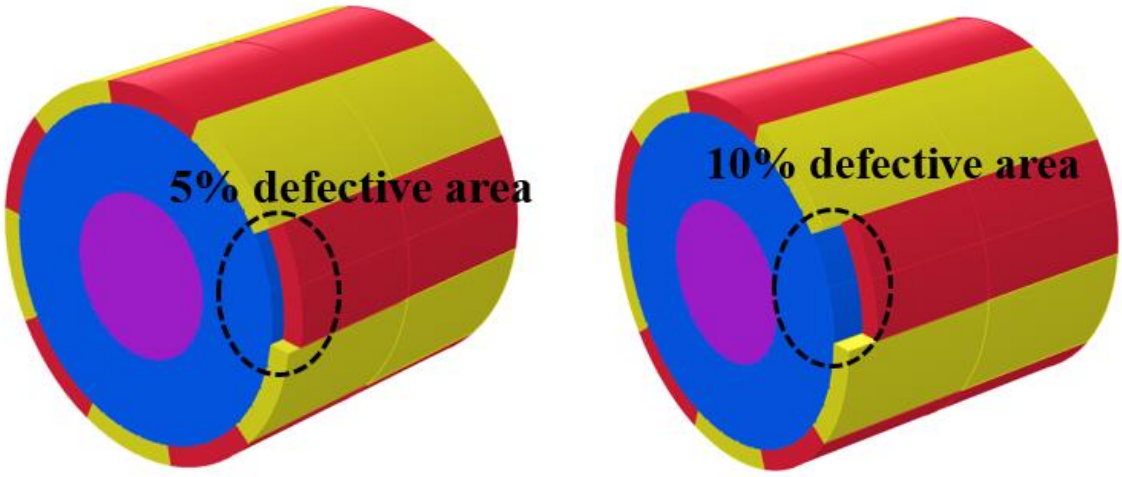

(a) (b)

Fig. 5.27 The 3D 10-pole rotor models with defective PM (a) 5% defect. (b) 10% defect.

5.4.1 Influence of PM Defect on Open-Circuit Air-Gap Flux Density and Phase Back-EMFs

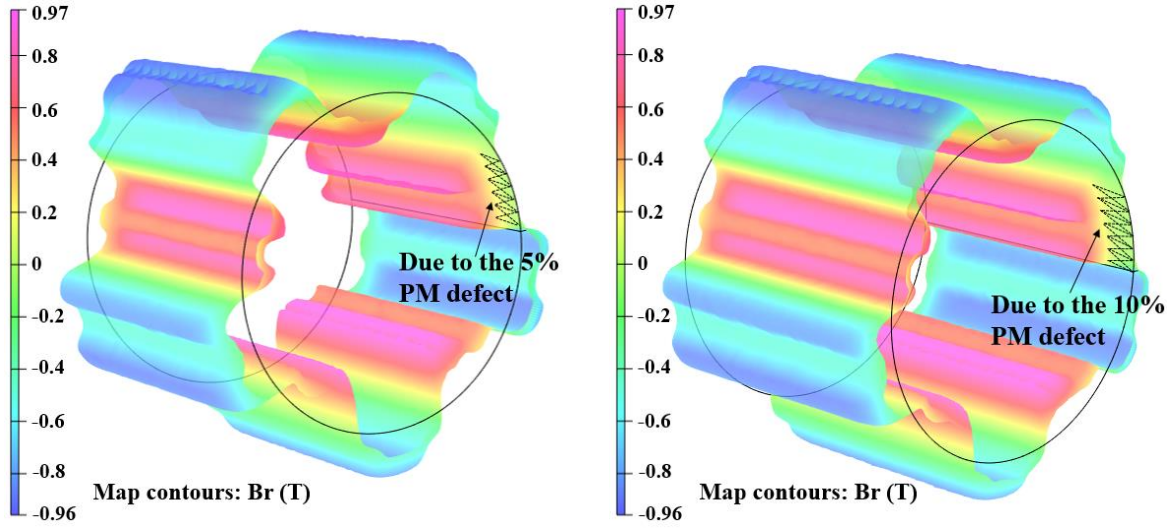

(a) (b)

Fig. 5.28 The colour maps of open-circuit air-gap flux density. (a) 5% defect. (b) 10% defect.

Under the healthy rotor condition, the mechanical period is p times of the electrical period. However, when the rotor PMs are defected, such relationship will be changed. Hence, in this section, the following calculations are all within one mechanical revolution (360 Mech. Deg.).

when the PM defect occurred, the electromagnetic performance will be globally affected, such as the flux density, flux linkage, back-EMF and torque characteristics, etc. This is due to the global change of the air-gap magnetic field generated by the defective PMs, as shown in Fig. 5.28.

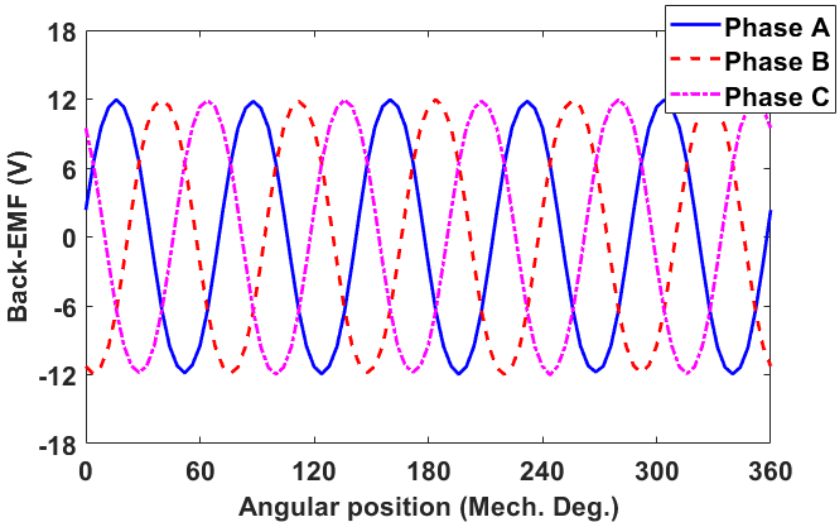

(a)

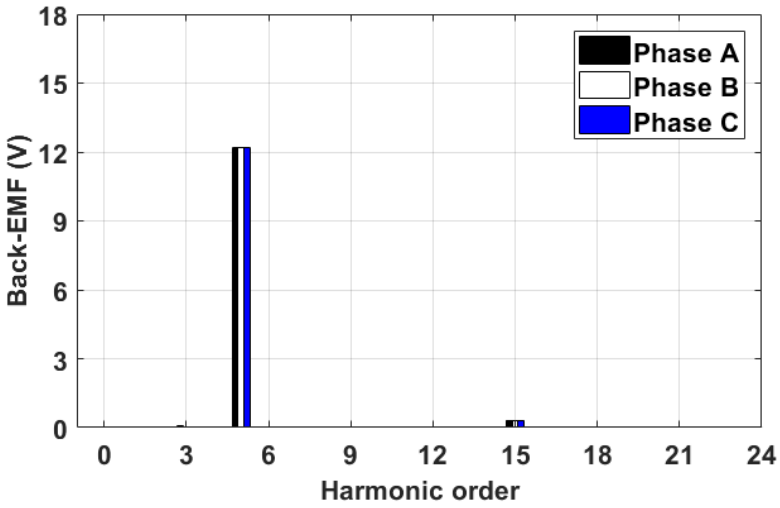

(b)

Fig. 5.29 The phase back-EMF waveforms and spectra of 12-slot/10-pole modular PM machines having 2mm FGs with 5% PM defect. (a) Waveforms (b) Spectra.

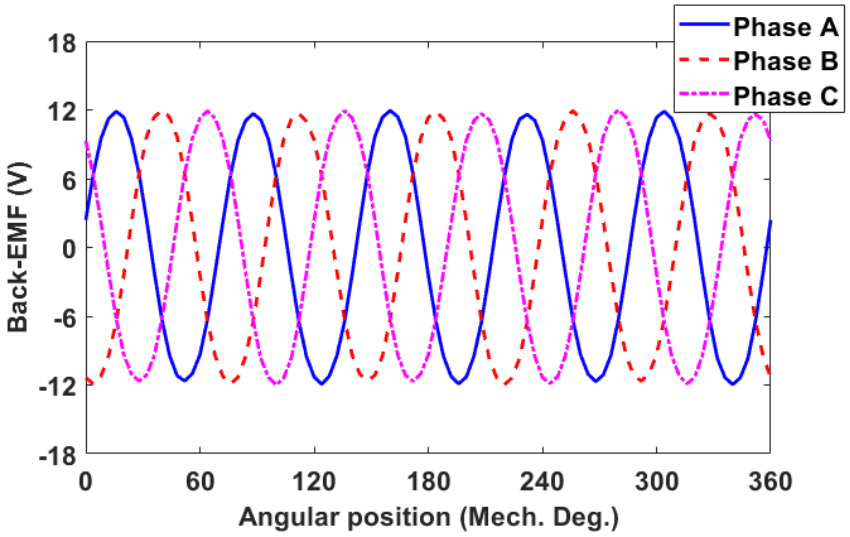

(a)

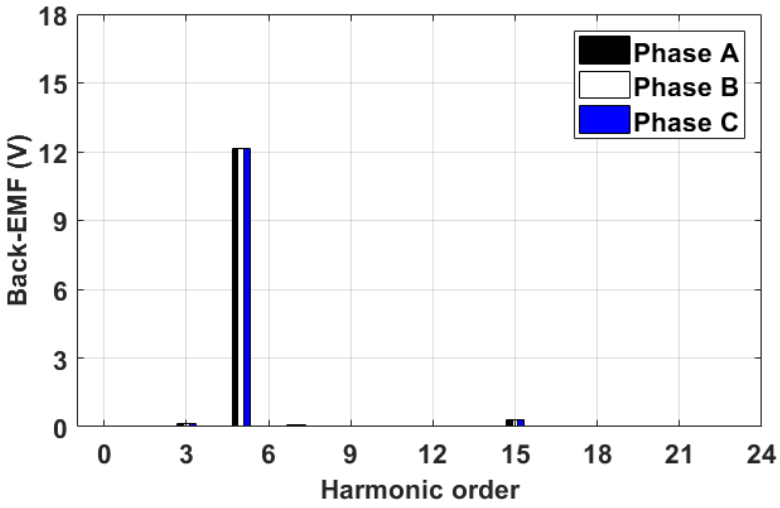

(b)

Fig. 5.30 The phase back-EMF waveforms and spectra of 12-slot/10-pole modular PM machines having 2mm FGs with 10% PM defect. (a) Waveforms (b) Spectra.

In Fig. 5.29 and Fig. 5.30, the waveforms and spectra of the phase back-EMFs of 12-slot/10-pole modular PM machines having 2mm FG with 5% or 10% PM defects are shown as examples. It is found that the magnitudes of three phase fundamental back-EMFs are still identical but decreased due to the defective PM. Furthermore, it can also be seen that the larger area of the PM is defected, the more negative impact on the fundamental phase back-EMF will be. However, The influence on the fundamental phase back-EMFs is not proportional to the

defective area, as shown in Table 5.10. It is worth noting that no extra even order harmonics are introduced due to PM defect and the three-phase back-EMFs still remain balanced.

Since the PM defect exerts some negative impact on the fundamental phase back-EMFs, as detailed in (5.5), the average torque will be decreased accordingly, as can be proven in Fig. 5.38.

TABLE 5.10 THE COMPARISON OF MAGNITUDES OF THE FUNDAMENTAL PHASE BACK-EMFS

Magnitudes (V)	Phase A	Phase B	Phase C
Healthy	12.36V	12.36V	12.36V
5% defect	12.2V	12.19V	12.19V
10% defect	12.13V	12.13V	12.13V

5.4.2 INFLUENCE OF FG WIDTHS AND SLOT/POLE NUMBER COMBINATIONS OF MODULAR PM MACHINES WITH PM DEFECT

5.4.2.1 PHASE BACK-EMF

The influence of FG widths on fundamental phase back-EMFs of modular PM machines with PM defect have been calculated and compared in Fig. 5.32. It is found that the influence of FG widths on the fundamental phase back-EMFs are similar regardless of the modular PM machines with or without PM defect.

The changing ratios of fundamental phase back-EMFs are also calculated and listed in Table 5.11. It can be seen that for the 12-slot/10-pole modular PM machines, the changing ratio is decreased with the increase in the FG width. However, for the 12-slot/14-pole modular PM machines, the changing ratio is increased with the increase in the FG width. This means that the severity of influence due to the PM defect on phase back-EMF can be mitigated with the increase in the FG widths for the 12-slot/10-pole modular PM machines while for the 12-slot/14-pole modular PM machines, the severity of such influence is aggravated.

In order to explain the phenomena observed above, the colour maps of the radial open-circuit flux density *Br* of 12-slot/10-pole modular PM machines with 10% PM defect having 2mm or 4mm FG width are shown in Fig. 5.31. It is worth noting that initial rotor position is

set as the *d*-axis, which is aligned with the phase A. By doing so, the flux linkage of the phase A can be maintained to be the maximum.

It can be seen from Fig. 5.31 that the maximum open-circuit flux density is 1.57T when FG width is 2mm. However, when the FG width changes to 4mm, the maximum open-circuit flux density at the same rotor position increases to 1.65T. This means that the increase in FG widths helps to increase the open-circuit flux density for the 12-slot/10-pole modular PM machines with PM defect. As a result, the decrease of the phase back-EMFs of the 12-slot/10-pole modular PM machines with PM defect can be mitigated. Hence, the changing ratio is reduced.

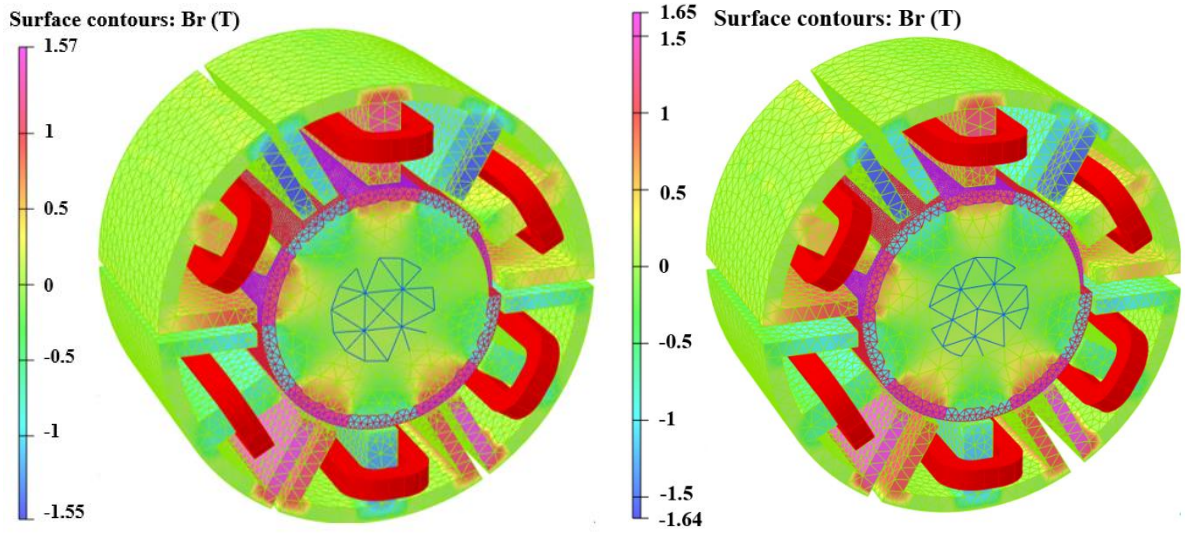

(a) (b)

Fig. 5.31 The colour map of radial flux density *Br* of the 12-slot/10-pole modular PM machines with 10% PM defect under the open-ciruit condition. (a) FG=2mm. (b) FG=4mm.

It is also found that the changing ratios of the 12-slot/14-pole modular PM machines are generally higher than those of the 12-slot/10-pole modular PM machines for both the 5% and 10% PM defects. As a result, similar to the radial segment displacement scenarios, the PM defect withstand capability of modular PM machines having 12-slot/10-pole is also better compared with the 12-slot/14-pole modular PM machines.

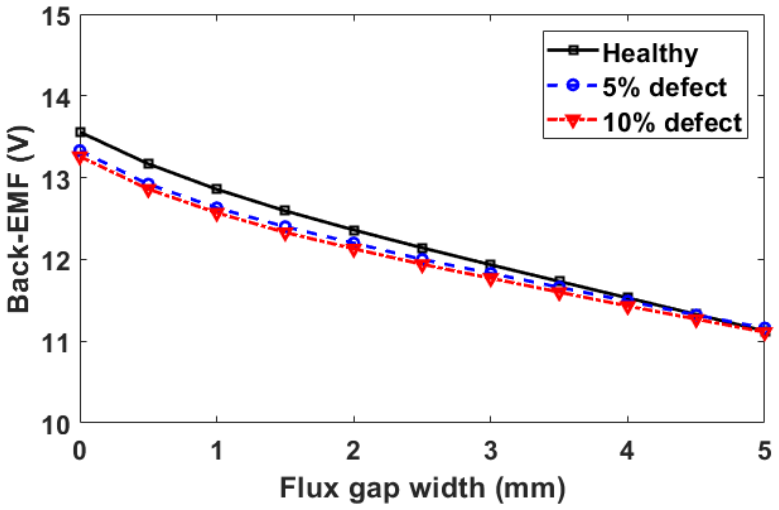

(a)

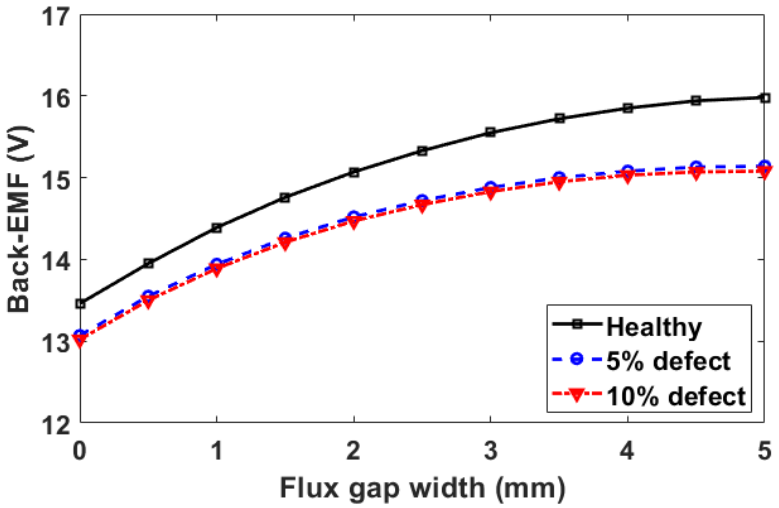

(b)

Fig. 5.32 The fundamental phase back-EMFs versus the FG width of modular PM machines with PM defects. (a) 12-slot/10-pole. (b) 12-slot/14-pole.

TABLE 5.11 THE CHANGING RATIOS OF FUNDAMENTAL PHASE BACK-EMFS OF THE MODULAR AND NON-MODULAR PM MACHINES WITH PM DEFECT

FG widths (mm)	5% defect (12slot-10pole/12slot-14pole)	10% defect (12slot-10pole/12slot-14pole)
0.0	-1.68% / -2.9%	-2.2% / -3.27%
0.5	-1.89% / -2.87%	-2.34% / -3.23%
1.0	-1.77% / -3.13%	-2.24% / -3.47%
1.5	-1.54% / -3.39%	-2.09% / -3.73%
2.0	-1.29% / -3.65%	-1.86% / -3.98%
2.5	-1.17% / -3.98%	-1.66% / -4.31%
3.0	-0.87% / -4.31%	-1.38% / -4.63%
3.5	-0.61% / -4.58%	-1.12% / -4.9%
4.0	-0.34% / -4.86%	-0.86% / -5.17%
4.5	-0.07% / -5.08%	-0.51% / -5.46%
5.0	0.33% / -5.26%	-0.12% / -5.63%

5.4.2.2 COGGING TORQUE

The cogging torque waveforms as well as their spectra of 12-slot/10-pole and 12-slot/14-pole modular PM machines having 2mm FG with PM defect are depicted in Fig. 5.33 and Fig. 5.34. It is found that the cogging torque periodicity of the modular PM machines are changed due to PM defect since the rotor symmetry is changed from 5 or 7 to 1 for the 10-pole or 14-pole rotor, respectively. By way of example, for the healthy 12-slot/10-pole modular PM machines, the cogging torque periodicity is 30 within a mechanical revolution which denote the order of the first appeared cogging torque harmonic is 30^{th}, as shown in Fig. 5.33 (b). Nevertheless, for the modular PM machines with the PM defect, the LCM between the stator and rotor symmetries becomes 6 which denotes the first appeared cogging torque harmonic will be the 6^{th} order harmonic instead, as validated in Fig. 5.33 (b). It is worth noting that the very tiny sub-harmonics observed from Fig. 5.33 (b) are mainly due to the numerical error. The aforementioned explanations can also be applied to the cogging torque analyses of the 12-slot/14-pole modular PM machines with PM defect.

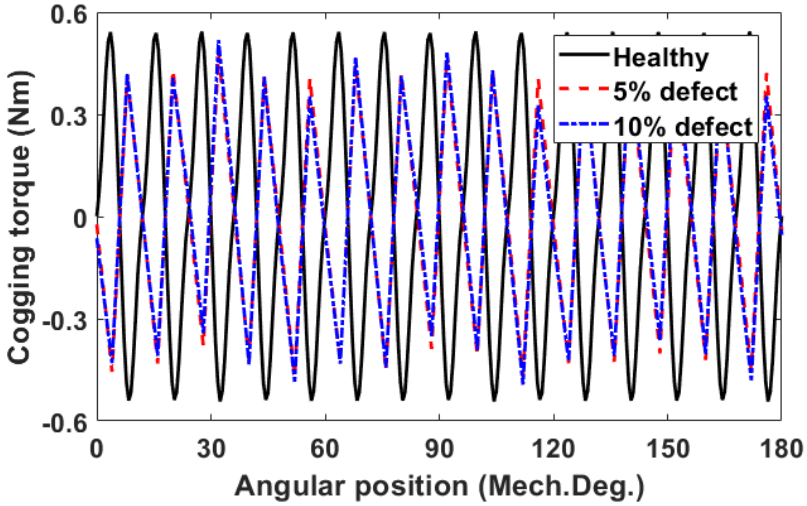

(a)

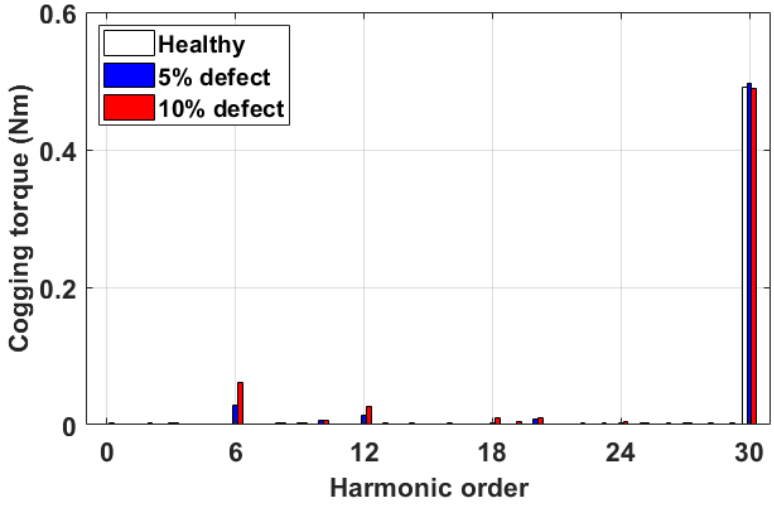

(b)

Fig. 5.33 The cogging torque waveforms and spectera of the 12-slot/10-pole modualr PM machines having 2mm FGs with or without PM defect. (a) Waveforms. (b) Spectra.

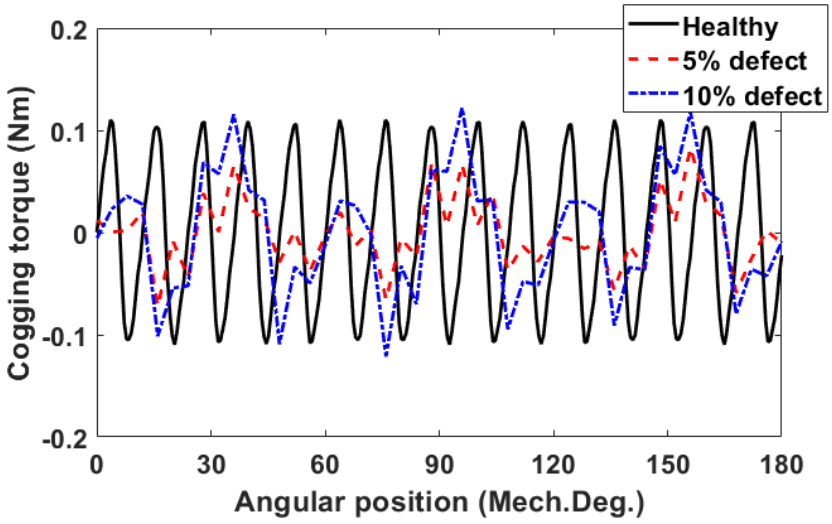

(a)

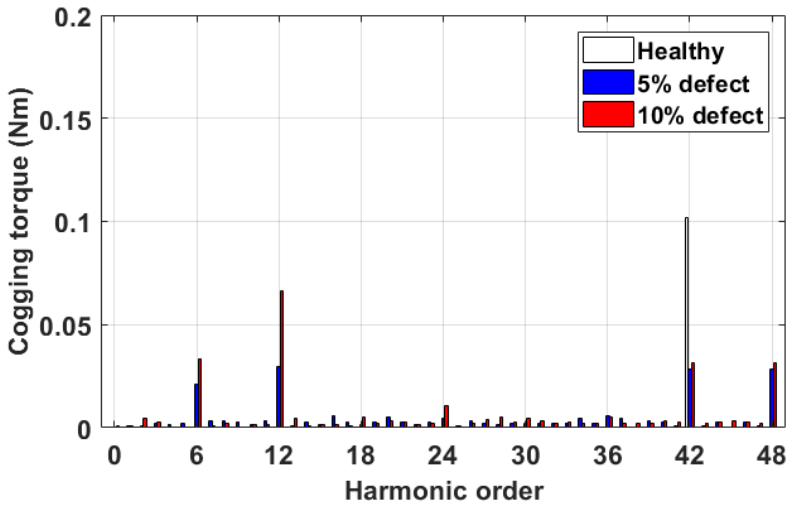

(b)

Fig. 5.34 The cogging torque waveforms and spectera of the 12-slot/14-pole modualr PM machines having 2mm FGs with or without PM defect. (a) Waveforms. (b) Spectra.

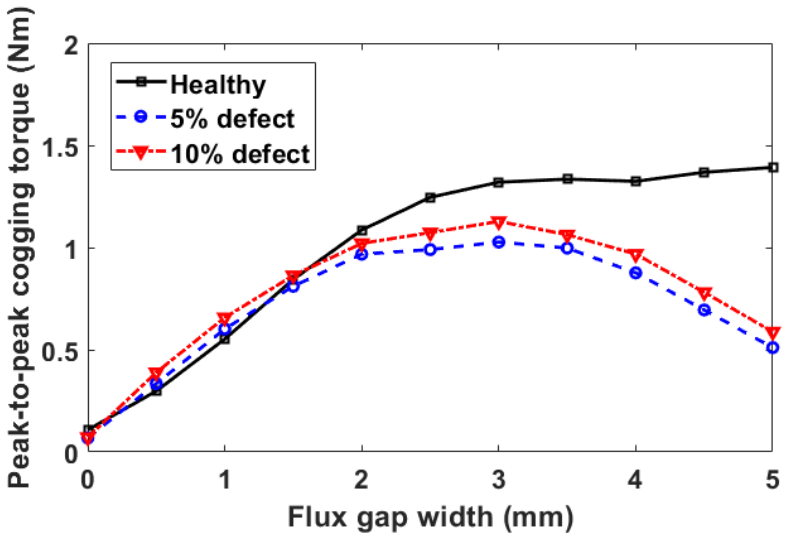

(a)

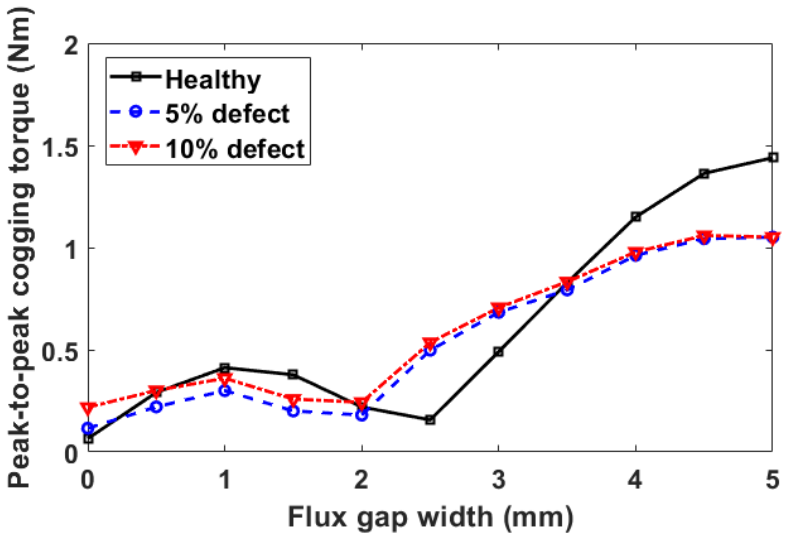

(b)

Fig. 5.35 The peak-to-peak cogging torque of modualr PM machines with or without PM defect. (a) 12-slot/10-pole. (b) 12-slot/14-pole.

The waveforms of the peak-to-peak cogging torque against FG widths of 12-slot/10-pole and 12-slot/14-pole modular PM machines with or without PM defect are depicted in Fig. 5.35. For the 12-slot/10-pole modular PM machines, when the FG width is smaller than 3mm, the peak-to-peak cogging torque of modular PM machines with PM defect is increased with the increase in the FG widths. Similar trend can be observed for the modular PM machines without PM defect. Nevertheless, when the FG width becomes bigger than 3mm, different from the

peak-to-peak cogging torque of the modular PM machines without PM defect, the peak-to-peak cogging torque of the modular PM machines with PM defect starts to decrease with the increase in the FG widths, as shown in Fig. 5.35 (a). Nevertheless, for the 12-slot/14-pole modular PM machines, the variation trend of the peak-to-peak cogging torque against the FG widths are similar, as shown in Fig. 5.35 (b).

It is worth noting that the peak-to-peak cogging torques of modular PM machines with 5% PM defect are always slightly smaller than those of the modular PM machines with 10% PM defect. This is true for both the 12-slot/10-pole and 12-slot/14-pole modular PM machines.

The changing ratio of peak-to-peak cogging torque of the modular PM machines with the PM defects are listed in Table 5.12. It can be seen that for both 12-slot/10-pole and 12-slot/14-pole modular PM machines, the changing ratio can be mitigated significantly by selecting the FG widths properly.

TABLE 5.12 THE CHANGING RATIOS OF PEAK-TO-PEAK COGGING TORQUE OF THE MODULAR AND NON-MODULAR PM MACHINES WITH PM DEFECT

FG widths (mm)	5% defect (12slot-10pole/12slot-14pole)	10% defect (12slot-10pole/12slot-14pole)
0.0	-36.2% / 77.98%	-33.21% / 235.53%
0.5	12.36% / -24.21%	30.57% / 3.38%
1.0	8.93% / -27.23%	18.96% / -12.5%
1.5	-3.99% / -46.88%	2.29% / -31.54%
2.0	-10.86% / -17.88%	-5.98% / 10.54%
2.5	-20.52% / 217.34%	-13.86% / 241.02%
3.0	-22.2% / 39.22%	-14.53% / 43.93%
3.5	-25.27% / -4.38%	-20.37% / 0.47%
4.0	-33.81% / -16.3%	-26.88% / -14.84%
4.5	-49.21% / -23.46%	-42.93% / -22.31%
5.0	-63.32% / -26.98%	-57.78% / -26.95%

5.4.2.3 ON-LOAD TORQUE

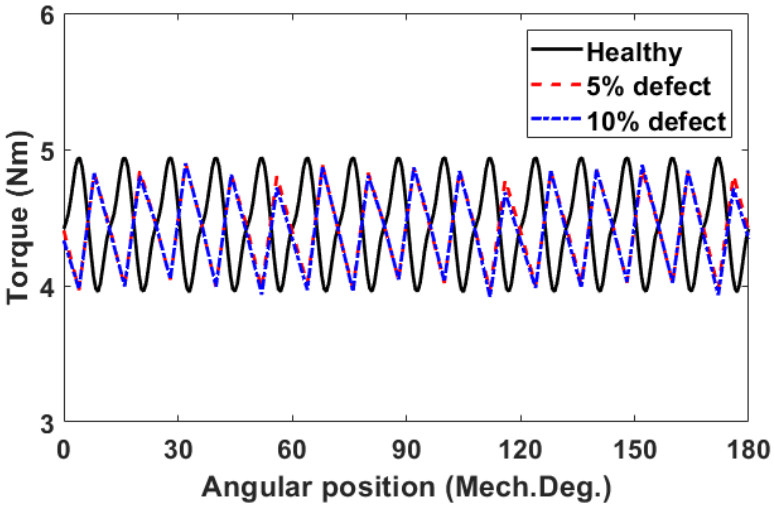

(a)

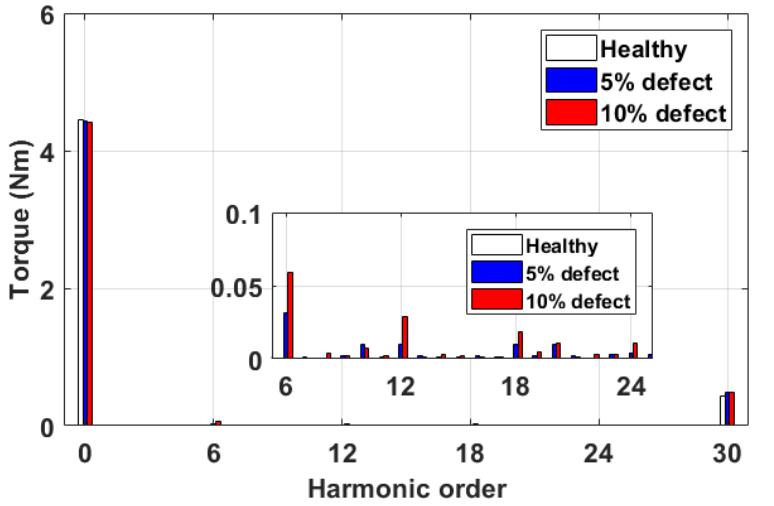

(b)

Fig. 5.36 The torque waveforms and spectera of 12-slot/10-pole modualr PM machines having 2mm FGs with or without PM defect. (a) Waveforms. (b) Spectra.

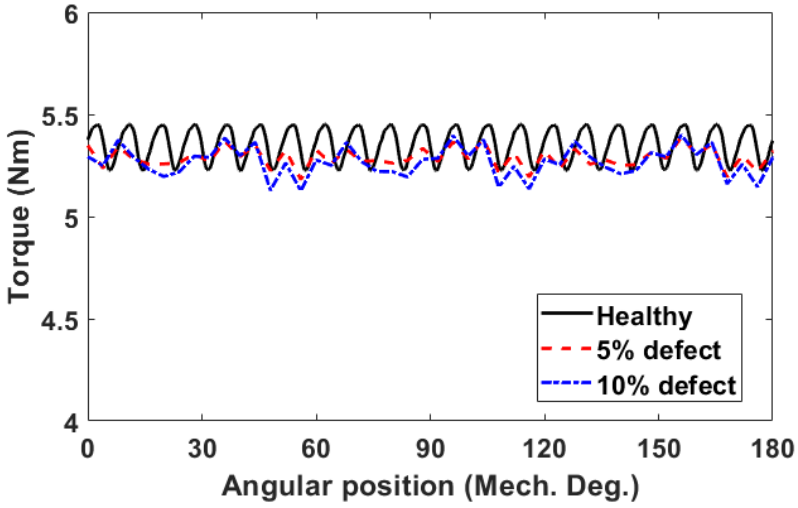

(a)

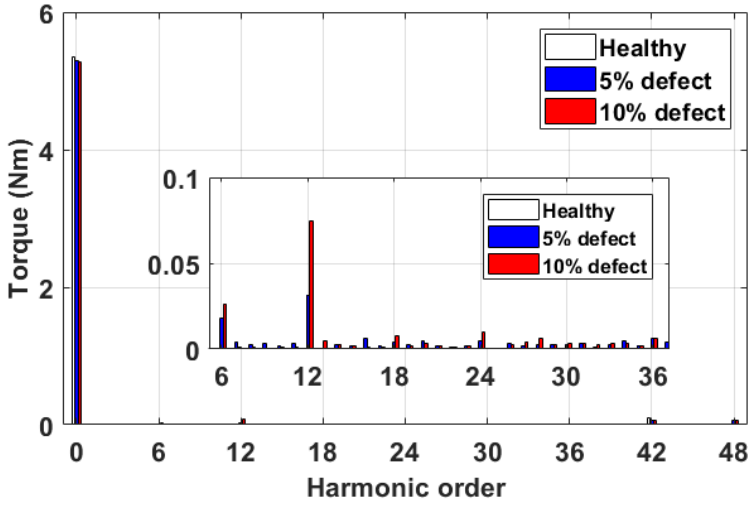

(b)

Fig. 5.37 The torque waveforms and spectera of 12-slot/14-pole modualr PM machines having 2mm FGs with or without PM defect. (a) Waveforms. (b) Spectra.

The on-load torque waveforms and spectra of 12-slot/10-pole and 12-slot/14-pole modular PM machines with or without PM defect having 2mm FGs are shown in Fig. 5.36 and Fig. 5.37. It can be seen from the Fig. 5.36 (b) and Fig. 5.37 (b) that the first appeared torque ripple harmonics of on-load torque within one mechanical revolution becomes the 6^{th} rather than 30^{th} for the 12-slot/10-pole healthy modular PM machines and the 42^{nd} for the 12-slot/14-pole healthy modular PM machines. The main reason of such newly introduced 6^{th} and its multiple

order harmonics is the 6th order harmonic and its multiple orders of the cogging torque which has been well demonstrated in the section 5.4.2.2.

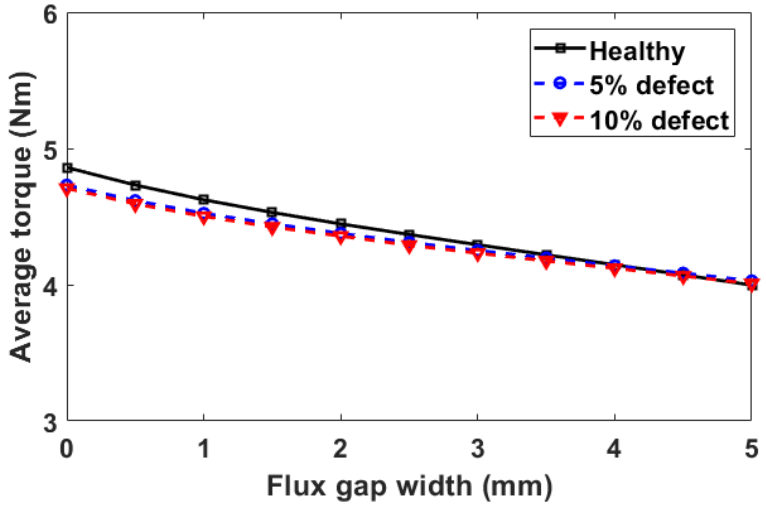

(a)

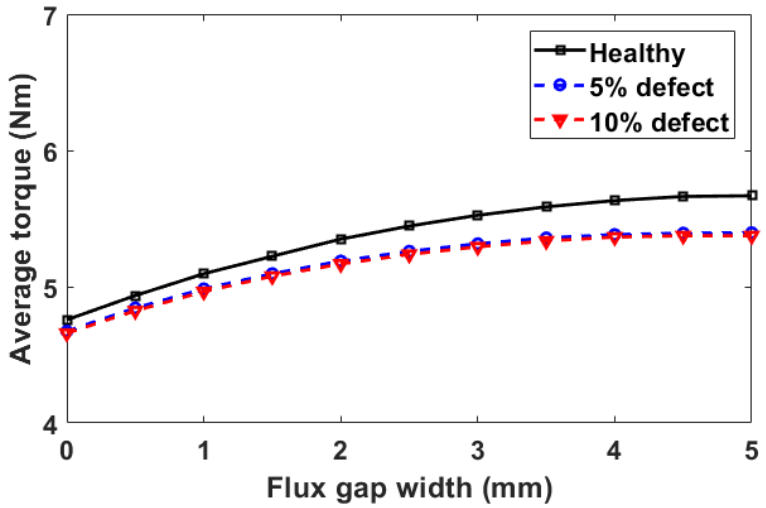

(b)

Fig. 5.38 The average torque of modualr PM machines with or without PM defect. (a) 12-slot/10-pole. (b) 12-slot/14-pole.

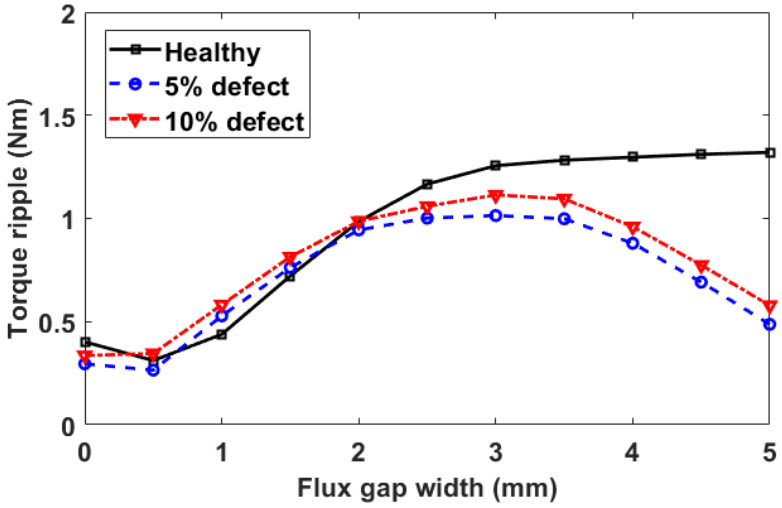

(a)

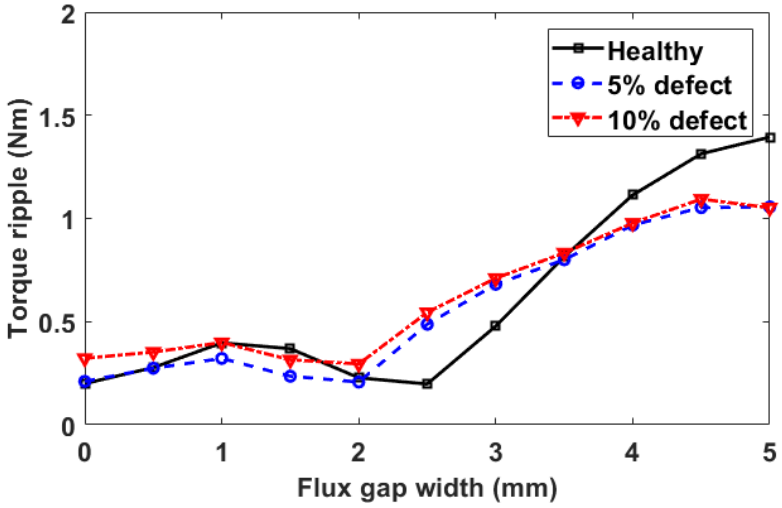

(b)

Fig. 5.39 The torque ripple of modualr PM machines with or without PM defect. (a) 12-slot/10-pole. (b) 12-slot/14-pole.

The average toque and torque ripple against FG width of modular PM machines with or without PM defect is depicted in Fig. 5.38 and Fig. 5.39. Since the average torque has a close relationship with the fundamental phase back-EMF, the influence of FG width on fundamental phase back-EMF will be reflected in average torque, as proven in Fig. 5.38. Again, due to the fact that the cogging torque plays a dominant role in torque ripple, the influence from the FG widths on the cogging torque of modular PM machines with PM defect will be reflected in the

performance of the torque ripple.

The changing ratio of the average torque is listed in Table 5.13. In term of the average torque, it can be found that the severity of the PM defect can be mitigated with the increase in the FG widths for the 12-slot/10-pole modular PM machines. Whilst for the 12-slot/14-pole modular PM machines, such influence is aggravated with the increase in the FG widths.

Additionally, the changing ratios of average torque of 12-slot/10-pole modular PM machines are smaller than those of the 12-slot/14-pole modular PM machines when the FG width is bigger than 1mm while when the FG width is smaller than 1mm, the changing ratios of the 12-slot/14-pole modular PM machines are smaller regardless of the PM defect area. Although such special phenomenon is observed, the conclusion such as the 12-slot/10-pole modular PM machines have better PM defect withstand capability in terms of the average torque is still valid. This is due to the fact that only few cases do not follow the conclusion made above but the majority cases are supporting that conclusion

TABLE 5.13 THE CHANGING RATIOS OF AVERAGE TORQUE OF THE MODULAR AND NON-MODULAR PM MACHINES WITH PM DEFECT

FG widths (mm)	5% defect (12slot-10pole/12slot-14pole)	10% defect (12slot-10pole/12slot-14pole)
0.0	-2.67% / -1.77%	-3.15% / -2.07%
0.5	-2.42% / -1.85%	-2.92% / -2.27%
1.0	-2.15% / -2.18%	-2.63% / -2.57%
1.5	-1.85% / -2.45%	-2.36% / -2.8%
2.0	-1.56% / -3.01%	-2.01% / -3.41%
2.5	-1.32% / -3.4%	-1.8% / -3.82%
3.0	-0.98% / -3.79%	-1.44% / -4.19%
3.5	-0.55% / -4.08%	-1.06% / -4.48%
4.0	-0.18% / -4.43%	-0.62% / -4.76%
4.5	0.32% / -4.76%	-0.2% / -5.09%
5.0	0.78% / -4.78%	0.27% / -5.17%

5.4.2.4 UMF

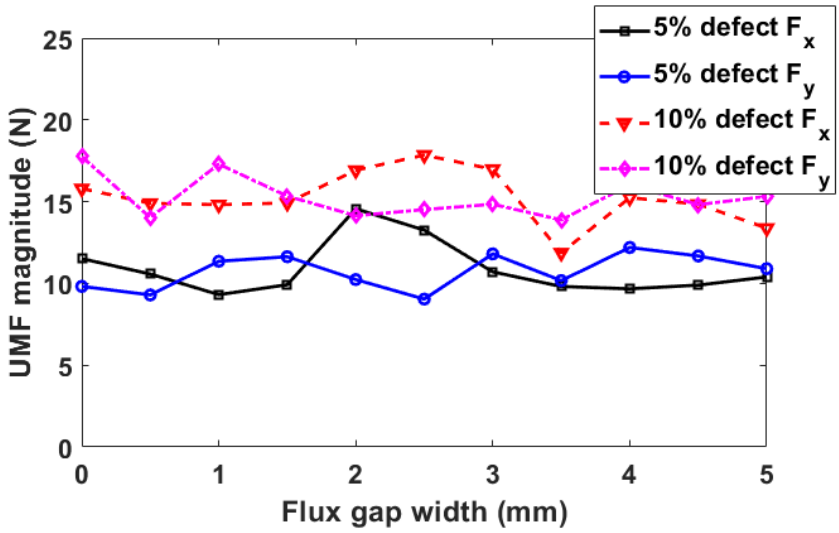

(a)

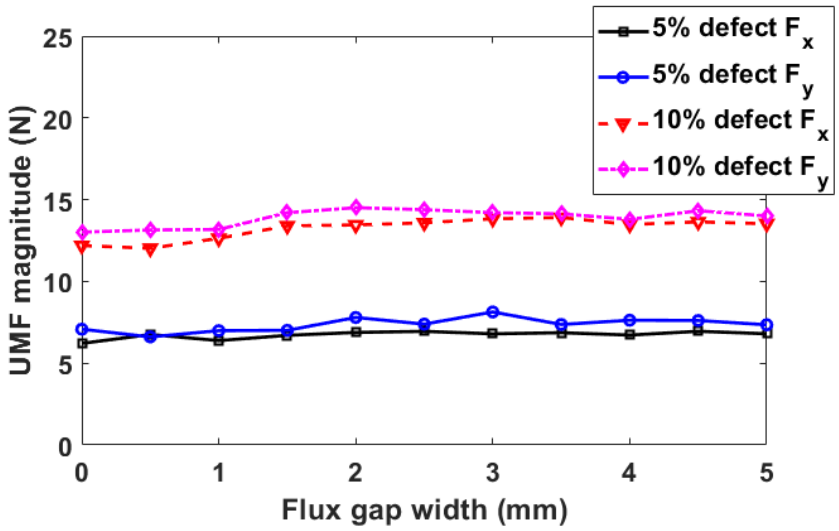

(b)

Fig. 5.40 The UMF magnitudes versus FG widths of modular PM machines with PM defect. (a) 12-slot/10-pole. (b) 12-slot/14-pole.

The variations of the UMF magnitudes of modular PM machines with PM defect are depicted in Fig. 5.40. It is found that for both the 12-slot/10-pole and 12-slot/14-pole modular PM machines, the UMF magnitudes of the PM machines with 10% PM defect are generally higher than those of the 5% PM defect cases regardless of the FG widths. It is also worth noting

that, with 5% PM defect, the magnitudes of F_x and F_y of the 12-slot/10-pole modular PM machines are bigger than those of the 12-slot/14-pole modular PM machines. This is also true for the 10% PM defect cases. Therefore, different from the previous conclusions for the phase back-EMF, the cogging torque and the on-load torque, the 12-slot/14-pole modular PM machines have better PM defect manufacturing tolerance withstand capability in terms of the UMF.

Moreover, for the 12-slot/10-pole modular PM machines with either 5% or 10% PM defect, the magnitudes of F_x and F_y can be mitigated to some extent by appropriately selecting the FG width. However, for the 12-slot/14-pole cases, the magnitudes of the UMF cannot be mitigated.

5.4.3 EXPERIMENTAL VALIDATION

In order to validate the previous FE predictions, An existing prototypes of modular PM machines having healthy rotor and the newly introduced defective rotor have been used and tested, as shown in Fig. 5.41. It is worth noting that the rotor shown in Fig. 5.41 (c) is a 10-pole surface mounted PM rotor with half of a N-pole magnet removed. This arrangement is made from the practicality point of view, mainly because the existing prototype in the laboratory has two pieces of magnets per pole. As a result, removing one piece (50% magnet defect) is much more practical, and also allows us to avoid building a new rotor with 5% or 10% magnet defect, which might be time consuming and also costly.

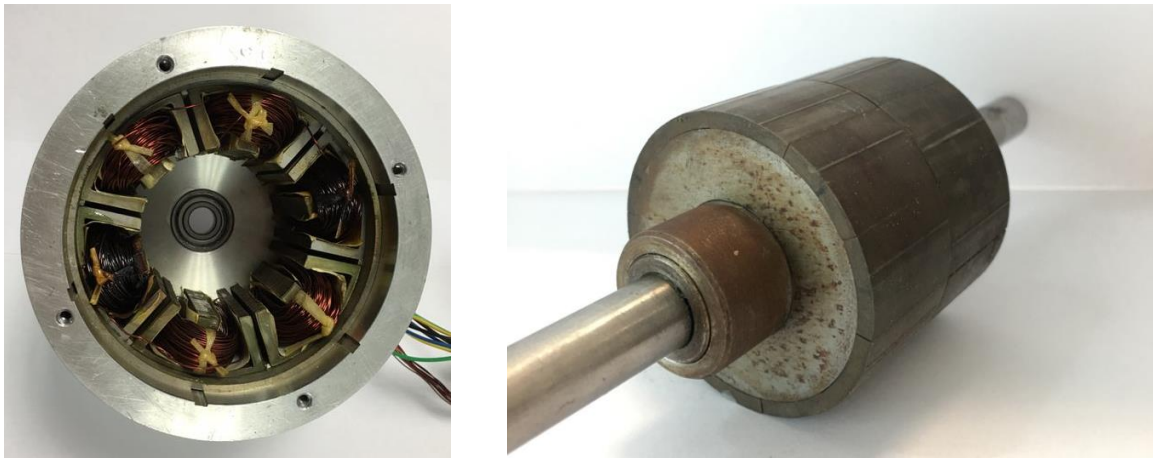

(a) (b)

(c)

Fig. 5.41 The prototype 12-slot/10-pole modular PM machines. (a) The modular stator. (b) The healthy rotor. (c) The defective rotor.

The 3D FE model of 12-slot modular PM machine with the aforementioned defective rotor has also been built and simulated. The colour maps of the open-circuit flux density of the modular PM machine with defective rotor are shown in Fig. 5.42. It is evident that the open-circuit air-gap flux density becomes asymmetric and a near zero flux density zone can be observed for the area with magnet removed, as shown in Fig. 5.42 (b).

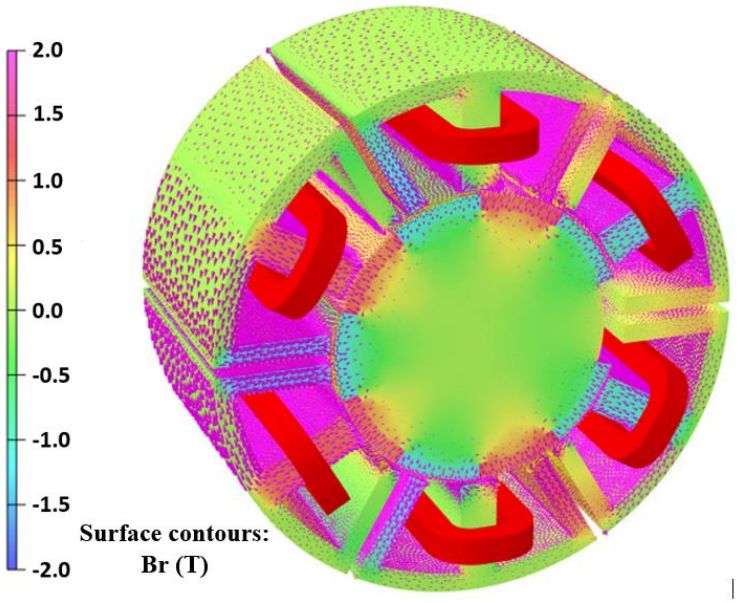

(a)

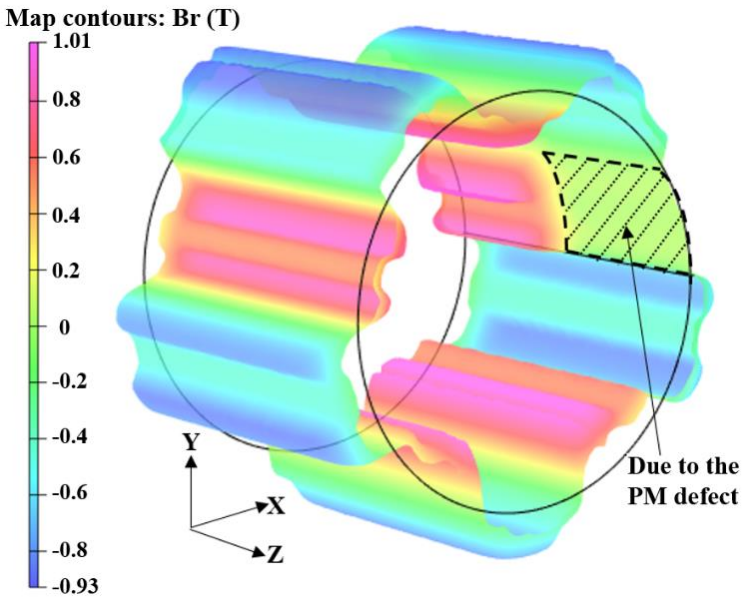

(b)

Fig. 5.42 The colour maps of open-circuit flux density. (a) Entire model. (b) Middle of the air-gap.

5.4.3.1 PHASE BACK-EMF

At the rated speed (400 rpm), the back-EMF of phase A of the 12-slot modular PM machine with the healthy and defective rotors has been calculated by FE and validated by tests, as shown in Fig. 5.43.The defective rotor changes the periodicity of the phase back-EMF and introduce extra harmonic contents that do not exist in the machines with healthy rotor, such as, 1st, 2nd order harmonics, etc. Moreover, the beginning part of the EMF is lower due to the defective magnet.

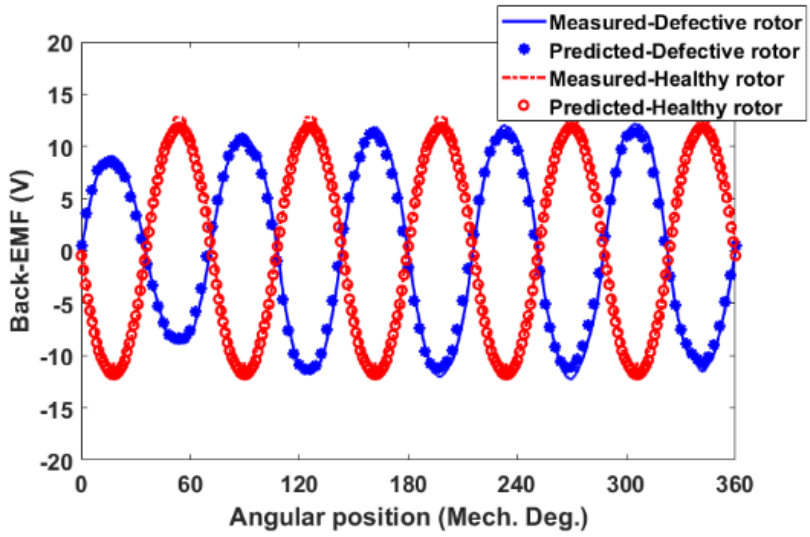

(a)

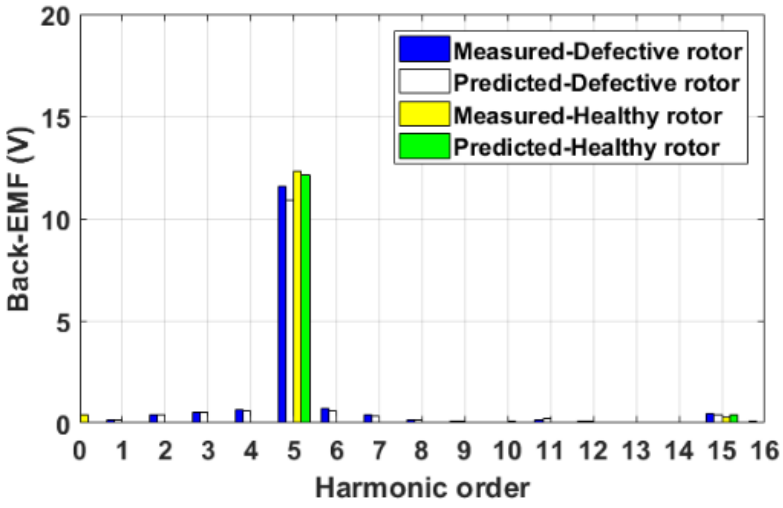

(b)

Fig. 5.43 The predicted and measured back-EMFs of the modular PM machine with healthy and defective rotors. (a) Waveforms. (b) Spectra.

5.4.3.2 COGGING TORQUE AND STATIC TORQUE

The method of measuring static torque and cogging torque is described in [67] and the test rig is illustrated in Fig. 2.15 (a). The rotor shaft is connected to a balance beam which provides the possibility of using the digital scale to measure the force produced by the prototype. Hence, by doing so, the rotor needs to be stationary while the stator is rotated instead to vary the rotor

position. As a result, both the cogging torque and the static torque can be measured for different rotor positions.

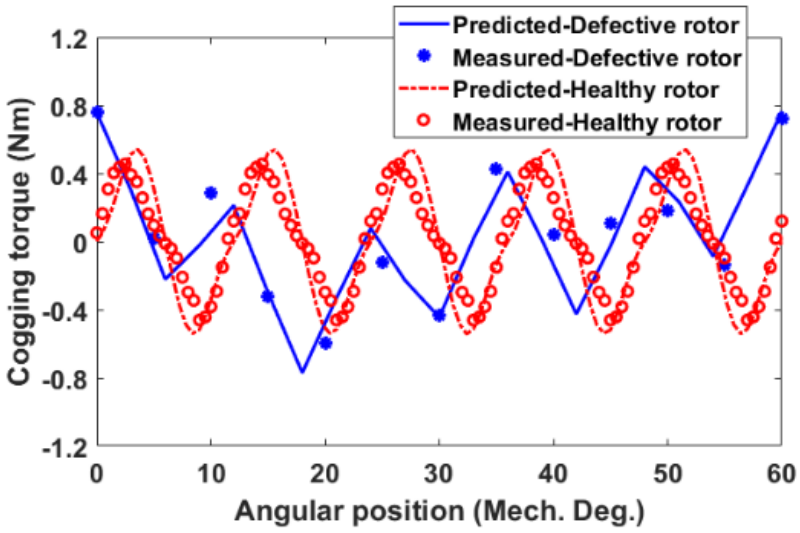

(a)

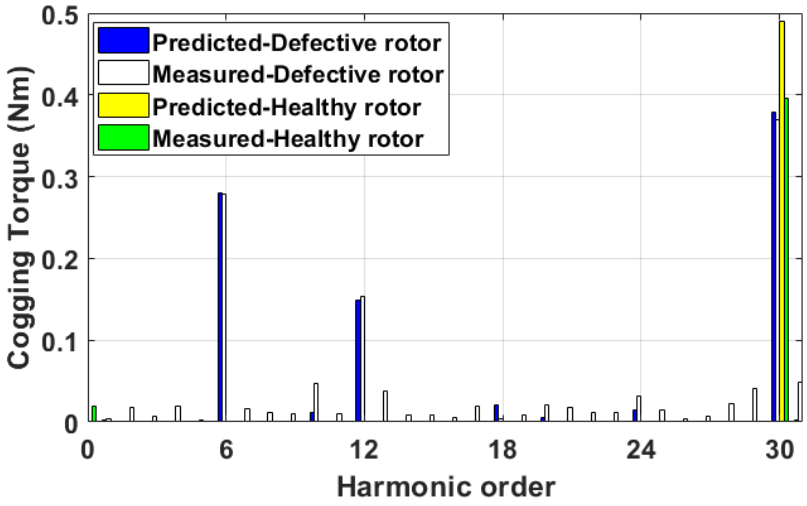

(b)

Fig. 5.44 Predicted and measured cogging torques of the modular PM machine with healthy and defective rotors. (a) Waveforms. (b) Spectra.

Fig. 5.44 shows the measured and predicted cogging torques of the modular PM machine with defective and healthy rotors. For the healthy rotor case, N_{cm} equals to 30 if N_{FG} is 6 and $2p$ is 10, and hence, there are 5 cogging torque periods within 60 Mech. Deg., which is shown in Fig. 5.44 as the dashed line. However, for the case of defective rotor, the value of N_{cm}

becomes 6 since the rotor is asymmetric. Therefore, the periodicity of cogging torque is 60 Mech. Deg., as shown by the solid line in Fig. 5.44. Furthermore, the peak-to-peak cogging torque of the modular PM machine with defective rotor is bigger than that of the modular PM machine with healthy rotor. This is mainly due to its asymmetric rotor and hence smaller N_{cm}.

Using similar method as for the cogging torque measurement, the on-load static torque can be measured by supplying the prototype with DC currents ($I_A = I, I_B = I_C = -I/2$, with I = 3A). The predicted and measured static torques of the modular PM machines with healthy and defective rotors are shown in Fig. 5.45. It can be seen that the static torque with defective rotor is smaller while it has larger ripple. This is mainly due to the reduction in the phase back-EMF (see Fig. 5.43) while the increase in the cogging torque (see Fig. 5.44).

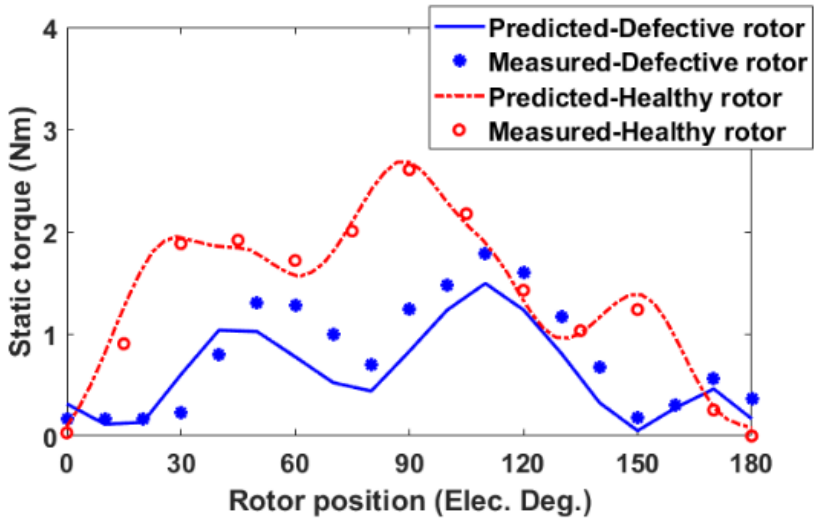

Fig. 5.45 The predicted and measured static torque of modular PM machine (I_A=3A). 3A DC current is chosen to avoid machine overheating.

5.5 CONCLUSION

The influences of radial and circumferential stator segment displacements and PM defect on the 12-slot/10-pole and 12-slot/14-pole modular PM machines have been investigated in this chapter. By theoretically analysing the influence of radial and circumferential stator segment displacements on the phase back-EMFs as well as the on-load torque, the most serious cases can be identified. It is found that the radial stator segment displacement mainly exerts influence on the magnitudes of the phase back-EMFs due to the change in the air-gap length while the circumferential stator segment displacement exerts limited impacts on the magnitudes but significant impacts on the phase angles of the phase back-EMFs.

For the radial stator segment scenario, the most influenced cases are generally those segments that belong to the same phase and are displaced in the same direction. But for the circumferential stator segment displacement scenarios, the most influenced cases are those having the biggest phase angle difference of the resultant three-phase back-EMFs. With regard to the manufacturing tolerance scenario of PM defect, two representative cases are studied which are the 5% and 10% area of one magnet pole are defected.

It demonstrated that the influence of FG widths on electromagnetic performance of the modular PM machines with radial stator segment displacement is similar to that of the healthy modular PM machines regardless of the slot/pole number combinations. In Table 5.14, the influence of the FG widths on changing ratios are summarized. It can be found that the modular structure can help to improve the manufacturing tolerance of radial stator segment displacement withstand capability for the PM machines. The influence of FG widths on electromagnetic performance of the modular PM machines with PM defect have also been demonstrated, as shown in Table 5.15. Similarly, the modular structure can also help to mitigate the effect from PM defect.

However, for the circumferential stator segment displacement scenario, the influence from such manufacturing tolerance on phase back-EMF and average torque is limited. But the peak-to-peak cogging torques are significantly increased due to the change of the stator symmetry.

Furthermore, compared with the 12-slot/14-pole modular PM machines, the 12-slot/10-pole modular PM machines have the better radial stator segment displacement withstand capability. This is the same for the PM defect except the case where the 12-slot/14-pole modular PM machines have slightly better withstand capability in terms of UMF. For the circumferential

stator segment displacement, the 12-slot/14-pole modular PM machines also have the better withstand capability of UMF.

The prototypes of the modular PM machines with PM defect rotor have been built and tested in order to validate the predictions and conclusion. Generally good agreement between the calculated and tested results has been observed.

TABLE 5.14 THE CHANGING RATIO AND THE UMF MAGNITUDES OF THE MODULAR PM MACHINE WITH RADIAL STATOR SEGMENT DISPLACEMENT

Changing ratio	Fundamental phase back-EMF	Cogging torque	Average torque	UMF
12-slot/10-pole	↓	√	~	$\mathbf{F_x}$: ↑ $\mathbf{F_y}$: ↓
12-slot/14-pole	↓	√	↓	$\mathbf{F_x}$: ↑ $\mathbf{F_y}$: ↓

TABLE 5.15 THE CHANGING RATIO OF THE MODULAR PM MACHINE WITH PM DEFECT

Changing ratio	Fundamental phase back-EMF	Cogging torque	Average torque	UMF
12-slot/10-pole	5% defect ↓	√	5% defect ↓	$\mathbf{F_x}$: √
	10% defect ↓		10% defect ↓	$\mathbf{F_y}$: √
12-slot/14-pole	5% defect ↑	√	5% defect ↑	$\mathbf{F_x}$: Δ
	10% defect ↑		10% defect↑	$\mathbf{F_y}$: Δ

- √ Represents the values can be reduced by selecting the FG widths appropriately.
- Δ Represents the values cannot be reduced by selecting the FG widths appropriately.
- ↓ Represents the changing ratio is decreased with the increase in the FG widths.
- ↑ Represents the changing ratio is increased with the increase in the FG widths.

Chapter 6 CONCLUSIONS AND FUTURE WORKS

6.1 CONCLUSIONS

This thesis mainly investigates some novel modular PM machines including the design of multi-phase modular PM machines, the cogging torque and torque ripple reduction of modular PM machines and the manufacturing tolerances of modular PM machines. The general conclusions obtained from the research demonstrated in thesis are detailed in this section.

The multi-phase modular PM machines with fractional-slot and single-layer concentrated winding is studied in the Chapter 2. The optimal slot/pole number combinations can be identified with the help of analysing the winding-factor. It is found that employing the modular structure can significantly reduce the main sub-harmonics of the air-gap flux density due to armature windings. For the multi-phase (or any phase number) modular PM machines having $N_s > 2p$, the FGs exert negative effects on the electromagnetic performance. While for the machines having $N_s < 2p$, the performance such as average torque and torque ripple can be improved by properly selecting the FG width.

In the chapter 3, an effective cogging torque mitigation method by the slot-opening shift is proposed for modular PM machines. The slot openings are divided into two groups in a special way. By shifting those two groups of slot-openings in the opposite directions with the desired shift angle, the synthesised cogging torque waveforms due to the shifted slot openings could be almost opposite to the cogging torque waveform due to the FGs, and thus cancel each other. Four cases are studied to validate the efficiency of the proposed method. A reduction up to 85% of the resultant cogging torque can be achieved. It is worth noting that the three-phase back-EMF waveforms are still balanced although their amplitudes might be slightly reduced and no extra harmonics are introduced due to the slot openings shift.

Another cogging torque and torque ripple reduction method for modular PM machines by adopting the C-core stator segments is investigated in Chapter 4. It is found that the resultant cogging torque and torque ripple can be reduced by 96.4% and 57.6% respectively compared with those of E-core modular PM machines. Especially, for the 12-slot/10-pole modular PM machine, the average torque can be enhanced by 6.3% when the C-core modular structure is employed.

The influence of the manufacturing tolerances on modular PM machines is studied in Chapter 5. Three manufacturing tolerance scenarios which are the radial stator segment displacement, circumferential stator segment displacement and PM defect are considered. It is

found that the radial stator segment displacement and PM defect exert influence on the magnitudes of phase back-EMFs while the circumferential stator segment displacement exerts limited influence on the magnitudes but significant influence on the phase angles of back-EMFs. Moreover, the modular structure has been found to be able to improve the withstand capability against the manufacturing tolerance due to radial stator segment displacement and PM defect. However for the circumferential stator segment displacement cases, the influence from such manufacturing tolerance scenario is limited with respect to the phase back-EMF and average torque. But the resultant cogging torques are dramatically increased due to the changed stator symmetry. In addition, compared with the 12-slot/14-pole modular PM machines, the 12-slot/10-pole modular PM machines have the better radial stator segment displacement and PM defect withstand capability except that the 12-slot/14-pole modular PM machines have the slightly better PM defect withstand capability in terms of UMF. Similarly, for the circumferential stator segment displacement withstand capability in terms of UMF, the 12-slot/14-pole modular PM machines are also better.

In summary, the main contributions from this thesis can be concluded that: 1) The slot-opening design for reducing the cogging torque of the E-core modular PM machines. 2) The improved C-core modular PM machine design for reducing the cogging torque and torque ripple. Other contributions such as the design and study of the multi-phase modular PM machines and the investigation on the manufacturing tolerance of the modular PM machines are also detailed in this thesis.

Last but not the least, it is worth mentioning that although the research carried out in this thesis are based on the small size modular PM machines (for experimental validation purpose), the conclusions detailed in this chapter might be extended to other large PM machines, such as the ones used for wind power applications.

6.2 FUTURE WORKS

Although several research on the novel modular PM machines have been carried out in this thesis, there are still a lot of work to be done in the future, such as:

- The extension employment of the novel modular structure to other PM machines.
- The investigation of modular PM machines with both modular stator and modular rotor.
- The further investigation of the manufacturing tolerances of modular PM machines.

- The thermal management of PM machines using the novel modular structure.
- The study on large modular PM machines having different numbers of the stator segments.
- The design of the optimal manufacturing method for modular PM machines.

REFERENCES

[1] Z. Q. Zhu and Y. X. Li, "Modularity techniques in high performance permanent magnet machines and applications," *CES Trans. Electr. Mach. Syst.*, vol. 2, no. 1, pp. 93-103, Mar. 2018.

[2] J.R. Hendershot and T.J. Miller, *Design of brushless permanent-magnet machines* 2010.

[3] Z. Q. Zhu and D. Howe, "Electrical machines and drives for electric, hybrid, and fuel cell vehicles," *Proc. IEEE,* vol. 95, no. 4, pp. 746-765, Apr. 2007.

[4] K. T. Chau, C. C. Chan, and C. Liu, "Overview of permanent-magnet brushless drives for electric and hybrid electric vehicles," *IEEE Trans. Ind. Electron.*, vol. 55, no. 6, pp. 2246-2257, Jun. 2008.

[5] M. Andriollo, M. De Bortoli, G. Martinelli, A. Morini, and A. Tortella, "Design improvement of a single-phase brushless permanent magnet motor for small fan appliances," *IEEE Trans. Ind. Electron.*, vol. 57, no. 1, pp. 88-95, Jan. 2010.

[6] C. N. Bhende, S. Mishra, and S. G. Malla, "Permanent magnet synchronous generator-based standalone wind energy supply system," *IEEE Trans. Sustainable Energy.*, vol. 2, no. 4, pp. 361-373, Oct. 2011.

[7] P. Roshanfekr, T. Thiringer, M. Alatalo, and S. Lundmark, "Performance of two 5 MW permanent magnet wind turbine generators using surface mounted and interior mounted magnets," in *2012 XXth Int. Conf. Electr. Mach.*, Marseille, France, Sept. 2-5, 2012, pp. 1041-1047.

[8] F. Libert and J. Soulard, "Design study of different direct-driven permanent-magnet motors for a low speed application," in *Nordic Workshop Power Ind. Electron.*, Trondheim, Norway, Jun. 2014.

[9] https://cleantechnica.com/2015/04/15/zero-gearbox-adds-massive-new-offshore-wind-turbine-opportunities/largest-offshore-wind-turbine-generator/.

[10] G. Shrestha, H. Polinder, D. Bang, and J. A. Ferreira, "Structural flexibility: a solution for weight reduction of large direct-drive wind-turbine generators," *IEEE Trans. Energy Convers.*, vol. 25, no. 3, pp. 732-740, Jun. 2010.

[11] H. Akita, Y. Nakahara, N. Miyake, and T. Oikawa, "New core structure and manufacturing method for high efficiency of permanent magnet motors," in *Ind. Appl. Conf. 38th IAS Annu. Meeting.*, Salt Lake City, USA. Oct. 12-16, 2003, pp. 367-372.

[12] F. Libert and J. Soulard, "Manufacturing methods of stator cores with concentrated windings," in *3rd IET Int. Conf. Electron. Mach. Drives*, Apr. 4-6, 2006, pp. 676-680.

[13] X. Ge and Z. Q. Zhu, "Sensitivity of manufacturing tolerances on cogging torque in interior permanent magnet machines with different slot/pole number combinations," *IEEE Trans. Ind. Appl.*, vol. 53, no. 4, pp. 3557-3567, Jul.-Aug. 2017.

[14] X. Ge and Z. Q. Zhu, "Influence of manufacturing tolerances on cogging torque in interior permanent magnet machines with eccentric and sinusoidal rotor contours," *IEEE Trans. Ind. Appl.*, vol. 53, no. 4, pp. 3568-3578, Jul.-Aug. 2017.

[15] T.Y. Lee, M.K. Seo, Y.J. Kim, and S. Y. Jung, "Cogging torque of surface-mounted permanent magnet synchronous motor according to segmented-stator core effect," in

2016 XXII Int. Conf. Electr. Mach. (ICEM), Lausanne, Switzerland, Sept. 4-7, 2016, pp. 200-206.

[16] http://www.swd-technology.com/en/products/segmentierung-und-zahnsegmente/.

[17] http://www.yumalaminations.com/lamination-stacks-for-servo-motors/80mm-servo-motors-2.html.

[18] J. Yuan, C. Shi, and J. Shen, "Analysis of cogging torque in surface-mounted permanent magnet machines with segmented stators," in *2014 17th Int. Conf. Electr. Mach. Syst. (ICEMS)*, Hangzhou, China, Oct. 22-25, 2014, pp. 2513-2516.

[19] G. Dajaku and D. Gerling, "Different novel methods for reduction of low space harmonics for the fractional slot concentrated windings," in *15th Int. Conf. Electr. Mach. Syst. (ICEMS)*, Sapporo. Japan. Oct. 21-24, 2012, pp. 1-6.

[20] G. Dajaku， and D. Gerling, "A novel 12-teeth/10-poles PM machine with flux barriers in stator yoke," in *XXth Int. Conf. Electr. Machines (ICEM)*, Marseille, France, Sept. 2-5, 2012, pp. 36-40.

[21] G. Dajaku, W. Xie, and D. Gerling, "Reduction of low space harmonics for the fractional slot concentrated windings using a novel stator design," *IEEE Trans. Magn.*, vol. 50, no. 5, May. 2014.

[22] B.C. Mecrow, A.G. Jack, J.A. Haylock, U. Hoefer, and P. G. Dickinson, "Simplifying the manufacturing process for electrical machines," in *Power Electron. Mach. Drives (PEMD)*, Edinburgh, UK, Mar. 31-2 Apr. 2004, pp. 169-174.

[23] M.F. Momen and S. Datta, "Analysis of flux leakage in a segmented core brushless permanent magnet motor," *IEEE Trans. Energy Convers.*, vol. 24, no. 1, pp. 77-81, Mar. 2009.

[24] Z. Q. Zhu, Z. Azar, and G. Ombach, "Influence of additional air gaps between stator segments on cogging torque of permanent-magnet machines having modular stators," *IEEE Trans. Magn.*, vol. 48, no. 6, pp. 2049-2055, Jun. 2012.

[25] M. Kitamura, Y. Enomoto, J. Kaneda, and M. Komuro, "Cogging torque due to roundness errors of the inner stator core surface," *IEEE Trans. Magn.*, vol. 39, no. 3, pp. 1622-1625, May. 2003.

[26] J. Shen, C. Wang, D. Miao, M. Jin, D. Shi, and Y. Wang, "Analysis and optimization of a modular stator core with segmental teeth and solid back iron for PM electric machines," in *2011 IEEE Int. Conf. Electr. Mach. Drives. (IEMDC)*, Niagara Falls, Canada, May. 15-18, 2011., pp. 1270-1275.

[27] G. Geng and E. Spooner, "Cancellation of noise and vibration in modular permanent-magnet wind turbine generators," in *Seventh Int. Conf. Elect. Mach. Drives.*, Sept. 11-13, 1995, Durham, UK., pp. 467-471.

[28] Z. Chen and E. Spooner, "A modular, permanent-magnet generator for variable speed wind turbines," in *7th Int. Conf. Electr. Mach. Drives.*, Durham, UK, Sep. 11-13, 1995, pp. 453-457.

[29] E. Spooner and A. Williamson, "Modular, permanent-magnet wind-turbine generators," in *Conf. Rec. IEEE Ind. Appl. Conf. 31st IAS Annu. Meeting*, San Diego, USA, Oct. 6-10, 1996, pp. 497-502.

[30] E. Spooner, A. C. Williamson, and G. Catto, "Modular design of permanent-magnet

generators for wind turbines," *IEE Proc. Elec. Power Appl.*, vol. 143, no. 5, pp. 388-395, Sep. 1996.

[31] E. Spooner and A. C. Williamson, "Parasitic losses in modular permanent-magnet generators," *IEE Proc. Elec. Power Appl.*, vol. 145, no. 6, pp. 485-496, Nov. 1998.

[32] Z. Chen, E. Spooner, W.T. Norris, and A. C. Williamson, "Capacitor-assisted excitation of permanent-magnet generators," *IEE Proc. Elec. Power Appl.*, vol. 145, no. 6, pp. 497-508, Nov. 1998.

[33] G. Dajaku and D. Gerling, "Low costs and high-efficiency electric machines," in *2nd Int. Elec. Drives. Production Conf. (EDPC)*, Nuremberg, Germany, Oct. 15-18, 2012.

[34] G. Dajaku, "Elektrische Maschine," *Patent DE 10 201 2103 677.2*, 4. May, 2012.

[35] S. Spas, G. Dajaku, and D. Gerling, "Comparison of PM machines with concentrated windings for automotive application," in *2014 Int. Conf. Electr. Machines (ICEM)*, Berlin, Germany, Sept. 2-5, 2014, pp. 1996-2000.

[36] G. J. Li, Z. Q. Zhu, W. Q. Chu, M. P. Foster, and D. A. Stone, "Influence of flux gaps on electromagnetic performance of novel modular PM machines," *IEEE Trans. Energy Convers.*, vol. 29, no. 3, pp. 716-726, Apr. 2014.

[37] G. J. Li, Z. Q. Zhu, M. Foster, and D. Stone, "Comparative studies of modular and unequal tooth PM machines either with or without tooth tips," *IEEE Trans. Magn.*, vol. 50, no. 7, Jun. 2014.

[38] G. J. Li, Z. Q. Zhu, M. P. Foster, D. A. Stone, and H. L. Zhan, "Modular permanent-magnet machines with alternate teeth having tooth tips," *IEEE Trans. Ind. Electron.*, vol. 62, no. 10, pp. 6120-6130, Apr. 2015.

[39] M. J. Jin, C. F. Wang, J. X. Shen, and B. Xia, "A modular permanent-magnet flux-switching linear machine with fault-tolerant capability," *IEEE Trans. Magn.*, vol. 45, no. 8, pp. 3179-3186, Aug. 2009.

[40] A. Zulu, B. C. Mecrow, and M. Armstrong, "Permanent-magnet flux-switching synchronous motor employing a segmental rotor," *IEEE Trans. Ind. Appl.*, vol. 48, no. 6, pp. 2259-2267, Nov.-Dec. 2012

[41] A. S. Thomas, Z. Q. Zhu, and L. J. Wu, "Novel modular-rotor switched-flux permanent magnet machines," *IEEE Trans. Ind. Appl.*, vol. 48, no. 6, pp. 2249-2258, Nov.-Dec. 2012.

[42] N. Bianchi, S. Bolognani, and M. D. Pre, "Impact of stator winding of a five-Phase permanent-magnet motor on postfault operations," *IEEE Trans. Ind. Electron.*, vol. 55, no. 5, pp. 1978-1987, May. 2008.

[43] W. Cao, B. C. Mecrow, G. J. Atkinson, J. W. Bennett, and D. J. Atkinson, "Overview of electric motor technologies used for more electric aircraft (MEA)," *IEEE Trans. Ind. Electro.*, vol. 59, no. 9, pp. 3523-3531, Aug. 2012.

[44] L. Szabo and M. Ruba, "Segmental stator switched reluctance machine for safety-critical applications," *IEEE Trans. Ind. Appl.*, vol. 48, no. 6, pp. 2223-2229, Dec. 2012.

[45] A. Nollau and D. Gerling, "Novel cooling methods using flux-barriers," in *Int. Conf. Electr. Mach. (ICEM)*, Berling, Germany, Sep. 2-5, 2014, pp. 1328-1333.

[46] A. Nollau and D. Gerling, "A flux barrier cooling for traction motors in hybrid drives," in *IEEE Int. Electr. Mach. Drives. Conf. (IEMDC)*, Coeur d'Alene, USA, May. 10-13,

2015, pp. 1103-1108.

[47] G. J. Li, B. Ren, and Z. Q. Zhu, "Design guidelines for fractional slot multi-phase modular permanent magnet machines," *IET Electr.Power. Appl.*, vol. 11, no. 6, pp. 1023-1031, Jul. 2017.

[48] J. Wang, V. I. Patel, and W. Wang, "Fractional-slot permanent magnet brushless machines with low space harmonic contents," *IEEE Trans. Magn.*, vol. 50, no. 1, 2014.

[49] N. Bekka, M. E. Zaim, N. Bernard, and D. Trichet, "Optimization of the MMF function of fractional slot concentrated windings," in *2014 Int. Conf. Electr. Mach. (ICEM)*, Berlin, Germany, Sep. 2-5, 2014, pp. 616-622.

[50] N. Bianchi and M. D. Pre, "Use of the star of slots in designing fractional-slot single-layer synchronous motors," *IEE Proc. Elec. Power Appl.*, vol. 153, no. 3, pp. 459-466, May. 2006.

[51] J. M. Apsley, S. Williamson, A. C. Smith, and M. Barnes, "Induction motor performance as a function of phase number," *IEE Proc. Elec. Power Appl.*, vol. 153, no. 6, pp. 898-904, Nov. 2006.

[52] E. A. Klingshirn, "High phase order induction motors-Part I-description and theoretical considerations," *IEEE Trans. Power Apparatus Syst.*, vol. PAS-102, no. 1, pp. 47-53, Jan. 1983.

[53] A. M. E. Refaie, M. R. Shah, R. Qu, and J. M. Kern, "Effect of number of phases on losses in conducting sleeves of surface PM machine rotors equipped with fractional-slot concentrated windings," *IEEE Trans. Ind. Appl.*, vol. 44, no. 5, pp. 1522-1532, Sept.-Oct. 2008.

[54] L. Parsa and H. A. Toliyat, "Multi-phase permanent magnet motor drives," in *38th Ind. Appl. Conf. (IAS) Annu. Meeting*, Salt Lake City, USA, Oct. 12-16, 2003, pp. 401-408.

[55] L. Parsa, H. A. Toliyat, and A. Goodarzi, "Five-phase interior permanent-magnet motors with low torque pulsation," *IEEE Trans. Ind. Appl.*, vol. 43, no. 1, pp. 40-46, Jan.-Feb. 2007.

[56] S. Sadeghi, L. Guo, H. A. Toliyat, and L. Parsa, "Wide operational speed range of five-phase permanent magnet machines by using different stator winding configurations," *IEEE Trans. Ind. Electron.*, vol. 59, no. 6, pp. 2621-2631, Jun. 2012.

[57] H. A. Toliyat, S. P. Waikar, and T. A. Lipo, "Analysis and simulation of five-phase synchronous reluctance machines including third harmonic of airgap MMF," *IEEE Trans. Ind. Appl.*, vol. 34, no. 2, pp. 332-339, Mar.-Apr. 1998.

[58] K. Huilin, L. Zhou, and J. Wang, "Harmonic winding factors and MMF analysis for five-phase fractional-slot concentrated winding PMSM," in *2013 Int. Conf. Electr. Mach. Syst. (ICEMS)*, Busan, South Korea, Oct. 26-29, 2013, pp. 1236-1241.

[59] M. Barcaro, N. Bianchi, and F. Magnussen, "Six-phase supply feasibility using a PM fractional-slot dual winding machine," *IEEE Trans. Ind. Appl.*, vol. 47, no. 5, pp. 2042-2050, Sep.-Oct. 2011.

[60] A. S. Abdel-Khalik, S. Ahmed, and A. M. Massoud, "A six-phase 24-slot/10-pole permanent-magnet machine with low space harmonics for electric vehicle applications," *IEEE Trans. Magn.*, vol. 52, no. 6, Jun. 2016.

[61] V. I. Patel, J. Wang, W. Wang, and X. Chen, "Six-phase fractional-slot-per-pole-per-phase permanent-magnet machines with low space harmonics for electric vehicle

application," *IEEE Trans. Ind. Appl.*, vol. 50, no. 4, pp. 2554-2563, Jul.-Aug. 2014.

[62] M. Barcaro, N. Bianchi, and F. Magnussen, "Analysis and tests of a dual three-phase 12-slot 10-pole permanent-magnet motor," *IEEE Trans. Ind. Appl.*, vol. 46, no. 6, pp. 2355-2362, Nov.-Dec. 2010.

[63] Y. Demir and M. Aydin, "A novel dual three-phase permanent magnet synchronous motor with asymmetric stator winding," *IEEE Trans. Magn.*, vol. 52, no. 7, Jul. 2016.

[64] N. Bianchi, M. D. Pre, and L. Alberti, *Theory and design of fractional-slot PM machines*: CLEUP, 2007.

[65] Z. Q. Zhu, S. Ruangsinchaiwanich, and D. Howe, "Synthesis of cogging-torque waveform from analysis of a single stator slot," *IEEE Trans. Ind. Appl.*, vol. 42, no. 3, pp. 650-657, May.-Jun. 2006.

[66] G. J. Li, B. Ren, Z. Q. Zhu, Y. X. Li, and J. Ma, "Cogging torque mitigation of modular permanent magnet machines," *IEEE Trans. Magn.*, vol. 52, no. 1, Jan. 2016.

[67] Z. Q. Zhu, "A simple method for measuring cogging torque in permanent magnet machines," in *IEEE Power & Energy Soc. General Meet.*, Calgary, Canada. Jul. 26-30, 2009.

[68] Z. Q. Zhu and D. Howe, "Influence of design parameters on cogging torque in permanent magnet machines," *IEEE Trans. Energy Convers.*, vol. 15, no. 4, pp. 407-412, Dec. 2000.

[69] T. M. Jahns and W. L. Soong, "Pulsating torque minimization techniques for permanent magnet AC motor drives-a review," *IEEE Trans. Ind. Electron.*, vol. 43, no. 2, pp. 321-330, Apr. 1996.

[70] N. Bianchi and S. Bolognani, "Design techniques for reducing the cogging torque in surface-mounted PM motors," *IEEE Trans. Ind. Appl.*, vol. 38, no. 5, pp. 1259-1265, Sep.-Oct. 2002.

[71] C. S. Koh and J. S. Seol, "New cogging-torque reduction method for brushless permanent-magnet motors," *IEEE Trans. Magn.*, vol. 39, no. 6, pp. 3503-3506, Nov. 2003.

[72] G. Zhang, F. Wang, and Y. Shen, "Reduction of rotor loss and cogging torque of high speed PM machine by stator teeth notching," in *2007 Int. Conf. Electr. Mach. Syst. (ICEMS)*, Seoul, South Korea, Oct. 8-11, 2007, pp. 856-859.

[73] Y. Yang, X. Wang, X. Leng, D. Wang, and S. Liu, "Reducing cogging torque in surface-mounted permanent magnet motors by teeth notching," in *2nd. Conf. Ind. Electro. Appl.(ICIEA)* Harbin, China, May. 23-25, 2007, pp. 265-268.

[74] Y. U. Park, J. H. Cho, and D. K. Kim, "Cogging torque reduction of single-phase brushless DC motor with a tapered air-gap using optimizing notch size and position," *IEEE Trans. Ind. Appl.*, vol. 51, no. 6, pp. 4455-4463, Nov.-Dec. 2015.

[75] V. Keloth, M. Mijas, P. A. Manu, P. Thomas, V. M. Menon, and R. P. Praveen, "Analysis of cogging torque reduction techniques of a slotless PMBLDC motor," in *2014 Annu. Int. Conf. Emerging Research Areas: Magn. Mach. Drives. (AICERA/iCMMD)*, Kottayam, India, Jul. 24-26, 2014.

[76] C. Breton, J. Bartolome, J. A. Benito, G. Tassinario, I. Flotats, C. W. Lu, and B. J. Chalmers, "Influence of machine symmetry on reduction of cogging torque in permanent-magnet brushless motors," *IEEE Trans. Magn.*, vol. 36, no. 5, pp. 3819-

3823, Sep. 2000.

[77] M. Lukaniszyn, M. JagieLa, and R. Wrobel, "Optimization of permanent magnet shape for minimum cogging torque using a genetic algorithm," *IEEE Trans. Magn.,* vol. 40, no. 2, pp. 1228-1231, Mar. 2004.

[78] J. Y. Lee, J. H. Chang, D. H. Kang, S. I. Kim, and J. P. Hong, "Tooth shape optimization for cogging torque reduction of transverse flux rotary motor using design of experiment and response surface methodology," *IEEE Trans. Magn. ,* vol. 43, no. 4, pp. 1817-1820, Apr. 2007.

[79] S. Saravanan, M. A. N. Doss, S. Jeevananthan, and S. Vidyasagar, "Reduction of cogging torque by adopting semi circled permanent magnet," in *2011 1st Int. Conf. Electr. Energy. Syst. (ICEES)*, Newport Beach, Canada, Jan. 3-5, 2011, pp. 149-153.

[80] Y. Yang, X. Wang, C. Zhu, and C. Huang, "Reducing cogging torque by adopting isodiametric permanent magnet," in *2009 4th Conf. Ind. Electro. Appl (ICIEA)* Xi'an, China, May. 25-27, 2009, pp. 1028-1031.

[81] J. G. Lee, Y. K. Lee, and G. S. Park, "Effects of V-skew on the cogging torque in permanent magnet synchronous motor," in *Int. Electr. Mach. Syst. (ICEMS)*, Busan, South Korea, Oct. 26-29, 2013, pp. 122-124.

[82] M. S. Islam, S. Mir, and T. Sebastian, "Issues in reducing the cogging torque of mass-produced permanent-magnet brushless DC motor," *IEEE Trans. Ind. Appl.,* vol. 40, no. 3, pp. 813-820, May.-Jun. 2004.

[83] R. Islam, I. Husain, A. Fardoun, and K. McLaughlin, "Permanent-magnet synchronous motor magnet designs with skewing for torque ripple and cogging torque reduction," *IEEE Trans. Ind. Appl.,* vol. 45, no. 1, pp. 152-160, Jan.-Feb. 2009.

[84] C. C. Hwang, S. B. John, and S. S. Wu, "Reduction of cogging torque in spindle motors for CD-ROM drive," *IEEE Trans. Magn.,* vol. 34, no. 2, pp. 468-470, Mar. 1998.

[85] Z. Q. Zhu, S. Ruangsinchaiwanich, N. Schofield, and D. Howe, "Reduction of cogging torque in interior-magnet brushless machines," *IEEE Trans. Magn.,* vol. 39, no. 5, pp. 3238-3240, Sep. 2003.

[86] Z. Q. Zhu and D. Howe, "Analytical prediction of the cogging torque in radial-field permanent magnet brushless motors," *IEEE Trans. Magn.,* vol. 28, no. 2, pp. 1371-1374, Mar. 1992.

[87] T. Liu, S. Huang, J. Gao, and K. Lu, "Cogging torque reduction by slot-opening shift for permanent magnet machines," *IEEE Trans. Magn.,* vol. 49, no. 7, pp. 4028-4031, Jul. 2013.

[88] G. Dajaku and D. Gerling, "New methods for reducing the cogging torque and torque ripples of PMSM," in *2014 4th Int. Electr. Drives Prod. Conf. (EDPC)*, Nuremberg, Germany, Sep. 30-Oct. 1. 2014.

[89] G. J. Li, B. Ren, and Z. Q. Zhu, "Cogging torque and torque ripple reduction of modular permanent magnet machines," in *XXII Int. Conf. Elec. Mach. (ICEM)*, Lausanne, Switzerland, Sept. 4-7, 2016, pp. 193-199.

[90] A. M. El-Refaie, "Fractional-slot concentrated-windings synchronous permanent mgnet mchines: oportunities and challenges," *IEEE Trans. Ind. Electron.,* vol. 57, no. 1, pp. 107-121, Sept. 2010.

[91] W. Q. Chu and Z. Q. Zhu, "On-load cogging torque calculation in permanent magnet

machines," *IEEE Trans. Magn.,* vol. 49, no. 6, pp. 2982-2989, Dec. 2012.

[92] K. Wang, Z. Q. Zhu, and G. Ombach, "Torque enhancement of surface-mounted permanent magnet machine using third-order harmonic," *IEEE Trans. Magn.,* vol. 50, no. 3, pp. 104-113, Oct. 2013.

[93] W. Q. Chu and Z. Q. Zhu, "Average torque separation in permanent magnet synchronous machines using frozen permeability," *IEEE Trans. Magn.,* vol. 49, no. 3, pp. 1202-1210, Oct. 2012.

[94] K. Wang, Z. Q. Zhu, G. Ombach, and W. Chlebosz, "Average torque improvement of interior permanent-magnet machine using third harmonic in rotor shape," *IEEE Trans. Ind. Electron.,* vol. 61, no. 9, pp. 5047-5057, Oct. 2013.

[95] W. Q. Chu and Z. Q. Zhu, "Reduction of on-load torque ripples in permanent magnet synchronous machines by improved skewing," *IEEE Trans. Magn.,* vol. 49, no. 7, pp. 3822-3825, Jul. 2013.

[96] S. Park and K. Kim, "Torque ripple reduction method with asymmetric pole for wound-field synchronous motor," *IEEE Trans. Magn.,* vol. 51, no. 3, Mar. 2015.

[97] X. Luo and T. A. Lipo, "A synchronous/permanent magnet hybrid AC machine," *IEEE Trans. Energy Convers.,* vol. 15, no. 2, pp. 203-210, Jun. 2000.

[98] A. J. P. Ortega and L. Xu, "Analytical prediction of torque ripple in surface-mounted permanent magnet motors due to manufacturing variations," *IEEE Trans. Energy Convers.,* vol. 31, no. 4, pp. 1634-1644, Dec. 2016.

[99] A. J. P. Ortega and L. Xu, "Investigation of effects of asymmetries on the performance of permanent magnet synchronous machines," *IEEE Trans. Energy Convers.,* vol. 32, no. 3, pp. 1002-1011, Sept. 2017.

[100] H. Qian, H. Guo, Z. Wu, and X. Ding, "Analytical solution for cogging torque in surface-mounted permanent-magnet motors with magnet imperfections and rotor eccentricity," *IEEE Trans. Magn.,* vol. 50, no. 8, Aug. 2014.

[101] I. Coenen, M. v. d. Giet, and K. Hameyer, "Manufacturing tolerance: estimation and prediction of cogging torque influence by magnetization faults," *IEEE Trans. Magn.,* vol. 48, no. 5, pp. 1932-1936, May. 2012.

[102] I. Coenen, C. P. Mbo'o, and K. Hameyer, "Statistical evaluation of manufacturing tolerances in electrical machines by simulation and measurement," in *Fourth Int. Conf. POWERENG*, Istanbul, Turkey, May. 13-17, 2013.

[103] L. Wu, R. Qu, B. Song, H. Bi, O. Jing, G. Yang, and C. Du, "Analysis of cogging torque in surface permanent magnet machine with manufacturing tolerances," in *IEEE IECON 41st Annu. Conf.,* Yokohama, Japan, Nov. 9-12, 2015 pp. 4732-4737.

[104] Z. Q. Zhu, L. J. Wu, and M. L. M. Jamil, "Influence of pole and slot number combinations on cogging torque in permanent-magnet machines with static and rotating eccentricities," *IEEE Trans. Ind. Appl.,* vol. 50, no. 5, pp. 3265-3277, Feb. 2014.

[105] D. G. Dorrell, M. F. Hsieh, and Y. Guo, "Unbalanced magnet pull in large brushless rare-earth permanent magnet motors with rotor eccentricity," *IEEE Trans. Magn.,* vol. 45, no. 10, pp. 4586-4589, Sep. 2009.

[106] L. Gasparin, A. Cernigoj, S. Markic, and R. Fiser, "Additional cogging torque components in permanent-magnet motors due to manufacturing imperfections," *IEEE Trans. Magn.,* vol. 45, no. 3, pp. 1210-1213, Mar. 2009.

[107] M. Nakano, Y. Morita, and T. Matsunaga, "Reduction of cogging torque due to production tolerances of rotor by using dummy slots placed partially in axial direction," *IEEE Trans. Ind. Appl.*, vol. 51, no. 6, pp. 4372-4382, Nov.-Dec. 2015.

[108] W. Li, A. Li, and H. Wang, "Anisotropic fracture behavior of sintered rear-earth permanent magnets," *IEEE Trans. Magn.*, vol. 41, no. 8, pp. 2339-2342, Aug. 2005.

[109] J. A. Farooq, A. Djerdir, and A. Miraoui, "Analytical modeling approach to detect magnet defects in permanent-magnet brushless motors," *IEEE Trans. Magn.*, vol. 44, no. 12, pp. 4599-4604, Dec. 2008.

[110] W. l. Roux, R. G. Harley, and T. G. Habetler, "Detecting rotor faults in low power permanent magnet synchronous machines," *IEEE Trans. Power Electron.*, vol. 22, no. 1, pp. 322-328, Jan. 2007.

[111] M. Zafarani, T. Goktas, and B. Akin, "A comprehensive magnet defect fault analysis of permanent-magnet synchronous motors," *IEEE Trans. Ind. Appl.*, vol. 52, no. 2, pp. 1331-1339, Mar.-Apr. 2016.

[112] J.-C. Urresty, J.-R. Riba, and L. Romeral, "A back-EMF based method to detect magnet failures in PMSMs," *IEEE Trans. Magn.*, vol. 49, no. 1, pp. 591-598, Jan. 2013.

[113] T. Goktas, M. Zafarani, and B. Akin, "Discernment of broken magnet and static eccentricity faults in permanent magnet synchronous motors," *IEEE Trans. Energy Convers.*, vol. 31, no. 2, pp. 578-587, Jun. 2016.

[114] T. Goktas, M. Zafarani, K. W. Lee, B. Akin, and T. Sculley, "Comprehensive analysis of magnet defect fault monitoring through leakage flux," *IEEE Trans. Magn.*, vol. 53, no. 4, Apr. 2017.